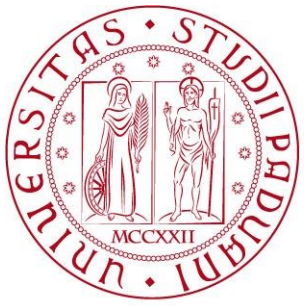

UNIVERSITÀ DEGLI STUDI DI PADOVA

Head Office: Università degli Studi di Padova

Department of Industrial Engineering

Ph.D. COURSE IN: INDUSTRIAL ENGINEERING

CURRICULUM: ENERGY ENGINEERING

SERIES: XXXV

SUSTAINABILITY IN ROAD TRANSPORT REFRIGERATION: REDUCTION OF DIRECT AND INDIRECT EMISSIONS THROUGH ELECTRIFICATION AND NATURAL REFRIGERANTS

Thesis written with the financial contribution of the National Research Council - Construction Technologies Institute (Italy)

Coordinator: Prof. Anna Stoppato

Supervisor: Dr. Silvia Minetto

Ph.D. Student: Francesco Fabris

Abstract

The increasing urbanization and globalization phenomena, together with the COVID-19 outbreak which characterized the last years, caused an overall growth of the home-delivered food consumption, of the transport and preservation of pharmaceutical products and of the online grocery shopping, leading to a significant rise of the importance of refrigerated transport. Temperature-controlled transport of the products represents a crucial aspect of the Cold Chain, to manage the goods temperature, ensure their quality and safety throughout the whole delivery process and avoid product waste. Within the temperature-controlled transport sector, road transport through the employment of refrigerated vehicles represents the primary transportation option.

The operation and the control of a transport refrigeration unit is generally more challenging compared to a stationary cooling unit, due to specific issues as initial temperature conditions of the cargo, strong variability of external ambient conditions, frequent door openings with consequent infiltration of external air, highly variable range of thermal loads and accelerations and vibrations linked to the vehicle motion. At the same time, climate change issues need to be carefully considered and faced, to control and limit Green-House Gases emissions in the atmosphere to prevent the harmful effect of climate change on humans and environment.

In such a scenario, the refrigerated road transport sector needs to develop and implement strategies and solutions to guarantee the correct preservation of the transported products quality along their Cold Chain, but at the same time to minimize its negative impacts on the environment. Therefore, a reduction of both the indirect emissions, linked to the system operation and efficiency, and the direct emissions, linked to refrigerant leakage in the atmosphere, needs to be achieved.

The present thesis contains the results of the studies carried out during three years of PhD activity, conducted at the Construction Technology Institute (ITC) of the National Research Council (CNR) in Padova, Italy, which has focused on the development of possible solutions to reduce the indirect and direct environmental impact of the road refrigerated transport sector.

Firstly, a baseline numerical assessment of the environmental impact of traditionally employed HFC refrigeration systems will be carried out. The results will highlight the crucial influence of the cooling unit power supply technology. Numerical simulations will assess that the fuel consumption of a refrigerated truck presents an average +19.0% increase compared to non-refrigerated trucks, and that pollutant emissions (CO, NOx, THC, PM) present an increase in the range of +10÷35%. However, the use of an energy storage system can mitigate the increase of energy consumption due to the cooling unit presence, thanks to the optimization of the vehicle engine operation (the fuel consumption increase is reduced to only +5.7%). Moreover, the insertion of photovoltaic panels on the roof of the vehicle insulated box can lead

to a -95% reduction of the power drawn from the vehicle engine, in case of small battery pack capacity, and that with the use of a larger battery pack, a net +12% energy excess on a yearly basis can be achieved.

As a sustainable alternative to commonly used HFC refrigerants, R744 (CO_2) has then been selected as a long-term future proof refrigerant, reducing to zero the direct refrigerant emissions. Therefore, a novel R744 cooling unit design developed for road transport refrigeration applications will be proposed and its performance will be numerically evaluated. In hot summer conditions, the average mission Coefficient of Performance (COP) of the R744 cooling unit during a delivery mission of temperature-controlled products is equal to 1.40, while the baseline COP of the belt-driven R134a unit in the same conditions is equal to 1.31, highlighting the good performance of the R744 unit even compared to traditional HFC solutions. Supported by the positive numerical results, the installation, setup and first startup tests of the experimental setup of a R744 refrigeration unit will be described.

Moreover, the performance of MT single-temperature R744 cooling units and MT-LT multi-temperature R744 cooling units will be numerically assessed, suggesting optimal control strategies to maximize the system performance, assessing the crucial importance of the refrigeration cycle design, including specific components such as ejector to increase the unit efficiency, and highlighting the crucial issues linked to a non-stationary application as road transport refrigeration.

The results of this thesis will be useful to highlight that sustainable alternatives to replace the traditionally used HFC/HFO transport refrigeration systems are possible and under practical development, both in terms of improvement of the refrigerating system performance and efficiency, through innovative solutions and electrification, and in terms of development of highly efficient units employing natural refrigerants such as R744.

Keywords: Transport refrigeration; Emissions; CO_2; Ejector; Energy management; Solar-aided refrigeration; Dynamic simulation; Experimental evaluation; Cold Chain.

Table of contents

1. Introduction

The increasing urbanization and globalization phenomena which characterized the last decades led to a general change in consumer behavior and caused an overall growth of the home-delivered food consumption, leading to a significant rise of the importance of refrigerated transport [1]. Moreover, the COVID-19 outbreak, which characterized the recent years, caused a significant increase in the demand for grocery home deliveries and the trend is expected to continue in the next years, as the pandemic has introduced new habits. Recent research related to the UK market highlighted that the COVID-19 outbreak has strongly accelerated online grocery shopping [2], as weekly home delivery orders have registered a 38% increase compared to the pre-pandemic period. The same authors report that the home delivery sector is expected to experience a 41% growth in the next five years [2]. In addition, in this sanitary emergency scenario, also the need for conservation and transport of pharmaceuticals and vaccines has overwhelmingly emerged, underlining the crucial role of the refrigerated transport sector.

The cooling steps which guarantee the need to maintain perishable products in a specific temperature range throughout the entire supply chain are commonly named “Cold Chain”. The Cold Chain comprehends the whole process of production stage, initial pre-cooling, storage and transport of products, their distribution and final domestic refrigeration by the end-user [3]. In particular, the temperature-controlled transport of the products represents a crucial aspect of the Cold Chain, to manage the goods temperature, ensure their quality and safety throughout the whole delivery process and avoid product waste, as it is estimated in literature that approximately one third of all food produced globally is either lost or wasted along the food chain, before reaching the consumers [4]

Within the context of the Cold Chain, around 31% of food supply chain includes temperature-controlled transportation [5]. Since this kind of freight transport systems must provide temperature control in the environment where the products to be transported are stored, an additional amount of energy needs to be provided to run a refrigeration system and ensure the products quality and safety throughout the whole delivery process [6]. Within the temperature-controlled transport sector, road transport through the employment of refrigerated vehicles represents the primary transportation option. Consistently with the overall growth of the entire delivery sector reported above, a significant expansion in terms of volume, number of units and overall financial and energetic cost is foreseen for the truck industry in the upcoming years [7] [8].

The operation and the control of a transport refrigeration unit is generally more challenging compared to a stationary cooling unit, due to several issues linked to this specific applications, such as the initial temperature conditions of the cargo, the strong fluctuation and variability of the external ambient conditions, the frequent door openings with consequent infiltration of external air, the highly variable

range of loads in which the refrigerating system needs to operate during usual daily delivery missions and the accelerations and vibrations linked to the vehicle motion [9] [10] [11]. To address the specific issues linked to transport applications, Artuso et al. [12] developed a numerical model of an insulated box, installed on a refrigerated van, employed in a typical long-distance delivery mission and assessed how the load fluctuations and the mission structure impact on the instantaneous cooling power required by the insulated body. Moreover, Jara et al. [11] proposed a computational-experimental analysis of a refrigerated vehicle for food transport in which the authors developed a Computational Fluid Dynamics (CFD) model to evaluate the thermal behavior of the refrigerated vehicle and to assess the temperature distribution inside it.

At the same time, climate change issues need to be carefully considered and faced. Literature reports that over the last 50 years, an average increase of the global temperature of around 0.13°C per decade has been experienced, with an approximately doubled increase rate compared with the first 50 years of the century [13]. The same study reports that in the next 20 years an even larger increase rate of the global average temperature is forecast, reaching the value of around 0.2°C per decade [13]. The significant and continuous environmental temperature rise severely accelerates the rate of glaciers melting and sea level rise, thus requiring preventive and effective actions to control and limit Green-House Gases (GHG) emissions in the atmosphere to prevent the harmful effect of climate change on humans and environment [14].

The transport sector must consider the above-mentioned issues to limit its negative impact on the environment, as it is reported in literature that the transport activities are responsible for 22% of CO_2 emissions that significantly contribute to global warming [15] and that 15% of world's energy from fossil fuels is used to transport food under temperature-controlled conditions [16], identifying the sector as heavy energy consumer, especially in refrigerated transport applications, where additional energy is required to preserve the cold chain [14].

In such a scenario, the refrigerated road transport sector needs to develop and implement strategies and solutions to guarantee the correct preservation of the transported products quality along their Cold Chain, but at the same time to minimize its negative impacts on the environment. The overall environmental impact of a refrigeration system can be evaluated through the definition of the Total Equivalent Warming Impact (TEWI):

$$TEWI = (\alpha_{CO2} \cdot L \cdot E) + (x \cdot GWP) \tag{1.1}$$

As it can be observed from Eq. (1.1), two different contributions to the TEWI can be identified.

The first contribution represents the indirect emissions which characterize the refrigeration system during its operation, and it is evaluated as the product $(\alpha_{CO2} \cdot L \cdot E)$, in which the parameters represent the mass

of CO_2 emitted per unit of energy consumed during operation, the lifetime of the refrigeration system and the energy consumed in the time unit, respectively.

On the other hand, the second contribution represents the direct emissions linked to refrigerant mass leakages in the atmosphere, and it is evaluated as the product $(x \cdot GWP)$, in which the parameters represent the total mass of refrigerant leaked during the entire refrigeration unit lifetime and the global warming potential of the specific refrigerant compared to CO_2, respectively.

The indirect and the direct contribution to the overall environmental impact of the refrigerated road transport sector will be further discussed in the next sections.

1.1 Indirect emissions of road transport refrigeration systems

Current road transport refrigeration systems are mainly based on vapor compression cycle units [17] employing HFC (Hydrofluorocarbons) refrigerants such as R134a, R404A and R410A [18] [19].

Different types of vehicles are used for transport refrigeration applications, depending on the quantity of transported products and on the distance which needs to be covered during the transport operations. The vehicles employed in the refrigerated transport sector are typically classified as vans (40% of the total refrigerated vehicles in service worldwide), trucks (30%) and semi-trailers or trailers (30%) [18], with increasing dimensions, storage capacity and cooling power production capacity.

The most common drive systems for refrigerated transport vapor-compression systems are summarized in [17]. A direct belt drive is primarily used in small trucks and vans; in such a configuration, the compressor of the refrigeration unit is directly driven by the vehicle engine through a belt. A vehicle alternator unit is instead characterized by the connection of the vehicle engine shaft and a single alternator, which then charges the vehicle battery. An auxiliary alternator unit is defined in case of a dedicated large alternator, driven by a belt from the main traction engine, generating power to drive the electric motor in the refrigeration unit. Finally, the most popular solution for medium to large vehicles is an auxiliary diesel unit which drives the refrigerating system.

As it has been described in Eq. (1.1), indirect emissions of refrigeration systems are linked to the system operation, requiring an external energy source, and therefore to the emissions related to the production of the energy needed for the refrigeration system operation. Therefore, increasing the efficiency of refrigeration systems through the study of innovative solutions and of the system optimization would lead to a reduction of the electrical energy consumption of the cooling unit to provide a desired refrigerating effect and, consequently, to a reduction of the indirect environmental impact of the system. As mentioned above, in road transport cooling units the energy required for the cooling unit operation can not be supplied by the grid and, therefore, it has to be provided by the vehicle main engine (for small and middle-

sized vehicles) or by a dedicated diesel engine (for large trucks and semi-trailers). In both cases, the presence of the cooling unit requires additional operation of an internal combustion engine and, consequently, to additional emissions indirectly linked to the refrigeration system.

Literature review shows that different approaches have been adopted to evaluate the energetic and environmental impact of road transport refrigeration systems, falling under three general categories: numerical models based on parameters evaluation and optimization; experimental tests performed on existing equipment, without the development of an associated numerical model; instantaneous and unsteady numerical models accounting for the real-time behavior of the system, validated against experimental data.

With regards to the first approach, Tassou et al. [17] report that the fuel consumption of a transport refrigeration unit depends on several different circumstances (operating conditions, control strategy, transported products type, environmental conditions, vehicle type, fuel and engine characteristics). For dedicated engine diesel driven refrigeration, the authors account a fuel consumption (with an internal air temperature of 0°C) of 1.5 l/h for small-size refrigerated vans (under 6.5 m of length), 2.5 l/h for medium-size trucks (under 10.5 m of length) and 3.0 l/h for semi-trailers (above 13 m of length). The authors also state that multi-drop distribution will require a higher refrigeration capacity to counteract the infiltration load during door openings, leading to an average fuel consumption of the refrigeration units between 15% and 25% of the main engine fuel consumption, regardless of the vehicle type.

Wu et al. [14] presented a model to assess the carbon footprint of food transport refrigeration systems. The authors considered all the impacts on Green-House Gases (GHG) emissions of the cooling units and refrigerants during their production, transport, use, repair and recycling phases. The carbon footprint of three different refrigerants (R404A, R410A and R744) under various operating conditions was assessed, and the results showed that refrigeration systems employing R404A present the highest carbon footprint. Moreover, despite being characterized by the lowest Global Warming Potential (GWP), the use of R744 in refrigerated transport systems may lead to a higher carbon footprint compared with an R410A system in high environmental temperature operation due to a reduction in the cooling unit efficiency. The authors reported that 65-86% of the emissions related to the cooling unit comes from the energy consumption needed to power the unit and to carry the additional weight of the refrigeration system on the vehicle. Moreover, the results showed that using an auxiliary dedicated engine to power the cooling unit leads to higher CO_2 emissions compared with a unit directly driven by the vehicle engine or with an electrically powered unit.

Li [13] developed a numerical model based on the assessment of evaluation indexes to investigate the GHG emissions of a R452A food transport refrigeration system under various influencing factors during its entire life cycle. The cooling unit employing R452A is compared to a traditional R404A unit and results

show that the use of R452A can lead to a 5-15% emission reduction (accounting for both direct and indirect emissions). In addition, the author highlighted that the operating conditions highly influence emissions: a reduction of the external temperature from 32°C to 15.5°C can reduce up to 60% the emissions of fresh product transport, while an increase of the evaporating temperature set-point from -23°C to 10°C can lead to more than 80% emission reduction.

Stellingwerf et al. [6] proposed an optimization of the routing decisions during a delivery mission, through the development of a Load-Dependent Vehicle Routing Problem (LDVRP) model, with the purpose of reducing the fuel consumption and pollutant emissions in temperature-controlled road transportation. The refrigeration related emissions were included in the evaluation of the optimized routing decisions. Results showed that taking into account the emissions caused by refrigeration in road transportation can result in different optimal routes and speeds compared with the models determining the optimal routing decisions not accounting for refrigeration related emissions. In addition, numerical simulations evaluated that the emissions caused by refrigeration are responsible for around 40% of the total emissions from temperature-controlled transportation.

Barnitt et al. [20] performed experimental measures of emissions and fuel consumption of transport refrigeration units powered by a dedicated diesel internal combustion engine. Two different fuels (ultra-low sulfur diesel and gas-to-liquid diesel), two exhaust configurations (with stock muffler and with the addition of a particulate filter) and two engine operating speeds (1450 rev min^{-1} and 2200 rev min^{-1}) were considered in the tests. Test results indicated that gas-to-liquid diesel fuel reduces all the considered emissions (CO, CO_2, NO_x, THC, PM) regardless of the engine speed. Moreover, the results highlight that the employment of a diesel particulate filter reduces the emissions, in some cases almost entirely. Finally, operation with a simultaneous implementation of gas-to-liquid diesel and the particulate filter reduces the emissions at high engine speed; however, in this case an increase in NO_x at low engine speed was registered.

Lawton et al. [21] experimentally measured the emissions of a diesel engine powering a nose-mounted refrigeration unit serving a 13.6 m length semi-trailer used for multi-temperature (0°C and -20°C) transportation. Different temperature setpoints, operating conditions and varying internal load were considered during the tests. Experimental results highlighted that CO_2 emissions vary between 2 g/s and 3 g/s, NO_x emissions between 16 g/l and 22 g/l and PM emissions between 0.02 g/l and 0.04 g/l of diesel fuel, with external air temperature ranging between 10°C and 30°C. In addition, results highlighted that the auxiliary engine powering the refrigerating unit emits 25-66 times more NO_x than a Euro 6 truck engine, depending on the operating conditions.

Bagheri et al. [5] focused on the real-time performance of typical trailers used in food transportation industry through both a theoretical and an experimental approach. The studied cooling units were

powered by a dedicated diesel engine and served the cooling needs of large trailers. The authors developed a mathematical model to simulate the transient behavior of the cooling unit and to evaluate its thermal and performance characteristics. The model was then validated against experimental test data. The real-time COP of the refrigerated trailers varied in a range of 0.001-1.33 over the ON periods, highlighting a strong sensitivity of the refrigerating system to the operating conditions, while the average simulated COP of the trailers over the year was equal to 0.58. In addition, the authors estimated a fuel consumption of 3105 l of diesel per year to run the cooling unit, equivalent to a yearly emission of 8320 kg of CO_2. Finally, the authors suggested that this amount of yearly CO_2 emissions per truck-trailer could be reduced by replacing the engine-driven refrigerating unit with a battery-powered one.

Yang et al. [2] focused on the fuel consumption and on the pollutant emissions of refrigerated vehicles through the development of a dynamic numerical model to simulate the real-world emissions of refrigerated small trucks. The model was validated against data from experimental tests over a realistic driving profile (the London Drive Cycle). Numerical results show a 15% increase of the overall CO_2 emissions and a 18% increase of the NO_x emissions for the vans with refrigerating units, compared with standard equivalent vehicles dedicated to generic freight transport.

Considering the above-mentioned results available in literature, a preliminary evaluation of the indirect environmental impact of traditional transport refrigeration systems can be performed, to set a baseline value which will be further investigated in this thesis.

Using as a baseline reference the results presented in the above-mentioned studies available in literature, Bagheri et al. [5] report that a typical R404A refrigerated trailer (powered by a dedicated diesel engine) consumes around 3000 liters of diesel fuel per year. Assuming an emission factor of 2.578 kg of CO_2 emitted per liter of diesel fuel burnt [21] and a total service lifetime of 10 years, the indirect emissions of a standard transport refrigeration unit, representative of the current market, are equal to 77.3 t_{CO2}.

To further investigate the indirect environmental impact of road refrigerated transport systems and to fill the gap in the open literature, as most of the above-mentioned studies focused only on a part of the complete system (cooling unit or vehicle engine) while providing estimations for the remaining parts of the system, the first part of this thesis will focus on the development of a comprehensive dynamic numerical model, accounting for the dynamic behavior of the cooling unit, of the insulated box in which the products are stored and of the vehicle engine during a typical daily multi-drop delivery mission in urban environment. The impact of electrification on the reduction of the environmental impact of transport refrigeration systems will be presented, and the possible integration of a renewable energy source (solar energy) for sustainable production of the energy required by the cooling unit will be discussed.

1.2 Direct emissions of road transport refrigeration systems

As it has been described in Eq. (1.1), direct emissions of refrigeration systems depend on the leakage of the refrigerant to the environment due to piping imperfect seals, even accentuated by the vibrations linked to the vehicle motion which naturally characterize transport refrigeration systems.

Every refrigerant is characterized by a specific Global Warming Potential (GWP), which has been developed as a metric to compare the ability of 1 ton of a specific greenhouse gas to trap heat in the atmosphere, compared with 1 ton of the reference gas (CO_2) over a given time period, usually a 100-year averaging time [22].

As described in Section 1.1, current transport refrigeration systems mainly employ HFC refrigerants such as R134a, R404A and R410A [18] [19]. The GWP of these refrigerants is reported in Table 1.1.

Table 1.1 – Global Warming Potential of the most commonly used refrigerants in current road transport refrigeration applications. [23]

Refrigerant	Type	GWP 100
R134a	HFC	1300
R404A	HFC mixture	3260
R410A	HFC mixture	1720

Considering the high GWP of the most commonly used refrigerants in current road transport refrigeration, which implies a high negative direct environmental impact linked to the leakage of such gases, governmental agencies and policy makers are raising attention to the refrigerant choice and are setting new regulations to minimize the global warming.

In particular, to limit the use of the highly polluting refrigerants reported in Table 1.1 in the next years, the European Union approved the EU F-Gas Regulation 517/2014 [24], which will lead to a progressive phase out and to a following ban of the currently used synthetic refrigerants. An even stricter approach is now expected by the revision of the F-gas, which is currently on the way.

In this challenging scenario, new environmentally friendly refrigeration solutions based on the use of low-GWP refrigerants have to be studied and developed. The main possible alternatives to HFC refrigerants have been identified in HFO (Hydrofluoroolefins) refrigerants, HC (Hydrocarbons) refrigerants and natural refrigerants. The GWP of the refrigerants in these categories with the highest potential for HFC substitution is reported in Table 1.2.

Table 1.2 – Global Warming Potential of possible sustainable refrigerants for road transport refrigeration applications. [23]

Refrigerant	Type	GWP 100
R1234yf	HFO	<1
R290 (propane)	HC	3
R600a (isobutane)	HC	3
R717 (ammonia)	Natural refrigerant	0
R744 (CO_2)	Natural refrigerant	1

Considering the GWP of the environmentally sustainable refrigerants reported in Table 1.2 and the indicative value of indirect emissions calculated at the end of Section 1.1 (77.3 t_{CO2} for a standard R404A transport refrigeration system over a 10-year service lifetime), it is possible to evaluate the impact of the direct emissions on the total polluting emissions of a transport refrigeration unit. Considering an average annual refrigerant leakage value of 10% of the total refrigerant charge [17], the baseline R404A unit (charged with 7.3 kg of refrigerant, as reported in [5]) would produce direct emissions over the 10-year service lifetime equal to 23.8 t_{CO2}, which correspond to 30.8% of the indirect emissions of the cooling unit. The use of a natural refrigerant as R744 in the refrigeration unit allows to drastically reduce the direct emissions. Previous studies in literature report that, considering a fixed cooling power production with a R744 system instead of the traditional HFC system, the R744 charge would be 1.3-2.3 times the refrigerant charge of the HFC system [25, 26, 27]. Assuming conservatively a R744-HFC charge ratio equal to 2.3 kg_{R744}/kg_{HFC}, an equivalent R744 unit would be charged with 16.8 kg of R744 refrigerant, leading to a drop of the direct emissions over the same lifetime to only 0.02 t_{CO2}. Assuming the same COP of the cooling unit for both refrigerants in this simplified preliminary evaluation, the use of R744 refrigerant leads to a reduction of around -23.5% of the total direct + indirect emissions over the 10-year service lifetime of the refrigeration unit.

Moreover, it must be considered that transport emissions currently represent around 25% of the European Union's total greenhouse gas emissions [28]. For this reason, The European Commission adopted a set of proposals to make the EU's climate, energy, transport and taxation policies fit for reducing net greenhouse gas emissions by 55% by 2030: 30 million zero-emissions cars and 80 000 zero-emission lorries will be in operation and scheduled collective travel under 500 km should be carbon neutral within the EU by 2030, and zero-emission large aircraft will become ready for market by 2035 [29]. The final objective is to achieve a 90% reduction in transport-related greenhouse gas emissions by 2050 [28], through the use of sustainable energy sources (such as biofuels, hydrogen, e-fuels) or through electrification of the transport sector. In such a scenario, the emissions from the fossil fuels used in internal combustion engines of vehicles will be eliminated, increasing even more the influence of the

direct emissions linked to the type of refrigerant on the overall sustainability of the refrigerated transport sector.

The above-described considerations lead to the conclusion that the use of a low-GWP refrigerant can significantly reduce the negative environmental impact of transport refrigeration systems. Therefore, the most suitable refrigerant to be employed in this kind of applications has to be assessed.

The employment of HFO refrigerants as drop-in solution to HFC refrigerants has been extensively studied in recent years [30] [31]. The main field of application of pure HFO refrigerants in the road transport sector has been their utilization in mobile air conditioning systems, and several studies available in literature investigated the use of the HFO R1234yf refrigerant as a replacement for the HFC R134a refrigerant in this specific application [32] [33], as at present most of the newly sold cars in Europe are equipped with R1234yf refrigerant in their automotive air conditioning system [34]. R452A itself, which is used in transport refrigeration, is a mixture of HFC/HFO. However, additional environmental effects of HFOs, related to Trifluoroacetic Acid (TFA) and Polyfluoroalkyl Substances (PFAS), are still under evaluation [35] [36] and five European countries announced that they will soon (January 2023) submit a proposal to restrict all PFASs in the EU [37].

The use of ammonia as a refrigerant has been studied in recent years mainly regarding NH_3/CO_2 cascade refrigeration cycles [38] [39], absorption refrigeration cycles [40] [41] or heat pump applications [42] [43] [44]. Literature review shows that no studies regarding the application of ammonia as the refrigerant in transport refrigeration systems is available. In addition, the toxicity of ammonia even in very low concentrations in air and its capability to form a flammable mixture in air at 16 to 25% concentration by volume makes this fluid more challenging to utilize in refrigeration systems for transport applications.

Hydrocarbons are a group of fluids that are more and more looked upon as refrigerants for their ability to replace the environmental unfriendly HFCs [45] and their utilization has been studied in household [46] [47] or cold storage [48] air conditioning systems, as well as automotive air conditioning systems [49]. The most considered hydrocarbons to be used as refrigerants are R290 (propane), R600a (isobutane) and their mixtures [50] [51] [52] [53]. The possibility of employment of propane in transport refrigeration systems has been studied [54], and the first experimental systems have been recently tested [55]. However, all the hydrocarbon fluids are flammable and explosive, although in small systems the refrigerant charge is normally too low to form an explosive mixture with air in case of leakage. An updated regulation setting the standards for the use of mildly flammable and flammable refrigerants needs to be provided to regulate and allow the widespread use of hydrocarbons in refrigeration [56], as they are currently permitted for use only in limited amounts or only allowed when specific safety measures are implemented and verified [57].

Compared to all the low-GWP refrigerants above listed, CO_2 (R744) is the only refrigerant that is non-flammable, non-toxic, characterized by an ODP (Ozone Depletion Potential) equal to 0 and which can operate below 0°C. No other refrigerants can meet these properties simultaneously [58]. Furthermore, this refrigerant is inexpensive and, compared to HFCs, shows higher latent heat, specific heat, density and thermal conductivity and low viscosity [59].

Economic and technical aspects of CO_2 application provide the same positive perspective as the above-mentioned environmental factors and legal regulations. In fact, the thermodynamic properties of CO_2 lead to positive operating conditions in real cycles: lower pressure ratios than traditional halocarbons (and consequently, a higher efficiency of compressor operation); high volumetric refrigeration capacity and high heat transfer coefficients (providing for a lower specific volume, smaller size compressors and thus lower investment costs, and leading to smaller sizes of components and pipes); very low temperature drops with corresponding pressure drops (allowing designing smaller piping systems with higher velocities of flowing working fluids) [59]. Higher absolute pressure values than in classical units using R134a require higher design pressures, however design issues are mitigated by the smaller size of components.

On the other hand, CO_2 is characterized by a low critical temperature (30.9°C). This forces transcritical operation for adequate heat rejection to the ambient air in warm and hot climates. In addition, the transcritical operation leads to high expansion losses, which affect the Coefficient of Performance (COP) of the system in a negative way, making the technology sensitive to the discharge pressures at high ambient temperature [60] [61].

Starting from the early years [62], different cycle modifications have been proposed to improve the performances of the transcritical cycle [59]. After being proposed by Lorentzen in 1983 in a new arrangement [63], in recent years ejectors have been identified as simple and light devices to recover the expansion work in CO_2 transcritical cycles. In fact, the ejector partially utilizes the expansion work available when the high-pressure refrigerant is expanded in the motive nozzle of the ejector, reducing the compressor pressure ratio and thus the required compression work [64]. The use of ejectors looks particularly promising in commercial refrigeration [65].

The use of CO_2, according to transcritical cycles when required by the heat sink temperature, has been investigated and applied in many different fields. One of the most successful applications of transcritcal CO_2 cycles is commercial refrigeration: several reviews and research papers covering CO_2 refrigeration plants design and installations for food retail applications, focusing on the energetic, environmental and economic perspective, are available in literature [66] [25] [67] [68] [69]. In addition to the wide application of such a technology in commercial refrigeration sector, a systematic and comprehensive description of novel improvement technologies for transcritical CO_2 cycles can be found in [70] [71].

Although the use of CO_2 has been assessed as the standard option for new supermarket and commercial refrigeration integrated systems installations, and it is spreading in other applications, like water chillers or marine refrigeration, literature review shows that it is possible to find very few studies on numerical or experimental evaluations of a CO_2 refrigerating systems in road refrigerated transport applications.

Barta et al. [72] presented an in-depth review of the state-of-the-art in stationary and transport CO_2 refrigeration and air conditioning technologies. The Authors reported several studies regarding transcritical CO_2 transportation applications, which however largely fall into two main topics: automotive air-conditioning (AC) systems and cooling of shipping containers. No examples of research in CO_2 refrigerated truck applications are reported in the review.

Lawrence et al. [73] developed a numerical model, using the software Engineering Equation Solver, to predict the performance of a transcritical CO_2, multi-temperature, mobile refrigerated container system with ejector technology. The system performance was simulated at very harsh working conditions (ambient temperature of 57°C and -20°C for the lower temperature evaporator air). The numerical model was first utilized to compare the performance of a conventional direct expansion booster cycle in case of microchannel finned coil heat exchangers and in case of all round-tube plate fins heat exchangers, highlighting a 6.2% COP increase in the case of microchannel heat exchangers. In addition, the performance of the system utilizing an internal heat exchanger and a two-phase ejector was simulated, finding a 68.6% improvement in COP compared to a classical direct expansion cycle operating at the same environmental conditions.

The same authors [74] presented the design of a similar multi-evaporation temperature refrigerated container using CO_2 as the refrigerant, focusing on cycle architecture and component selection. The mobile refrigerated container system prototype was experimentally tested in steady state conditions, providing medium-temperature (MT) refrigeration at 3°C and low-temperature (LT) refrigeration at -20°C with external ambient conditions varying between 25°C and 50°C. The experimental results showed that as ambient temperature increases from 25°C to 50°C, MT cooling capacity ranges from 3.6 to 2.3 kW, LT cooling capacity ranges from 5.1 to 3.4 kW, and unit COP ranges from 1.48 to 0.75. A performance comparison between the tested CO_2 system and a baseline R404A mobile container unit was then conducted according to literature data, showing a good competitiveness of the CO_2 system compared to existing HFC system containers.

In another assessment of a similar two-evaporator, multi-stage transcritical CO_2 transportation refrigeration system, Barta et al. [75] assessed the effects of varying ambient temperature and flash tank pressure relative to evaporation pressure on compressor suction superheat, flash tank liquid level, and system COP. Results highlighted that the system COP is maximized for a given ambient condition when the flash tank is as close to the evaporation pressure as possible due to the presence of an expander.

However, at this flash tank pressure compressor superheat could become dangerously low, suggesting that a pressure differential should be retained, maintaining at the same time the liquid level in the flash tank at a high-enough level to not risk starving the tank of liquid.

Bodys et al. [76] implemented a numerical model, using the software Engineering Equation Solver, to investigate the effects of different possible cycle modifications to a baseline CO_2 refrigeration unit installed in a fishing vessel operating under Scandinavian conditions. The baseline case with a liquid ejector designed for Scandinavian conditions was simulated on the basis of a developed mathematical model and measurement data from an actual working installation. The energy demands of the refrigeration unit were assessed with heat sink temperatures of 21°C and 33°C, characteristic of the Mediterranean Sea and the waters of East Asia, respectively. To investigate system performance under high ambient conditions, the developed baseline model was modified by introducing an intermediate pressure receiver and parallel compression of the flash gas. Moreover, an additional model of a multi-ejector system was developed and simulated as well. In the case of the most advanced installation in warm East-Asian waters conditions (layout with three parallel compressors, high efficiency multi-ejector module and optimization of the pressure level of the intermediate pressure receiver) numerical simulations showed an increment of available evaporator load of 67% compared with the baseline refrigeration cycle.

Considering the same application, Söylemez et al. [77] presented a complete overview of the development and the currents status of CO_2 refrigeration systems utilized onboard fishing vessels, highlighting that this kind of systems can be employed in CO_2-only solutions, operating in low seawater temperature conditions, eventually including freezing functions, or in ammonia-CO_2 cascade systems, when additional freezing capacity is needed in vessels operating in higher seawater temperature conditions. The Authors reported that more than 50 CO_2-only cooling units have been installed on fishing vessels operating in cold-climate countries since 2016. However, for a wider application in hot climates, component-based improvements have to be carried out, and the number of energy efficient solutions needs to be further increased.

All the above-mentioned studies, however, are referred to refrigerated containers and fishing vessels applications, showing a lack of recent studies related to CO_2 refrigeration systems to be employed in road transport applications. One of the first studies related to CO_2 refrigerated vehicles purposes was published by Artuso et al. [78], where the Authors presented a numerical model of a new CO_2 vapor-compression system for refrigerated transport applications, comparing the performance of the cooling unit in three different configurations: the standard back-pressure with low-pressure receiver layout and two arrangements integrating a two-phase ejector. The performance of the system under different ambient and internal space temperatures are simulated with a numerical model developed with the commercial

software Simcenter Amesim v.17. Numerical results show that the ejector cycle configuration is convenient when the system is operating in a hot climate with a maximum COP increase (compared to the standard back-pressure configuration) equal to 15.9%, at 42°C ambient temperature and -5°C internal space temperature. The use of an auxiliary evaporator can extend the operating range of the ejector to lower values of ambient temperature, with a maximum COP improvement (over the standard back-pressure configuration) equal to 21.0% at 25°C ambient temperature and 5°C internal cargo space.

Following the approach presented by Artuso et al. [78], the second part of this thesis will focus on the development of a detailed dynamic numerical model of a R744 cooling unit, accounting for the dynamic behavior of the cooling unit and of the insulated box in which the products are stored during a typical daily multi-drop delivery mission in urban and extra-urban environment. Since the cooling unit design allows operation in multiple configurations, a control strategy to select the optimal configuration during operation will be developed. The yearly performance of the refrigeration system will be assessed, and the installation, setup and first experimental tests of the cooling unit prototype will be described. To fulfill the requirements of the current transport refrigeration market, which is focusing more and more on multi-temperature solutions, new R744 multi-temperature unit designs will be discussed, supported by the results of an experimental campaign conduced on a R744 ejector employed in low-temperature suction conditions.

2. Numerical modelling of the environmental impact of a traditional R134a transport refrigeration unit and evaluation of the improvements linked to electrification

As a first step in the evaluation of possible solutions to improve the environmental sustainability of the refrigerated transport sector, reduction of indirect GHG emissions through the improvement of the efficiency of current transport refrigeration systems needs to be addressed. In fact, an improvement of the performance of cooling systems would lead to a reduction of the energy requirement to obtain a desired cooling effect, thus reducing the GHG emissions related to the production of the energy source.

Traditionally, refrigerating systems employed in current temperature-controlled logistics rely on the use of HFC refrigerants such as R134a, R404A and R410A [17]. Moreover, for the vast majority of small to medium-size vans used for deliveries in urban environment, the cooling unit compressor is directly driven from the vehicle engine through a belt [17].

In this chapter, the numerical model of a R134a cooling unit serving the needs of a small refrigerated van in an urban delivery mission of perishable goods is developed, to represent the baseline technology in current refrigerated transport sector. The fuel consumption and the main pollutant emissions of the vehicle engine are also included in the model, to evaluate the impact of the cooling unit operation on the environment. Different connections between the vehicle engine and the cooling unit compressor are considered, as well as operation in different environmental temperature conditions.

Moreover, the implementation of a solar-aided refrigeration unit with the addition of photovoltaic panels on the roof of the insulated box of the vehicle is modelled, to assess the performance improvement of the system linked to the exploitation of the renewable solar source.

2.1 Refrigerating system description

The system considered for the numerical analysis of the baseline performance and environmental impact of current transport refrigeration units consists of a medium-size van, used for the urban delivery of temperature-sensitive goods, equipped with an insulated body that is kept under desired temperature conditions through the action of a cooling unit. The simplified schematic of the whole system is presented in Figure 2.1.

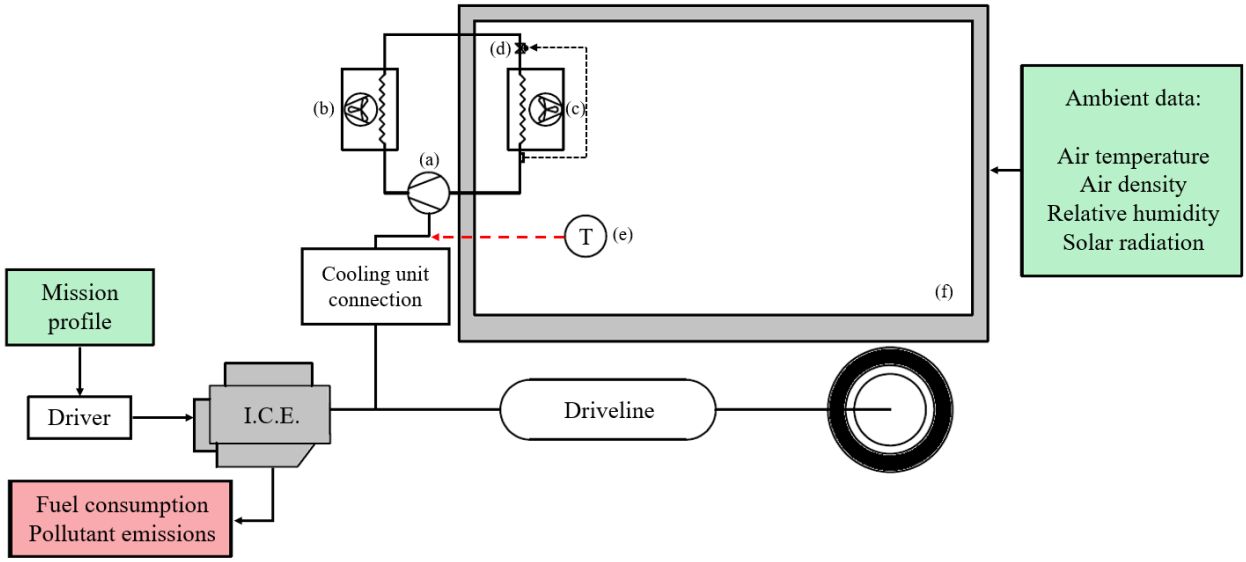

(a) Semi-hermetic compressor	(b) Condenser	(c) Evaporator
(d) Thermostatic expansion valve	(e) Thermostat	(f) Insulated body

Figure 2.1 – Simplified schematic of the modelled system.

The refrigerated truck presented in the figure above is employed for the numerical simulation of a daily multi-drop delivery mission of perishable products.

The mission profile (defined through the definition of the instantaneous vehicle target speed, the opening of the insulated box doors and the remaining fraction of the perishable goods inside the insulated box) is provided as an input of the model, as it will be described in detail in Section 2.3. The instantaneous environmental conditions, continuously changing throughout the day, are also provided as an input.

The numerical model of a driver control constantly checks the mission requirements regarding the truck motion and acts on the vehicle engine through acceleration, brake and gearbox-clutch controls to match the target speed profile. The Internal Combustion Engine (ICE), under the dynamic control of the driver model, produces the mechanical power required for both the motion of the truck and the cooling unit power supply. The transmission of mechanical power along the vehicle driveline is considered.

Depending on the ICE operating points along the mission, which are continuously changing to match the mission profile and the refrigeration needs requirements, the real-time fuel consumption and pollutant emissions of the engine are calculated by the model, thus allowing a direct evaluation of the impact of the presence of the cooling unit on the engine performance.

The cooling unit function is to keep the internal air temperature of the insulated box where the perishable goods to be delivered are loaded in a desired range, corresponding to the optimal storage conditions which can preserve the goods quality and safety requirements. To do so, a thermostat control turns ON

or OFF the cooling unit's compressor in order to maintain the internal air temperature between -1°C and 3°C.

Given the environmental conditions throughout the day, the conduction through the box walls, the internal and external convection, the solar radiation, the hot environmental air infiltration during door openings and the cooling effect coming from the refrigerating unit are considered for the instant energy balance inside the insulated box.

To assess the impact of the cooling unit power supply arrangement on the thermal and environmental performance of the system, three different connections of the cooling unit to the power line coming from the vehicle engine will be considered, whose simplified schematics are reported in Figure 2.2.

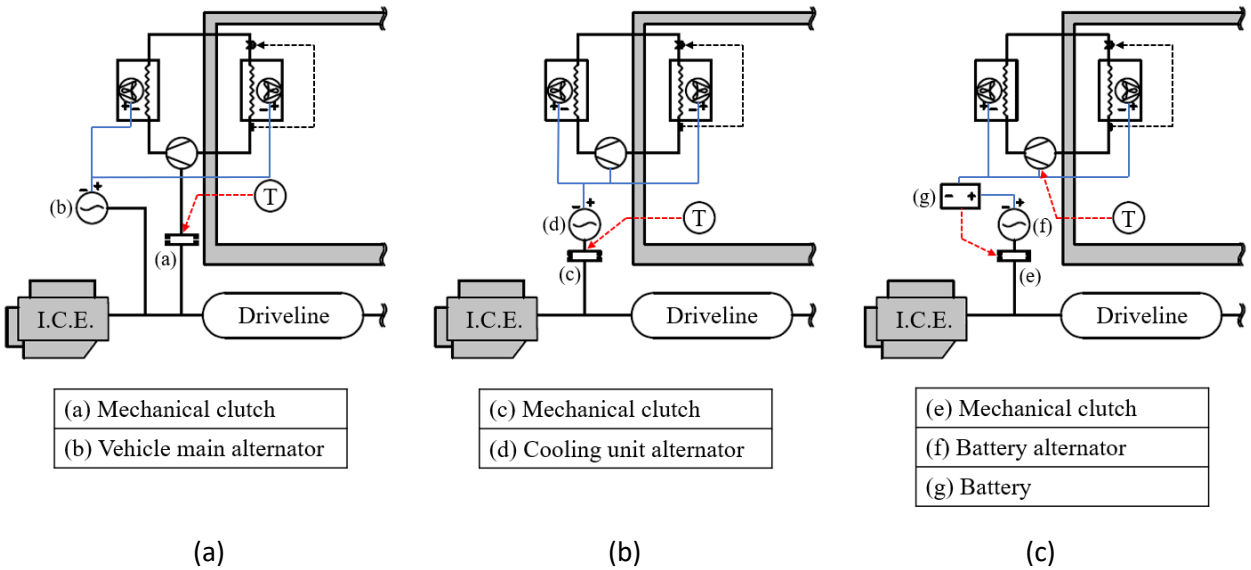

Figure 2.2 – Simplified schematics of the cooling unit's connection to the vehicle engine: (a) by means of a belt (BELT-CONF); (b) through an alternator (ALT-CONF); (c) through an alternator and a battery for energy storage (BAT-CONF).

In the first arrangement (Figure 2.2a), the cooling unit's compressor is directly driven by the vehicle engine by means of a belt, while the vehicle main alternator powers the heat exchangers fans. In this configuration, which will be referred to as BELT-CONF, the rotational speed of the cooling unit's compressor, during ON periods, is strictly tied to the vehicle engine rotational speed, meaning that the cooling capacity provided by the unit and the actual cooling demand of the insulated box are not necessarily coincident.

Conversely, in the second arrangement (Figure 2.2b) an alternator converts the mechanical power coming from the vehicle engine to the electrical power needed to feed both the cooling unit's compressor and the heat exchangers fans. In this configuration, which will be referred to as ALT-CONF, the compressor rotational speed and the vehicle engine rotational speed are decoupled. With such an arrangement, a

variable speed control of the compressor is allowed, leading to a consequent optimization of the cooling unit's performance according to the actual cooling demand of the insulated box.

Finally, in the third arrangement (Figure 2.2c) the mechanical energy coming from the vehicle engine is converted to electrical energy by an alternator and it is stored inside a battery, which then feeds the unit's compressor and the heat exchangers fans. In this configuration, which will be referred to as BAT-CONF, the power production by the vehicle engine and the power supply to the cooling unit are decoupled: the vehicle engine additional power production depends only on the charge level of the battery, which must be kept in conditions to provide the required power to the cooling unit. Such a solution allows both the optimization of the cooling unit's performance, matching the cooling demand of the insulated box and the unit's cooling capacity, and the optimization of the vehicle engine fuel consumption and pollutant emissions. In fact, the presence of the battery allows to keep the engine OFF during the pre-cooling activity which precedes the delivery mission and during long pauses and to perform a Start&Stop management of the engine during the urban drive, switching off the engine when the vehicle is still but yet ensuring the necessary power supply to the cooling unit, if needed.

2.2 Numerical model description

A dynamic numerical model of the refrigerated van is developed using the commercial multi-physics software Simcenter Amesim v.17. The numerical approach of the software is based on the discretization of real components in lumped parameters elements, connected to describe the entire system. Each element is described by nonlinear time-dependent differential equations involving the state variables. Equations are then assembled in a system of differential equations, according to the elements connection. The model dynamic is then solved by integrating the system of differential equations over time. This approach allows to solve fast dynamics without the limiting assumptions of the quasi-stationary formulation. The numerical solver adapts the integrating time step at every solving iteration, reducing it to increase the precision in correspondence of highly unsteady operation. A mixed (absolute and relative) residual error estimator is used to check the convergence at each time step. A more detailed description of the numerical solver of the software will be provided in Section 2.2.5.

The libraries of the software are composed of basic elements designed to model the dynamic behavior of the cooling unit, as well as the thermal dynamic response of the insulated cargo space, the transmission of mechanical power through driveline, the vehicle mechanical equilibrium during motion and its driving control to accurately follow the mission profile.

The numerical model of the elements of which the system consists of will be described in detail in the next sections.

2.2.1 Vehicle numerical model

The main focus of this chapter is to discuss the impact of the cooling unit on the whole vehicle energetic balance and not to reproduce in detail the mechanical components of the vehicle engine and driveline singularly. For this reason, the vehicle model was focused on the macroscopic physics involved, neglecting detailed component dynamics. The main truck geometries and layout are taken from the technical sheet of a typical light truck [79], and they are displayed in Figure 2.3.

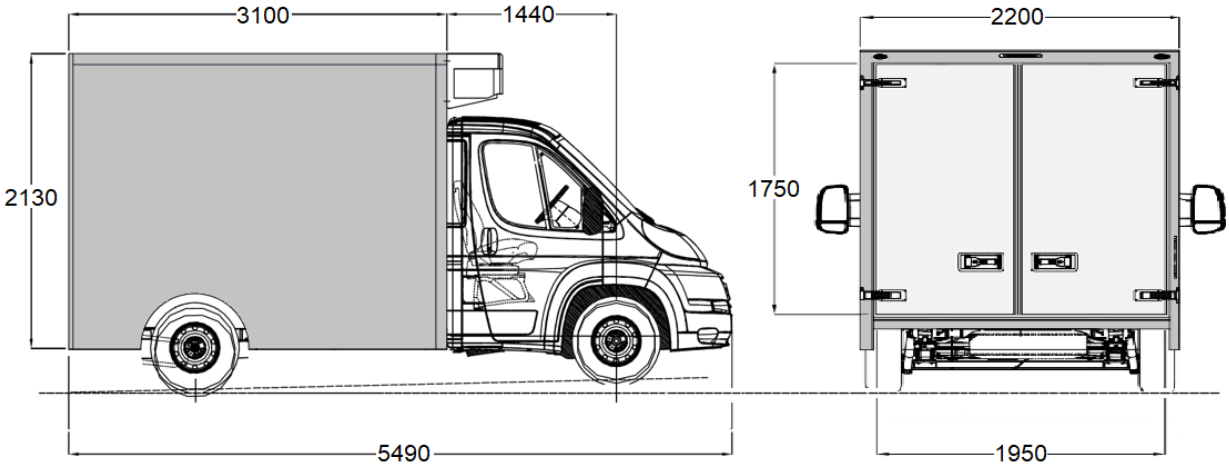

Figure 2.3 – Main dimensions (in mm) of the modelled van and insulated cargo space.

The vehicle is modelled as a translating mass. The assumptions of no slip between the tires and the ground, no climbing resistance due to road slope and absence of wind are made. Rolling friction and aerodynamic drag are taken into account as follows:

$$F_{drag} = \frac{1}{2}\,\rho_a\,A_{front}\,C_x\,{v_{truck}}^2 \tag{2.1}$$

$$F_{fric} = \mu_{fric}\,(m_{truck} + m_{goods})\,g \tag{2.2}$$

in which: ρ_a is the air density, A_{front} is the vehicle frontal area, C_x represents the air penetration coefficient and v_{truck} is the linear speed of the vehicle; μ_{fric} represents the Coulomb friction coefficient of the wheels on the road and $(m_{truck} + m_{goods})$ is the sum of the truck mass and the transported goods.

A six-ratio manual gearbox, characterized by the gear ratios reported in Table 2.1, was used as a driveline, assuming an efficiency of $\eta_{gearbox}$ = 0.9. The clutch which transmits the mechanical torque produced by the engine to the vehicle shaft is computed through the Coulomb frictional clutch model of the mechanical library of the software [80].

Table 2.1 - Gear ratios characterizing the manual gearbox of the vehicle [79].

Gear	Transmission gear ratio
1	1:3.727
2	1:1.952
3	1:1.290
4	1:0.875
5	1:0.673
6	1:0.585

The vehicle engine considered for this study is a 4 cylinders Euro4 turbo diesel 1.9L internal combustion engine, which is characterized by a total cylinder volume of 2287 cm^3, a maximum mechanical power of 108.5 kW ($P_{eng,max}$ at 4000 rev min^{-1}) and a maximum transmitted torque of 330.3 Nm ($M_{eng,max}$ at 2000 rev min^{-1}).

The engine mechanical power production and emissions are obtained through interpolation of the corresponding experimental bench test measurements of torque, fuel consumption and pollutant emissions reported in [81]. Figure 2.4 reports the interpolated map of the experimental data reported in [81]: fuel consumption (Figure 2.4a) and pollutant emissions, namely carbon monoxide (CO, Figure 2.4b), nitrogen oxides (NO_x, Figure 2.4c), total hydrocarbon (THC, Figure 2.4d) and particulate matter (PM, Figure 2.4e).

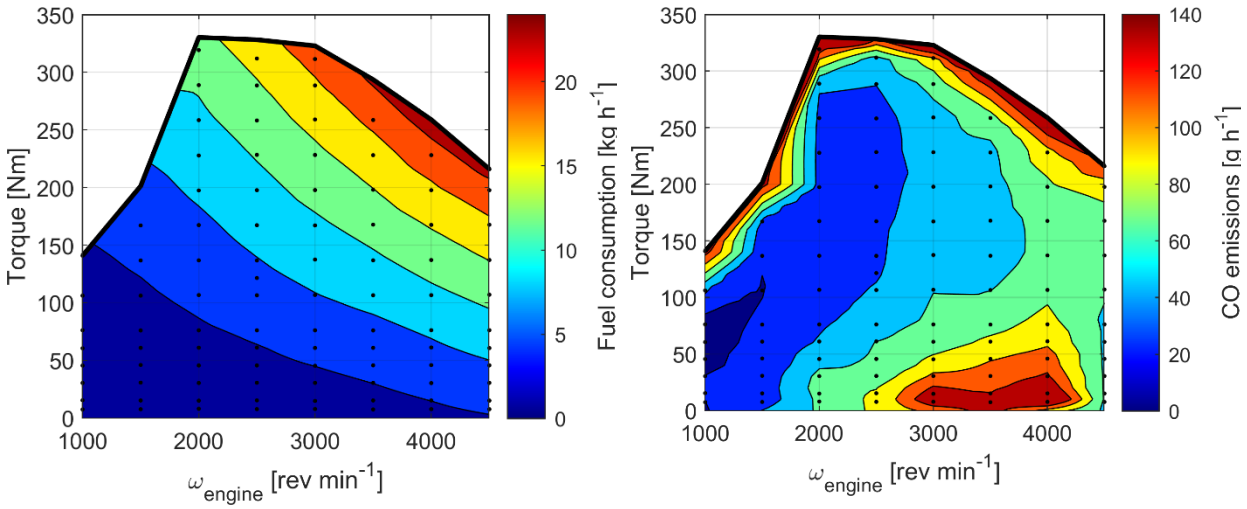

(a) (b)

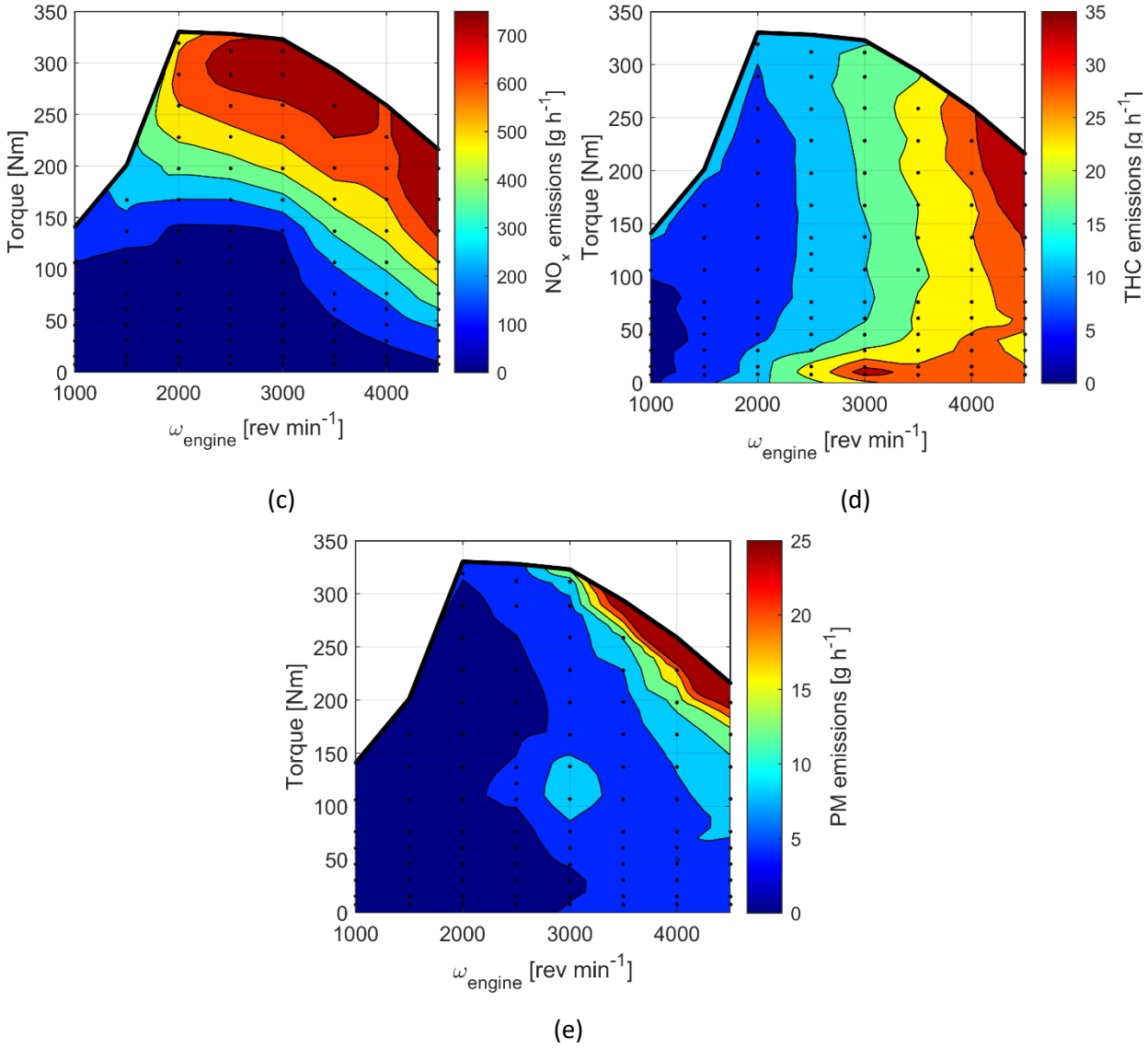

Figure 2.4 – Experimental data and interpolated map of the engine fuel consumption and of the pollutant emissions as a function of the engine torque and rotational speed: (a) fuel consumption; (b) CO emissions; (c) NO_x emissions; (d) THC emissions; (e) PM emissions.

The engine is supposed to be controlled by a Start&Stop control system that shuts down the engine during the vehicle stops. Some of the studied arrangements (BELT-CONF and ALT-CONF), will overwrite this feature, in order to allow the vehicle engine to provide the power required by the cooling unit even when the vehicle is still. With these configurations, the engine will be maintained at idle speed (1000 rev min^{-1}) during stops.

A Proportional-Integral (PI) controller is used to simulate the driver, based on the error between the target velocity and the vehicle actual velocity:

$$e_{speed} = v_{target} - v_{truck} \tag{2.3}$$

An open loop forward control is also implemented to increase the driver reactivity to the sudden velocity changes of the mission, including a derivative term computed on the target velocity. The driver output signal s is then computed as follows:

$$s = G_P\, e_{speed} + G_I \int e_{speed}\, dt + G_D\, \frac{dv_{target}}{dt} \tag{2.4}$$

Two different sets of parameters G_P, G_I, G_D are defined for the accelerator (a) and the breaking (b) signals. The accelerator signal and the braking signal are both limited in the range 0..1 and are used to compute the instant torque delivered by the engine or applied to the vehicle brakes, based on the maximum allowable values:

$$M_{eng} = a\, M_{eng,max}(\omega_{eng}) \tag{2.5}$$

$$M_{bra} = b\, M_{bra,max} \tag{2.6}$$

The gear to be engaged is controlled through the definition of the downshift engine rotary velocity $\omega_{eng,min}$ = 1100 rpm and the upshift engine rotary velocity $\omega_{eng,max}$ = 3000 rpm. When $\omega_{eng} > \omega_{eng,max}$, a higher gear is selected; when $\omega_{eng} < \omega_{eng,min}$, a lower gear is selected. When shifting from a gear ratio to another, the time needed for disengaging the clutch ($\Delta t_{clutch\ OFF}$ = 0.5 s), the time needed for engaging a gearbox ratio (Δt_{gear} = 0.5 s) and the time needed for re-engaging the clutch ($\Delta t_{clutch\ ON}$ = 1 s) are considered, so that a total delay of $\Delta t_{shift} = \Delta t_{clutch\ OFF} + \Delta t_{gear} + \Delta t_{clutch\ ON}$ = 2 s is forced between two gearshifts.

2.2.2 Refrigerated box numerical model

An insulated body with an internal volume of 11.89 m^3 is employed to store the perishable cargo to be transported by the truck. As traditionally realized in the market, the insulated box construction consists of polyurethane foam walls, sandwiched between layers of fiberglass and reinforced with metallic and wooden components, and with the addition of a plywood plate on the floor for supplementary mechanical resistance. Additional wooden and metallic structural components are also used to obtain the requested sturdiness of the walls [12]. Table 2.2 reports the main external dimensions, as well as the total internal and external surface that account for the six walls of the insulated body.

Table 2.2 – Main geometrical dimensions of the insulated body.

Element	Dimension
External height H_e	2.13 m
External length L_e	3.10 m
External width W_e	2.20 m
External surface S_e	36.22 m^2
Internal surface S_i	31.77 m^2
Internal volume V_i	11.89 m^3

The global heat transfer coefficient was evaluated through steady state experimental tests, carried out following the procedure defined in Annex 1 of the ATP agreement [82]. A representative scheme of test station and insulated truck body during a typical test, as well as a comprehensive description of the testing method, is provided in [12]. A global heat transfer coefficient K = 0.36 W m^{-2} K^{-1} was evaluated from the test: according to the ATP standards body types (IR classification), the considered refrigerated truck body as heavily insulated (K < 0.40 W m^{-2} K^{-1}).

The refrigerated box thermal characterization is modelled using a network of lumped models describing the insulated structure capacity and thermal resistance as well as the heat exchanges between the box and both the internal and external ambient conditions. It was demonstrated by Artuso et al. [12] that the whole insulated box can be modelled as a 0-D model defined by a series of 11 resistances ($R_0, \dots, R_{10}$) and 12 capacities ($C_0, \dots, C_{11}$). The extreme nodes of this series represent the internal and external average surface temperature of the box.

The capacity and resistive parameters of the box (C_i and R_i, respectively) are optimized to fit experimental data in steady state and under dynamic conditions.

A thermal-electric circuit analogy is used to model and solve the thermal equilibrium of the refrigerated box, referring to the schematic reported in Figure 2.5. This approach was originally presented by Artuso et al. [12] and it is here reported for the sake of completeness of the numerical model used for the simulations.

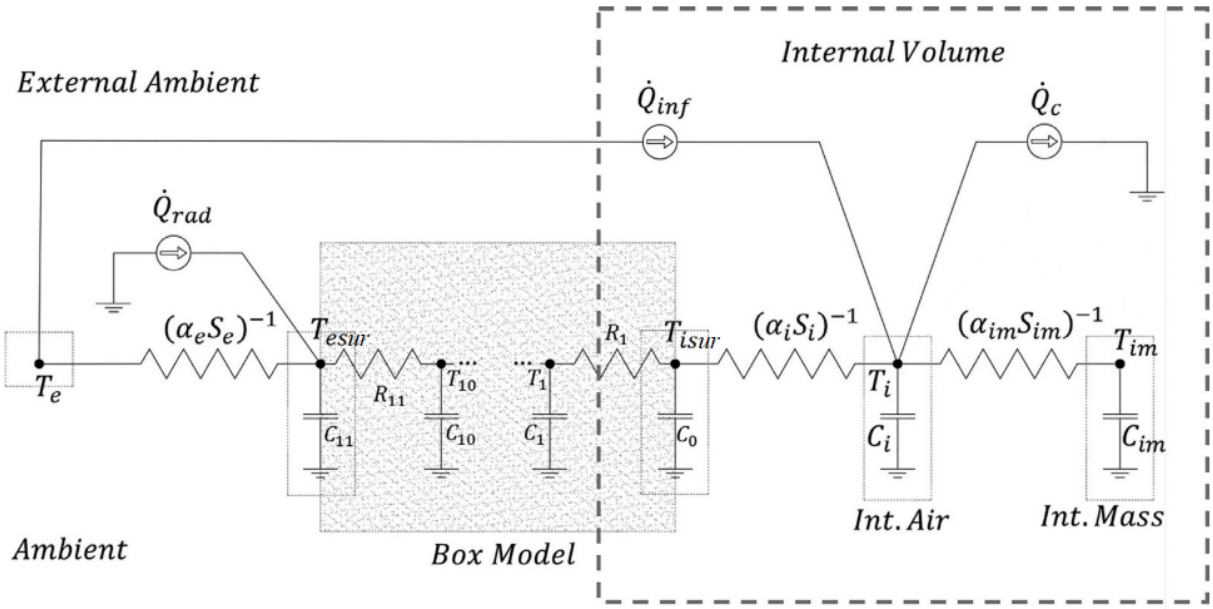

Figure 2.5 – Thermo-electric circuit analogy of the insulated body model, with internal and external elements [12].

The equations below describe the transient heat balance of the numerical model of the insulated box, which provides the mean temperature of the system components.

$$C_i \frac{dT_i}{dt} = -\dot{Q}_c + \alpha_i S_i (T_{isur} - T_i) + \alpha_{im} S_{im} (T_{im} - T_i) + \dot{Q}_{inf} \quad (2.7)$$

$$C_0 \frac{dT_{isur}}{dt} = \alpha_i S_i (T_i - T_{isur}) + \frac{1}{R_1} (T_1 - T_{isur}) \quad (2.8)$$

$$C_j \frac{dT_j}{dt} = \frac{1}{R_{j+1}} \left(T_{j+1} - T_j\right) + \frac{1}{R_j} \left(T_{j-1} - T_j\right) \ , \ j = 1, \dots, 10; \text{ with } T_0 = T_{isur} \text{ and } T_{11} = T_{esur} \quad (2.9)$$

$$C_{11} \frac{dT_{esur}}{dt} = \frac{1}{R_{11}} (T_{esur} - T_{10}) + \alpha_e S_e (T_{amb} - T_{esur}) + \dot{Q}_{rad} \quad (2.10)$$

$$C_{im} \frac{dT_{im}}{dt} = \alpha_{im} S_{im} (T_i - T_{im}) \quad (2.11)$$

The internal air volume transient heat balance is provided in Eq. (2.7). It is influenced by the cooling power provided by the refrigeration unit, by the convection with the internal wall temperature and with the perishable goods located inside the cargo space during the mission, and by the infiltration load given by the leakage of outside air into the insulated body during the opening of the vehicle's doors (modelled according to the study of Lafaye De Micheaux et al. [83]) or due to the imperfect seal of the doors during operation.

Eq. (2.9) describes the insulated box walls conductive model, as T_0 and T_{11} represent the internal and external mean surface temperatures.

Eq. (2.8) and Eq. (2.10) provide the internal and external surface heat balance, respectively. The net solar gain which influences the external surface is given by different contributions: the direct solar radiation, the diffusive incident solar radiation, the radiation heat exchanged between the surface and the sky and between the surface and the ground, referring to the six external surfaces and their respective orientation.

Eq. (2.11) describes the heat balance between the perishable cargo and the internal air.

A detailed description of the convective heat transfer coefficients used in the model, the complete formulation of the net solar gain and the validation of the modelling strategy are provided in [12].

2.2.3 Cooling unit numerical model

A basic R134a vapor compression unit is considered for the model presented in this chapter. The unit is charged with a total refrigerant mass equal to 2 kg of R134a, as common practice for refrigerated vehicles of similar size [17]. The modelled refrigeration unit provides a nominal cooling power of 3.3 kW, at the reference condition of T_i = 0°C and T_{amb} = 30°C and with compressor reference speed of 1450 rev min^{-1}. The performance maps of the cooling unit, working at full load and at reference speed in different operating conditions are reported in Figure 2.6, while the geometric dimensions of the main components

of the system, which are chosen among real components available in the market, are reported in Table 2.3.

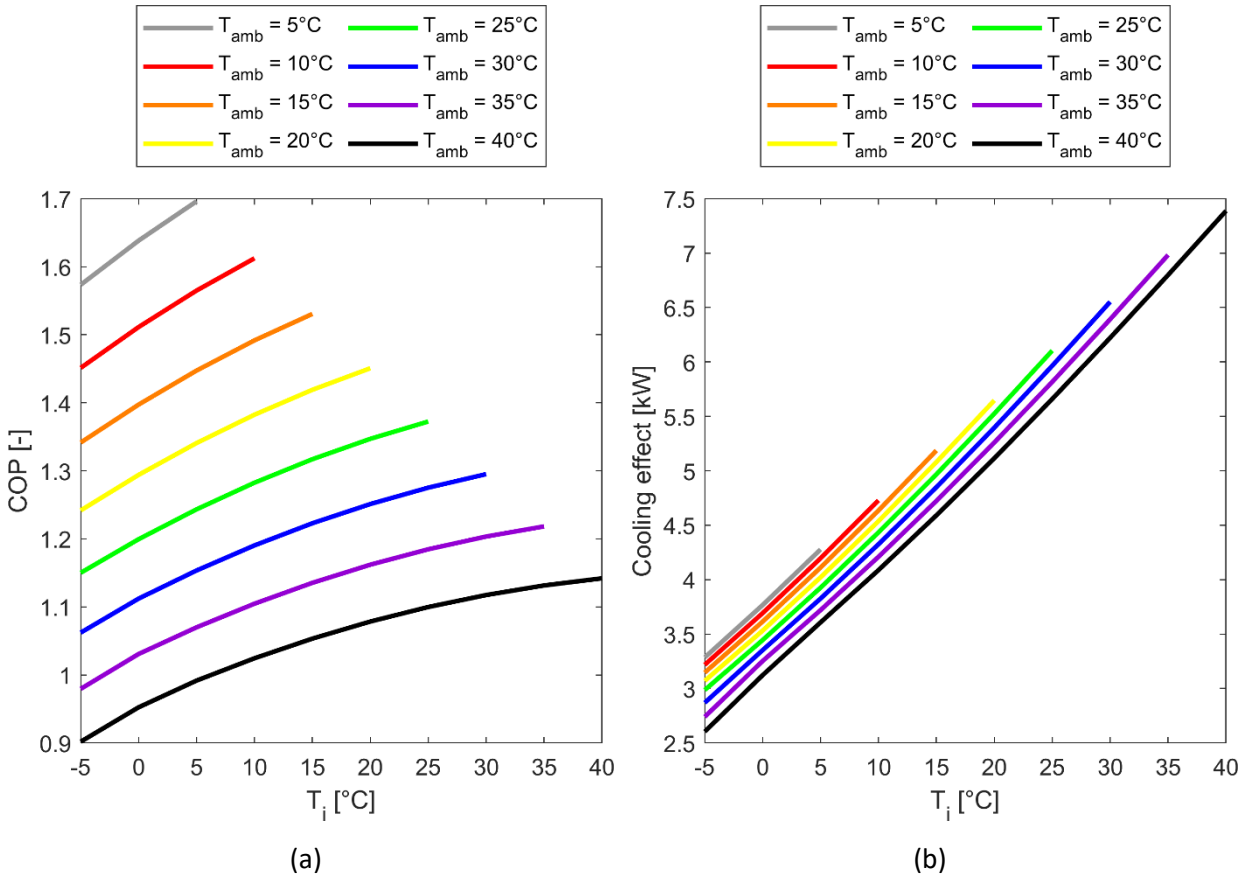

Figure 2.6 – Cooling unit performance at ω_{comp} = 1450 rev min^{-1}: (a) full-load COP; (b) cooling capacity.

Table 2.3 – Geometric dimensions of the main components of the cooling unit.

Component	**Geometric dimensions**
Compressor	Displacement, V_d = 400 cm^3
Condenser	External convective surface, $A_{e,cond}$ = 7.5 m^2
Evaporator	External convective surface, $A_{e,evap}$ = 8.9 m^2

The cooling unit is controlled by an ON/OFF thermostat with a 4°C hysteresis, to maintain the internal volume air temperature T_i between -1°C and 3°C.

As extensively described in Artuso et al. [78], the numerical model of the cooling unit is developed under the assumptions of homogeneous fluid model for the refrigerant, considering the two phases (liquid and vapor) to flow as a single phase characterized by mean fluid properties and with no slip and thermodynamic equilibrium between the two phases. The internal flow (refrigerant side) is considered one-dimensional, while the external flow (air side) is considered zero-dimensional. Moreover, the effect of gravity and the pressure losses along the pipes are neglected, since the assumption of short pipes is made, consistently with the unit's compactness. The thermodynamic properties of the R134a refrigerant

are evaluated through the Modified Benedict Webb Rubin (MBWR) equation [84], considering the pressure as a function of the fluid density and temperature.

The cooling unit is composed of a semi-hermetic compressor, a finned-coil condenser, a thermostatic expansion valve and a finned-coil evaporator.

2.2.3.1 Compressor

The semi-hermetic compressor utilized in the cooling unit modelled in this chapter was selected among the alternatives available in the market: in particular, a compressor specifically realized for transport applications was chosen [85], which can guarantee operation over a wide range of rotational speed (from 500 rev min^{-1} to 3500 rev min^{-1}). This choice was made following the current market's main technology, as it is reported in literature that in the majority of the van size vehicles utilized in transport refrigeration applications the cooling unit's compressor is directly driven by the vehicle engine [17].

The compressor was modelled using a fixed displacement (equal to V_d = 400 cm^3) compressor model. From the compressor operating data available in the data sheet provided by the manufacturer, the volumetric efficiency η_{vol} map and the overall compression efficiency η_{comp} map are interpolated as a function of the pressure ratio r_p and the rotational speed ω_{comp}. The overall compression efficiency η_{comp} is then conventionally divided into the mechanical efficiency η_{mec} (including the electrical one) and the isentropic efficiency η_{is}, including also heat dispersion through the compressor body.

Given the state of the refrigerant at the inlet and the discharge pressure, the compressor model calculates the mass-flowrate $\dot{m}_r$ developed (Eq. (2.12)), the electric power draw P_{comp} (Eq. (2.13)) and the state of the refrigerant (outlet enthalpy, Eq. (2.14)) at the outlet.

$$\dot{m}_r = \rho_{IN} \frac{\omega_{comp}}{60} V_d \eta_{vol} \tag{2.12}$$

$$P_{comp} = \frac{\dot{m}_r \Delta h_{is}}{\eta_{comp}} = \frac{\dot{m}_r \, \Delta h_{is}}{\eta_{mec} \eta_{is}} \tag{2.13}$$

$$h_{OUT} = \frac{\Delta h_{is}}{\eta_{is}} + h_{IN} \tag{2.14}$$

The compressor total efficiency, calculated as $\eta_{TOT} = \eta_{mec} \, \eta_{vol} \, \eta_{is}$, is presented in Figure 4 as a function of the pressure ratio r_p and of the rotational speed ω_{comp}.

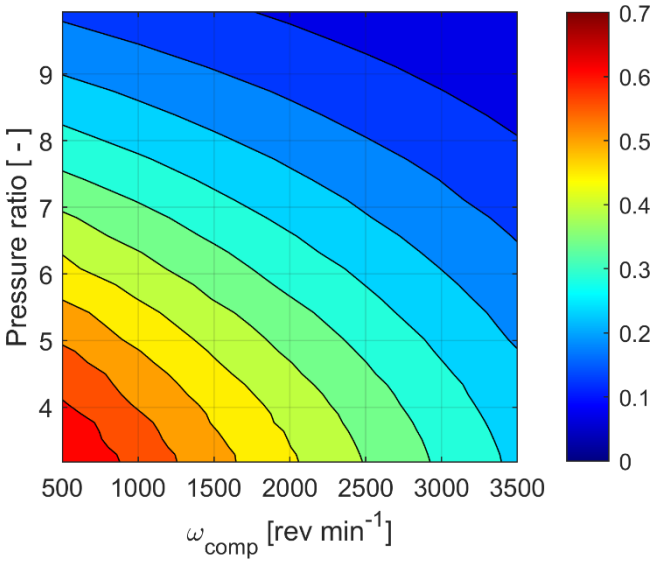

Figure 2.7 – Overall compressor efficiency [-] as a function of the compressor pressure ratio and rotational speed.

2.2.3.2 Heat exchangers

The evaporator and the condenser are characterized by an 8.9 m^2 and a 7.5 m^2 external heat exchanging surface, respectively.

The finned-coil heat exchangers are modelled as a simple tube in tube counter-flow configuration. The heat exchanger design is then discretized into N = 6 longitudinal lumped volumes, for both the evaporator and the condenser. Each discretized volume is then sub-divided in three nodes, one referring to the refrigerant flow, one to the state of tube wall and fins and one referring to the state of the air. The geometric dimensions of the heat exchanger are equally distributed in each lumped element.

This approach was originally presented by Artuso et al. [78] and it is reported in this chapter for the sake of completeness of the numerical model description. Figure 2.8 reports the schematics of such discretization in lumped-parameters volumes of the heat exchangers.

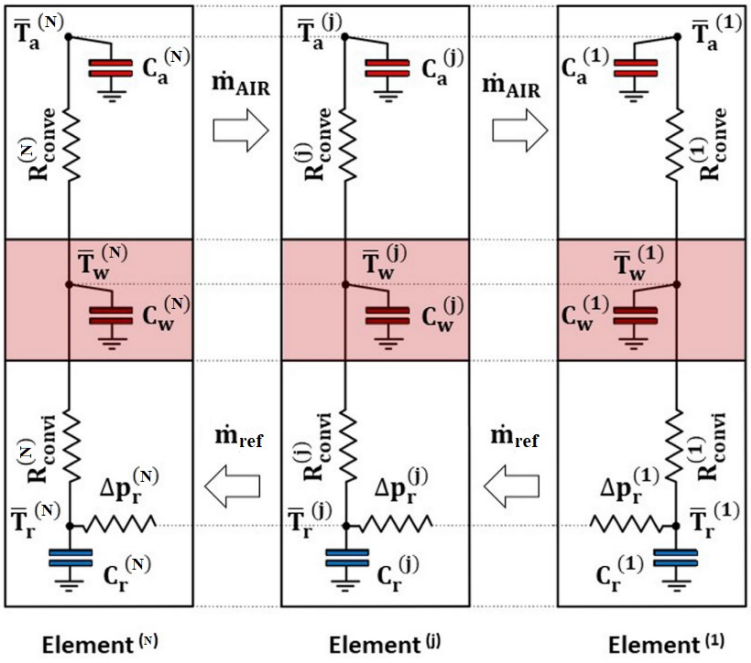

Figure 2.8 – Equivalent counter-flow heat exchanger discretization as a lumped-parameters system, with j=1,...,N (N = 6 for both the evaporator and the condenser) [78].

The internal flow is considered one-dimensional and fluid properties vary only in the direction of the flow. Each discretized volume in which the heat exchangers are divided is composed by a capacitive element and a resistive element (C_i and R_i, respectively). Eq. (2.15) and Eq. (2.16) describe the mass and energy balances, respectively, which are evaluated in each element, giving as a result the mean thermodynamic properties of the refrigerant flowing inside of the j-th tube element ($\bar{T}_r^{(j)}$, $\bar{p}_r^{(j)}$, $\bar{h}_r^{(j)}$).

$$V_r^{(j)} \left(\frac{\partial \bar{\rho}_r}{\partial p}\bigg|_h^{(j)} \frac{d\bar{p}_r^{(j)}}{dt} + \frac{\partial \bar{\rho}_r}{\partial h}\bigg|_p^{(j)} \frac{d\bar{h}_r^{(j)}}{dt} \right) = \dot{m}_r^{(j)} - \dot{m}_r^{(j-1)} \tag{2.15}$$

$$V_r^{(j)} \left[\left(\bar{h}_r^{(j)} \frac{\partial \bar{\rho}_r}{\partial p}\bigg|_h^{(j)} - 1 \right) \frac{d\bar{p}_r^{(j)}}{dt} + \left(\bar{h}_r^{(j)} \frac{\partial \bar{\rho}_r}{\partial h}\bigg|_p^{(j)} + \bar{\rho}_r^{(j)} \right) \frac{d\bar{h}_r^{(j)}}{dt} \right] = \dot{m}_r^{(j-1)} \bar{h}_r^{(j-1)} - \dot{m}_r^{(j)} \bar{h}_r^{(j)} - \dot{Q}_{convi}^{(j)} \tag{2.16}$$

The friction pressure drop and the acceleration pressure drop due to a change in the fluid's density along the flow axis are considered, while the contribution of the gravity to the total pressure gradient is neglected.

The internal convection between the refrigerant and the heat exchanger wall is computed through Eq. (2.17), where α_{convi} is the internal convective heat transfer coefficient and it is evaluated with the use of empirical correlations available on literature, as it will be reported later in Table 2.4.

$$\dot{Q}_{convi}^{(j)} = {\alpha_{convi}}^{(j)} {A_{convi}}^{(j)} \left({\bar{T}_W}^{(j)} - {\bar{T}_r}^{(j)} \right) \tag{2.17}$$

The wall and fins are lumped together in a single discretized element. The mean wall temperature ${\bar{T}_W}^{(j)}$ is evaluated through the formulation of the energy conservation for the wall elements reported in Eq. (2.18), neglecting the conduction heat flow through adjacent wall elements.

$${C_W}^{(j)} \frac{d{\bar{T}_W}^{(j)}}{dt} = \dot{Q}_{convi}^{(j)} - \dot{Q}_{conve}^{(j)} \tag{2.18}$$

The external convection is evaluated through Eq. (2.19) and gives as a result the mean thermodynamic properties of the air flowing outside of the j-th tube element (${\bar{T}_a}^{(j)}$, ${\bar{p}_a}^{(j)}$, ${\bar{h}_a}^{(j)}$). In this case, a zero-dimensional flow and negligible conduction in air flow direction are assumed; moreover, the pressure has the same value in each element, since the airflow pressure losses are neglected. The external convective heat transfer coefficient α_{conve} is evaluated with the use of Colburn j-factor correlation, as it will be reported later in Table 2.4.

$$\dot{Q}_{conve}^{(j)} = {\alpha_{conve}}^{(j)} {A_{conve}}^{(j)} \left({\bar{T}_a}^{(j)} - {\bar{T}_W}^{(j)} \right) \tag{2.19}$$

Table 2.4 reports the list of the empirical correlations utilized in the refrigerant side and air side in the heat exchangers model.

Table 2.4 – Empirical correlations utilized for the heat exchangers models.

Heat exchanger side	**Item**	**Used correlations**
Refrigerant side	α_{convi}	<u>Both evaporator and condenser:</u> Single phase: Gnielinski, 1976 [86] <u>Evaporator:</u> Two-phase: VDI for horizontal tube, 1992 [87] <u>Condenser:</u> Two-phase: Shah, 1979 [88]
	Δp_r	Friedel, 1979 [89]
Air side	α_{conve}	Colburn j-factor [90]

2.2.3.3 Expansion device

The last component of the cooling unit considered in the model is the expansion device, which is modelled as a thermostatic expansion valve, whose opening is regulated in order to maintain a fixed superheating at the outlet of the evaporator. The throttling process is considered isenthalpic and the valve is considered adiabatic. The effect of choked flow is neglected. The mass flow rate through the throttle is determined through the application of Eq. (2.20), where C_q represents the flow coefficient, A_{op} the actual cross area, ρ_{in} the inlet density and Δp_{valve} the pressure difference across the valve.

$$\dot{m}_{valve} = C_q A_{op} \sqrt{\rho_{IN} \Delta p_{valve}} \tag{2.20}$$

The flow coefficient C_q is computed through the default orifice model of the two-phase flow library of the software and it is an indirect function of the opening ratio of the expansion valve, expressed as the ratio between the actual cross flow area A_{op} and the maximum opening area $A_{op,MAX}$. The opening ratio of the thermostatic expansion valve is modulated with a Proportional-Integral (PI) controller in order to maintain a fixed superheating ΔT_{SH} = 10 K at the outlet of the evaporator.

2.2.4 Cooling unit control

The three different connections between the vehicle engine and the cooling unit described in Section 2.1 (BELT-CONF, ALT-CONF, BAT-CONF) were approached separately in the model. For each of these system arrangements a specific control strategy was implemented, with the objective of optimizing the operating conditions of both the engine and the cooling unit's compressor.

In the belt-driven configuration (BELT-CONF) the cooling unit's compressor is run by a belt-driven pully, directly connected to the engine shaft, with a fixed speed ratio between the two components, as reported in Eq. (2.21):

$$\omega_{comp} = \tau_{belt}\, \omega_{eng} \tag{2.21}$$

The value of the speed ratio τ_{belt} must be defined as a tradeoff between the best compressor efficiency, which is obtained for low rotational speed, and the need of simultaneously provide the required cooling power to preserve the quality of the perishable goods transported during the mission.

As a unit intended to serve a transport refrigeration application, the refrigeration system is designed to operate under ample and frequent fluctuations of the air temperature inside the insulated box, due to the door openings linked to the multiple deliveries of the cargo to be performed along the day. In such a scenario, the capacity of the cooling unit to promptly recover the ideal temperature inside the refrigerated box after a door opening is a crucial feature of the system, as it has been pointed out in literature [10]. However, for the BELT-CONF an accurate and dynamically controlled balance between these contrasting needs (compression efficiency and cooling capacity) is not completely possible, since the engine rotational speed ω_{eng} depends on the mission profile and the actual engaged gear, and consequently so does the compressor speed ω_{comp}, which is tied to the engine speed.

A value of τ_{belt} = 0.75 was assumed to scale the allowed engine rotational speed (which varies between the downshift and upshift velocities, 1100 rev min^{-1} and 3000 rev min^{-1} respectively) to a range where the compressor can provide satisfactory cooling power and efficiencies (825 – 2250 rev min^{-1}). The clutch (a)

in Figure 2.2a is controlled by the cooling unit thermostat, to engage or disengage the compressor according to the refrigerated box internal air temperature.

Conversely, in the electrically-driven system arrangements (ALT-CONF and BAT-CONF), an alternator and an electric motor are placed between the vehicle engine and the cooling unit's compressor, to decouple the rotational speed of these two components.

Both the alternator and the electric motor were modelled considering a conversion efficiency of 85% (η_{alt} = 0.85 and η_{el} = 0.85, respectively), a nominal voltage of 12 V and a nominal power of 1150 W. The nominal power value is equal to the steady-state mechanical power needed to keep an internal air temperature of 0°C with external environment at 30°C and engine at idle speed (1000 rev min^{-1}), as evaluated with a simple preliminary study. For the BAT-CONF, a battery is also present between the alternator and the electric motor, and it is modelled as a high-capacity truck commercial battery with a nominal capacity of 100 Ah, corresponding to a stored energy of $C_{bat,max}$ = 4.32 MJ at a voltage of 12 V.

The speed decoupling between the vehicle shaft and the cooling unit's compressor obtained using the electrical conversion allows designing more complex control systems of the compressor working condition compared to the BELT-CONF. In particular, the desired speed for the compressor can be set regardless of the engine operating conditions; therefore, the sensitivity of the compressor's efficiency and the unit's cooling capacity to the rotational speed must be assessed.

For this reason, the compressor response to the rotational speed $\omega_{comp}$was evaluated in terms of energy draw and time needed to pull down the insulated cargo space T_i to the desired value of 3°C, after five minutes in which the doors are kept completely open to an external environment characterized by a temperature of T_{amb} = 40°C and a relative humidity of RH_{amb} = 80%. These test conditions have been chosen to effectively represent high load operating conditions of the refrigerating system.

The results of this sensitivity study are reported in Figure 2.9, where the compressor energy draw was normalized to the minimum energy draw value corresponding to operation at compressor minimum speed (500 rev min^{-1}).

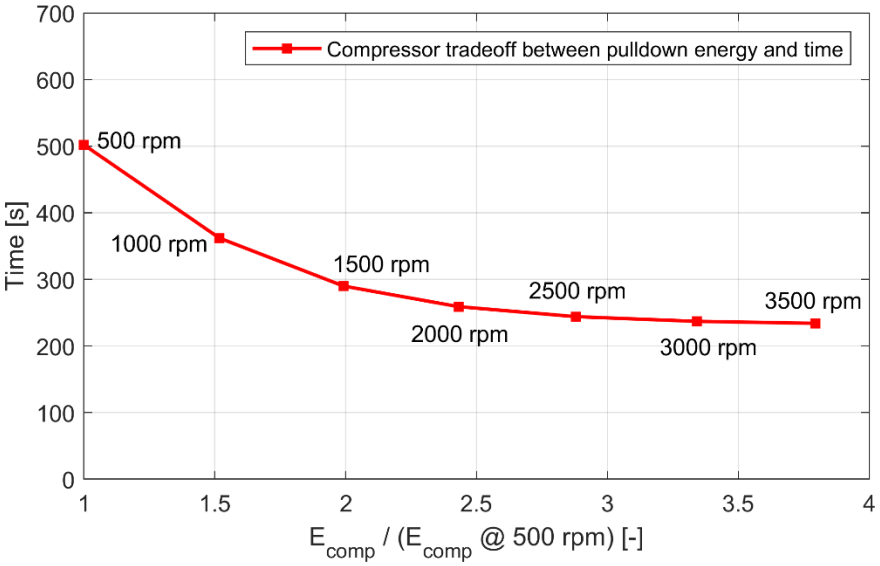

Figure 2.9 – Tradeoff between time and normalized compressor energy needed to recover an internal temperature of T_i = 3°C after five minutes of external air infiltration (T_{amb} = 40°C and RH_{amb} = 80%), for different compressor rotational velocities.

Following this preliminary study, three different operation regimes were set for the electrical-driven configurations:

- Pulldown (pre-cooling): during the pre-cooling activity preceding the mission start, in which the empty refrigerating box is cooled down to the desired operation temperature after spending the whole night in thermal equilibrium with the external environment, the best efficiency (obtained at 500 rev min^{-1}) is chosen. During this period, the perishable cargo is still not loaded inside the refrigerated box and consequently there is no risk of goods quality degradation if the set-point temperature range is recovered in more time. For this reason, the most energy saving setup was preferred;
- Pulldown (mission): when the refrigerated box is loaded with the perishable cargo, the fast recovery of the desired temperature set-point, for example after a door opening, is of crucial importance. For this reason, when the internal temperature is higher than the maximum allowed conservation temperature ($T_i \geq 3°C$) a rotational speed of ω_{comp} = 2000 rev min^{-1} is selected to minimize the time in which the goods are exposed to high temperatures. Observing the results presented in Figure 2.9, a further increase in the compressor speed do not lead to a sensible reduction of the pulldown time, while significantly decreasing the overall compression efficiency;
- Maintenance: when the internal air temperature presents values which do not undermine the perishable cargo correct conservation, since the refrigerated box internal conditions are within the temperature set-point range ($T_i < 3°C$), there is not a strict requirement for high cooling capacity. For this reason, in such conditions the achievement of the maximum compression

efficiency was preferred by setting operation at the minimum rotational speed for the cooling unit's compressor (ω_{comp} = 500 rev min^{-1}).

The resulting cooling unit's compressor speed control strategy is summarized in Table 2.5 for all the configurations considered in the model.

Table 2.5 – Cooling unit's compressor rotational speed control for BELT-CONF, ALT-CONF and BAT-CONF.

BELT-CONF	Entire mission	$\omega_{comp} = 0.75\ \omega_{eng}$
ALT-CONF **BAT-CONF**	Pulldown (Pre-Cooling)	ω_{comp} = 500 rev min^{-1}
	Pulldown (Mission)	ω_{comp} = 2000 rev min^{-1}, for $T_i \geq 3°C$
	Maintenance	ω_{comp} = 500 rev min^{-1}, for $T_i < 3°C$

The two electrical configurations (ALT-CONF and BAT-CONF) differ on the control system actuating the compressor and the clutches (c) in Figure 2.2b and (e) in Figure 2.2c.

In fact, in the alternator electrical layout (ALT-CONF) the alternator clutch connecting the vehicle main shaft to the alternator and the electrical motor feeding the cooling unit's compressor work simultaneously, meaning that there is an instantaneous supply of power to the refrigerating system, according to the refrigerated box thermostat status.

Conversely, in the battery electrical layout (BAT-CONF) the compressor is still controlled by the box thermostat, but the required power is not necessarily simultaneously produced by the vehicle engine, since it is retrieved from the battery, where the energy is stored as a function of its charge level, acting on the mechanical clutch connecting the alternator to the main shaft.

Eq. (2.22) reports the mechanical torque required by the alternator to produce the desired amount of electrical power to charge the battery, as a function of its charge level, normalized on the maximum nominal energy storage capacity. Following this charge control strategy, it is possible to obtain a fast recharge when the battery charge level is below 0.5 (to avoid the possibility of insufficient energy storage when the cooling unit must be switched on), while for a charge level above 0.5 the charge regulator linearly decreases the produced power to avoid over-charge and consequent damaging of the battery. The value of $M_{alt,max}$ was set to 10.95 Nm, equal to the torque needed to provide the alternator nominal power of 1150 W at engine idle speed (1000 rev min^{-1}).

$$\begin{aligned} M_{alt} &= M_{alt,max} && \text{for } C_{bat} < 0.5\ C_{bat,max} \\ M_{alt} &= \frac{M_{alt,max}}{0.5\ C_{bat,max}}(C_{bat,max} - C_{bat}) && \text{for } C_{bat} \geq 0.5\ C_{bat,max} \end{aligned} \tag{2.22}$$

2.2.5 Numerical solver

After the discretization of the system components in lumped parameters elements as described in the previous sections, the whole model can be defined by 107 state variables for BELT-CONF, 104 state variables for ALT-CONF and 105 state variables for BAT-CONF. The state variables will be solved through systems of differential equations as a function of time. From the definition of the state variables, the whole set of variables (1883, 1879 and 1887 for the three configurations, respectively), derived algebraically from the state variables, are computed and saved for post-process of the results. The numerical solver adapts the integrating time step at every iteration, reducing it to increase the precision in correspondence of highly unsteady operation. However, the final variable values are saved for post-process with a frequency of 1 Hz.

A residual error of 10^{-7} was chosen on the state variables to check their convergence at each time step: for each state variable y_i, the error must satisfy the conditions $\varepsilon_i < 10^{-7}(1 + y_i)$, thus interpreting the tolerance as an absolute value for small variables ($y_i \ll 1$) and as a relative error for variables with high magnitude ($y_i \gg 1$).

The implementation of a lumped parameters model implies the reduction of partial differential equations (PDEs) describing the physical system to a system of either ordinary differential equations (ODEs) or differential algebraic equations (DAEs). The integration of ODEs is handled by the software through the use of explicit Runge-Kutta or linear multistep methods, while DAEs are solved following the differential/algebraic system solver algorithm. The solving algorithm choice is managed by the numerical solver, since the software is designed to provide an optimization of the numerical solving process, as extensively described in [91].

2.2.6 Model initialization

The model requires initialization values for the lumped parameters elements, as a necessary input to be used in the first iteration of the solving process. To ensure a non-arbitrary initialization, in particular for the thermal profile of the insulated box and of the cooling unit pipelines and heat exchangers elements, the numerical model included the simulation of a time period of six hours before the start of the actual delivery mission which will be described in the next section. During this period the van is empty, the cooling unit is switched off and the vehicle engine is still. Thus, in this initialization period, the modelled system is influenced only by the ambient conditions of the night and early morning and it is free to reach the real thermal equilibrium which will represent the real initial conditions of the system at the beginning of the actual delivery mission.

Moreover, for BAT-CONF, the battery charge level initialization was obtained with an iterative numerical evaluation of the daily mission, using as a starting condition the battery charge level obtained at the end

of the previous run. This procedure allowed identifying the initial battery charge level which leads to obtain the same charge level at the end of the mission, meaning that no energy storage or energy drain from the battery occurs between start and ending of the mission. Such an approach allows a fair comparison of the total energy usage with the other two configurations modelled (BELT-CONF and ALT-CONF).

2.3 Delivery mission structure

The objective of the study presented in this chapter is to assess the thermal performance of a transport refrigeration unit and at the same time to evaluate the fuel consumption and the pollutant emissions of the vehicle during a typical transport mission. To this extent, the refrigerated vehicle modelled in this chapter is supposed to be employed in an urban range daily multi-drop delivery mission of temperature-controlled goods.

The mission simulates a typical daily local distribution activity, where a refrigerated vehicle travels from a distributor's warehouse located in a countryside area to multiple retail points located across an urban area, performing a delivery of part of the refrigerated cargo at every stop, and then comes back to the distributor's warehouse at the end of the day.

The mission profile is defined through the delineation, with a frequency of 1 Hz, of the vehicle target speed, of the periods in which the refrigerated box doors are opened to the environment to allow the unloading process of part of the cargo, and of the fraction of the perishable goods that are discharged at every delivery point, as a function of time.

The first two hours of the mission are dedicated to the precooling of the insulated box (pulldown), to bring it to the desired temperature range set-point after the night, where the cooling unit was switched off and the insulated box was in thermal equilibrium with the warm external environment. In the pulldown phase, the refrigerating unit provides cooling power according to the thermostat and with the doors closed. During this process, for the BELT-CONF and the ALT-CONF, the vehicle engine must be kept switched on, even if the vehicle is still, to provide the required power to the cooling unit. Conversely, for the BAT-CONF the vehicle engine can be maintained off for the whole pulldown period, since the required energy can be drawn from the battery, which will be recharged later during the mission, when the engine will be switched on to perform the actual driving part of the mission.

After the pulldown, 400 kg of meat products are considered to be loaded in the vehicle insulated box under controlled temperature conditions (4°C). The perishable goods will be distributed evenly in 7 deliveries in the morning and 7 deliveries in the afternoon, in a short-range urban area driving mission. Following what is reported in literature, the heat capacity of the meat is considered to be equal to 3.25 kJ kg^{-1} K^{-1} [92] and the convective heat transfer coefficient equal to 8 W m^{-2} K^{-1} [93].

Standard WLTC (Worldwide harmonized Light vehicles Test Cycle [94]) profiles are used to define the delivery mission profile by setting the target vehicle speed, with a frequency of 1 Hz. Two WLTC Rural followed by two WLTC SubUrban cycles are used to represent the drive from the distributor's warehouse to the urban area in which the deliveries have to be performed, while the urban drive between delivery points is represented through two WLTC Urban cycles.

To consider the unloading time of the cargo at the delivery points, a five-minute stop is accounted in the mission profile. After a lunch break of approximately one hour, the mission is continued in the afternoon with the same structure. After the last delivery, the vehicle drives back to the logistic facilities and it stays there for the whole night empty and with no refrigerating unit operation.

The complete mission structure is reported in Table 2.6.

Table 2.6 – Delivery mission structure.

Start time [hh.mm]	**Duration [hh.mm]**	**Activity**	**Travel distance [km]**
06.00	02.00	Pulldown (Pre-Cooling)	-
08.00	01.00	Loading	-
09.00	0.30	2x Rural + 2x SubUrban Driving Cycles	22
09.30	2.48	7x Delivery Cycles	42
	0.19	2x Urban Driving Cycles	6
	0.02	Stop	-
	0.03	Delivery	-
12.18	0.30	2x Rural + 2x SubUrban Driving Cycles	22
12.48	1.12	Stop	-
14.00	0.30	2x Rural + 2x SubUrban Driving Cycles	22
14.30	2.48	7x Delivery Cycles	42
	0.19	2x Urban Driving Cycles	6
	0.02	Stop	-
	0.03	Delivery	-
17.18	0.30	2x Rural + 2x SubUrban Driving Cycles	22
17.48	1.12	Stop	-
TOTAL	**11.48**	**-**	**172**

The mission is considered to be performed in a hot European climate city, to evaluate the system performance under harsh environmental conditions. Therefore, the ambient conditions of a mean summer day in the city of Athens are also provided as a model input. The environmental temperature, relative humidity and solar radiation intensity, available in the Energy Plus online database [95], were collected for all the days of August and then averaged hourly to obtain the climatic profile of the delivery mission day. Therefore, the results presented in Section 2.4 will be referred to the mean August day in the city of Athens.

However, an additional analysis of the system behavior under different climatic conditions has been carried on. In this case, the thermal performance of the cooling unit and the environmental impact of the

vehicle engine have been compared between two different climates: a hot European summer day (evaluated as above described) and a mild European summer day (evaluated following the same procedure above described, starting from the Energy Plus weather database [95] for the month of August in the city of Strasbourg). Therefore, the results presented in Section 2.5 will refer to the comparison between the mean August day in the cities of Athens and Strasbourg, representative of hot and mild European climatic conditions, respectively.

2.4 Influence of the cooling unit connection to the vehicle engine

The numerical model results were saved with a frequency of 1 Hz. As a first step, the influence of the different connections of the cooling unit to the vehicle engine is evaluated. Firstly, the effects of the cooling unit's compressor speed control on the internal air temperature, on the food cargo temperature and on the ON/OFF management of the refrigerating system will be considered. After that, the overall energy management of the vehicle power line will be investigated comparing the three different arrangements. Finally, the fuel consumption and the pollutant emissions will be presented, pointing out the impact of the connection between the cooling unit and the vehicle prime engine on the results.

2.4.1 Cooling unit performance

To evaluate in detail the dynamic mechanical and thermal behavior of the system, a limited period of the delivery mission will be firstly highlighted, to better appreciate the variations of the system parameters with time, while the general considerations on the overall daily results will be presented later in this section.

Therefore, the period between 09:50 and 10:15, covering the first delivery of the day and the following urban drive, is considered. At the beginning of this period, the vehicle is still, the engine is shut down and the insulated box doors are open, since the unloading operations of part of the cargo are in place. After the delivery, the engine is turned back on and the vehicle starts moving to the following retail point while performing the driving cycle described in Section 2.3. After arriving the following distribution point, the vehicle stops again, and another drop of the cargo is performed.

The main mechanical parameters which describe the vehicle and the engine during the considered period of the delivery mission are reported in Figure 2.10, considering operation in BELT-CONF. In Figure 2.10a, the target speed of the vehicle, corresponding to the standard urban driving cycle described in Section 2.3, is presented and compared with the actual speed of the truck, achieved through the dynamic driver control acting on the accelerator, brake, gearbox and clutch controls. Figure 2.10b reports instead the resulting engine rotational speed, directly influenced by the driver control, and the engaged gear,

dependent on the definition of the upshift and downshift rotational speed (3000 rev min^{-1} and 1100 rev min^{-1}). When the vehicle is still, the gear is put in neutral and the engine is at idle speed (1000 rev min^{-1}).

It can be noticed looking at the first minutes of the highlighted period that during the delivery stop the vehicle engine is switched off since, when the refrigerated box doors are open, the cooling unit is turned off as well. On the contrary, during the urban driving cycle the engine must be kept on even when the vehicle is still, because the necessary power has to be provided to the cooling unit, when required by the thermostat. This kind of behavior will be improved with the implementation of a battery as an energy storage device, as it will be described in the next section.

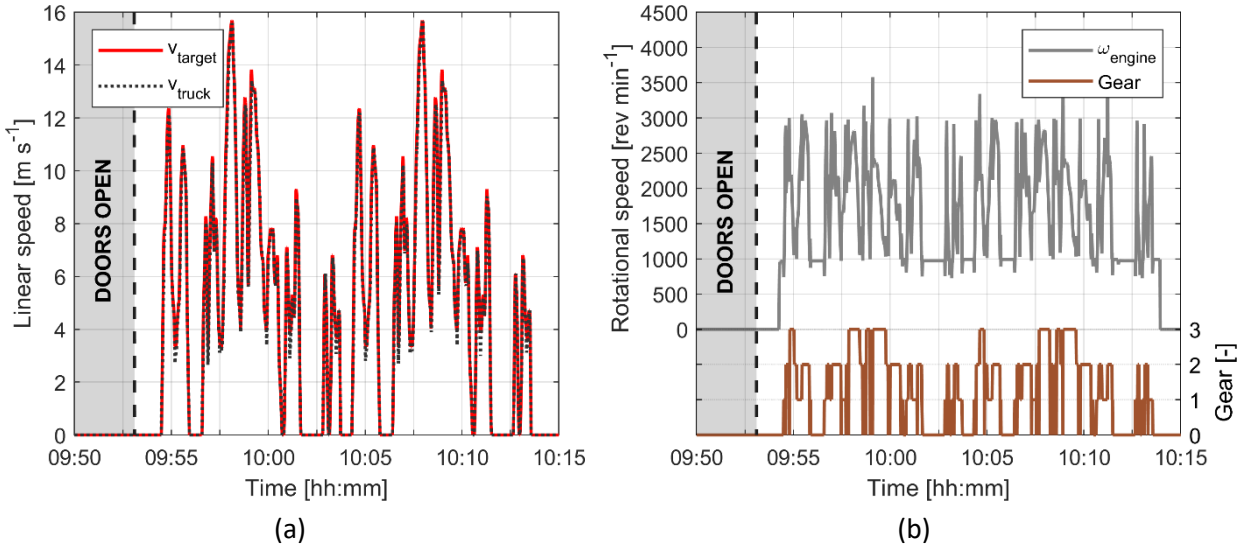

Figure 2.10 – First cargo delivery of the mission and urban drive to the following distribution point, with BELT-CONF: (a) vehicle linear speed; (b) engine rotational speed and engaged gear.

Focusing on the same mission period between 09:50 and 10:15, the cooling unit's compressor speed, both in BELT-CONF and ALT-CONF (controlled following the strategy summarized in Table 2.5), is presented in Figure 2.11 along with the air temperature inside the insulated box for each of the considered configurations.

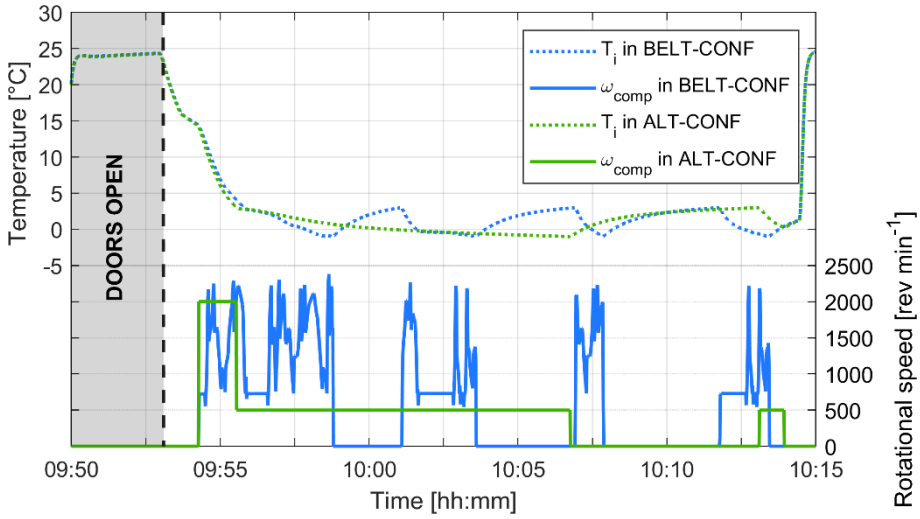

Figure 2.11 – Internal air temperature and compressor speed during the highlighted portion of the mission, with BELT-CONF and ALT-CONF.

Consistently with the control strategy presented in Table 2.5, for the BELT-CONF the compressor speed is directly linked to the vehicle engine speed through the scaling parameter τ_{belt} = 0.75, and the ON/OFF regulation is handled by the thermostat according to the internal air temperature. Conversely, for the ALT-CONF the compressor speed is untied from the engine speed and it is set by the alternator to 2000 rev min^{-1} when the internal air temperature is above the maximum acceptable value of 3°C (right after the insulated box doors closing) and to 500 rev min^{-1} for the maintenance of the desired temperature range.

It can be clearly appreciated from Figure 2.11 that the cooling unit compressor management has a direct and significant effect on the internal air temperature profile and, consequently, on the ON/OFF management of the unit. In fact, the heavily varying compressor speed registered in BELT-CONF causes an irregular cooling profile of the insulated box and consequent uneven ON/OFF cycles of the cooling unit, since the cooling capacity provided by the evaporator is not constant. The preservation of the ideal temperature conditions inside the refrigerated box is therefore subordinate to the vehicle driving conditions.

On the other hand, in ALT-CONF the constant compressor speed set by the alternator leads to a constant cooling capacity provided by the evaporator, resulting in a management of the internal air conditions which is independent from the delivery mission performed by the vehicle. In addition, setting a constant compressor speed of 500 rev min^{-1} after the pulldown contributes to longer ON periods of the cooling unit compared with BELT-CONF. This leads to a lower average internal air temperature during the highlighted urban drive section of the mission, meaning that better preservation conditions of the perishable cargo are achieved.

As it was reported in Table 2.5, ALT-CONF and BAT-CONF share the same cooling unit compressor control strategy. This leads to very limited differences between these configurations in terms of thermal performance of the refrigerating system, related only to the fact that, in BAT-CONF, the unit can be turned on even when the vehicle engine is switched off.

The air temperature inside the insulated box, averaged for each section of the delivery mission, is presented in Figure 2.12, along with the temperature of the transported goods. In accordance with the observation above presented, the average internal air temperature is lower in ALT-CONF than in BELT-CONF for most of the delivery mission time, as a result of the different compressor speed management. The hot ambient air infiltrating inside the refrigerated box during the deliveries, when the doors are opened, results in a cumulative effect in the transported cargo: in fact, a steep temperature increase of the food occurs at each delivery and, since the cooling unit can provide only a limited refrigerating energy between consecutive deliveries, a progressive increase of the cargo temperature takes place. However, accordingly to the better internal air temperature conditions, the ALT-CONF is more efficient in contrasting this increase, thus resulting in an overall improved food conservation during the delivery mission.

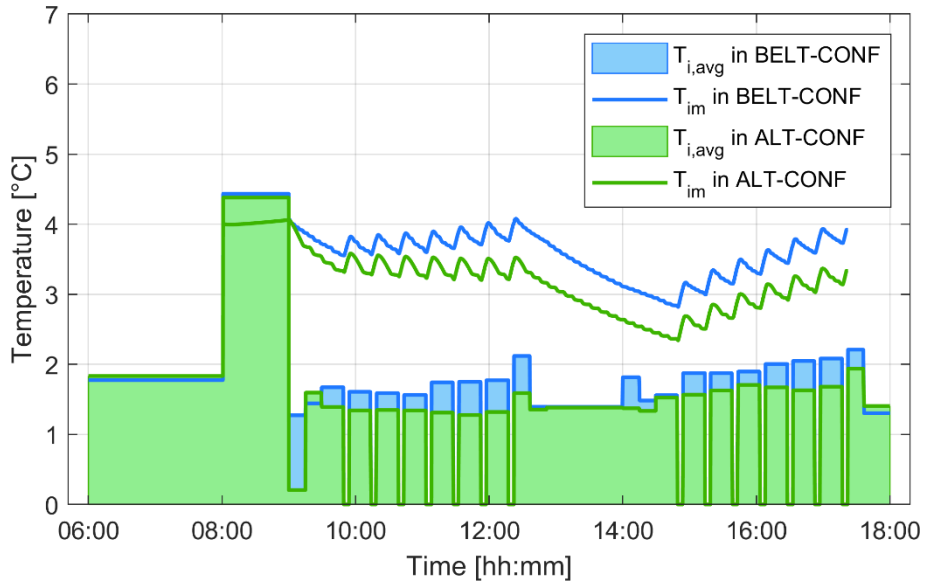

Figure 2.12 – Internal air temperature averaged on each section of the delivery mission and transported cargo temperature, with BELT-CONF and ALT-CONF.

The performance of the refrigerating system related to the whole delivery mission can be evaluated through the system COP (defined in Eq. (2.23)) and Duty Cycle (defined in Eq. (2.24)). It has to be pointed out that, given the highly unsteady operating conditions of the cooling unit, the instantaneous COP of the system would be highly fluctuating, strongly influenced by the highly variating operation of the system; therefore, an average mission COP is defined referring to the overall energy characterizing the entire mission rather than on instantaneous power.

$$COP = \frac{E_{evap}}{E_{comp} + E_{fans}} \quad (2.23)$$

$$\text{Duty cycle} = \frac{t_{ON}}{t_{ON}+t_{OFF}} \quad (2.24)$$

The average mission COP and Duty Cycle are reported in Table 2.7 for BELT-CONF, ALT-CONF and BAT-CONF. It can be observed that the control of the cooling unit's compressor rotational speed and its disconnection from the vehicle engine rotational speed lead to a 26% increase of the mission COP and a 39.3% increase of the mission unit's Duty Cycle. Consistently with what was previously pointed out, ALT-CONF and BAT-CONF do not present any significant difference regarding the cooling unit operation, since the main difference between these two configurations will have a more significant impact on the vehicle engine operation.

Table 2.7 – Average mission Coefficient of Performance and Duty Cycle for BELT-CONF, ALT-CONF and BAT-CONF.

	BELT-CONF	**ALT-CONF**	**BAT-CONF**
COP [-]	1.31	1.65 (+26.0%)	1.65 (+26.0%)
Duty cycle [-]	0.28	0.39 (+39.3%)	0.39 (+39.3%)

The overall mechanical energy distribution in the system, considering the cooling unit's compressor and fans, the whole cooling unit power junction, the vehicle driveline and the engine production, is reported in Table 2.8 for each of the three configurations considered in this chapter.

From the results it can be observed that, while the energy required by the sole cooling unit's compressor is significantly lower in the electrically-driven configurations (-23.0% for the ALT-CONF and -21.2% for the BAT-CONF, compared to BELT-CONF), the energy required by the heat exchangers fans increases (+38.9% in both cases) due to the increase of the unit's Duty Cycle. On the whole, the additional mechanical energy that the vehicle engine must produce to provide power to the refrigerating system (namely, the compressor and the heat exchangers fans) is higher in ALT-CONF and BAT-CONF than in BELT-CONF (+8.4% and +10.6%, respectively).

As previously discussed, the introduction of an alternator to control the compressor speed significantly reduces the energy required by the sole compressor, which is run at an optimized speed, but it requires two energy conversions (from mechanical to electrical and then from electrical to mechanical), resulting in an overall energy transmission efficiency of 0.72 for ALT-CONF and BAT-CONF. On the contrary, BELT-CONF is characterized by an energy transmission efficiency of 0.94, linked only to the mechanical losses along the power line. The improvement of using an alternator to decouple compressor and engine speeds

therefore relies more in the significant positive thermal effect for the perishable goods than in the overall energy production of the engine.

The mechanical energy dedicated to the vehicle motion shows minimal variations between the three configurations (-0.4% for ALT-CONF and -1.6% for BAT-CONF compared to BELT-CONF), due mainly to the different operating points of the engine, which depend on the power demand from the cooling unit, and a total mechanical energy production of the engine which remains almost constant (±0.4% for ALT-CONF and BAT-CONF compared to BELT-CONF).

However, as it was stated above, even if the variation of the engine overall energy production is limited, the electrically-driven configurations (ALT-CONF and BAT-CONF) present a significantly improved thermal performance of the system, as shown in Figure 2.11 and Figure 2.12.

Table 2.8 – Energy demand of the cooling unit and energy production of the vehicle engine during the delivery mission for BELT-CONF, ALT-CONF and BAT-CONF.

	BELT-CONF	**ALT-CONF**	**BAT-CONF**
E_{comp} **[MJ]**	25.08	19.32 (-23.0%)	19.76 (-21.2%)
E_{fan} **[MJ]**	2.88	4.00 (+38.9%)	4.00 (+38.9%)
$E_{cooling\ unit}$ **[MJ]**	29.74	32.23 (+8.4%)	32.88 (+10.6%)
$E_{vehicle}$ **[MJ]**	273.52	272.30 (-0.4%)	269.02 (-1.6%)
$E_{engine,TOT}$ **[MJ]**	303.26	304.53 (+0.4%)	301.90 (-0.4%)

2.4.2 Fuel consumption and pollutant emissions

The model results are useful to evaluate, along with the thermal performance of the refrigerating unit, the environmental impact of a refrigerated vehicle and, in general, of the perishable goods delivery sector within the cold chain, in terms of fuel consumption and pollutant emissions. These parameters are in direct dependency of the dynamic engine operation: as described in Section 2.2.1, the engine operating points are defined by the instantaneous values of torque and rotational speed along the delivery mission.

Considering the same delivery mission period corresponding to the first delivery and the following urban drive (from 09:50 to 10:15) considered in the previous section, the effect of the presence of the cooling unit on the engine operating points is highlighted in Figure 2.13. To this extent, a dynamic simulation of the same vehicle performing the same mission profile without the cooling unit (namely, the engine only had to produce the power needed for the vehicle motion) was run, and the results were used to evaluate the variation in the engine operation after the introduction of the energy drain by the cooling unit.

The operating points of the engine, sampled with a frequency of 1 Hz during the considered period of the mission, are reported in Figure 2.13a for both the vehicle without the cooling unit and for BELT-CONF. The upward shift of the BELT-CONF operating points compared to the other data set represent the additional torque that the engine has to produce to drive the cooling unit's compressor. This behavior can be appreciated even more accurately in Figure 2.13b, where the difference between the produced torque in BELT-CONF and in the case of no cooling unit is presented. The additional torque demand linked to the presence of the cooling unit is observed to be varying between 5 Nm and 30 Nm approximately.

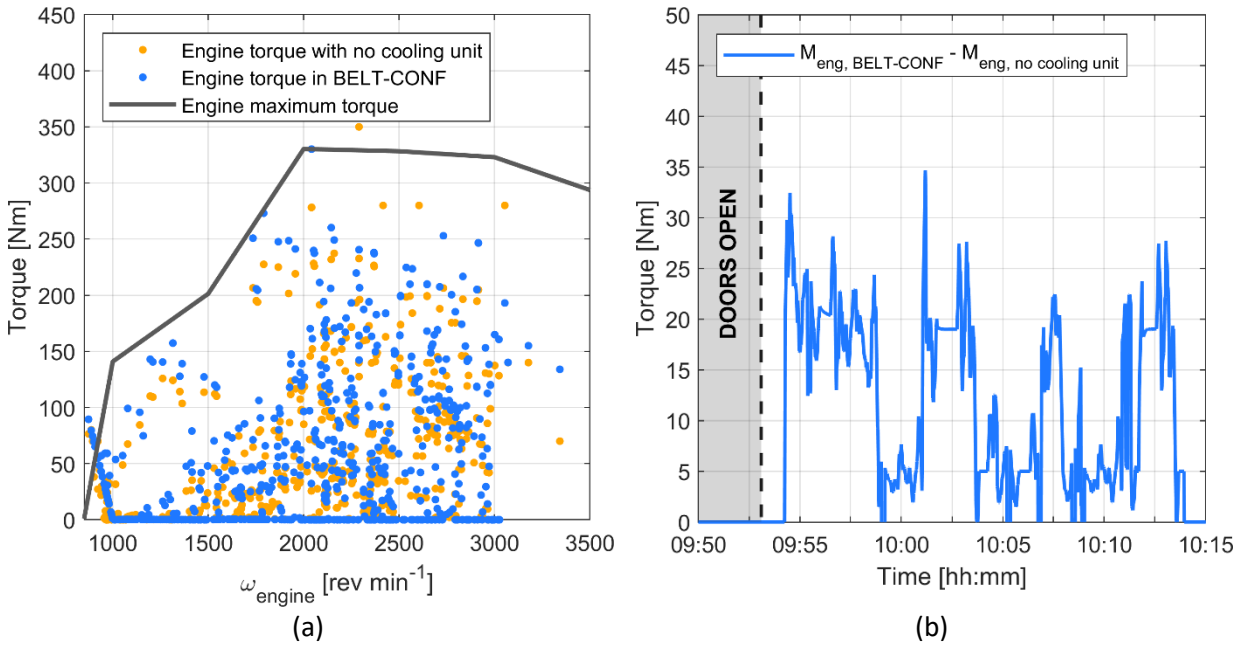

Figure 2.13 – First cargo delivery of the mission and urban drive to the following distribution point: (a) engine operating points in BELT-CONF and with no cooling unit; (b) torque production increase in BELT-CONF due to the presence of the cooling unit.

Considering the whole daily delivery mission and not only the portion above highlighted, the effect of the presence of the cooling unit on the fuel consumption and main pollutant emissions (CO, NO_x, THC, PM) of the vehicle engine can be appreciated from Figure 2.14. To highlight the impact of the cooling unit and its connection to the engine, the data are presented as increase compared to the reference vehicle without the refrigerating system.

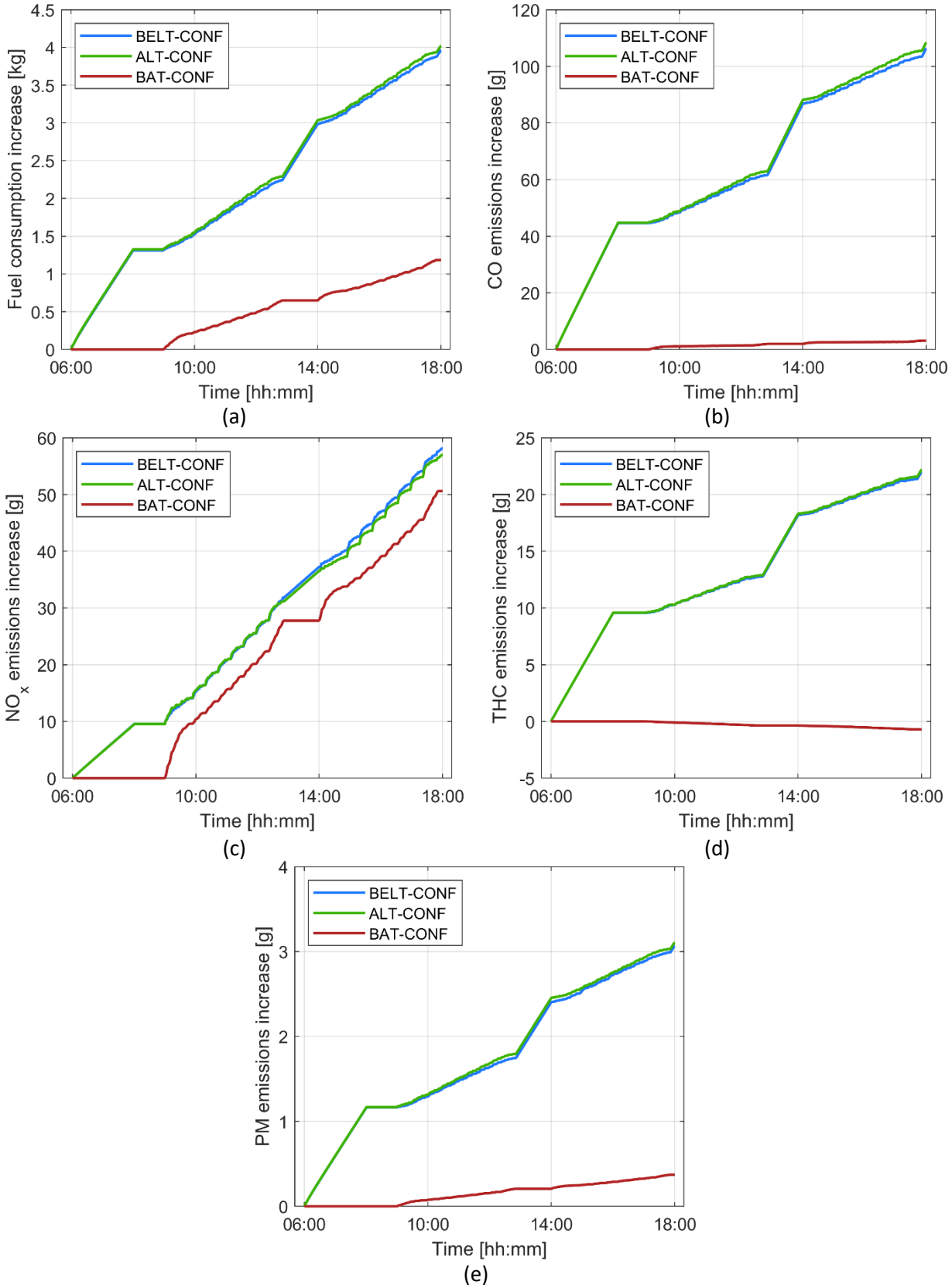

Figure 2.14 – Engine operation along the delivery mission for BELT-CONF, ALT-CONF and BAT-CONF: (a) fuel consumption increase; (b) CO emissions increase; (c) NO_x emissions increase; (d) THC emissions increase; (e) PM emissions increase, compared with no cooling unit operation.

Firstly, it can be clearly observed that, for BAT-CONF, fuel consumption and pollutant emissions are completely avoided during the first two hours of pulldown before the start of the actual delivery mission and during the long pause at the middle of the mission: in this configuration, the vehicle engine can be kept turned off during these sections of the mission, since the energy required to run the cooling unit is provided using the energy stored inside the battery pack. Conversely, in BELT-CONF and ALT-CONF the engine must be kept switched on for the entire mission because no energy storage system is present, thus resulting in significant fuel consumption and pollutant emissions also during these mission sections.

From Figure 2.14a, it can be observed that the fuel consumption increase is almost identical between BELT-CONF and ALT-CONF, while in BAT-CONF the fuel consumption increase is significantly lower, thanks to the possibility to switch off the engine when the vehicle is still and to avoid the fuel consumption associated with the forced operation of the engine at idle speed just to provide power to the cooling unit. However, it can be observed that, even in BAT-CONF, the additional power production that has to be provided by the engine to recharge the battery leads to a tangible increase in fuel consumption compared to the reference case of the vehicle without the cooling unit. Nevertheless, the fuel consumption increase rate along the driving sections of the mission is lower in BAT-CONF than in BELT-CONF and ALT-CONF: even if the overall energy produced by the engine is almost unchanged in the three configurations (as reported in Table 2.8), the energy required to recharge the battery in BAT-CONF is produced in more efficient engine operating points and in moments of the mission which are not necessarily corresponding to the moments in which power is demanded by the cooling unit, and therefore the overall energy demand of the cooling unit has a lower impact on the fuel consumption than in BELT-CONF and ALT-CONF.

Regarding the pollutant emission increase linked to the presence of the cooling unit, Figure 2.14b-e show that the engine performance response during the mission is significantly different depending on the type of pollutant considered. From Figure 2.14b and Figure 2.14e it can be observed that the CO and the PM emissions increase compared to the reference case without cooling unit is very limited in BAT-CONF, while in BELT-CONF and ALT-CONF the increase is remarkably higher. Actually, Figure 2.14d shows that the THC emissions in BAT-CONF are even slightly less than the ones of the vehicle with no cooling unit. As discussed above regarding the fuel consumption, such a behavior implies that the BAT-CONF approach to power the cooling unit, namely disconnecting power demand and power production, leads to an overall improved and more efficient management of the engine operation compared to BELT-CONF and ALT-CONF. Moreover, it can be concluded from these results that the engine operation at idle speed (low torque and low rotational speed) is responsible for a huge amount of CO, THC and PM emissions: in fact, most of these pollutants emissions increase in BELT-CONF and ALT-CONF compared to the reference vehicle with no cooling unit correspond to the pulldown at the beginning of the mission and to the long pause around half of the mission, when the vehicle is still but the engine can not be turned off to be ready to provide the required power to the cooling unit.

Conversely, Figure 2.14c highlights that the increase of NO_x emissions compared to the reference truck is significant for all of the three configurations considered in this chapter. Such a behavior implies that, for this specific type of pollutant, the greater part of the emissions is not linked to the engine ON/OFF management during long pauses or to the operation at low torque load: in fact, the increase of NO_x emissions compared with the not refrigerated vehicle is mostly linked to the additional torque dedicated to the cooling unit that the engine has to produce during the vehicle motion, when the torque demand is already high, since the power needed for the vehicle motion has to be produced.

The overall fuel consumption and pollutant emissions increases displayed in Figure 2.14 are summarized in Table 2.9. In agreement with what was observed above, the performance of the engine in BELT-CONF and in ALT-CONF presents very limited variations, as for both configurations the cooling unit's compressor is a direct load on the engine torque production. Averaging the results of these two configurations, which represent the vast majority of the solutions used in the current refrigerated road transport sector, an evaluation of the impact of the cooling unit on the engine environmental performance can be provided. On the average, the presence of the cooling unit leads to a 19.0% increase of the fuel consumption, a 33.2% increase of the CO emissions, a 9.5% increase of the NOx emissions, a 32.2% increase of the THC emissions and a 23.5% increase of the PM emissions compared to a vehicle with no cooling unit.

However, the introduction of an energy storage device as a battery can significantly mitigate the impact of the presence of the cooling unit on the engine operations, offering the possibility to switch off the engine when the vehicle is still and to produce the additional energy dedicated to the refrigerating system only when the vehicle is in motion. As a result, in BAT-CONF the numerical results show a 5.7% increase of the fuel consumption, a 1.0% increase of the CO, a 8.4% increase of the NOx, a 1.0% decrease of the THC and a 2.8% increase of the PM emissions compared with the case with no cooling unit, thus minimizing the environmental implications of the presence of the refrigerating system.

Table 2.9 – Overall fuel consumption and pollutant emissions of the vehicle during the daily delivery mission with no cooling unit and for BELT-CONF, ALT-CONF and BAT-CONF.

	No cooling unit	**BELT-CONF**	**ALT-CONF**	**BAT-CONF**
Fuel consumption [kg]	21.03	25.00 (+18.9%)	25.05 (+19.1%)	22.22 (+5.7%)
CO emissions [g]	323.87	430.12 (+32.8%)	432.22 (+33.5%)	326.99 (+1.0%)
NO_x emissions [g]	603.50	661.66 (+9.6%)	660.53 (+9.4%)	654.10 (+8.4%)
THC emissions [g]	68.63	90.60 (+32.0%)	90.81 (+32.3%)	67.93 (-1.0%)
PM emissions [g]	13.20	16.27 (+23.3%)	16.31 (+23.6%)	13.57 (+2.8%)

In conclusion, comparing the results of the direct-load and indirect-load management of the cooling unit, the implementation of an energy storage device, such as a battery pack, can lead to a 11.1% reduction of the fuel consumption, a 24.0% reduction of the CO, a 1.1% reduction of the NOx, a 25.0% reduction of the THC and a 16.6% reduction of the PM emissions between BAT-CONF and the traditionally implemented BELT-CONF, as reported in Table 2.10.

Table 2.10 – Reduction of fuel consumption and pollutant emissions with BAT-CONF, compared to BELT-CONF.

	BELT-CONF	**BAT-CONF**
Fuel consumption [kg]	25.00	22.22 (-11.1%)
CO emissions [g]	430.12	326.99 (-24.0%)
NO_x emissions [g]	661.66	654.10 (-1.1%)
THC emissions [g]	90.60	67.93 (-25.0%)
PM emissions [g]	16.27	13.57 (-16.6%)

The results of the presented numerical evaluation are compared with the fuel consumption and pollutant emissions data available in open literature in Table 2.11. The data reported in the table are referred only to the impact of the cooling unit and do not regard the entire vehicle. The data considered for this study represents the average fuel consumption and emissions increase registered in BELT-CONF and ALT-CONF, since in these configurations the cooling unit represents a direct load on the engine. Moreover, an emission factor of 2.578 kg of CO_2 emitter per liter of diesel fuel burnt has been considered, according to literature [21].

Despite the direct comparison of the published data is misleading due to significant differences in the units size, operating conditions, truck type and dependency on the traction engine, it is worth noticing a reasonable agreement between this study and the results reported by Tassou et al. [17], Bagheri et al. [5] and Yang et al. [2], where the data are normalized on the consumption (or emission) of the vehicle prime engine.

Table 2.11 – Comparison between fuel consumption and pollutant emissions results of this study and results previously published in literature.

	Present study	**Tassou et al.** [17]	**Bagheri et al.** [5]	**Yang et al.** [2]	**Lawton et al.** [21]	**Barnitt et al.** [20]
Fuel consumption	+19.0% 0.4 l/h	+18.9%	+14.3%	+15%	-	2.1-5.0 l/h
CO_2 emissions	+19.0% 0.3 g/s	+18.9%	+14.3%	+15%	2.2-3.0 g/s	-
CO emissions	+33.2% 9.1 g/h	-	-	-	-	30.8-61.8 g/h
NO_x emissions	+9.5% 12.3 g/l_{fuel} 4.9 g/h	-	-	+18%	16-22 g/l_{fuel}	53.9-123.3 g/h
THC emissions	+32.2% 1.9 g/h	-	-	-	-	24.9-37.3 g/h
PM emissions	+23.5% 600 mg/l_{fuel} 0.3 g/h	-	-	-	20-40 mg/l_{fuel}	6.5-17.6 g/h
Methodology	Dynamic model	Literature review	Analytical evaluation	Dynamic model	Experimental campaign	Experimental campaign
Notes	Medium-size vehicle with cooling unit powered by vehicle engine	Data collected for 17 fleets; medium rigid vehicles	Trailer with dedicated diesel engine; assumption on the dedicated engine efficiency	Light commercial vehicle; constant cooling load assumption; no long idle speed operation in the mission	13.6 m semi-trailer with dedicated diesel engine; only PM 2.5 considered	14.6 m semi-trailer with dedicated diesel engine

2.5 Influence of the climatic conditions

To evaluate the influence of ambient climatic conditions on the operation of the cooling system and on the environmental impact of the refrigerated vehicle, a daily delivery mission with the same structure as the one presented in Table 2.6 was numerically simulated in a mean summer day in the city of Strasbourg, representative of mild European climatic conditions, and the results were compared with the ones obtained for the city of Athens.

For this evaluation, the BELT-CONF layout was considered for both cases, as the direct-drive configuration is representative of the most widespread technology in the current market for small to medium size refrigerated vehicles [17] and, consistently with the results presented in Section 2.4, it is the configuration

which has the most significant effect on the engine environmental performance, compared with the reference van with no cooling unit.

The internal air temperature, averaged for each section of the delivery mission, and the temperature of the transported goods are reported in Figure 2.15, as well as the external ambient temperature throughout the day, for both the Athens and Strasbourg cases.

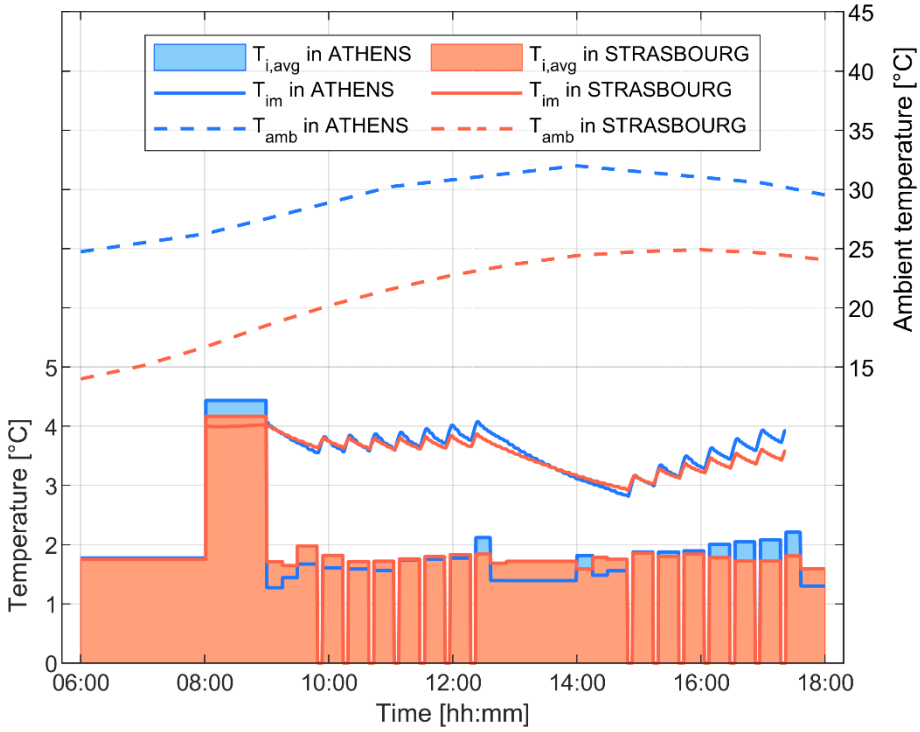

Figure 2.15 – Internal air temperature averaged on each section of the delivery mission, transported cargo temperature and external ambient temperature, for Athens and Strasbourg.

The temperature trend is the same in Athens and Strasbourg, showing a clear cumulative effect associated to the door openings during the delivery phase of the mission, as a result of ambient air infiltrating inside the refrigerated box. In addition, it can be observed that, despite an external ambient temperature which is significantly higher in Athens than in Strasbourg (with a temperature difference in a 5-10°C range along the day), the effect on the average internal air temperature and on the transported goods temperature is very limited. In some sections of the mission, the average internal air temperature is even higher in Strasbourg than in Athens, and this is due to the fact that, since the external ambient temperature is lower, the heat to be removed from the refrigerated box is lower as well, and therefore the cooling unit is turned on for less time, thus resulting in a slightly higher average temperature of the internal air.

The difference in the cooling unit ON/OFF management between Athens and Strasbourg can be more clearly appreciated with the results presented in Figure 2.16, which reports the cooling capacity and the cooling demand the refrigerating unit, averaged for each section of the delivery mission.

The average cooling demand of the unit (Eq. (2.25)) is evaluated as the total amount of refrigerating energy provided for each of the j sections of the mission, divided by the total duration of the corresponding mission section, in which the cooling unit is turned on and off by the thermostat to keep the internal temperature in the desired range. This parameter therefore represents the actual cooling needs of the system during the mission sections and it is directly linked to the ON/OFF management of the unit itself.

Conversely, the average cooling capacity of the unit (Eq. (2.26)) is evaluated as the total amount of refrigerating energy divided by the ON duration in each of the j sections of the mission. This parameter represents the average cooling power that the unit provides during ON periods, but since such a refrigerating effect would bring the internal air temperature under the minimum desired temperature of -1°C, the thermostat controls the unit to perform ON/OFF cycles and keep T_i in the desired range.

$$(Q_{demand})_j = \left(\frac{E_{evap}}{t_{ON} + t_{OFF}}\right)_j \tag{2.25}$$

$$(Q_{capacity})_j = \left(\frac{E_{evap}}{t_{ON}}\right)_j \tag{2.26}$$

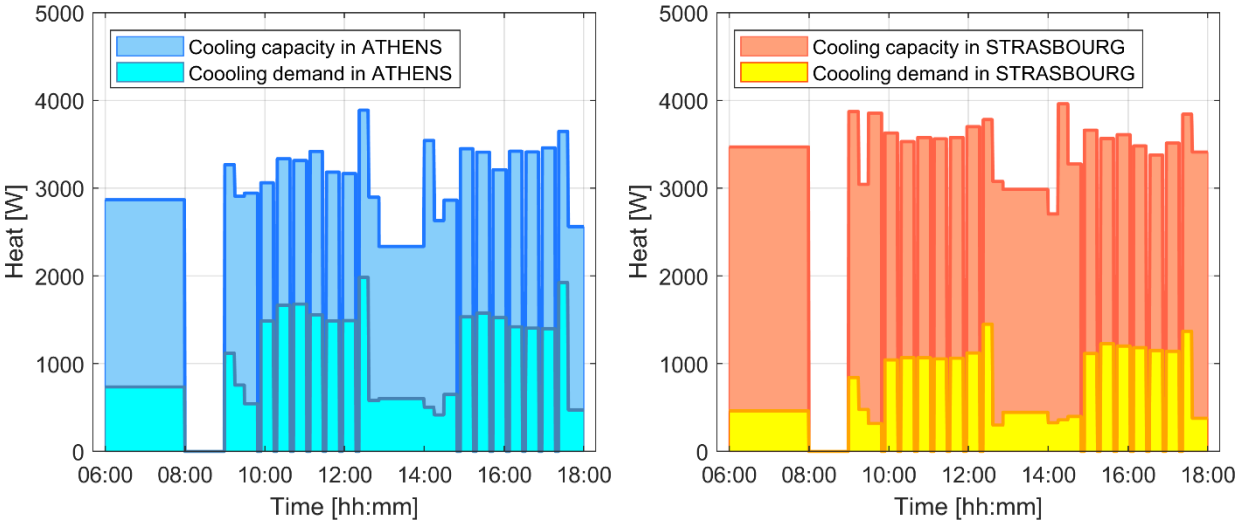

(a) (b)

Figure 2.16 – Cooling capacity and cooling demand averaged on each section of the delivery mission: (a) Athens; (b) Strasbourg.

Comparing Figure 2.16a and Figure 2.16b, it can be observed that the refrigerating system cooling capacity is higher in Strasbourg, as a consequence of the lower ambient temperature; for the same reason, the cooling demand of the system is lower in Strasbourg, because less heat needs to be removed from the refrigerated box. Therefore, it can be concluded that in hot climatic conditions (Athens) a higher Duty Cycle of the refrigerating unit will be experienced, compared to mild climatic conditions (Strasbourg).

On the other hand, for both Athens and Strasbourg, it is possible to notice that a higher ratio between cooling demand and cooling capacity is observed during the urban drive sections of the mission, in between the products deliveries. Such a behavior is connected to fact that the vehicle is performing urban driving cycles, characterized by an average lower speed, meaning that also the engine presents lower rotational speed and frequent idle speed operation. As a consequence, also the cooling unit compressor speed is lower, since the compressor is directly driven by the engine in BELT-CONF. This leads to a slightly reduced cooling capacity compared with the sections in which the vehicle is performing rural and suburban driving cycles. Furthermore, during the urban sections of the mission, the cooling demand is higher, to counteract the effects of hot air infiltrating inside the refrigerated box during door opening to deliver the transported goods.

Table 2.12 reports the average mission COP and Duty Cycle, evaluated through Eq. (2.23) and Eq. (2.24) respectively, for Athens and Strasbourg. The lower ambient temperature in Strasbourg allows obtaining a higher mission COP than in Athens, because of the lower energy required by the cooling unit's compressor, due to the lower pressure ratio between condensation and evaporation pressures. On the other hand, the lower cooling demand and the higher cooling capacity of the refrigeration system in Strasbourg, induced by the lower external ambient temperature, directly reduce the cooling unit Duty Cycle compared to Athens.

Table 2.12 – Average mission Coefficient of Performance and Duty Cycle for BELT-CONF in Athens and in Strasbourg.

	BELT-CONF ATHENS	**BELT-CONF STRASBOURG**
COP [-]	1.31	1.59
Duty cycle [-]	0.28	0.18

Alongside the analysis of the thermal behavior of the system under different climatic conditions, the impact of external ambient temperature on the environmental performance of the system was also considered. Following the same approach used Table 2.9, the overall fuel consumption and pollutant emissions related to the delivery mission (performed with BELT-CONF system layout) are reported in Table 2.13 for Athens and Strasbourg; the respective fuel consumption and emissions increase compared to the reference case with no cooling unit are also included in the table.

It can be observed that the fuel consumption is lower in Strasbourg than in Athens, due to the lower Duty Cycle of the cooling unit induced by the less severe ambient temperature during the day and the higher system COP. Pollutant emissions follow the same trend, presenting slightly lower values for Strasburg except for the THC emissions, which displays a minimal increase. When compared to the non-refrigerated reference case, the presence of the cooling unit in Strasbourg leads to a 17.5% increase of the fuel

consumption, a 32.7% increase of the CO emissions, a 8.6% increase of the NOx emissions, a 32.3% increase of the THC emissions and a 22.7% increase of the PM emissions compared to a vehicle with no cooling unit.

Table 2.13 – Overall fuel consumption and pollutant emissions of the vehicle during the daily delivery mission with no cooling unit and for BELT-CONF in Athens and in Strasbourg.

	No cooling unit	**BELT-CONF ATHENS**	**BELT-CONF STRASBOURG**
Fuel consumption [kg]	21.03	25.00 (+18.9%)	24.72 (+17.5%)
CO emissions [g]	323.87	430.12 (+32.8%)	429.68 (+32.7%)
NO_x emissions [g]	603.50	661.66 (+9.6%)	655.10 (+8.6%)
THC emissions [g]	68.63	90.60 (+32.0%)	90.79 (+32.3%)
PM emissions [g]	13.20	16.27 (+23.3%)	16.19 (+22.7%)

However, the numerical results highlight that the reduction of fuel consumption and pollutant emissions in mild climatic conditions compared to hot climatic conditions is very limited. Table 2.14 reports the relative variation of the considered parameters from Athens to Strasbourg. It can be observed from the results that the variation of the environmental impact of the cooling unit presence with climatic conditions is always comprised in the ±1% range, approximately.

Considering the results presented in Figure 2.15, Figure 2.16, Table 2.12 and Table 2.14, it can be concluded that the external climatic conditions do not have a strong influence on the improvement of the conditions in which the transported goods are stored during the mission and on the environmental performance of the system, but they can present a more remarkable impact on the Duty Cycle and on the ON/OFF management of the refrigerating unit.

Overall, comparing the effects of the variation of the cooling unit connection to the vehicle engine presented in Section 2.4 and of the variation of the external climatic conditions presented in Section 2.5, it can be concluded that an optimization of the cooling unit power supply system and of the vehicle engine management can lead to significant improvements on both the thermal and the environmental impact of the refrigerated transport sector, regardless of the climatic conditions.

Table 2.14 – Reduction of fuel consumption and pollutant emissions in Strasbourg, compared to Athens.

	BELT-CONF ATHENS	BELT-CONF STRASBOURG
Fuel consumption [kg]	25.00	24.72 (-1.1%)
CO emissions [g]	430.12	429.68 (-0.1%)
NO_x emissions [g]	661.66	655.10 (-1.0%)
THC emissions [g]	90.60	90.79 (+0.2%)
PM emissions [g]	16.27	16.19 (-0.5%)

2.6 Implementation of photovoltaic generators in a solar-aided cooling unit

The numerical results presented in Section 2.4 highlighted that the switch from a belt-driven compressor of the cooling unit to an electrical-controlled one, through the use of an alternator and of a battery pack, can significantly improve the performance of the refrigerating system under all aspects.

In fact, with the disconnection of the compressor from the vehicle engine and with an optimized compressor speed control the average air temperature inside the insulated box can be lowered, granting a better preservation of the transported goods (as illustrated in Figure 2.12); moreover, the average efficiency of the unit during the delivery mission can be improved (as testified by the COP increase reported in Table 2.7); finally, with the use of a battery pack, also the environmental impact of the cooling unit can be significantly mitigated (as highlighted by the fuel consumption and pollutant emissions reduction presented in Table 2.9 and Table 2.10).

The electrification of the refrigeration unit compressor suggested by the above-mentioned numerical results opens to the integration of renewables in the system, in particular to solar energy exploitation through photovoltaic (PV) panels, which can reduce even more the reliance of the cooling unit on fossil fuels and, as a consequence, the environmental impact of transport refrigeration systems.

Literature regarding the use of photovoltaic driven or aided refrigeration unit in the transport sector is limited and often dated, considering mostly plug-in long-distance transport applications [96] [97] [98] [99]. Conversely, in this section the refrigerated vehicle considered for the integration of PV technology will be a small size van employed in short-distance deliveries, as done in Section 2.4 and Section 2.5.

To reduce the battery capacity and to guarantee the required cooling effect, a hybrid solution is considered. The system runs normally on a battery pack that can be pre-charged from the electrical grid and is recharged by the solar panels when the solar radiation is available. Nevertheless, to extend the

system autonomy, the system can also rely on the vehicle internal combustion engine to guarantee functionality and food safety.

A preliminary stationary experimental tests campaign was previously performed to characterize the main components and to verify the robustness of the system design, whose results were used as a background for the numerical research activity carried out during the Ph.D. period. Based on the results of the preliminary experimental tests, dynamic numerical simulations of the complete system are run to assess the impact of the renewable energy on the energy consumption of the truck assuming a daily delivery mission in an urban area, presenting the results both on a daily and a seasonal scale.

2.6.1 Stationary experimental tests

An experimental campaign on a stationary setup was performed in June 2019 [100] to characterize the main components and to verify the robustness of the system design and it will be mentioned in this thesis as the necessary background to describe the environment in which the data used for post-process and for the results analysis, which was carried out during the Ph.D. research period, were collected.

For the stationary experimental campaign, the insulated body of a small refrigerated truck, available in the market, was selected as the preliminary test case. The insulated box main geometrical dimensions are reported in Table 2.15. The box was made of a polyurethane foam coated both on the internal and external sides with 1.5 mm fiberglass layer. Due to the insulated box limited size, no wooden reinforcements were included in the roof or the sidewalls, while a plywood plate and an array of wood beams reinforced the floor.

Table 2.15 – Main geometrical dimensions of the insulated body.

Element	Dimension
External height H_e	2.00 m
External length L_e	3.00 m
External width W_e	2.00 m
External surface S_e	32.00 m^2
Internal volume V_i	9.75 m^3

The insulated box was equipped with a simple R134a vapor compression refrigeration unit with the same schematic as the one presented in Figure 2.1, as it is representative of the standard technology in current transport refrigeration applications. The set-point value of the air temperature conditions inside the insulated box was set to 0°C. The compressor was driven by a DC electrical motor and it ran at constant speed. Consequently, the cooling capacity was modulated through an ON/OFF controller with a 3°C hysteresis between the maximum allowed temperature of 2°C and the minimum allowed temperature of -1°C.

The global heat transfer coefficient was evaluated through steady state experimental tests, carried out following the procedure defined in Annex 1 of the ATP agreement [82]. A global heat transfer coefficient K = 0.36 W m^{-2} K^{-1} was evaluated from the test: according to the ATP standards body types (IR classification), the considered refrigerated truck body as heavily insulated (K < 0.40 W m^{-2} K^{-1}).

The baseline reference system was then modified in order to include the photovoltaic generators, connected through a charge regulator to a battery pack powering the cooling unit. The photovoltaic generators were sized to cover the roof of the insulated box. Due to the limited area available (6 m^2), six panels are installed, leading to a nominal power of 940 W for 5.4 m^2 of active surface. A charge-controller was used in order to optimize the panel conversion efficiency and to transform the panel voltage to 24 V recharging the battery pack. The charge controller was also used to reduce the generated power when the battery pack reached the maximum charge. Four high capacity Pb–Ca car batteries were used, obtaining a maximum stored energy of $C_{bat,max}$ = 8.64 MJ at a voltage of 24 V.

The cooling unit compressor and fans were powered directly by the battery pack. However, in order to guarantee the cooling power required to maintain the refrigerated box at the design temperature, a backup power line, connected to the vehicle alternator, was included in the system. This line can be used to power the cooling unit in case the battery pack is fully discharged, due to a limited or non-sufficient production from the photovoltaic generators, and also to recharge the battery pack and run the system from the electrical grid when the vehicle is not is use or during the pulldown before the loading of the transported cargo.

The simplified schematic of the experimental setup is reported in Figure 2.17, while the actual experimental setup is presented in Figure 2.18.

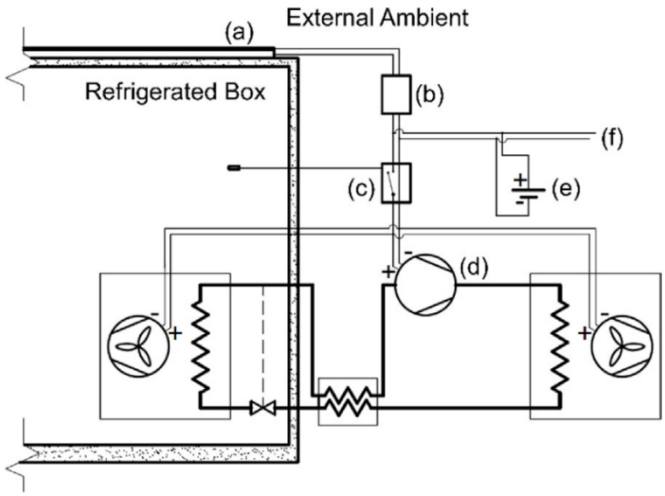

Figure 2.17 – Refrigeration system integrated with photovoltaic generators: (a) photovoltaic panels; (b) charge regulator; (c) thermostat; (d) compressor; (e) battery pack; (f) backup line connected to the vehicle alternator.

Figure 2.18 – Stationary experimental setup.

The insulated box was positioned in full sun position, with the solar panel fixed over the roof of the insulated box. The prototype was equipped with temperature and humidity sensors to monitor both the internal and the external temperature. The power flows were monitored by recording the battery voltage and the electric currents by means of Hall effect current transducers.

The experimental facility was located at the Construction Technology Institute of the National Research Council in Padova and it was placed so to be unaffected by the shadows of the surrounding buildings. As previously mentioned, the data were recorded in June 2019, and they were used to perform the results analysis which will be described below. Data acquisition was carried out using an Arduino Mega board logging the data with a period of two seconds.

Two different sets of data are considered to present the results. In the first set of data (Scenario A) the pull-down was performed: the cooling unit was switched on after two days of inactivity at 8:30 in the morning and then maintained active for the rest of the week. In the second set of data (Scenario B), the unit was running continuously since the first start of the system 5 days before.

Starting from Scenario A, the power produced by the photovoltaic generators from 6:00 to 21:00 and the solar radiation are presented in Figure 2.19a. Before 08:30, the charge regulator limits the power production, since the battery pack is already at full charge. Once the cooling unit is switched on at 08:30, the charge regulator allows the PV panels to produce the maximum power, in order to recover the energy drained from the battery pack to power the unit during the pulldown.

During the morning, the power required to perform the pulldown of the insulated box to the temperature setpoint is high, and the production of the PV panels follows the same trend of the solar radiation (Figure 2.19b). Since the cooling unit was turned on after two days of inactivity, in which the insulated box was in thermal equilibrium with the warm external environment, the ON period is significantly longer than the OFF period of a complete ON/OFF cycle set by the thermostat.

After 12:00, instead, the insulated box has reached the desired temperature setpoint and the thermal inertia gained after the whole morning helps reducing the length of the ON period and increasing the OFF period of a complete ON/OFF cycle (Figure 2.19c). For this reason, the energy produced by the PV panels becomes sufficient to fully recharge the battery pack, and the charge regulator progressively limits the power production at the end of the ON/OFF cycle.

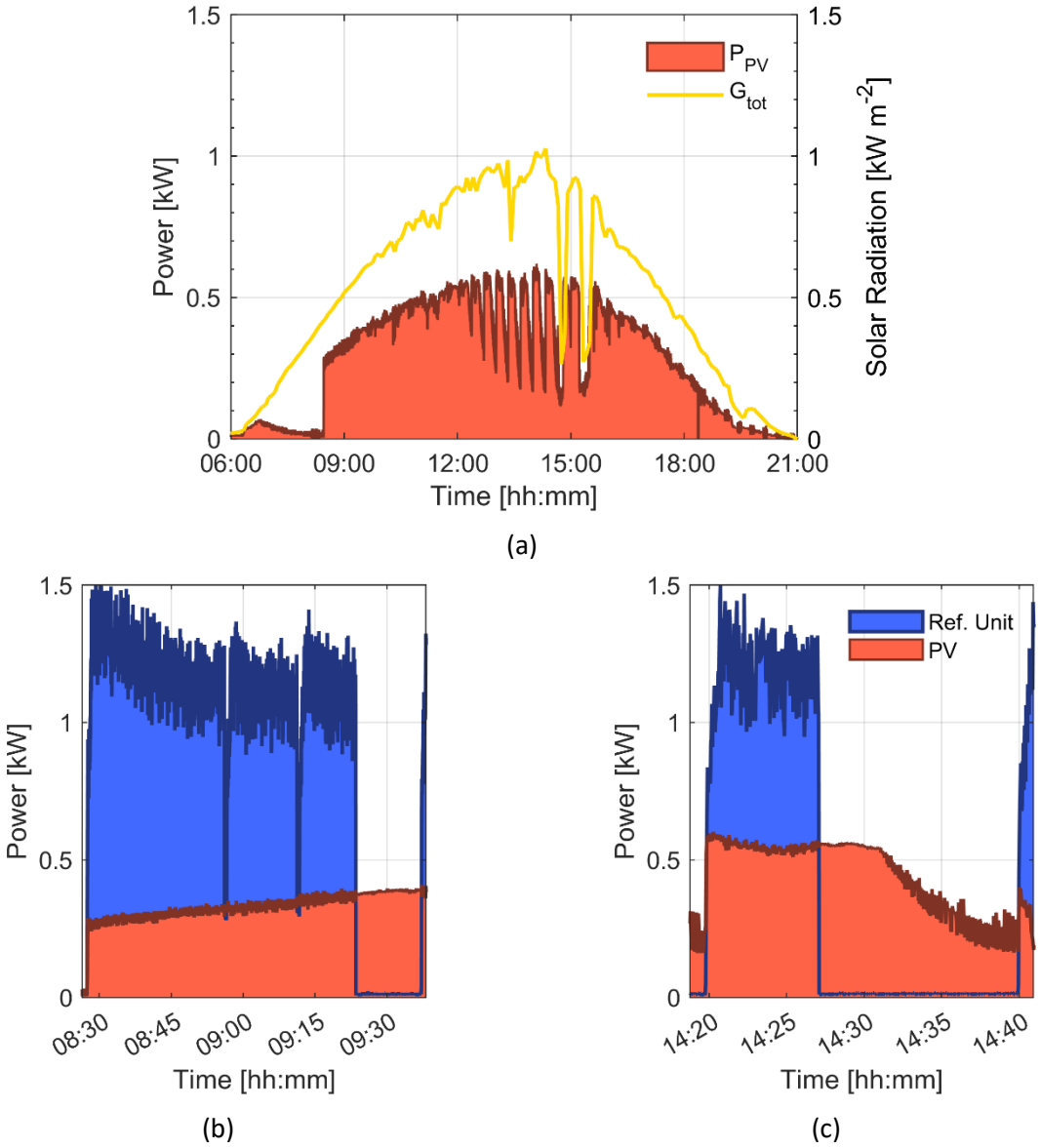

Figure 2.19 – Solar power production in Scenario A: (a) daily power production and solar radiation; (b) and (c) highlight of the cooling unit power consumption and solar production during an ON/OFF cycle.

To allow the comparison between the energy continuously produced by the PV panels and the energy consumed by the cooling unit, which works on ON/OFF cycles, the energy data balances are averaged for every ON/OFF cycle in Figure 2.20.

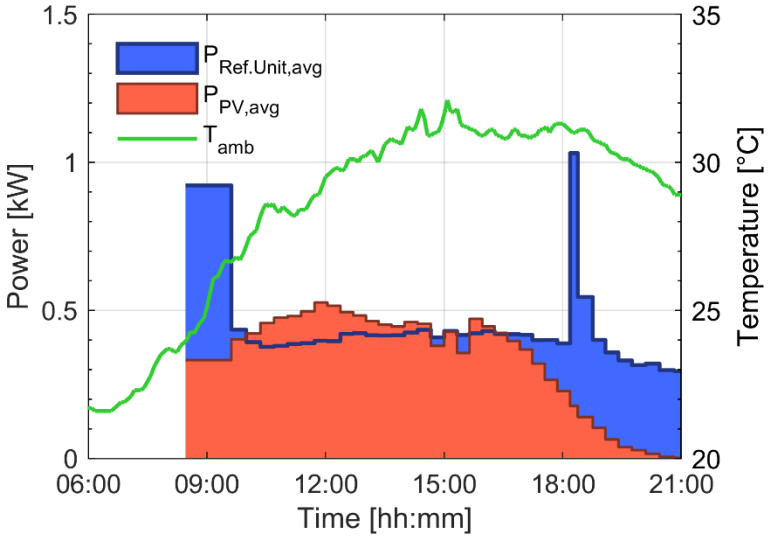

Figure 2.20 – Cooling unit power consumption and power generated by PV panels averaged over every ON/OFF cycle in Scenario A.

Figure 2.21 presents the cumulative energy demand of the cooling unit considering the overall consumed energy during the day, as defined in Eq. (2.27), and the net energy trend, normalized on the nominal battery capacity, as defined in Eq. (2.28), assuming the batteries are fully charged before the start of the day.

$$e_{Ref.Unit} = 1 - \frac{\int_{00:00}^{t} P_{Ref.Unit}\, d\tau}{C_{bat,max}} \tag{2.27}$$

$$e_{Net} = 1 - \frac{\int_{00:00}^{t} \left(P_{Ref.Unit} - P_{PV}\right) d\tau}{C_{bat,max}} \tag{2.28}$$

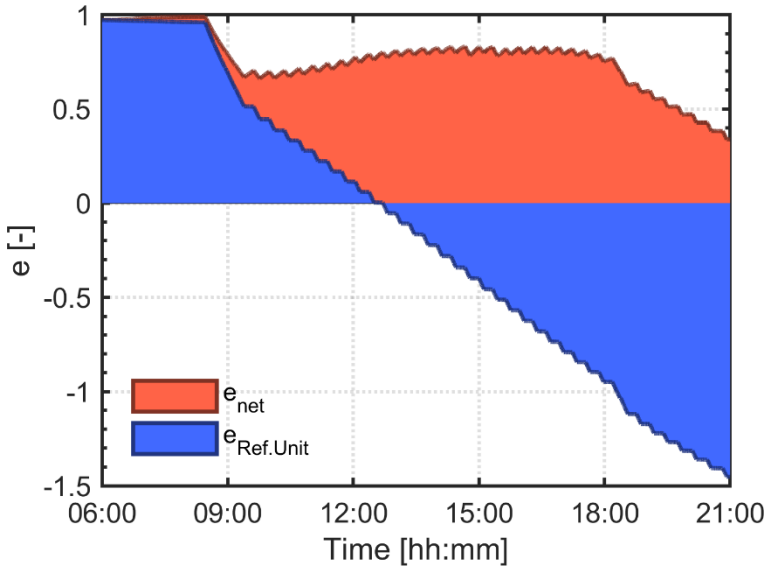

Figure 2.21 – Cumulative net energy consumption and cooling unit energy consumption in Scenario A.

As expected, the first ON/OFF cycle is characterized by a high power consumption of the cooling unit, as the internal temperature is lowered from ambient temperature conditions to the desired temperature

setpoint of 0°C. During this ON/OFF cycle, the PV panels can recover only partially the energy required by the cooling unit, and consequently the battery pack charge level decreases.

On the contrary, in the middle hours of the day, when the PV panels can produce more energy than the average energy consumed by the cooling unit, an increase in the battery charge level occurs, which then becomes stable at around 84% of the full capacity.

However, at late afternoon (around 18:00), the solar radiation decreases significantly, while the power required by the cooling unit is still high, due to the warm external temperature conditions, resulting in a decrease of the battery pack charge level. Furthermore, a scheduled electrical defrost is performed at 18:00 (represented by the peak in the refrigeration unit power request in Figure 2.20), speeding up even more the battery discharge.

The same data presented for Scenario A are evaluated also for the Scenario B, in which the insulated box is already at the desired temperature range, since the cooling unit was kept operating continuously for five days from the initial switch on occurred in Scenario A. For this reason, in Scenario B no initial pulldown was necessary. This scenario can be representative of a truck not fully unloaded between two consecutive working days, where the cooling unit is powered using the engine or the grid energy during the night.

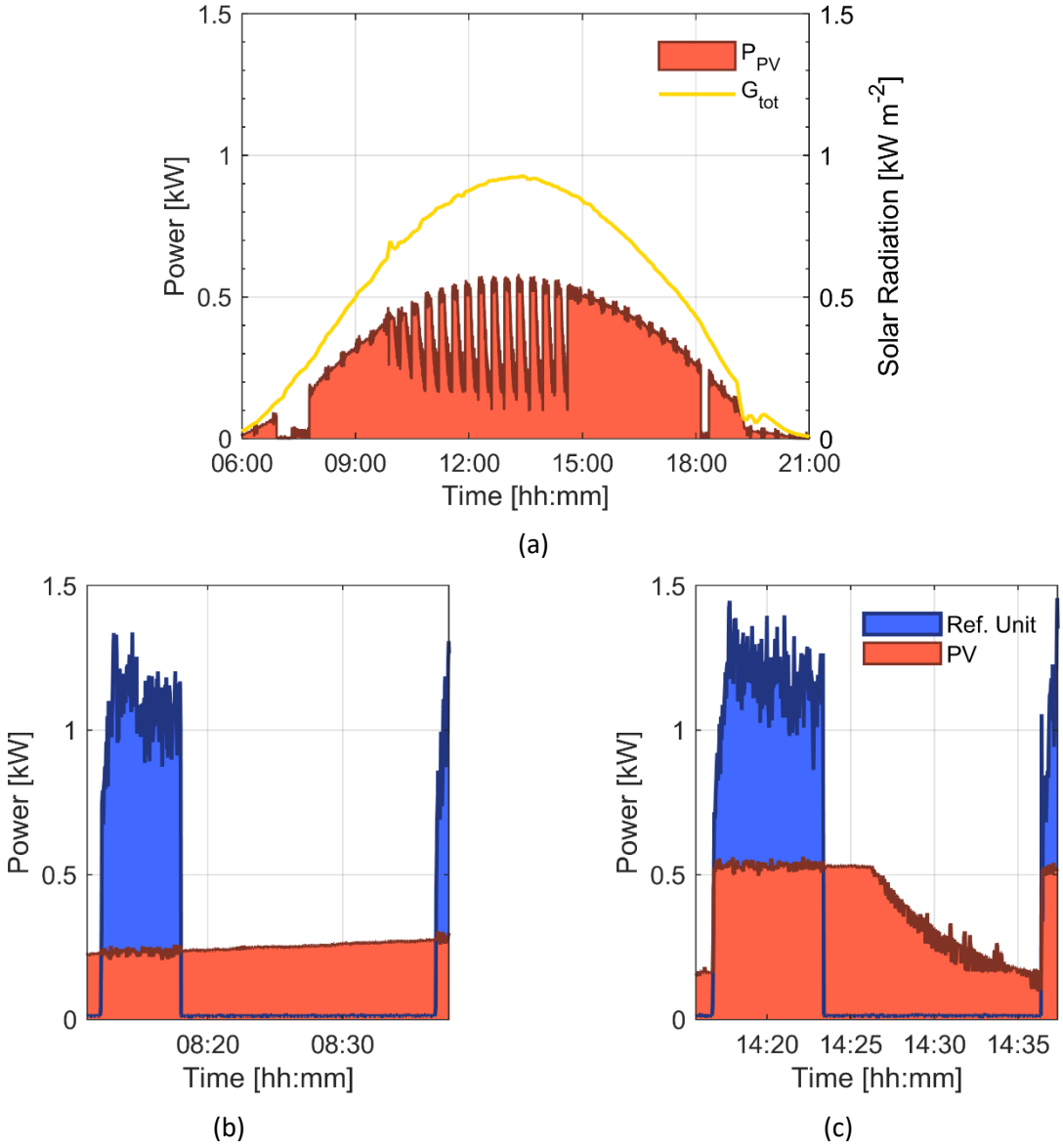

Figure 2.22 – Solar power production in Scenario B: (a) daily power production and solar radiation; (b) and (c) highlight of the cooling unit power consumption and solar production during an ON/OFF cycle.

Despite the PV panels can contribute to the net energy balance only during daytime, when the solar radiation is available, it can be clearly observed from Figure 2.22b and Figure 2.22c that the length of the ON periods and the overall length of the ON/OFF cycles in Scenario B is reduced compared with the ones registered in Scenario A. Moreover, Figure 2.22a highlights that the reduction of the power produced by the PV panels imposed by the charge regulator begins significantly earlier in the day compared to Scenario A.

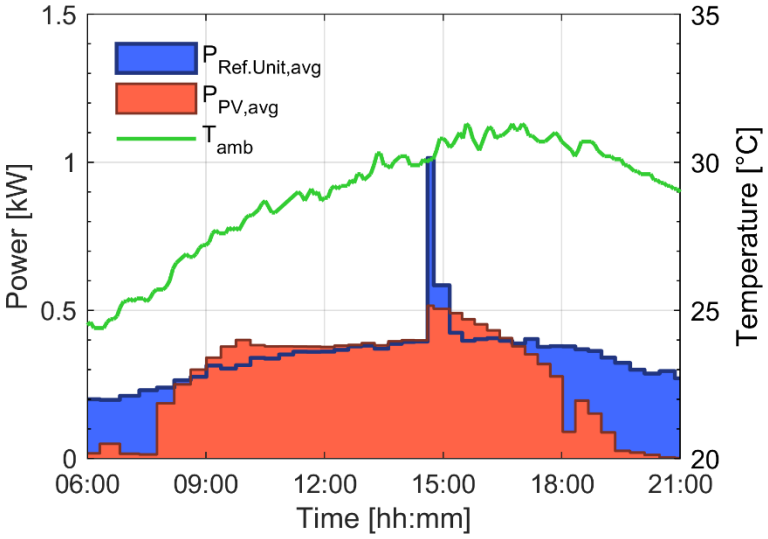

Figure 2.23 – Cooling unit power consumption and power generated by PV panels averaged over every ON/OFF cycle in Scenario B.

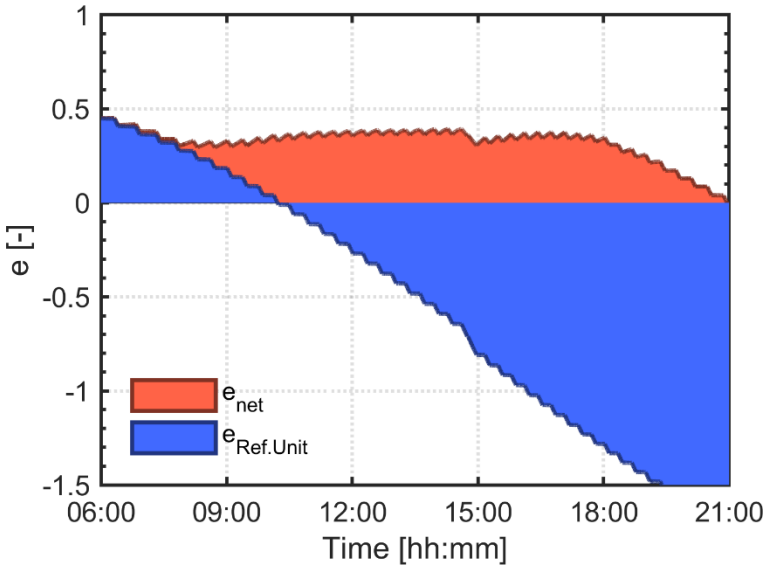

Figure 2.24 – Cumulative net energy consumption and cooling unit energy consumption in Scenario B.

In order to quantify the impact of the solar energy in the system, the energy produced by the PV panel is normalized on the overall consumption of the cooling unit, as described in Eq. (2.29):

$$\beta(t) = \frac{E_{Net} - E_{Ref.Unit}}{1 - E_{Ref.Unit}} = \frac{\int_{00:00}^{t} P_{PV}\, d\tau}{\int_{00:00}^{t} P_{Ref.Unit}\, d\tau} \tag{2.29}$$

The β ratio depends on the time and decreases as the evaluation time is moved to the late afternoon, due to the decrease of the solar radiation occurring towards sunset. Table 2.16 reports the β ratio for both Scenario A and Scenario B, considering the evaluation time at 13:00, 18:00 and 24:00, representative of a half-day, full working day and continuous use of the unit, respectively.

Table 2.16 – Ratio between solar energy production and cooling unit overall consumption.

Scenario	Reference ending time 13:00	Reference ending time 18:00	Reference ending time 24:00
Scenario A	83.7%	88.6%	65.5%
Scenario B	53.7%	70.0%	56.0%

The experimental results presented in Table 2.16 highlight the ability of the PV panels to cover major part of the overall cooling unit energy demand and, consequently, to significantly reduce the energy supplied to the unit by an external energy source.

2.6.2 Numerical simulation of the yearly performance during a delivery mission

The limited extent of the experimental campaign and the stationary nature of the experimental setup prevent any generalization of the experimental results to the system actual working conditions, which correspond to the refrigeration of a small van employed in a delivery of temperature-controlled goods. To estimate the impact of such a solution on a mobile application, a numerical model is developed and used to simulate the system during a daily delivery mission under different ambient conditions.

The numerical model of the refrigeration system is developed using the commercial software Simcenter Amesim v.17. The refrigerated box numerical model and the cooling unit numerical model are developed following the same assumptions, the same discretization in lumped volumes and the same governing equations described in Section 2.2.2 and Section 2.2.3, respectively. In addition to the already described insulated box and cooling unit numerical models, the solar system is modelled as follows.

The PV panels are located on the top of the insulated box, in direct contact with the box roof. Following this assumption, the overall cooling demand of the insulated box is slightly increased, as a consequence of the local increase of both the surface emissivity (ϵ_{box} = 0.70, ϵ_{roof} = 0.8) and the short-wave surface absorptivity ($a_{s,box}$ = 0.15, $a_{s,roof}$ = 0.9) compared to the white fiberglass composite. Nevertheless, this type of installation is preferred for transport refrigeration applications, since the presence of an air gap between the PV panels and the insulated box roof would not increase the cooling demand but it would lead to potentially greater issues such as vibrations, noise and structural problems during the vehicle motion.

The PV generators efficiency in standard conditions is assumed equal to η_{PV} = 0.21, as defined in the datasheet provided by the manufacturer.

The electrical converted power is evaluated as described in Eq. (2.30), in which A represents the total surface of the PV panels, G_{dh} represents the diffuse solar radiation and $\bar{n} \cdot \bar{G}_f$ represents the direct solar radiation in the normal direction.

$$P_{PV} = \eta_{PV} A (G_{dh} - \bar{n} \cdot \bar{G}_f) \tag{2.30}$$

The delivery mission considered for the numerical simulation of the system is characterized by the same structure described in Section 2.3 (Table 2.6). A reference mean day for each month of the year in the city of Athens has been chosen for an annual evaluation of the system performance in European hot areas. The environmental temperature, relative humidity and solar radiation intensity, available in the Energy Plus online database [95], were collected for all the days of each month of the year and then averaged hourly to obtain the climatic profile of the mean day of each of the months of the year. The use of a reference mean day as the representation of each month is functional to evaluate the average performance of the system, since the sky cover and the solar radiation can have significant discontinuities between consecutive days, leading to results that are excessively dependent on the day chosen as a reference.

Firstly, the numerical results obtained from the delivery mission simulations in the months of August and May, representative of hot and mid-season operating conditions respectively, are presented and discussed, to assess the influence of the ambient temperature conditions on the unit performance.

The evolution during the daily mission of the temperature of the air inside the insulated box T_i averaged over each ON/OFF cycle, the temperature of the transported goods T_{im} and the ambient temperature T_{amb} is reported in Figure 2.25. In both cases, the numerical results highlight the ability of the cooling unit to maintain a stable internal temperature T_i throughout the whole mission, quickly recovering the desired conditions after every door opening.

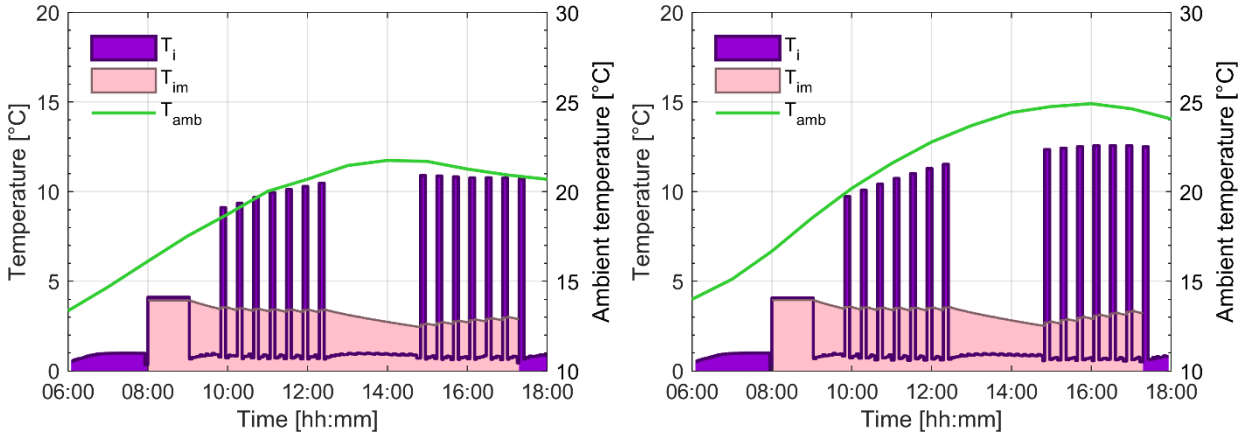

Figure 2.25 – Internal, external and transported goods temperatures, averaged on each ON/OFF cycle: (a) May; (b) August.

Similarly to what has been investigated with the results of the stationary experimental campaign, the power consumption of the refrigeration system and the power production of the PV panels is compared in Figure 2.26.

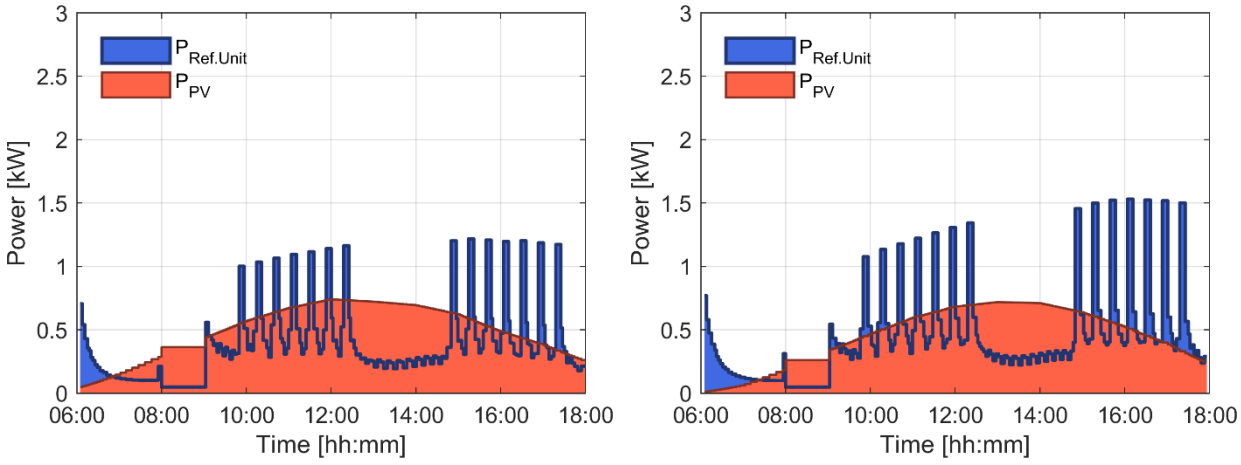

Figure 2.26 – Cooling unit power consumption and PV panels generated power, averaged on each ON/OFF cycle: (a) May; (b) August.

The power demand from the cooling unit presents several peaks which exceed the power generated by the PV panels. These power demand peaks correspond to three different situations along the delivery mission:

- The pulldown of the insulated box from the initial conditions, in which the box is in thermal equilibrium with the external environment after a whole night of inactivity, to the desired internal temperature range conditions, occurring in the first two hours in the early morning (from 06:00 to 08:00);
- The first switch on of the cooling unit after the loading operations of the products to be transported (at 09:00), which is shorter than the initial pulldown since the loading operations take place in a controlled environment with temperature fixed at 4°C;
- The first switch on of the cooling unit after each of the delivery stops, in which the doors are opened and part of the transported cargo is unloaded, causing external air infiltrations (occurring seven times in the morning and seven times in the afternoon).

As it was described in the system schematic presented in Figure 2.17, the energy demand of the cooling unit is supplied by the battery pack, as long as the batteries have a sufficient charge level to provide the requested energy. When the batteries are totally discharged and the instant power requested by the refrigeration unit is greater than the power provided by the photovoltaic panels, the refrigerating unit relies on an external power source, i.e. the vehicle alternator. At the same time, the battery pack can store the power produced by the PV panels that exceeds the instant consumption of the refrigerated unit. The system operation is then significantly affected by the battery pack nominal capacity: larger batteries increase the system autonomy, reducing the need of an external power source, but at the same time they increase the system mass and cost.

Therefore, three different battery pack capacities (2.16 MJ, 4.32 MJ and 8.64 MJ, corresponding to a capacity of 25 Ah, 50 Ah and 100 Ah at a voltage of 24 V, respectively) are considered in the simulations, to assess the effect of the battery pack capacity on the system operation. In every case, the battery pack capacity is initialized to half of the maximum nominal capacity at the beginning of the delivery mission.

The stored energy in the battery pack for each of the different capacities considered in the model are reported in Figure 2.27. Negative values of the battery charge level represent the energy required by the cooling unit which is not supplied by the battery pack, since the batteries are completely discharged, and which have to be provided by the external energy source.

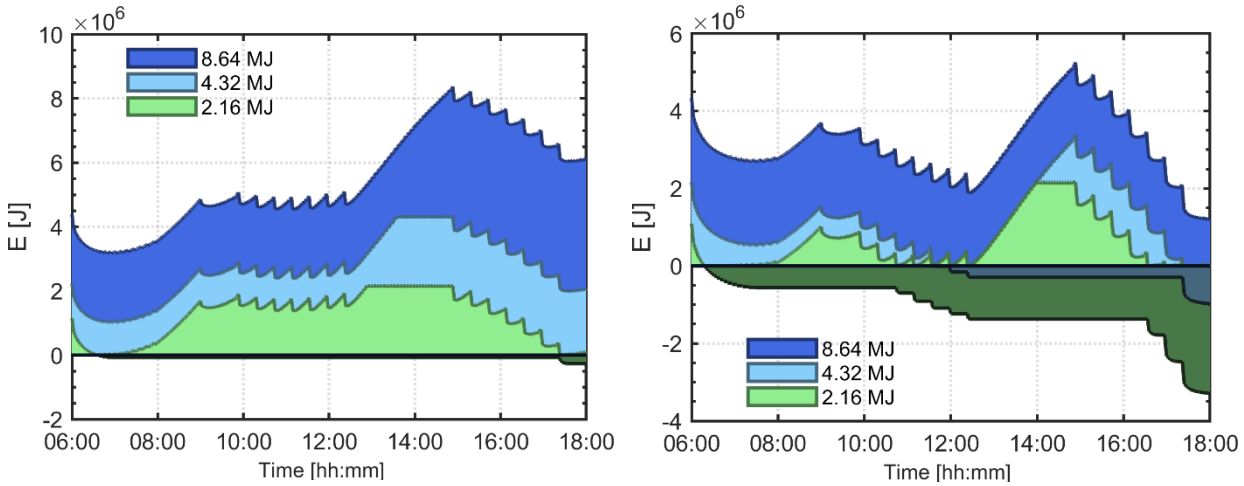

Figure 2.27 – Battery pack charge level: (a) May; (b) August. Negative values represent the energy provided by the external source.

It can be observed that, during the driving sections and during the long pause between the morning deliveries and the afternoon deliveries, the PV panels contribute significantly to provide the necessary energy to the cooling unit and to simultaneously charge the battery pack with the excess energy production, both for May and August. On the other side, the charge level during the pulldown and the actual delivery sections of the mission is strongly affected by the external ambient temperature conditions.

In May, the mild ambient temperature leads to a lower cooling demand to maintain the temperature inside the insulated box within the desired range and, consequently, to a lower energy draw of the compressor and heat exchangers fans. The energy required to reset the desired internal air temperature is lower than the overall energy produced by the PV panels, and a progressive recharge of the battery pack occurs. Under these climatic conditions, all the battery pack capacities can run the system without relying on the backup power supply.

On the contrary, in August the hot ambient temperature leads to a significantly higher cooling demand inside the insulated box and to a consequent increase of the colling unit energy consumption. The

increased energy demand of the cooling unit leads to different behaviors for each of the considered battery packs. The two higher capacity batteries present almost the same behavior once the graph is shifted accordingly to the different initial value. For both the cases, the battery packs reach the same overall daily balance of −1.25 MJ. However, while the larger one (8.64 MJ) does not draw power from the external backup source, the 4.32 MJ capacity one is fully discharged twice, requiring the system to run on the external vehicle alternator at the end of each delivery session (late morning and late afternoon). On the other side, when the smallest battery pack is considered, the limited nominal capacity does not allow to completely exploit the available solar source, as the charge regulator limits the PV panels power production when the battery is fully charged at around 14:00. Consequently, the overall energy balance at the end of the mission is worse compared to the other two cases (−2.75 MJ), as part of the available solar energy was wasted due to the limited battery pack capacity.

After focusing on May and August simulations to highlight the influence of specific parameters on the system performance, the yearly results are presented in Figure 2.28.

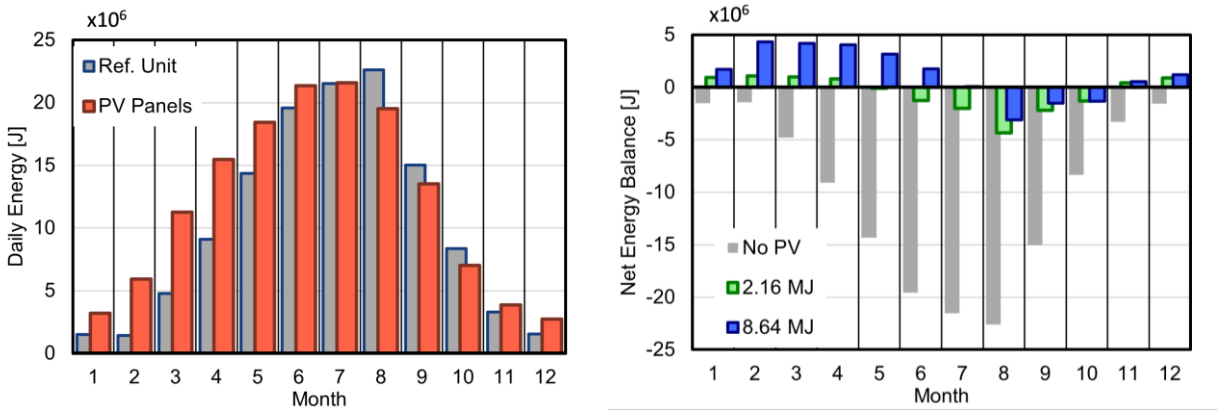

(a) (b)

Figure 2.28 – Yearly system performance: (a) daily energy produced by the PV panels and consumed by the cooling unit; (b) net daily energy balance for different battery pack capacities.

Figure 2.28a reports the total energy produced by the PV panels during the day considered for the delivery mission simulation, as well as the total energy consumed by the cooling unit, for each month of the year. The energy produced by the PV panels exceeds the one consumed by the cooling unit for most of the months in the year, with the exception of August, September and October.

On the other hand, Figure 2.28b reports the net energy balance of the daily mission for each month of the year. Following the results presented in Figure 2.27, which highlighted the crucial influence of the battery pack nominal capacity on the net energy balance of the mission, the smallest capacity (2.16 MJ) and highest capacity (8.64 MJ) are considered and compared to a baseline case without the presence of the PV panels, in which the cooling unit power demand is supplied entirely by the vehicle alternator. The presence of the photovoltaic system significantly reduces the energy drained from the external source for

both the considered battery pack capacities. The main difference between the two arrangements is visible during the first half of the year, where the largest capacity leads to a significant net energy gain, which can contribute to sustain the vehicle auxiliary systems such as lightning and air conditioning systems.

The ambient data used for the numerical simulations presented above already accounts for the effect of sky cover, due to fog or clouds, since the solar radiation is evaluated through a monthly average of the single days data. However, since the delivery mission takes place in an urban environment, the effect of shading induced by the presence of buildings (known as urban canyon effect [101]) has to be considered as an additional factor which could lower the available solar radiation to the refrigeration system PV panels.

The actual amount of direct radiation collected by the PV panels can be obtained only assuming the structure of the urban environment: urban canyon aspect ratio, average length and orientation. In order to discuss the impact of the urban environment three abstract cases are considered:

- A best-case scenario (full-DSR) in which no effect of additional shading due to the urban environment is considered. This scenario is characterized by the full presence of the Direct Solar Radiation (DSR) and corresponds to the environmental conditions already considered for the whole results analysis presented above;
- A worst-case scenario (no-DSR) in which complete shading of the DSR is considered for the whole delivery mission time, and therefore only the Diffuse Horizontal Radiation (DHR) contributes to the Global Horizontal Radiation (GHR);
- An intermediate condition (partial-DSR) in which the DSR is assumed to be obscured only when the refrigerated vehicle is driving in the urban environment.

The influence of the additional shading due to the urban canyon effect on the net energy balance of the daily delivery mission is presented in Figure 2.29.

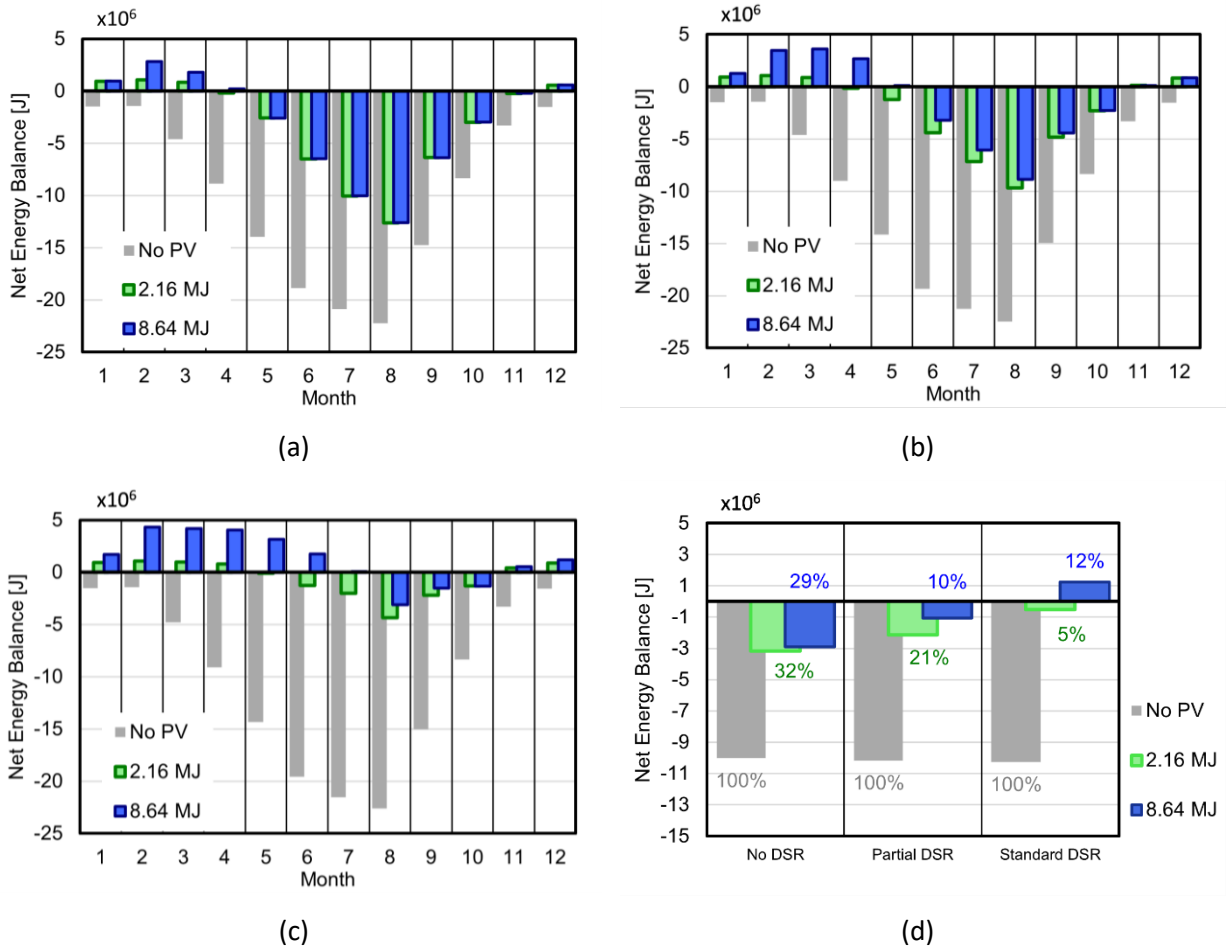

Figure 2.29 – Net energy balance as a function of the shading conditions, with no PV panels and with battery pack capacity of 2.16 MJ and 8.64 MJ: (a) no DSR (worst-case scenario); (b) partial DSR; (c) full DSR (best-case scenario); (d) yearly average net energy balance (percentage expressed with the case of no PV panels as a reference).

The largest battery pack can be exploited efficiently only in case of limited shading (Figure 2.29b-c), when the PV panels are able to collect the direct solar radiation. In fact, in case of no DSR (when only diffuse radiation is available, Figure 2.29a), the net energy balance of the mission is almost identical between the two cases involving the PV panels, regardless of the battery pack capacity.

The average yearly results are summarized in Figure 2.29d, where the baseline case of absence of the PV panels is used as the comparison to express the percentage of the net energy balance of the delivery mission.

The presence of the PV panels significantly reduces the energy draw of the cooling unit from the external source even in case of complete absence of direct solar radiation, providing more than two thirds of the required energy on a yearly basis. However, as above mentioned, in case of no DSR the increase of the battery pack capacity from 2.16 MJ to 8.64 MJ does not lead to a proportional reduction in energy saving ($\Delta E \cong 3\%$). The system becomes more and more efficient as more direct solar radiation is considered, lowering the energy request to the 5% (2.16 MJ battery pack) or producing a net energy excess of the 12%

(8.64 MJ battery pack) when no urban canyon effect is taken into account, compared to the baseline case with no PV panels. In this case, the battery pack capacity increase can be fully exploited, leading to a significant reduction in energy saving ($\Delta E \cong 17\%$).

2.7 Conclusions

This chapter presented the dynamic numerical simulation of a medium-size van for the urban delivery of temperature-controlled goods. The vehicle was equipped with an insulated box in which the perishable products were stored, and which was kept under the desired temperature conditions throughout an urban multi-drop delivery mission by a R134a vapor compression refrigerating system. The software Simcenter Amesim v.17 was used for the development of the numerical model of the entire system, including the simulation of the unsteady operation of both the cooling unit and the vehicle engine, as well as the thermal energy balance of the insulated box. The fuel consumption and the pollutant emissions of the engine were evaluated throughout the delivery mission. Moreover, operation under different climatic conditions (Athens, representative of hot European climate, and Strasbourg, representative of mild European climate) was considered.

Three different system layouts, which differ regarding the type of connection between the cooling unit compressor and the vehicle prime engine, were modelled. In the first configuration, a direct-drive connection between the vehicle main shaft and the refrigerating system compressor was considered. In the second configuration, the introduction of an alternator untied the compressor rotational speed to the engine rotational speed, allowing an optimization of the compressor efficiency and of the refrigerating system cooling effect. In the third configuration, the use of an energy storage device, namely a battery, was proposed to produce, store and provide the required energy to the refrigerating system, thus leading to the possibility to switch off the vehicle engine during some sections of the delivery mission.

As a direct extension of the third configuration, the additional presence of photovoltaic panels mounted above the roof of the insulated box is considered, producing energy from a renewable source which can be stored inside the battery pack and then used by the cooling unit, thus reducing the overall energy draw of the refrigeration system from the vehicle engine.

The main results obtained in this chapter can be summarized as follows:

- Considering operation in hot European climatic conditions (Athens), the average mission COP of the refrigerating system is equal to 1.31 with a direct connection between cooling unit and vehicle engine (BELT-CONF) and to 1.65 when an alternator is used to decouple the rotational speed of the engine and of the compressor, providing an optimization of the latter (ALT-CONF and BAT-CONF). In addition, an overall Duty Cycle equal to 0.28 for the belt-driven configuration and to

0.39 for the electrically-driven configurations is calculated. The introduction of the alternator to disconnect the cooling unit from the engine leads to a 26% increase of the mission COP and a 39.3% increase of the Duty Cycle of the refrigerating system.

- The compressor connection to the vehicle engine has a significant effect on the temperature of the air inside the insulated box, and consequently on the temperature of the transported cargo. In the belt-driven configuration, the heavily varying compressor speed causes irregular ON/OFF cycles of the refrigerating unit and a not constant cooling capacity profile. Conversely, in the electrically-driven configurations the compressor speed is set and optimized by the alternator regardless of the vehicle engine operating conditions, and as a consequence a better management of the internal air conditions can be achieved. In particular, the decoupling of the engine rotational speed and of the compressor rotational speed leads to a lower internal air temperature on the average, thus improving the preservation of the transported cargo during the delivery mission.
- The introduction of a battery as an electrical energy storage dedicated to the cooling unit operation (BAT-CONF) leads to the disconnection between the power demand of the refrigerating system and the power production to be performed by the engine. In fact, for BELT-CONF and ALT-CONF, the power required by the cooling unit was produced instantly by the engine; for this reason, the vehicle engine can not be turned off in any part of the mission. Conversely, in BAT-CONF, the engine can be switched off when the vehicle is still, as the power required by the cooling unit is withdrawn from the battery, which will be then recharged when the engine is already switched on to perform the mission driving cycles.
- While the compressor operation is optimized in ALT-CONF and in BAT-CONF than in BELT-CONF, leading to an energy consumption reduction for this specific component (-23.0% and -21.2% respectively), on the whole the mechanical energy that the engine must produce to run the cooling unit is higher in ALT-CONF and in BAT-CONF than in BELT-CONF (+8.4% and +10.6% respectively). The use of an alternator, in fact, leads to a lower overall energy transmission efficiency for ALT-CONF and BAT-CONF (0.72) because it requires two energy conversions (from mechanical to electrical and then from electrical to mechanical), while the BELT-CONF is characterized by an energy transmission efficiency of 0.94 linked only to mechanical losses along the power line.
- The presence and the operation of the cooling unit during the daily delivery mission lead to a 19.0% increase of the fuel consumption, a 33.2% increase of the CO emissions, a 9.5% increase of the NOx emissions, a 32.2% increase of the THC emissions and a 23.5% increase of the PM emissions, on the average, compared to the same vehicle performing the same delivery mission without powering a cooling unit. However, when the use of a cooling unit is mandatory to

preserve the cold chain, the use of a battery can significantly mitigate the impact of the presence of the cooling unit on the engine operation, giving the possibility to switch off the engine when the vehicle is still and to produce the additional energy dedicated to the cooling unit only during the driving sections of the mission. The implementation of the battery to store the energy produced by the engine and to allow a Start&Stop management of the engine itself can lead to a 11.1% reduction of the fuel consumption, a 24.0% reduction of the CO emissions, a 1.1% reduction of the NOx emissions, a 25.0% reduction of the THC emissions and a 16.6% reduction of the PM emissions compared with the use of a direct belt connection between the engine shaft and the cooling unit.

- Considering operation in BELT-CONF in mild European climatic conditions (Strasbourg), the average mission COP of the refrigerating system becomes equal to 1.59 thanks to the less severe external temperature level. On the other hand, the overall Duty Cycle drops down to 0.18, because of the lower need to remove heat from the insulated box.
- The external climatic conditions do not have a strong influence on the improvement of the internal air conditions in which the transported goods are stored during the mission as well as on the environmental performance of the system. Overall, the variation of the fuel consumption and of the pollutant emissions due to the cooling unit presence with climatic conditions is always comprised in the ±1% range, approximately. However, the external climatic conditions present a more remarkable impact on the Duty Cycle and on the ON/OFF management of the refrigerating unit, as they have a direct influence on both the cooling capacity and the cooling demand of the system.
- The introduction in the refrigeration system schematic of photovoltaic panels for energy production from the renewable solar source is evaluated. Firstly, a stationary experimental test is conducted, demonstrating the ability of the solar system to significantly contribute to the overall energy balance under early summer conditions, providing 65.5% of the energy required to run the cooling unit on the first full day of activity and 56.0% of the energy on the last full day after five consecutive days of activity.
- Numerical simulations of the solar-aided refrigeration system employed in a typical daily delivery mission in an urban environment highlight that the presence of the PV panels can reduce by 95% the power drawn from the vehicle engine, in case of small battery pack capacity (2.16 MJ). With the use of a larger battery pack (8.64 MJ), the performance of the system can be improved up to 17%, leading to a net +12% energy excess on a yearly basis.
- Even in case additional shading due to the presence of buildings limits the direct solar radiation available to the PV panels, the energy production obtained from diffuse radiation only leads to a 68% reduction of the power drawn from the vehicle engine, in case of small battery pack capacity

(2.16 MJ). Full shading conditions, however, limit the ability to exploit a larger battery pack capacity, as the switch to a 8.64 MJ battery pack leads to a 3% improvement of the net energy balance on a yearly basis.

3 Design, modelling and application of a R744 cooling unit for single-temperature refrigerated transport applications

After the evaluation of the indirect environmental impact of current road transport refrigeration systems based on HFC refrigerants, the improvement of the environmental sustainability of these kind of cooling units needs to be addressed through the implementation of low-GWP refrigerants. In particular, R744 (CO_2) is selected for its negligible impact on Green-House Effect, for its thermodynamic and safety characteristics, as well as for the ever-growing development of stationary refrigeration applications employing this natural refrigerant.

In this chapter, the design of a R744 cooling unit designed to provide MT refrigeration in road temperature-controlled transport applications is presented and the numerical model of a R744 cooling unit serving the needs of a small refrigerated van in an urban delivery mission of perishable goods is developed. The steady state performance and the unsteady operation of the system performing ON/OFF cycles to maintain a desired temperature range inside the insulated box will be evaluated considering three possible system configurations. Results will be useful to develop a configuration control strategy of the cooling unit, to maximize the cooling effect or the system COP as a function of the operating conditions. The numerical simulation of a short-range multi-drop delivery mission (for every month of the year) and of a long-range single-drop delivery mission (for the hottest month of the year) will be carried out to evaluate the performance of the cooling unit when employed during delivery missions of temperature-controlled goods, both in urban and extra-urban environment.

3.1 Refrigerating system design

The refrigerating system considered in this chapter consists of a R744 cooling unit designed to provide Medium-Temperature (MT) refrigeration in road temperature-controlled transport applications. Consistently with the usual temperature range in which chilled goods are transported in refrigerated vehicles, the cooling effect of the unit is designed to be provided at an air temperature inside the insulated box ranging between approximately -5°C to 5°C.

The cooling unit schematic is presented in Figure 3.1. Depending on the external environmental conditions, the system can operate in both subcritical and transcritical mode. The presence of four solenoid valves (S-1, S-2, S-3 and S-4 in the figure) allows running the refrigerating unit according to three different operating cycles.

The reference cycle is given by a classical low-pressure receiver cycle employing a simple high-pressure valve (HPV) for the refrigerant expansion and for the simultaneous control of the pressure at the outlet

of the gas cooler. In warm and hot environmental temperature conditions, the refrigerating system can also operate following an ejector transcritical cycle, exploiting the parallel between the HPV and a fixed-geometry two-phase ejector. The introduction of an auxiliary evaporator in the line between the ejector outlet nozzle and the liquid separator can provide a further modification of the ejector transcritical cycle. The different configurations will be presented in detail later in this section.

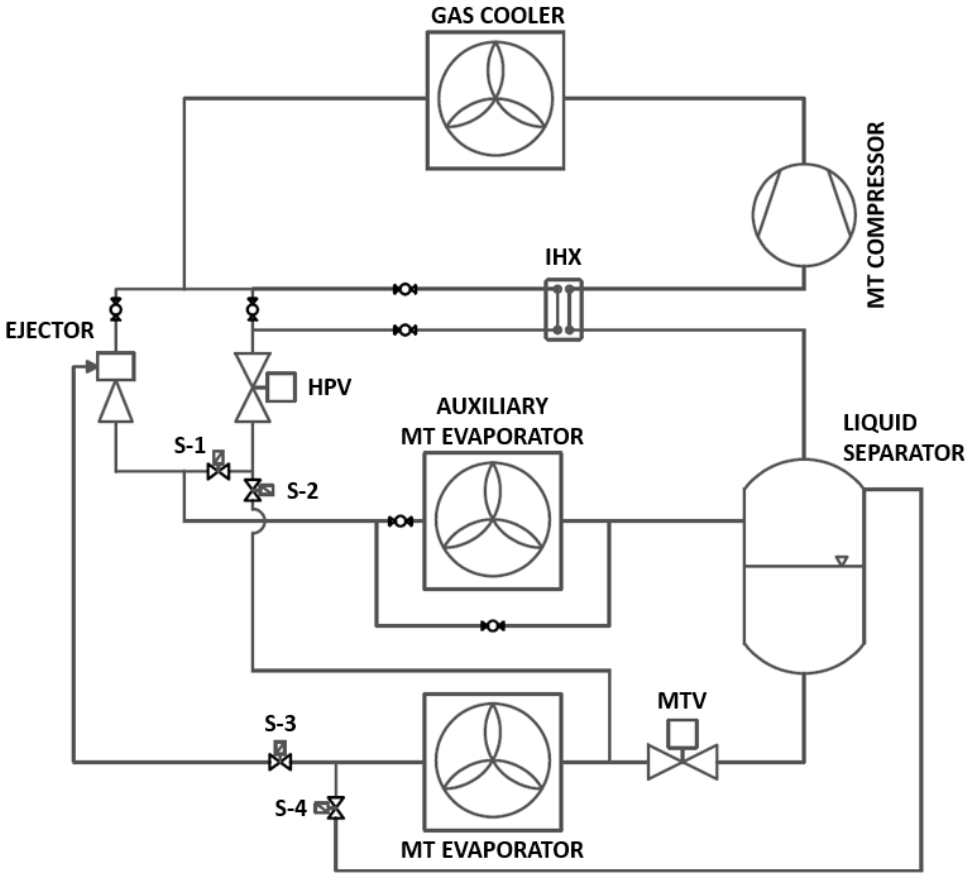

Figure 3.1 – Schematic of the refrigerating system.

The refrigerating unit, operating in the classical back-pressure configuration and with an environmental temperature equal to T_{amb} = 30°C, an internal air temperature in the insulated box equal to T_i = -2°C and with the compressor operating at the nominal rotational speed of 1450 rev min^{-1}, provides a nominal MT cooling power of 5.3 kW. The geometric dimensions of the main components of the system, which are chosen among real components available in the market, are reported in Table 3.1. The throat diameter of the ejector, equal to 1 mm, is the minimum throat diameter available on the market, as ejectors are currently designed and produced mostly to meet commercial refrigeration needs, characterized by significantly higher cooling capacities, and therefore ejectors are commonly developed to work in multi-ejector racks composed by multiple ejector cartridges with increasing capacity [102].

Table 3.1 – Geometric dimensions of the main components of the cooling unit.

Component	**Geometric dimensions**
MT compressor	Displacement, V_d = 27.5 cm^3
Gas cooler/Condenser	External convective surface, $A_{e,gc}$ = 29.8 m^2
MT evaporator	External convective surface, $A_{e,evap}$ = 39.4 m^2
MT auxiliary evaporator	External convective surface, $A_{e,evap\ AUX}$ = 8.9 m^2
Internal heat exchanger (IHX)	Convective surface, A_{IHX} = 0.39 m^2
Fixed geometry ejector	Motive nozzle throat diameter d_{EJ} = 1 mm

The different configurations available for the refrigerating unit are implemented through the opening/closing of the solenoid valves S-1, S-2, S-3 and S-4.

The back-pressure (BP) configuration is obtained closing the S-1 and S-3 solenoid valves and opening the S-2 and S-4 valves. The schematic of the refrigeration unit operating in the BP configuration is presented in Figure 3.2a, highlighting the different pressure levels in the system: the red color is used to refer to the high pressure (HP), while the green color refers to medium pressure (MP). To provide a better understanding of the refrigerating cycle in this configuration, Figure 3.2b reports the pressure-specific enthalpy (p-h) diagram of the R744 refrigerant during steady-state operation with external ambient temperature equal to T_{amb} = 30°C, internal air temperature in the insulated box equal to T_i = -2°C and compressor operating at the nominal rotational speed of ω_{comp} = 1450 rev min^{-1}.

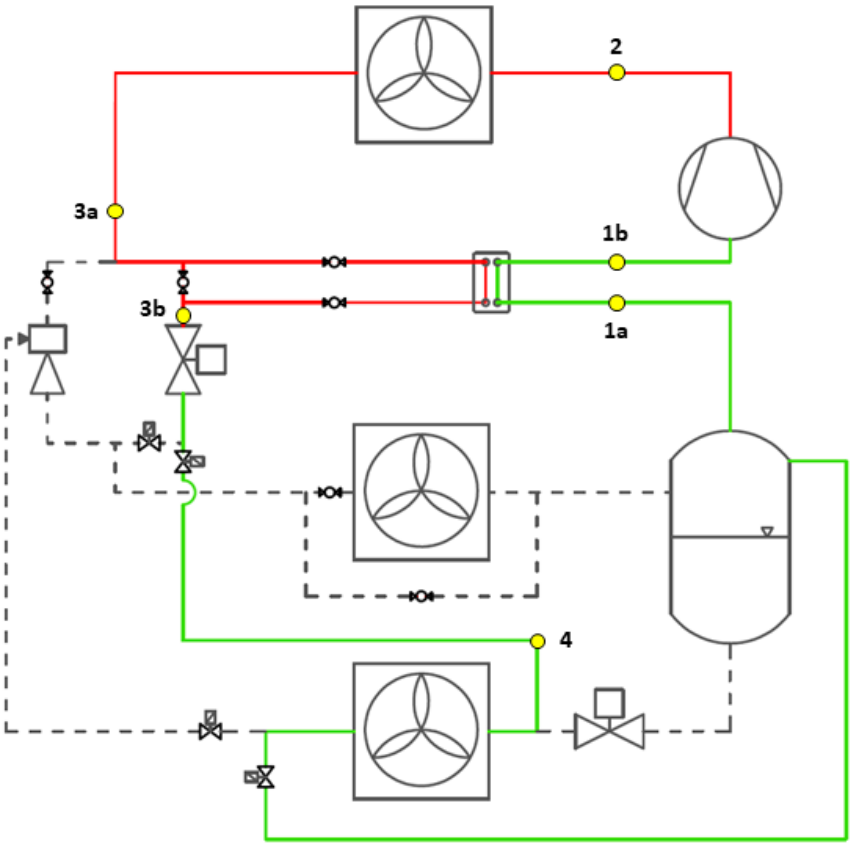

(a)

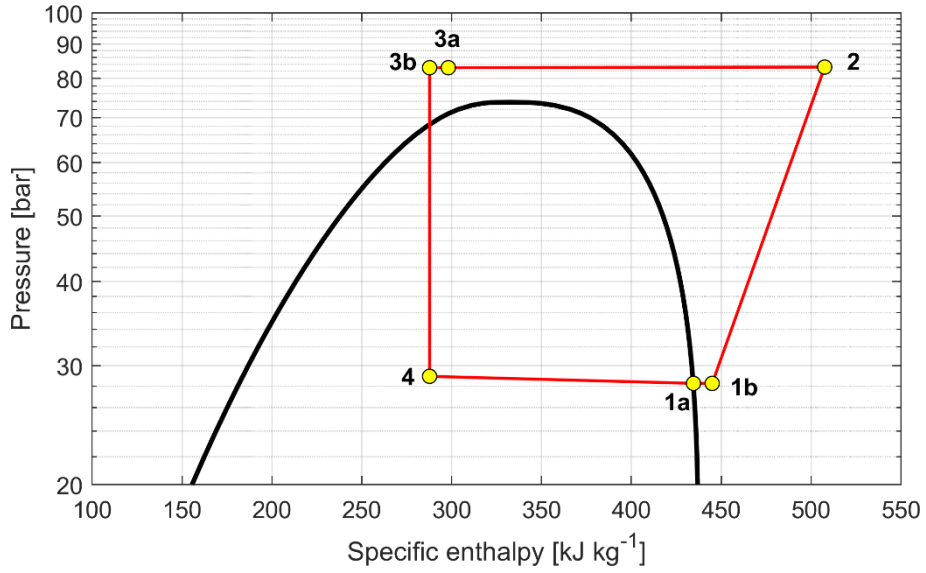

(b)

Figure 3.2 –Refrigerating system in back-pressure (BP) configuration: (a) operational schematic; (b) p-h diagram of the system operating points with T_{amb} = 30°C, T_i = -2°C and ω_{comp} = 1450 rev min^{-1}.

In this configuration, the refrigerant leaves the liquid separator in the state of saturated vapor (1a), it is superheated in the internal heat exchanger (IHX) and then it enters the compressor suction line (1b). After compression to the HP pressure level (2), which can be subcritical or supercritical according to the external ambient conditions, the refrigerant flows in the gas cooler/condenser coils and rejects heat to the external environment (3a), before flowing into the HP side of the IHX and being additionally cooled down (3b). Afterwards, the refrigerant enters the HPV valve, which provides also the control of the optimal pressure at the outlet of the gas cooler (as it will be described in Section 3.2), and it is expanded to the MT evaporation pressure level (4). The two-phase mixture then flows in the MT evaporator coils, it is evaporated and eventually superheated and then flows back to the liquid separator.

The ejector (EJ) configuration is obtained opening the S-1 and S-3 solenoid valves, closing the S-2 and S-4 valves and bypassing the MT auxiliary evaporator. The schematic of the refrigeration unit operating in the EJ configuration is presented in Figure 3.3a, highlighting the different pressure levels in the system: following the same color convention presented above, red refers to high pressure (HP) and green to medium pressure (MP). In addition, the yellow color is used to refer to the intermediate pressure (IP) of the liquid separator. As done for the BP configuration, Figure 3.3b reports the pressure-specific enthalpy (p-h) diagram of the R744 refrigerant during steady-state operation in the EJ configuration, with the same input parameters (T_{amb} = 30°C, T_i = -2°C and ω_{comp} = 1450 rev min^{-1}).

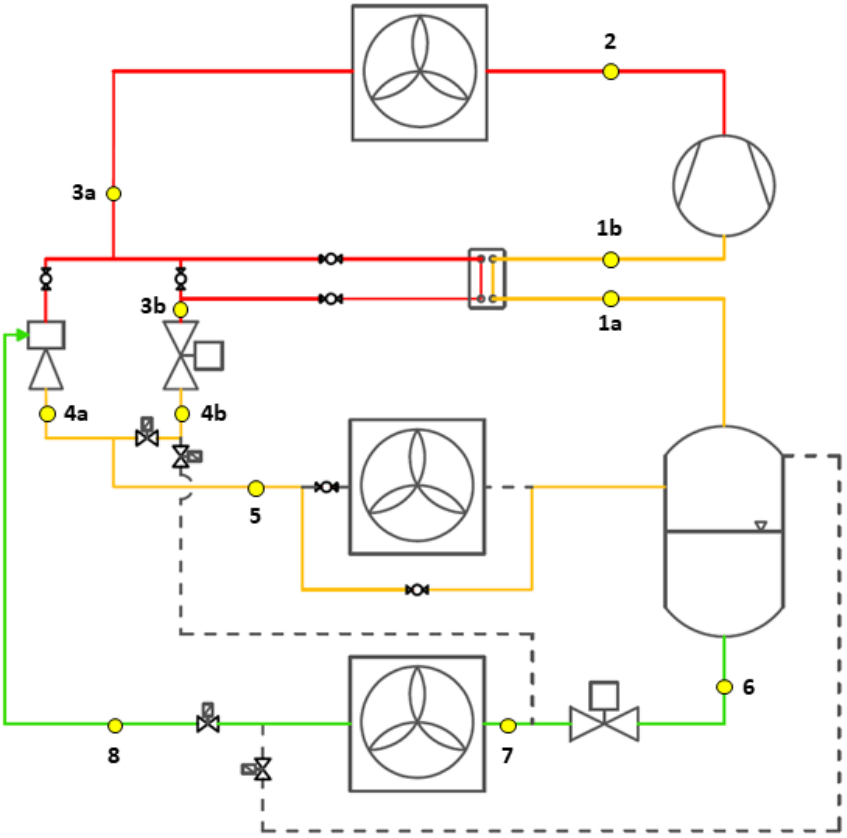

(a)

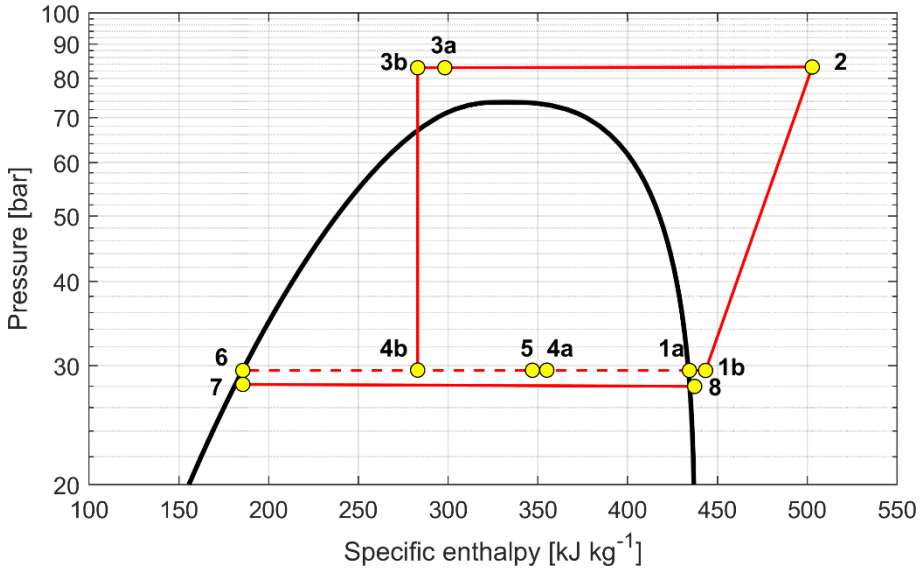

(b)

Figure 3.3 –Refrigerating system in ejector (EJ) configuration: (a) operational schematic; (b) p-h diagram of the system operating points with T_{amb} = 30°C, T_i = -2°C and ω_{comp} = 1450 rev min^{-1}.

In this configuration, a parallel between the two-phase ejector and the HPV is enforced: the ejector operates with a fixed geometry, so it is not possible to handle the whole range of operating points (corresponding to significantly different mass flow rates of the refrigerant) employing only the ejector. For this reason, the HPV is kept in parallel to the ejector, to handle the mass flow rate exceeding the one

processed by the ejector motive nozzle. In case the ejector is able to process all the mass flow rate, a valve can be inserted upstream of the ejector motive nozzle, to guarantee the operation of the HPV and the control of the high-pressure optimal value. According to the findings of Elbel and Hrnjak [103], the presence of an internal heat exchanger in front of the ejector motive nozzle reduces the motive flow enthalpy and, consequently, the ejector pressure lift, without increasing the cooling capacity. For this reason, the internal heat exchanger placed in the bypass branch connected only to the HPV valve, in order to provide the refrigerant superheat required to guarantee absence of liquid at the compressor suction. The mass flow rate at the outlet of the ejector-HPV parallel (5) is sent to the liquid separator bypassing the MT auxiliary evaporator. From the separator, the vapor phase is sent to the IHX (1a) and then to the compressor (1b), while the liquid phase (6) is expanded in a mechanical throttling valve (MTV) to the MT evaporation pressure (7) and then evaporated in the heat exchanger coils. The refrigerant at the outlet of the evaporator (8) is then entrained by the ejector from the MP pressure level to the IP pressure level. In this configuration, the ratio between the vapor mass flow rate $\dot{m}_V$ elaborated by the compressor (1a) and the total mass flow rate $\dot{m}_V + \dot{m}_L$, in which $\dot{m}_L$ represents the liquid mass flow rate sent to the MT evaporator (6), has to match the value of the vapor quality downstream of the ejector-HPV parallel (5), to fulfill the continuity equation of each phase in the liquid separator.

$$\frac{\dot{m}_{V,1a}}{\dot{m}_{V,1a} + \dot{m}_{L,6}} = x_5 \tag{3.1}$$

The EJ configuration can be therefore used, working at the specific ejector lift condition ($\Delta p_{lift} = p_{receiver} - p_{MT\ evap}$) which fulfills Eq. (3.1), just as long as the ejector characteristic allows this condition to be satisfied with a positive pressure lift ($p_{receiver} > p_{MT\ evap}$), as extensively described in [78].

The ejector + auxiliary evaporator (EJ,AUX) configuration is obtained from the EJ configuration closing the bypass of the MT auxiliary evaporator and adding an additional evaporation process between the ejector-HPV parallel and the liquid separator. The schematic of the refrigeration unit operating in the EJ,AUX configuration is presented in Figure 3.4a, highlighting the different pressure levels in the system with the same color convention used above. As done for the BP and EJ configurations, Figure 3.4b reports the pressure-specific enthalpy (p-h) diagram of the refrigerant during steady-state operation in the EJ,AUX configuration, still with the same input parameters (T_{amb} = 30°C, T_i = -2°C and ω_{comp} = 1450 rev min^{-1}).

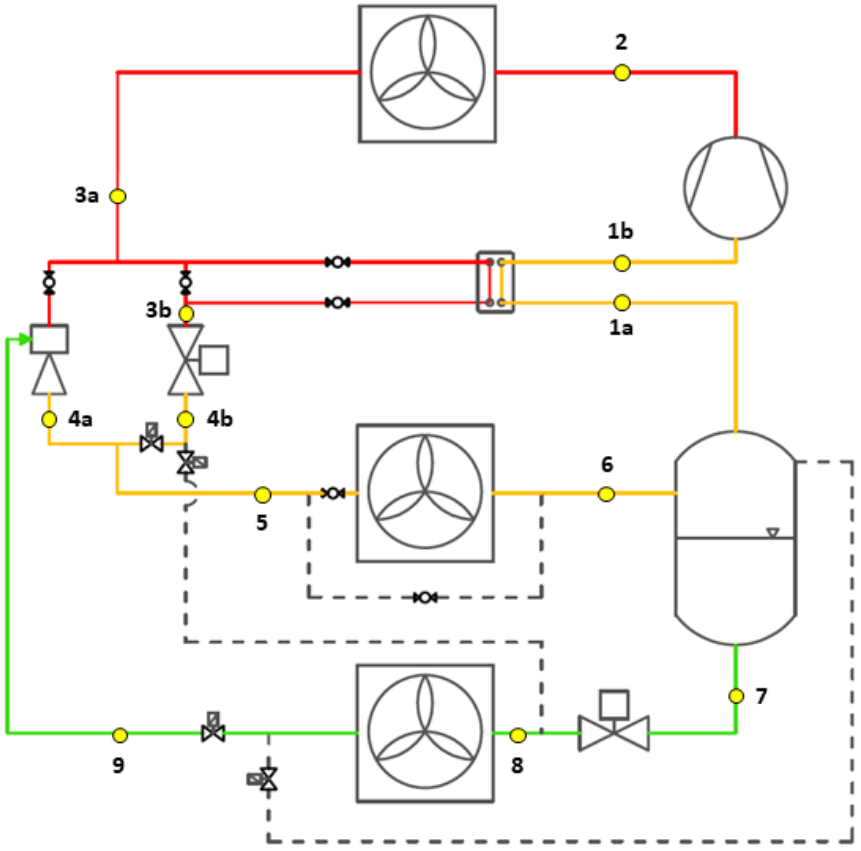

(a)

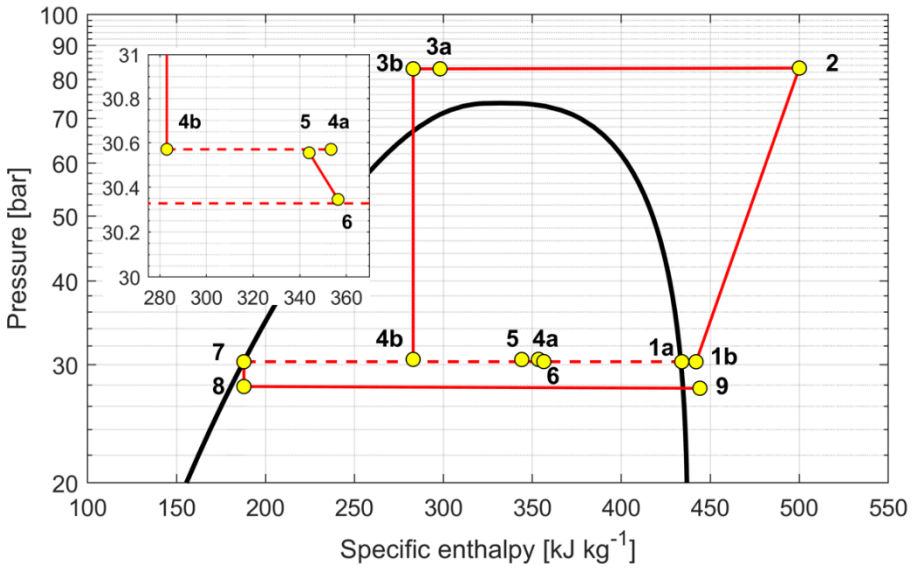

(b)

Figure 3.4 – Refrigerating system in ejector + auxiliary evaporator (EJ,AUX) configuration: (a) operational schematic; (b) p-h diagram of the system operating points with T_{amb} = 30°C, T_i = -2°C and ω_{comp} = 1450 rev min^{-1}.

The refrigerating cycle in this configuration follows almost entirely what was described for the EJ configuration, with the significant difference that, in this configuration, the vapor quality of the two-phase

mixture obtained at the mixing point between the ejector and the HPV (5) does not necessarily coincide with the vapor quality required to fulfill the liquid separator continuity equation, since an additional quality increase in the two-phase mixture can be provided by the auxiliary evaporator (6), as it is highlighted in the zoomed portion of the p-h diagram presented in Figure 3.4b.

$$\frac{\dot{m}_{V,1a}}{\dot{m}_{V,1a} + \dot{m}_{L,7}} = x_6 \neq x_5 \tag{3.2}$$

The exploitation of the auxiliary MT evaporator therefore introduces an additional degree of freedom in the system optimization, since the ejector can be employed also in operating conditions which would not fulfill the equilibrium of the phases at the liquid separator, thus allowing the feasibility of the ejector operation in different points of its pressure lift – entrainment ratio characteristic.

This solution has been proven to have a significant effect on the extension of the ejector cycles applicability towards low ambient temperature operating conditions, while still granting an improvement of the system performance compared to the traditional BP configuration, as extensively presented and discussed in [78].

3.2 Numerical model description and validation

The refrigerating system modelled in this chapter is supposed to be charged with a total refrigerant mass equal to 25 kg of R744. The numerical model of the cooling unit is developed using the commercial software Simcenter Amesim v.17.

The assumptions under which the numerical model of the cooling unit has been developed are the same listed in Section 2.2.3: homogeneous fluid model for the refrigerant, considering the two phases to flow as a single phase in thermal equilibrium and characterized by mean fluid properties; internal flow (refrigerant side) considered one-dimensional; external flow (air side) considered zero-dimensional; the effect of gravity and the pressure losses along the pipes are neglected, since the assumption of short pipes is made. The thermodynamic properties of the R744 refrigerant are evaluated through the Modified Benedict Webb Rubin (MBWR) equation [84], considering the pressure as a function of the fluid density and temperature.

The cooling unit is composed of a semi-hermetic compressor, a finned-coil condenser/gas cooler, two finned-coil evaporators, a high-pressure expansion valve (HPV), a manual throttling valve (MTV), a liquid separator and a two-phase ejector.

3.2.1 Compressor

The semi-hermetic compressor is modelled following the same numerical approach described in Section 2.2.3. However, for this refrigerating system, a specific compressor developed for R744 supercritical units, characterized by a fixed displacement of V_d = 27.5 cm^3 and operating at fixed nominal speed of ω_{comp} = 1450 rev min^{-1}, was chosen among the alternatives available in the market [104]. The volumetric efficiency η_{vol} map and the overall compression efficiency η_{comp} map are interpolated as a function of the pressure ratio r_p and the rotational speed ω_{comp} from the compressor operating data provided by the manufacturer. The compressor mass-flowrate, its electric power draw and the refrigerant outlet enthalpy are evaluated with the same approach presented in Section 2.2.3 (Eq. (2.12), Eq. (2.13) and Eq. (2.14), respectively).

3.2.2 Heat exchangers

The heat exchangers (condenser/gas cooler, MT evaporator and MT auxiliary evaporator) are modelled following the same numerical approach described in Section 2.2.3, based on the discretization of the heat exchangers in N lumped volumes, each of them then sub-divided in three nodes (internal flow refrigerant, wall and fins, external flow air), as presented in Figure 2.8. The geometric dimensions of the heat exchangers, reported in Table 3.1, are equally distributed in each lumped element in which the respective heat exchanger is divided in the numerical model design.

As already presented in Section 2.2.3, for each lumped element, the mass and energy balance are evaluated through Eq. (2.15) and Eq. (2.16), respectively, while the internal convection, the conduction through the wall and fins and the external convection are evaluated through Eq. (2.17), Eq. (2.18) and Eq. (2.19), respectively. The empirical correlations employed to determine the convective heat transfer coefficients and the pressure losses in the refrigerant side are the same reported in Table 2.4.

Differently from the R134a heat exchangers numerical model described in Section 2.2.3, in which the heat exchangers were discretized into N = 6 lumped volumes, for the R744 refrigerating system described in this chapter, both the MT main evaporator and the MT auxiliary evaporator were discretized into N = 10 lumped volumes, while the condenser/gas cooler was discretized into N = 12 lumped volumes. The choice to increase the number of discretized elements in the R744 heat exchangers model compared to the R134a model leads to an increase in the accuracy of the CO_2 transition during the phase change processes; in particular, a denser discretization was chosen for the gas cooler since during transcritical operation the properties of CO_2 present significant variations along the heat exchanger.

The optimal condenser/gas cooler outlet conditions (pressure and temperature) are enforced through the implementation of two PI (Proportional-Integral) controllers and are set to follow a four-zones control strategy, as the one presented by Dugaria et al. [105]. The condenser/gas cooler R744 target outlet

temperature $T_{gc,OUT}^{design}$ (enforced by a PI controller acting on the gas cooler fans speed) and high pressure $p_{gc,OUT}^{design}$ (enforced by a PI controller acting on the HPV opening cross-sectional area) are reported in Table 3.2 as a function of the external ambient temperature T_{amb}.

Table 3.2 – Four working zones operation of the condenser/gas cooler as a function of the external air temperature.

Temperature range	**High pressure operation**	**Control logic**
$T_{amb} < 8°C$	Subcritical	$p_{gc,OUT}^{design} = p_{sat}(T_{gc,OUT} + 7°C)$ $T_{gc,OUT}^{design} = 10°C$
$8°C \leq T_{amb} < 17°C$	Subcritical	$p_{gc,OUT}^{design} = p_{sat}(T_{amb} + 9°C)$ $T_{gc,OUT}^{design} = T_{amb} + 7°C$
$17°C \leq T_{amb} \leq 27°C$	Transition	$p_{gc,OUT}^{design} = 65.8\ \text{bar} + 0.9(T_{amb} - 17°C)$ $T_{gc,OUT}^{design} = 24°C + 0.6(T_{amb} - 17°C)$
$T_{amb} > 27°C$	Transcritical	$p_{gc,OUT}^{design} = 2.7\ T_{gc,OUT} - 6.1\ \text{bar}$ $T_{gc,OUT}^{design} = T_{amb} + 3°C$

3.2.3 Expansion devices

The expansion devices in the cooling unit (the HPV and the MTV) are numerically modelled following the same approach that was used in Section 2.2.3 to model the thermostatic throttling valve. The throttling process is considered isenthalpic, the valve is considered adiabatic and the effect of choked flow is neglected. The mass flow rate through the throttle is determined through Eq. (2.20), in which the flow coefficient C_q is an indirect function of the opening ratio of the expansion valve. As mentioned above, the opening ratio of the HPV is modulated with a PI controller to achieve the optimal pressure at the outlet of the gas cooler, while the opening ratio of the MTV is set manually as a fixed input of the model.

3.2.4 Liquid separator

In addition to the refrigerating system elements whose numerical model was already described in Section 2.2.3, the cooling unit described in this chapter includes a liquid separator (or liquid receiver) and a two-phase ejector.

In two-phase flow applications, a liquid separator is used to manage refrigerant charge fluctuations due to variations in the system operating conditions, unsteady operation and variability of external boundary conditions. Moreover, it separates the liquid phase, which is sent to the evaporator, from the vapor phase, that is sent to the compression stage, thus avoiding liquid flow back to the compressor.

The liquid separator is modelled as a cylindrical-shape tank with constant cross-sectional area, homogeneous pressure in the entire volume and homogeneous densities for the liquid phase and the vapor phase, in their respective volumes. Heat exchange due to convection between the separator and the external environmental air is taken into account.

Since the refrigerating system presented in this chapter is designed to operate in refrigerated road transport applications, providing cooling effect in an insulated box installed on a small van-size vehicle used for temperature-controlled deliveries, in such a scenario the liquid separator is assumed to be installed below the refrigerated box, fixed to the vehicle chassis. This layout prevents solar radiation to heat up the receiver, limiting pressure drifts during long OFF periods, as this issue will be further discussed in Section 3.6.4, and protects it from accidental collisions. Following these assumptions, convection was considered as the main heat exchange process.

When the vehicle is not moving (and therefore, also in case of stationary steady-state numerical evaluation of the system performance), natural convection between the liquid separator and the external air is considered and the heat exchange is computed through the empirical correlation presented by Churchill and Chu [106], as reported in Eq. (3.3). On the other hand, when the vehicle is moving, forced convection between the liquid separator and the environmental air is considered and the heat exchange is computed through the empirical correlation presented by Hilpert [107], as reported in Eq. (3.4).

$$\overline{Nu}_l = \left\{ 0.825 + \frac{0.387\, Ra_l^{1/6}}{\left[1 + \left(\frac{0.492}{Pr}\right)^{9/16}\right]^{8/27}} \right\}^2 \tag{3.3}$$

$$\overline{Nu}_d = c\, Re_d^m Pr^{1/3} \tag{3.4}$$

The mean refrigerant pressure $\bar{p}_{receiver}$ and specific enthalpy $\bar{h}_{receiver}$ are used to compute the state of the refrigerant leaving the receiver (in the state of saturated liquid and vapor, respectively) and the percentage of liquid volume inside the liquid separator, which is used to determine the height of the liquid-vapor interface.

3.2.5 Ejector

The ejector performance is modelled after the results of the study by Banasiak et al. [108], who performed an experimental evaluation of the performance of a high-pressure lift multi-ejector pack designed for R744 refrigerating systems and developed the interpolating functions which describe the ejector operation as a function of the boundary conditions. The multi-ejector evaluated by Banasiak et al. [108] is composed by different cartridges characterized by increasing size: the ejector included in the numerical model of the cooling unit presented in this chapter corresponds to the smallest ejector cartridge (named

VEJ1) experimentally evaluated in that research paper, which also provides the geometrical description of the fixed-geometry ejector cartridge.

The ejector motive nozzle mass flow rate $\dot{m}_{motive}$ and the ejector entrainment ratio, which is defined as the ratio between the suction nozzle mass flowrate $\dot{m}_{suction}$ and the motive nozzle mass flow rate as reported in Eq. (3.5), are expressed following the interpolating functions reported in [108] as a function of motive nozzle inlet pressure and density, suction nozzle inlet pressure and ejector outlet pressure.

$$\phi = \frac{\dot{m}_{suction}}{\dot{m}_{motive}} \tag{3.5}$$

The suction nozzle mass flow rate can be then evaluated directly by the entrainment ratio definition given in Eq. (3.5), while the value of the mass flow rate at the ejector outlet is computed as reported in Eq. (3.6). On the other hand, the state of the refrigerant at the ejector outlet is computed with the formulation of energy conservation principle, as reported in Eq. (3.7).

$$\dot{m}_{discharge} = (1 + \phi)\dot{m}_{motive} \tag{3.6}$$

$$h_{discharge} = \frac{(h_{motive} + \phi\, h_{suction})}{(1 + \phi)} \tag{3.7}$$

3.2.6 Heat exchangers numerical model validation

The numerical modelling approach of the heat exchangers was validated against data reported in datasheets of existing heat exchangers available in the market. The heat exchangers selected for the numerical model validation are characterized by different rated power (from hundreds of kW of thermal power to some kW of thermal power) and different technology (finned coils heat exchanger with air as a secondary fluid or plate heat exchanger with water as a secondary fluid), to verify the accuracy of the modelling approach under significantly different operating conditions.

The performance of the heat exchangers reported in manufacturers' datasheets is compared with the one evaluated with the heat exchanger numerical model in Table 3.3 through the evaluation of the exchanged thermal power in steady-state operation under the operating conditions provided by the technical datasheets, i.e. the inlet conditions of the primary and secondary fluids in the heat exchangers.

Table 3.3 – Validation of the heat exchangers numerical model against datasheet data of heat exchangers available in the market.

Heat exchanger	Thermal power (datasheet) [kW]	Thermal power (numerical model) [kW]	Numerical model error
LUVE EAV8S 7222H CO_2 – Air finned coil evaporator	250.3	253.3	+1.2%
LUVE EAV8S 7222H CO_2 – Air finned coil gas cooler	246.3	238.2	-3.4%
SWEP B185H 100P CO_2 – Water plate gas cooler	135.7	134.9	-0.6%
LUVE F35HC 215 CO_2-Air finned coil evaporator	9.5	9.3	-2.1%

The exchanged thermal power calculated with the numerical model presents relative errors always less than ±5% compared to the exchanged thermal power declared by the manufacturers in the heat exchangers datasheets, regardless of the rated power or the heat exchanger type.

3.3 Steady-state performance of the refrigerating system

An extensive study of the steady-state performance of the refrigeration system was previously published by Artuso et al. [78]. The main results of that study are briefly reported in this section for the sake of completeness and to provide the necessary baseline results which complement the evaluation of the unsteady performance of the refrigeration system which will be described in Section 3.4 and which will be used to define the cooling unit control strategy in the numerical simulations of daily delivery missions of perishable goods.

The steady-state performance of the cooling unit is evaluated through the definition of the system Coefficient of Performance (COP), as reported in Eq. (3.8):

$$COP = \frac{Q_{evap,TOT}}{P_{comp}} = \frac{Q_{evap} + Q_{evap,AUX}}{P_{comp}} \tag{3.8}$$

Steady-state numerical simulations of the cooling unit have been carried out providing the temperature of the air inside the refrigerated box (T_i), i.e. the temperature of the air entering the evaporators coils, and the temperature of the external air (T_{amb}), i.e. the temperature of the air entering the gas cooler coils, as fixed inputs of the model. Steady-state operation is reached when none of the operating parameters of the system changes with time. A simulation time of 7200 s was proven to be long enough

for the system to reach steady-state operation and for the solutions to be independent from the system initialization.

The cooling unit performance was evaluated under different combinations of T_i (varying between -5°C and 15°C) and T_{amb} (varying between 15°C and 45°C) and with operation in each of the three system configurations described in Section 3.1: backpressure (BP) configuration, ejector (EJ) configuration and ejector + auxiliary evaporator (EJ,AUX) configuration. The cooling unit's compressor was run at the nominal speed of ω_{comp} = 1450 rev min^{-1} in each of the numerical simulations.

While in BP configuration the evaporation pressure results from the system equilibrium depending on the internal and external temperatures, in EJ configuration and in EJ,AUX configuration the evaporation pressure is a free parameter that can be varied acting on the opening ratio of the manual throttling valve (MTV), as previously described in Section 3.1. For each pair of temperatures (T_i, T_{amb}) which identify a steady state working point, the opening degree of the MTV was set to maximize the COP, leading to optimal evaporation pressures which are different between EJ and EJ,AUX configurations, as extensively discussed in [78].

The system performance maps are reported in Table 3.4, Table 3.5 and Table 3.6 for BP configuration, EJ configuration and EJ,AUX configuration operation, respectively.

Table 3.4 – Steady-state COP [-] of the cooling system in BP configuration.

T_{amb} [°C]/T_i [°C]	-5	0	5	10	15
15	2.85	3.33	3.88	4.53	5.34
17	2.62	3.05	3.55	4.12	4.82
20	2.43	2.83	3.28	3.80	4.42
22	2.31	2.68	3.10	3.60	4.18
25	2.13	2.47	2.86	3.31	3.83
27	1.91	2.22	2.56	2.96	3.40
30	1.74	2.01	2.32	2.66	3.05
32	1.59	1.83	2.11	2.42	2.77
35	1.40	1.62	1.85	2.12	2.41
38	1.24	1.43	1.64	1.87	2.12
40	1.15	1.33	1.52	1.73	1.96
42	1.07	1.23	1.41	1.60	1.81
45	0.97	1.11	1.27	1.44	1.63

Table 3.5 – Steady-state COP [-] of the cooling system in EJ configuration.

T_{amb} [°C]/T_i [°C]	-5	0	5	10	15
15	2.14	2.17	2.20	2.24	2.27
17	2.15	2.19	2.22	2.26	2.29
20	2.20	2.25	2.30	2.34	2.39
22	2.24	2.29	2.33	2.38	2.44
25	2.18	2.31	2.37	2.42	2.47
27	1.97	2.30	2.36	2.41	2.48
30	1.90	2.11	2.37	2.61	2.72
32	1.78	1.98	2.22	2.47	2.76
35	1.62	1.80	2.00	2.23	2.48
38	1.47	1.62	1.80	2.01	2.22
40	1.36	1.51	1.67	1.86	2.06
42	1.28	1.41	1.55	1.72	1.90
45	1.12	1.26	1.38	1.52	1.68

Table 3.6 – Steady-state COP [-] of the cooling system in EJ,AUX configuration.

T_{amb} [°C]/T_i [°C]	-5	0	5	10	15
15	3.03	3.55	4.18	4.89	5.87
17	2.79	3.27	3.82	4.50	5.43
20	2.58	3.02	3.53	4.14	5.00
22	2.46	2.86	3.34	3.91	4.68
25	2.26	2.62	3.34	3.57	4.20
27	2.12	2.47	2.87	3.34	3.91
30	1.83	2.12	2.46	2.85	3.30
32	1.67	1.93	2.23	2.58	2.96
35	1.45	1.69	1.95	2.24	2.56
38	1.26	1.48	1.70	1.96	2.23
40	1.14	1.36	1.57	1.79	2.03
42	1.03	1.24	1.44	1.64	1.86
45	0.88	1.09	1.27	1.44	1.63

According to the performance results above reported, it is possible to evaluate which of the three possible system configurations leads to the highest COP for each of the considered combinations of T_i and T_{amb}. The best performing configuration for each of the operating points (T_i, T_{amb}) is reported in Figure 3.5.

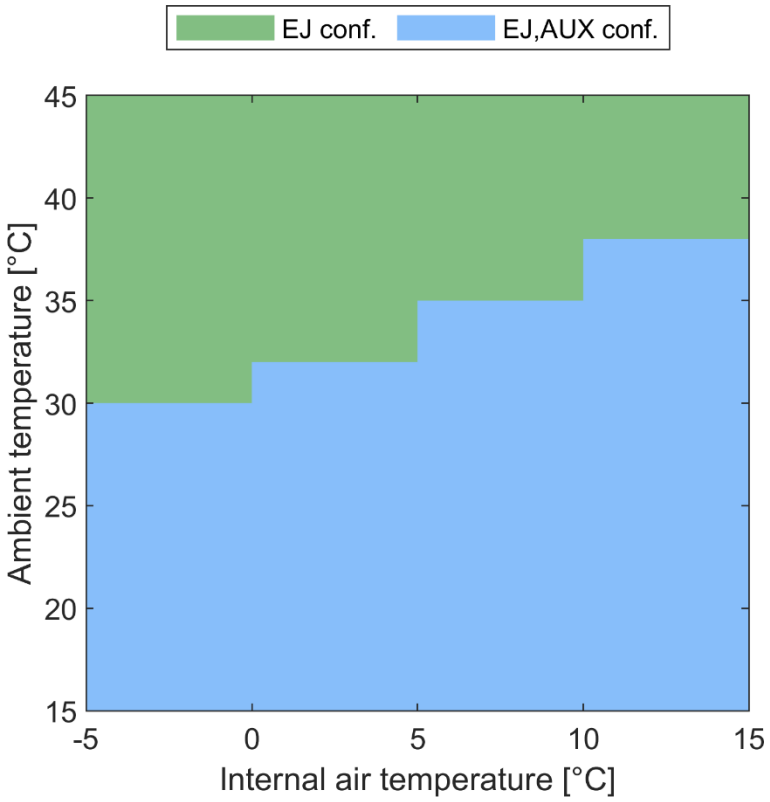

Figure 3.5 – Map of the best performing configuration under different steady-state conditions.

From the results reported in Figure 3.5, it can be noticed that operation in EJ configuration leads to a higher COP under higher external air temperatures, while the introduction of the auxiliary evaporator and operation in EJ,AUX configuration leads to the best performance under lower external air temperatures, thus extending the possibility to operate according to an ejector-supported cycle even with low environmental air temperature conditions. Moreover, it can be noticed that the baseline BP configuration is outperformed by the ejector-supported configurations in each of the considered combinations of internal and external air temperature conditions.

3.4 Cooling unit control strategy in unsteady operation

As described in Section 3.1, the cooling unit described in this chapter is designed to provide Medium-Temperature (MT) refrigeration in road temperature-controlled transport applications.

Operation aiming at the achievement of controlled air temperatures inside a refrigerated box mounted on a transport vehicle presents significant elements of variability: the fluctuations of the climatic conditions throughout a daily delivery mission, a significantly unsteady cooling load depending on the real-time energy balance of the refrigerated box, a consequent wide range of loads in which the cooling unit is forced to work during the delivery mission, the motion of the vehicle itself, the frequent door openings and the consequent infiltrations of external air inside the insulated box [10] [9] [11].

For the above-mentioned reasons, operation in road transport applications is strongly unsteady, and the development of a control strategy based on steady-state performance results can lead to non-optimized operation during the different parts of the delivery mission. Therefore, the performance of the cooling unit was numerically evaluated also in dynamic operating conditions.

To this extent, dynamic simulations of the operation of the cooling unit employed to maintain the temperature of the air inside the refrigerated box in a desired temperature range (-1°C $< T_i <$ 3°C), necessary for the perishable goods correct conservation, have been carried out considering the effective thermal loads occurring at various ambient temperatures.

Differently from the evaluation of the steady-state performance of the cooling unit, in which the steady-state COP can be evaluated through instant power (Eq. (3.8)), in unsteady operation the COP has to be evaluated considering the total cooling energy provided by the evaporators ($E_{evap} + E_{evap,AUX}$) and the total energy required by the compressor (E_{comp}). Moreover, since in a delivery mission the total amount of energy spent to feed the cooling unit is fundamental for overall energetic considerations, also the energy supplied to the heat exchangers fans (E_{fans}) was considered in the COP evaluation.

As it was mentioned above, during dynamic operation the system thermostat acts on the compressor to perform ON/OFF cycles in order to maintain the internal air temperature in the desired range (-1°C $< T_i <$ 3°C). An ON/OFF cycle COP can be then defined as follows:

$$(COP)_{ON/OFF} = \left(\frac{E_{evap} + E_{evap,AUX}}{E_{comp} + E_{fans}} \right)_{ON/OFF} \tag{3.9}$$

in which the evaluation of the thermal and electrical energies is carried out on a single ON/OFF hysteresis cycle imposed by the cooling unit thermostat.

The dynamic simulations aimed at evaluating the performance of the cooling unit during the actual ON/OFF operation which will characterize the unit during delivery missions were carried out under the following assumptions:

- The external ambient temperature T_{amb} is set as a fixed input for the simulations;
- The dynamic energetic balance of the insulated box is evaluated considering internal convection, conduction through the box walls, external convection and solar radiation, as described in Section 2.2.2 (Eq. (2.7), Eq. (2.8), Eq. (2.9), Eq. (2.10) and Eq. (2.11));
- The vehicle is kept still (the external convective heat transfer coefficient does not consider the effects of vehicle motion);
- The Global Horizontal Radiation (GHR) effect is interpolated as a function of the temperature at 12:00 of a mean day for every month of the year in the city of Athens, representative of hot European climatic conditions. Solar irradiance and temperature data are collected from the

Energy Plus online database [95]. The solar radiation load acting on the refrigerated box is then evaluated through the above-mentioned GHR interpolating regression as a function of the external ambient temperature imposed as an input of the simulation;

- The doors are kept closed throughout the entire simulation (no infiltration load considered in the energetic balance of the insulated box);
- The simulations were kept running until consequent ON/OFF cycles imposed by the thermostat presented no relative variations in terms of the $COP_{ON/OFF}$ defined in Eq. (3.9). The dynamic performance of the cooling unit performing ON/OFF cycles can be therefore considered stable at the i-th cycle if:

$$\{(COP)_{ON/OFF}\}_i = \{(COP)_{ON/OFF}\}_{i-1} \tag{3.10}$$

Following the results reported in Section 3.3, which highlighted that the EJ configuration and the EJ,AUX configuration outperformed the BP configuration for every operating condition considered, the dynamic simulations of the cooling unit aimed at the evaluation of the ON/OFF performance of the system were carried out only for EJ and EJ,AUX configurations.

The stable ON/OFF cycle COPs are reported in Table 3.7 and Table 3.8 for EJ configuration and EJ,AUX configuration operation, respectively.

Table 3.7 – ON/OFF cycle COP [-] of the cooling system in EJ configuration to maintain -1°C $< T_i <$ 3°C.

T_{amb} [°C]/T_i [°C]	-1 / 3
22	1.00
25	1.19
27	1.44
30	1.58
32	1.57
35	1.49
38	1.26
40	1.13

Table 3.8 – ON/OFF cycle COP [-] of the cooling system in EJ,AUX configuration to maintain -1°C $< T_i <$ 3°C.

T_{amb} [°C]/T_i [°C]	-1 / 3
22	1.13
25	1.81
27	1.86
30	1.82
32	1.64
35	1.43
38	1.22
40	1.09

According to the performance results above reported, it is possible to evaluate which of considered configurations leads to the highest ON/OFF cycle COP for each of the considered T_{amb}. The ON/OFF cycle COP is compared between the considered configurations in Figure 3.6 and the resulting best performing configuration is reported in Table 3.9.

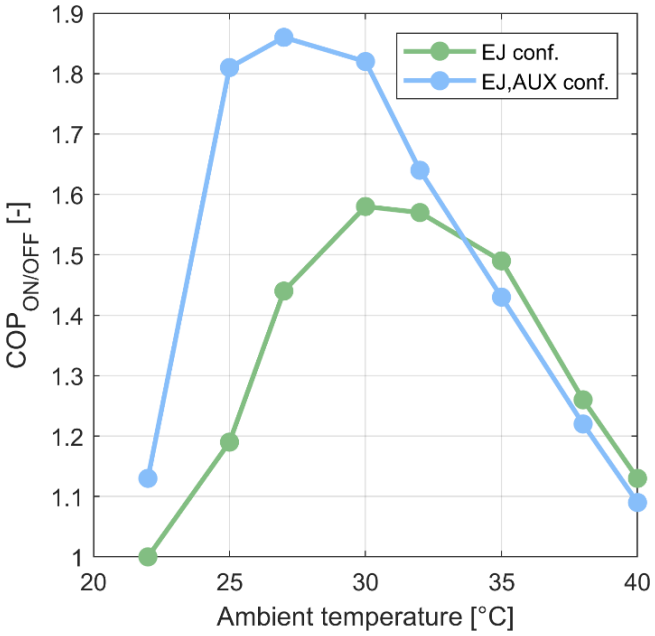

Figure 3.6 – ON/OFF cycle COP comparison between EJ and EJ,AUX configurations as a function of T_{amb}.

Table 3.9 – Map of the best performing configuration while operating ON/OFF cycles to maintain -1°C $< T_i <$ 3°C.

T_{amb} [°C]/T_i [°C]	-1 / 3
22	EJ,AUX
25	EJ,AUX
27	EJ,AUX
30	EJ,AUX
32	EJ,AUX
35	EJ
38	EJ
40	EJ

Following the results reported in Figure 3.6 and in Table 3.9, the final control strategy to select the best performing configuration during delivery missions, as a function of the ambient temperature, is reported in Figure 3.7.

In particular, when the internal air temperature presents values which do not undermine the perishable cargo correct conservation, since the refrigerated box internal conditions are within the temperature set-point range ($T_i < 3°C$), the best performing configuration in terms of $COP_{ON/OFF}$ is preferred. In this scenario, for $T_{amb} < T_{amb,switch}$ = 33°C, the EJ,AUX configuration is selected, while for $T_{amb} \geq T_{amb,switch}$ = 33°C, the EJ configuration leads to a better performance.

However, as it was previously discussed in Section 2.2.4, when the internal air conditions are outside of the desired temperature range, the fast recovery of the desired temperature set-point, for example after a door opening, is of crucial importance for the correct preservation of the transported goods. For this reason, when the internal temperature is higher than the maximum allowed conservation temperature ($T_i \geq 3°C$), the EJ;AUX configuration is selected regardless of the ambient temperature, to provide a higher overall cooling effect $\dot{Q}_{evap,TOT}$, due to the simultaneous use of both the evaporators, and contribute to a fast pulldown towards the correct temperature range inside the refrigerated box, when the best performing configuration is enforced.

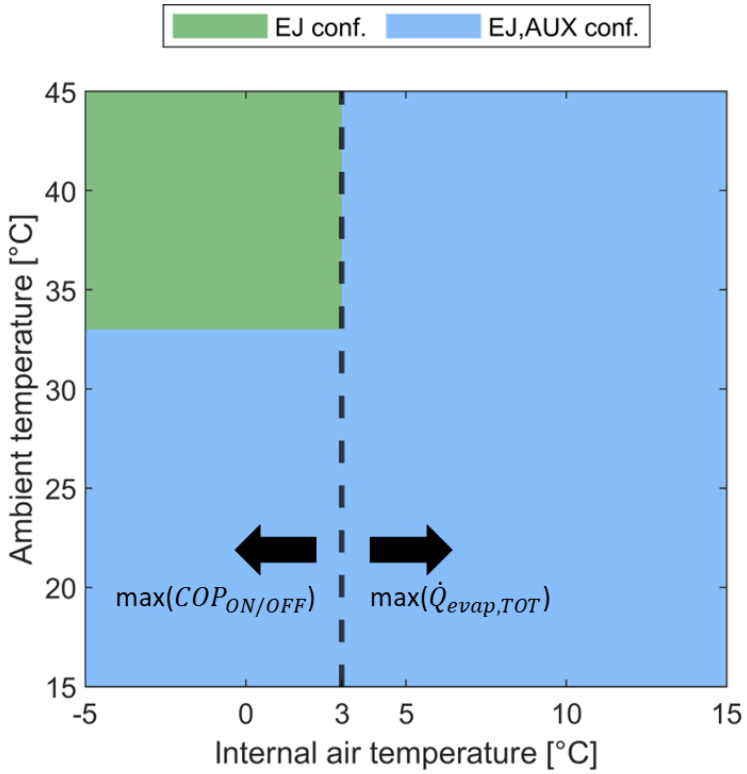

Figure 3.7 – Cooling unit configuration control during operation, as a function of T_{amb} and T_i, in order to maximize the ON/OFF cycle COP (for T_i < 3°C) or the cooling effect (for T_i > 3°C).

Following the configuration control map presented in Figure 3.7, during delivery missions a switching control system dynamically selects the optimal configuration as a function of time and of T_i and T_{amb}. Nevertheless, configuration switches are permitted only during compressor OFFs imposed by the thermostat, to avoid mechanical issues related to valves opening/closing during operation. As a result, as the compressor is turned ON by the thermostat, the switching control system selects the optimized configuration and holds it until next compressor OFF.

3.5 Numerical evaluation of a short-range multi-drop delivery

Firstly, the performance of the cooling unit during a short-range multi-drop delivery mission of temperature-controlled goods in an urban environment is evaluated.

3.5.1 Delivery mission structure

The perishable cargo to be delivered during the daily mission are stored inside an insulated body with external dimensions of internal volume of 11.89 m^3, whose main geometrical dimensions are reported in Table 3.10. A global heat transfer coefficient K = 0.36 W m^{-2} K^{-1} was evaluated following the procedure defined in Annex 1 of the ATP agreement [82].

Table 3.10 – Main geometrical dimensions of the insulated body (short-range mission).

Element	Dimension
External height H_e	2.13 m
External length L_e	3.10 m
External width W_e	2.20 m
External surface S_e	36.22 m^2
Internal surface S_i	31.77 m^2
Internal volume V_i	11.89 m^3

The mission simulates a typical daily local distribution activity, with the same structure and with the same inputs definition (vehicle target speed, openings of the doors, fraction of loaded goods) of the delivery mission presented in Section 2.3. Therefore, a two-hours pulldown brings the internal air temperature to the desired temperature range (-1°C $< T_i <$ 3°C) and precedes the charging of 400 kg of meat products inside the vehicle insulated box under controlled temperature conditions (4°C). The perishable goods will be distributed evenly in 7 deliveries in the morning and 7 deliveries in the afternoon, in a short-range urban area driving mission. The heat capacity and the convective heat transfer coefficient of the meat is the same described in Section 2.3. The vehicle target speed is set through standard WLTC profiles, defined with a frequency of 1 Hz. The stops have the same structure and duration of the ones described in Section 2.3. The complete mission structure is the same presented in Table 2.6, and it is reported here in Table 3.11 for the sake of completeness.

Table 3.11 – Delivery mission structure (short-range mission).

Start time [hh.mm]	Duration [hh.mm]	Activity	Travel distance [km]
06.00	02.00	Pulldown (Pre-Cooling)	-
08.00	01.00	Loading	-
09.00	0.30	2x Rural + 2x SubUrban Driving Cycles	22
09.30	2.48	7x Delivery Cycles	42
	0.19	2x Urban Driving Cycles	6
	0.02	Stop	-
	0.03	Delivery	-
12.18	0.30	2x Rural + 2x SubUrban Driving Cycles	22
12.48	1.12	Stop	-
14.00	0.30	2x Rural + 2x SubUrban Driving Cycles	22
14.30	2.48	7x Delivery Cycles	42
	0.19	2x Urban Driving Cycles	6
	0.02	Stop	-
	0.03	Delivery	-
17.18	0.30	2x Rural + 2x SubUrban Driving Cycles	22
17.48	1.12	Stop	-
TOTAL	**11.48**	**-**	**172**

The objective of this first part of the study was to evaluate the performance of the cooling unit under several different external conditions. Therefore, a reference mean day for each month of the year in the city of Athens has been chosen for an annual evaluation of the system performance in European hot areas. The environmental temperature, relative humidity and solar radiation intensity, available in the Energy Plus online database [95], were collected for all the days of each month of the year and then averaged hourly to obtain the climatic profile of the mean day of each of the months of the year. Differently from the approach presented in Section 2.3, the hourly ambient temperature is then corrected as reported in Mihalakakou et al. [109] to consider the ambient temperature increase in urban areas due to the Urban Heat Island (UHI) phenomenon since, as it was discussed in Section 3.4, the cooling unit optimal configuration control is significantly influenced by the external ambient temperature.

3.5.2 Effects of the configuration control

The effects of the cooling unit control strategy presented and described in Section 3.4 on the operation of the system are firstly investigated. To this extent, operation in the most severe environmental conditions is considered and, therefore, the last door opening and delivery of goods in the morning mission reported in Table 3.11 in the month of August is highlighted in Figure 3.8. The ON periods of the cooling unit, enforced by the system thermostat to keep the internal air temperature in the desired range, are also indicated in the figure.

Figure 3.8a reports the external ambient temperature T_{amb}, the temperature of the air inside the refrigerated box T_i and the relative humidity inside the refrigerated box RH_i for the considered period of

the delivery mission (from 12:19 to 12:39). For the same period, the thermal power exchanged by the main evaporator, by the auxiliary evaporator and by the gas cooler (respectively $\dot{Q}_{evap}$, $\dot{Q}_{evap,AUX}$ and $\dot{Q}_{gc}$) are reported in Figure 3.8b.

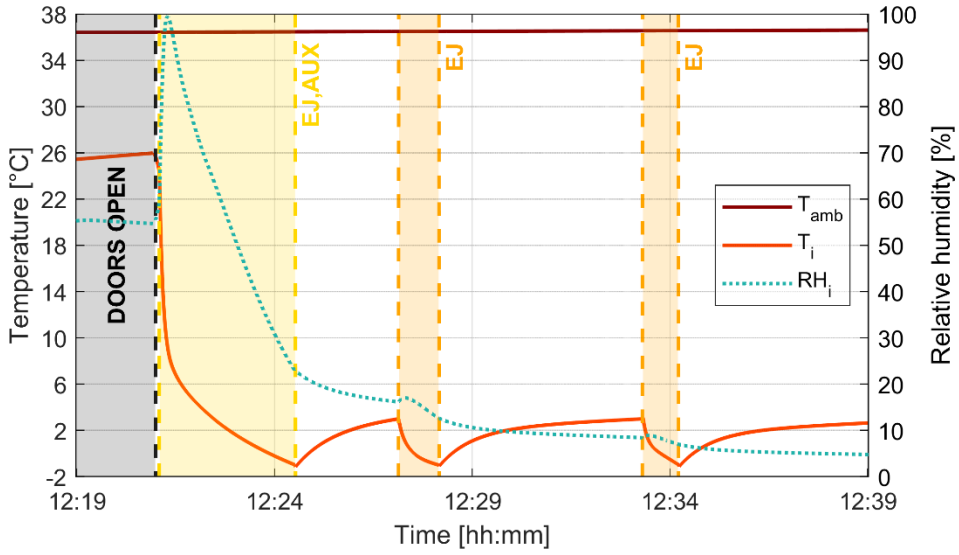

(a)

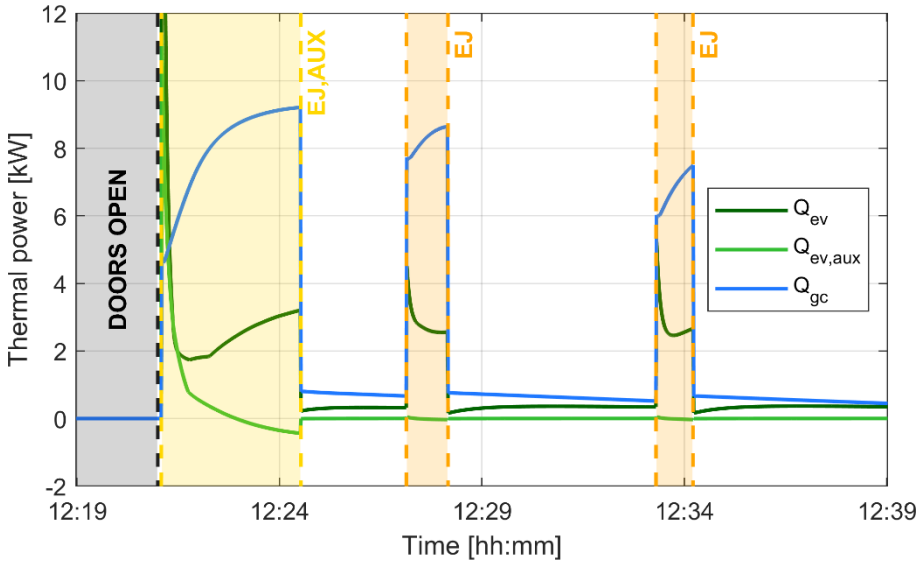

(b)

Figure 3.8 – Effects of the configuration control strategy on the system operation: (a) ambient temperature, internal air temperature, internal relative humidity; (b) thermal power exchanged by the main evaporator, auxiliary evaporator and gas cooler.

From Figure 3.8a it can be observed that, after the door opening to perform the delivery of part of the transported products, the internal air temperature is significantly higher than the maximum allowed internal temperature of 3°C, due to the infiltration of ambient air inside the insulated box. For this reason, when the doors are closed and the cooling unit is turned on, the first ON period is performed in EJ,AUX configuration, to maximize the cooling capacity of the refrigerating system and restore the desired

temperature range of the air inside the insulated box in the shortest time possible, consistently with the control strategy presented in Figure 3.7.

After the internal temperature is cooled down, hysteresis cycles are enforced by the thermostat to keep -1°C < T_i < 3°C, with closed doors. The second and the third ON periods, however, are performed in EJ configuration since, according to the control strategy presented in Figure 3.7, the internal air temperature does not exceed its maximum allowed value and, therefore, the maximization of the COP is preferred. Since the ambient temperature during the highlighted period is always higher than the value of $T_{amb,switch}$ = 33°C presented in Section 3.4, EJ configuration is selected for the second and third ON periods to guarantee the best performance of the refrigeration system.

The difference between the operation in EJ and EJ,AUX configurations can be clearly appreciated considering the thermal powers reported in Figure 3.8b. During the first ON after the door closing, performed in EJ,AUX configuration, both the main evaporator and the auxiliary evaporator provide a positive cooling effect inside the insulated box for the first minutes of the system operation. The auxiliary evaporator contribution to the total cooling effect is initially significant, when the internal air temperature is high. However, as T_i approaches the setpoint, its contribution becomes negligible and then even slightly negative for the last seconds of the ON period.

This behavior is due to the fact that T_i has become lower than the saturation temperature of the refrigerant flowing in the auxiliary evaporator coils, which depends on the intermediate pressure level of the separator $p_{separator}$ which in turn is tied to the pressure lift that can be provided by the ejector. At that point, operation in EJ,AUX configuration becomes counterproductive in terms of system performance and EJ configuration should be selected. However, the switch to the EJ configuration can not be performed during system operation to avoid valves opening and closing with flowing refrigerant. The valves are actuated right after the unit shut down, once the OFF setpoint is reached, and the following ON periods are performed in the EJ configuration.

In general, a fast recovery of the temperature range in which the transported products have to be maintained during transport is more important in terms of cold chain preservation than operation at the highest performance possible. In addition, the negative contribution of the auxiliary evaporator to the total cooling effect occurs only in the last seconds of the first ON period after door openings and therefore leads to a limited impact on the overall mission performance, but it provides a crucial contribution to the safety of the cold chain of the transported products.

3.5.3 Annual performance of the refrigerating system

The mission described in Table 3.11 is then performed for a representative day for every month in the year, whose average climatic conditions are obtained following the procedure described in Section 3.5.1,

to evaluate the performance of the system under the different environmental conditions which characterize a year in its entirety.

The total cooling energy provided by the refrigeration unit during the entire day of delivery mission is reported in Figure 3.9 for the reference day of every month of the year. The percentage of the cooling energy provided by the auxiliary evaporator and by the main evaporator, highlighting for the latter also the rate of cooling energy provided in EJ configuration and in EJ,AUX configuration, is also reported in the figure.

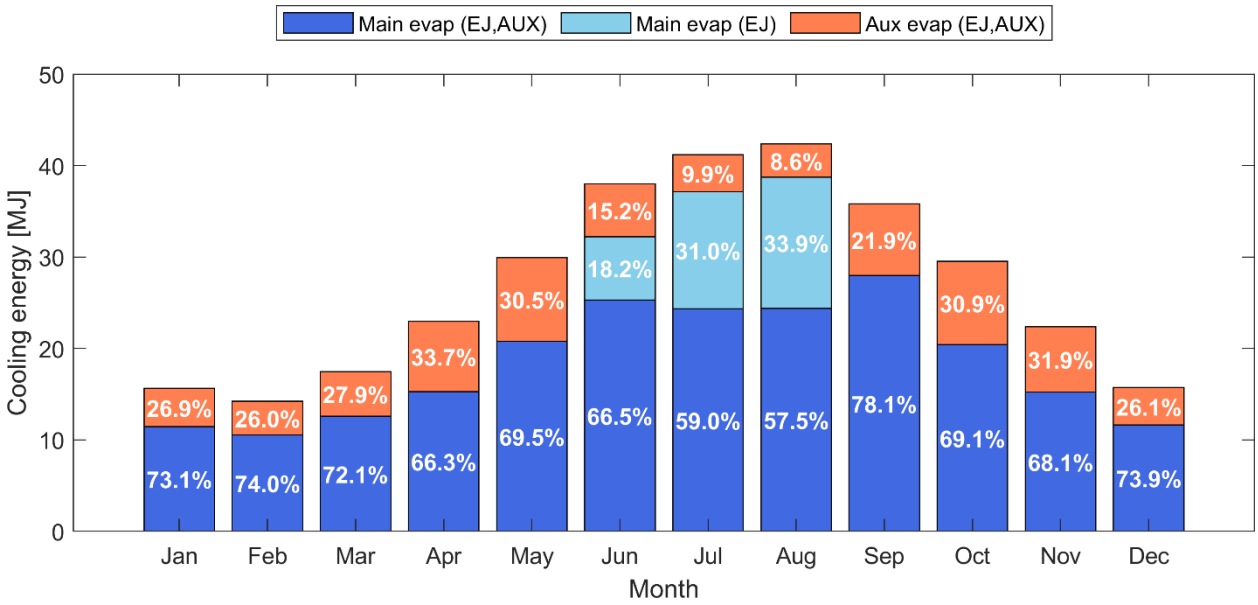

Figure 3.9 – Total cooling energy provided by the cooling unit for every month of the year, divided between main evaporator (in EJ and EJ,AUX configurations) and auxiliary evaporator.

The amount of cooling energy provided by the auxiliary evaporator is lower in the hottest months of the year (June, July and August). In these months, in fact, the ambient temperature is higher than the value of $T_{amb,switch}$ = 33°C for most of the mission time, and a significant part of the total cooling energy is therefore provided in EJ configuration, maximizing the system COP. For this reason, the overall contribution of the main evaporator to the total cooling energy is higher than in the other months.

However, even if the EJ configuration is selected for a large part of mission time, the amount of cooling energy provided in EJ,AUX configuration is still higher than the energy provided in EJ configuration. This behavior is due to the fact that the EJ,AUX mode is selected for the first hours in the morning, when the ambient temperature is still under 33°C and, notably, for the first ON period after each of the 14 door openings and deliveries to recover quickly the desired temperature range inside the insulated box, as discussed in Section 3.5.2. In fact, during these ON periods the cooling demand is the highest, in order to pull down the internal air temperature to controlled conditions. Moreover, for the same reason the first ON after a delivery is significantly longer than the following ones, thus leading to the increase of the overall portion of cooling energy provided in EJ,AUX configuration.

During the other months of the year, instead, the environmental temperature never exceeds the value of $T_{amb,switch}$ = 33°C, and therefore the EJ,AUX configuration always leads to the maximization of both the COP and of the cooling capacity for the temperature pulldowns after door openings.

The overall quantities of cooling energy provided in the different configurations and by the main and auxiliary evaporators are summarized in Table 3.12 for every month of the year.

Table 3.12 – Cooling energy provided in the different configurations and by the main and auxiliary evaporators for every month of the year.

	Jan	Feb	Mar	Apr	May	Jun	Jul	Aug	Sep	Oct	Nov	Dec
Total cooling energy [MJ]	15.6	14.2	17.4	23.0	29.9	38.0	41.2	42.4	35.8	29.5	22.4	15.7
Cooling energy in EJ config from main evaporator [MJ]	0.0	0.0	0.0	0.0	0.0	6.9	12.8	14.3	0.0	0.0	0.0	0.0
Cooling energy in EJ,AUX config [MJ]	15.6	14.2	17.4	23.0	29.9	31.1	28.4	28.0	35.8	29.5	22.4	15.7
Cooling energy in EJ,AUX config from main evaporator [MJ]	11.4	10.5	12.6	15.3	20.8	25.3	24.3	24.4	28.0	20.4	15.2	11.6
Cooling energy in EJ,AUX config from auxiliary evaporator [MJ]	4.2	3.7	4.8	7.7	9.1	5.8	4.1	3.6	7.8	9.1	7.2	4.1

Despite the EJ configuration is selected only for three months in the year, the total cooling energy provided in the reference days in June, July and August (38.0 MJ, 41.2 MJ and 42.4 MJ, respectively) accounts for the 37.4% of the total cooling energy provided in the entirety of the year reference days (325.1 MJ).

The optimization given by the of the configuration control during these high cooling demand months therefore leads to a significant improvement in the yearly performance of the system. In fact, the cooling energy provided in EJ configuration is equal to 6.9 MJ in June, 12.8 MJ in July and 14.3 MJ in August, combining for 10.5% of the yearly total cooling energy which, if operating in EJ,AUX configuration, would be provided not optimizing the system COP.

Since the system configuration optimization requires limited variations to the refrigeration system operational schematic, only linked to the eventual bypass of the auxiliary evaporator leading to a different load management between main and auxiliary evaporator when required, it can be concluded that switching between configurations during operation can lead to an improvement of the average performance of the system throughout the year.

To evaluate the overall mission performance of the system operating in unsteady conditions, the overall mission COP, defined in Eq. (3.11) as the ratio between the total cooling energy provided by the evaporators and the electrical energy required by the compressor and heat exchangers fans during the entire mission, is compared to the steady-state COP of the cooling unit, defined as in Eq. (3.8) and considering also the power draw by the heat exchangers fans, evaluated with varying ambient temperature and with a fixed internal air temperature T_i = 1°C, which is the mean value of the hysteresis cycle imposed by the refrigerating system thermostat.

Figure 3.10 reports the average mission COP for every month of the year, referred to the average ambient temperature registered during the daily mission, and the steady-state COP of the unit, evaluated with ambient temperature varying between T_{amb} = 10°C and T_{amb} = 40°C with a step of 2°C and with T_i = 1°C, as mentioned above.

$$COP = \frac{E_{evap} + E_{evap,AUX}}{E_{comp} + E_{fans}} \tag{3.11}$$

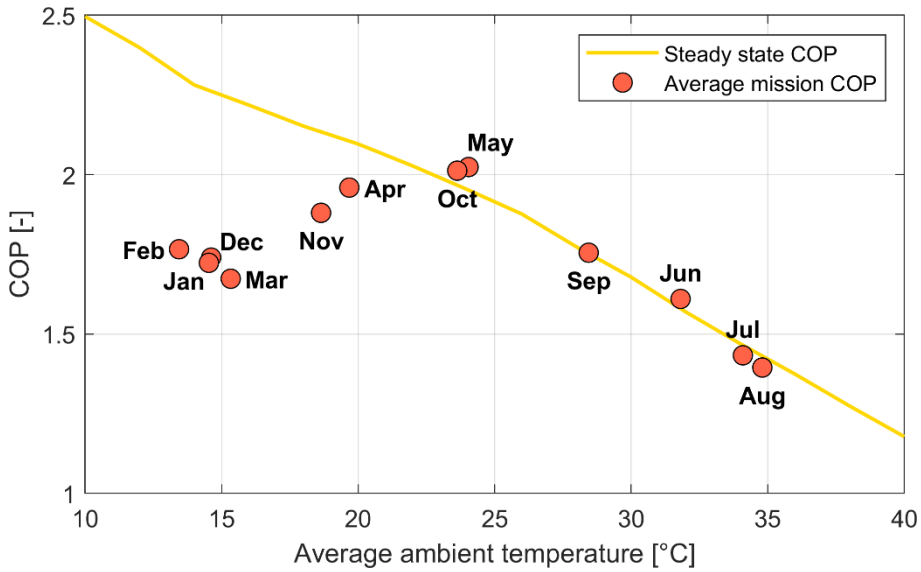

Figure 3.10 – Average delivery mission COP and steady-state COP as a function of the ambient temperature.

For high values of external ambient temperature, the average mission COP is in good agreement with the steady-state COP, decreasing as the ambient temperature increases. However, for low values of external ambient air temperature, the average mission COP presents significantly lower values compared to the steady-state ones, decreasing with decreasing temperature, while the steady-state ones increase with decreasing ambient temperature.

Such a behavior is related to the difference between the cooling power provided by the evaporators in steady-state operation and the actual cooling demand required by the system during the unsteady operation during the mission, defined in Eq. (3.12) as the ratio between the total cooling energy provided

by the evaporators and the time in which the cooling unit is switched on. A high difference between the rated cooling capacity of the cooling unit in steady-state operation and the actual cooling demand required during the mission leads to a low Duty Cycle, defined in Eq. (3.13) as the ratio between the time in which the cooling unit is switched on and the total mission time.

$$\dot{Q}_{evap,TOT} = \frac{E_{evap} + E_{evap,AUX}}{t_{ON}} \tag{3.12}$$

$$\text{Duty cycle} = \frac{t_{ON}}{t_{ON}+t_{OFF}} \tag{3.13}$$

The average ambient temperature, mission COP, cooling demand and Duty Cycle are reported for every month of the year in Table 3.13, while the steady state COP and cooling capacity of the system are summarized in Table 3.14.

Table 3.13 – Average performance of the cooling unit during the daily delivery mission, for every month of the year.

	Jan	**Feb**	**Mar**	**Apr**	**May**	**Jun**	**Jul**	**Aug**	**Sep**	**Oct**	**Nov**	**Dec**
Average ambient temperature [°C]	14.6	13.4	15.3	19.7	24.0	31.8	34.1	34.8	28.4	23.6	18.6	14.5
Average mission COP [-]	1.74	1.77	1.67	1.96	2.02	1.61	1.43	1.40	1.76	2.01	1.88	1.72
Average mission $\dot{Q}_{evap,TOT}$ [kW]	5.37	5.34	5.24	6.39	6.91	6.32	5.91	5.83	6.52	6.85	6.10	5.32
Average mission Duty Cycle [-]	0.068	0.062	0.077	0.083	0.100	0.138	0.162	0.168	0.127	0.100	0.085	0.069

Table 3.14 – Steady-state performance of the cooling unit operating with varying T_{amb} and T_i = 1°C.

T_{amb} [°C]	**10**	**12**	**14**	**16**	**18**	**20**	**22**	**24**	**26**	**28**	**30**	**32**	**34**	**36**	**38**	**40**
Steady state COP [-] (T_i = 1°C)	2.50	2.40	2.28	2.22	2.15	2.10	2.03	1.95	1.88	1.77	1.68	1.57	1.47	1.37	1.27	1.18
Steady state $\dot{Q}_{evap,TOT}$ [kW] (T_i = 1°C)	6.50	6.49	6.62	6.72	6.70	6.66	6.58	6.48	6.35	6.26	6.24	6.17	6.06	5.93	5.74	5.42

The steady-state cooling capacity of the system operating under the ambient temperature of the coldest month of the year (February, $T_{amb,Feb}$ = 13.4 °C), obtained through linear interpolation of the values presented in Table 3.14, is equal to 6.66 kW. For the same month, the average cooling demand evaluated with unsteady operation during the delivery mission is equal to 5.34 kW (-19.8%). Since the external ambient temperature is low, less cooling power is needed compared to the maximum rated cooling capacity of the system operating in steady-state under those conditions, thus reducing significantly the

Duty Cycle and leading to an average performance which is considerably far from the steady state operating conditions.

On the contrary, the steady-state cooling capacity evaluated through interpolation for the ambient temperature corresponding to the hottest month of the year (August, $T_{amb,Aug}$ = 34.8 °C) is equal to 6.01 kW, while the average cooling demand registered during the delivery mission in the same month is equal to 5.83 kW (-3.0%), leading to a significantly higher Duty Cycle and thus justifying the higher agreement between the steady-state COP and the average mission COP of the system for higher ambient temperature conditions.

3.6 Numerical evaluation of a long-range single-drop delivery

After the evaluation of the yearly cooling unit performance during a short-range multi-drop delivery mission in an urban environment, the behavior of the system during a long-range single-drop delivery mission is investigated.

3.6.1 Delivery mission structure

Since in a long-range delivery mission the main focus is to transport a high quantity of products from a storage point to another, an insulated body with higher storage capacity compared to the one considered in Section 3.5 is considered for this mission. The insulated body considered in this section is characterized by an internal volume of 20.30 m^3 and its main geometrical dimensions are reported in Table 3.15. A global heat transfer coefficient K = 0.39 W m^{-2} K^{-1} was evaluated for the insulated box considered for the long-distance mission, still following the procedure defined in Annex 1 of the ATP agreement [82].

Table 3.15 – Main geometrical dimensions of the insulated body (long-range mission).

Element	Dimension
External height H_e	2.74 m
External length L_e	3.40 m
External width W_e	2.60 m
External surface S_e	50.56 m^2
Internal surface S_i	44.96 m^2
Internal volume V_i	20.30 m^3

Differently from the short-range mission considered in Section 3.5, in this case the mission simulates the transport of perishable products from a distributor's storage point to another, in a long-distance single delivery. The mission is defined through the same input parameters (vehicle target speed, openings of the doors, fraction of loaded goods) of the delivery mission presented in Section 2.3 and in Section 3.5. A two-hours pulldown brings the internal air temperature to the desired temperature range (-1°C $< T_i <$ 3°C); after that, 600 kg of meat products are charged inside the vehicle insulated box under controlled

temperature conditions (4°C). The perishable goods will be dropped-off entirely in a single delivery at the end of the daily mission travel. The heat capacity and the convective heat transfer coefficient of the meat is the same described in Section 2.3. The vehicle target speed is set through standard WLTC profiles, defined with a frequency of 1 Hz. In this case, two Urban cycles followed by two SubUrban cycles are used to simulate the urban drive condition from the starting logistic facilities, located in an urban area, to the highway. Then the highway drive is defined following a single High cycle until the truck reaches the cruise speed of 100 km/h, which will be maintained for the whole highway travel. A one-hour lunch break is considered around midday, then the mission is continued with the highway path, followed by two SubUrban and Urban cycles to conclude the travel to the final delivery logistic facility. After the unloading operations, which are supposed to last for one hour such as the morning loading operations, the vehicle is parked at the owner's premises empty, with the cooling unit kept off, until the following morning. The complete mission structure is reported in Table 3.16.

Table 3.16 – Delivery mission structure (long-range mission).

Start time [hh.mm]	**Duration [hh.mm]**	**Activity**	**Travel distance [km]**
06.00	02.00	Pulldown (Pre-Cooling)	-
08.00	01.00	Loading	-
09.00	0.20	2x Urban Driving Cycles	6
09.20	0.15	2x SubUrban Driving Cycles	10
09.35	2.55	Highway drive at fixed speed	300
12.30	1.00	Stop	-
13.30	2.55	Highway drive at fixed speed	300
16.25	0.15	2x SubUrban Driving Cycles	10
16.40	0.20	2x Urban Driving Cycles	6
17.00	01.00	Unloading	-
18.00	-	Stop	-
TOTAL	**12.00**	**-**	**632**

Since the annual performance evaluation of the system has been already carried out in Section 3.5, in this case the operation in the hottest month of the year, August, has been considered. Therefore, a reference mean day for the month of August in the city of Athens has been considered for the simulation. The environmental temperature, relative humidity and solar radiation intensity are still collected from the Energy Plus online database [95] for the entire month of August and then averaged hourly to obtain the climatic profile of the mean day. Similarly to what was done in Section 3.5, the hourly ambient temperature is then corrected as reported in Mihalakakou et al. [109] to consider the Urban Heat Island (UHI) phenomenon. However, the UHI effect is considered exclusively during the pulldown, loading/unloading and urban driving cycles, which are supposed to happen in an urban environment, while the rest of the mission is performed in an extra-urban environment.

3.6.2 Effects of the configuration control

The performance of the cooling unit is evaluated through the COP and the Duty Cycle, defined in the same way as previously described in Eq. (3.11) and in Eq. (3.13), respectively. The average mission COP and Duty Cycle are reported in Table 3.17 together with the average ambient temperature registered during the mission day.

Table 3.17 – Average performance of the cooling unit during the daily delivery mission.

Average ambient temperature [°C]	31.5
Average mission COP [-]	1.60
Average mission Duty Cycle [-]	0.101

Figure 3.11 reports the steady-state COP of the cooling unit operating in both EJ configuration and EJ,AUX configuration, evaluated with fixed internal air temperature (T_i = 0°C) and varying ambient temperature, as previously reported in Table 3.5 and in Table 3.6. The average mission COP, referred to the average ambient temperature registered during the mission, is also included in the figure.

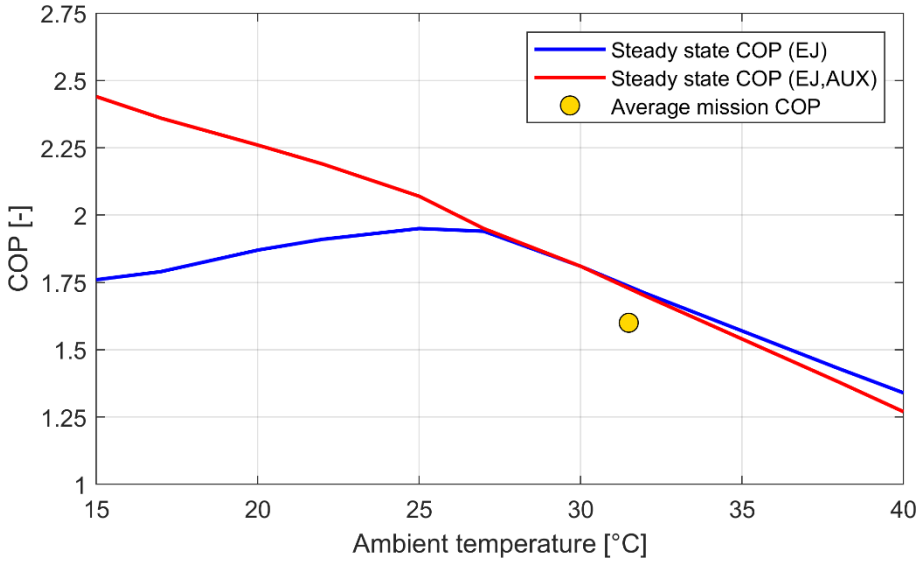

Figure 3.11 – Steady-state COP in EJ configuration and EJ,AUX configuration (evaluated for varying T_{amb} and T_i = 0°C) and average delivery mission COP, referred to the average mission ambient temperature.

As discussed for the short-range delivery missions in Section 3.5.3, the average mission COP presents a lower value compared with the steady-state COP evaluated at the same ambient temperature due to the low Duty Cycle caused by the ON/OFF cycles imposed by the thermostat during the mission, which leads to a deterioration of the system performance compared to the rated steady-state one.

Notably, in a long-range delivery mission with a single door opening at the end of the day, the deterioration of the average mission COP is even more appreciable than in a multi-drop delivery mission.

In fact, the absence of door openings leads to less heat infiltrations in the insulated box, thus reducing the cooling demand and the time in which the cooling unit has to be switched on.

The effects of the cooling unit control strategy presented and described in Section 3.4 on the operation of the system are then highlighted, as done in Section 3.5.2 for the short-range mission. Since in the long-distance mission no door openings are performed, the effects of the configuration control strategy can be appreciated mainly right after the end of the loading phase at the beginning of the mission. For this reason, the period between 8:55 and 9:35 is reported in Figure 3.12. The ON periods of the cooling unit, enforced by the system thermostat to keep the internal air temperature in the desired range, are also indicated in the figure.

Following the same structure presented in Section 3.5.2, Figure 3.12a reports the external ambient temperature T_{amb}, the temperature of the air inside the refrigerated box T_i and the relative humidity inside the refrigerated box RH_i for the considered period, while Figure 3.12b reports the thermal power exchanged by the main evaporator, by the auxiliary evaporator and by the gas cooler (respectively $\dot{Q}_{evap}$, $\dot{Q}_{evap,AUX}$ and $\dot{Q}_{gc}$).

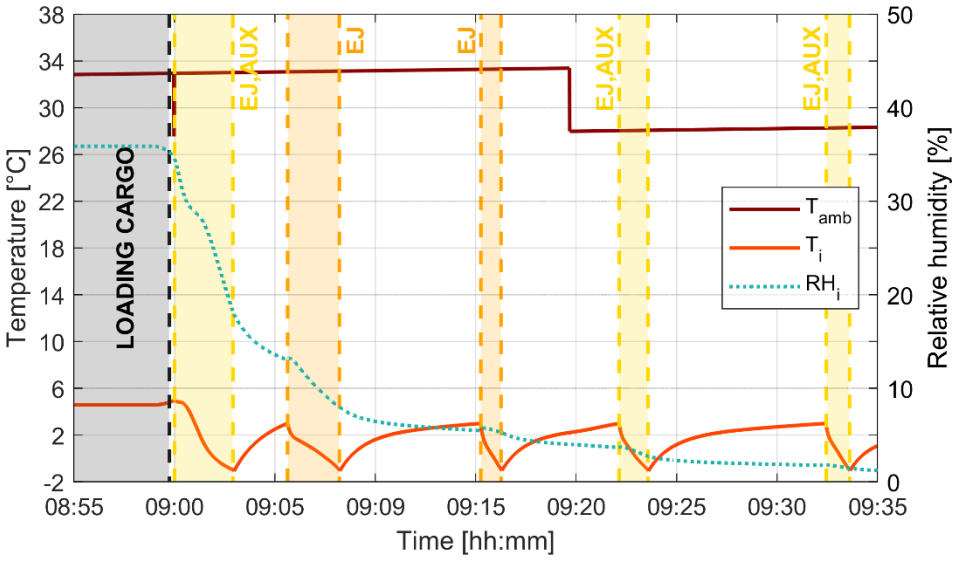

(a)

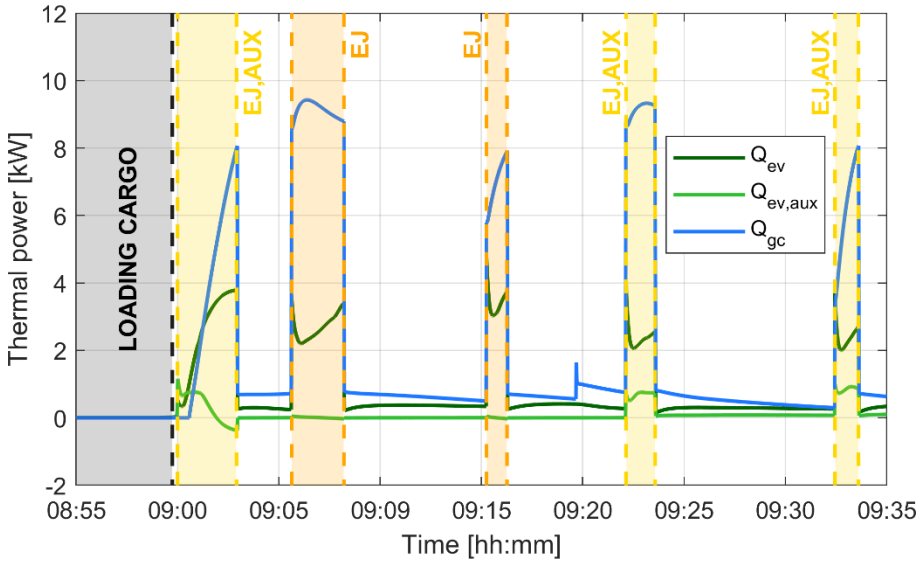

(b)

Figure 3.12 – Effects of the configuration control strategy on the system operation: (a) ambient temperature, internal air temperature, internal relative humidity; (b) thermal power exchanged by the main evaporator, auxiliary evaporator and gas cooler.

The configuration to be enforced at the beginning of every ON period imposed by the thermostat is set accordingly to the strategy summarized in Figure 3.7. After the door closing at the end of the loading phase, the first ON is performed in EJ,AUX configuration since T_i > 3°C and, regardless of the external ambient temperature, the maximization of the cooling effect is preferred, to recover quickly the temperature setpoint. Conversely, from the second ON period onwards the internal air temperature is always maintained in the desired range -1°C < T_i < 3°C by the thermostat and, therefore, the maximization of the system COP is preferred, depending on the external ambient temperature.

For this reason, the second and third ON periods are performed in EJ configuration, since the internal air temperature is in the desired range and the ambient temperature is higher than $T_{amb,switch}$ = 33°C. However, at 9:20 the vehicle finishes its urban driving cycles and it is supposed to move in an extra-urban environment while performing suburban and highway driving cycles. Moving away from the metropolitan area leads to a reduction of the external ambient temperature due to the removal of the temperature correction linked to the Urban Heat Island phenomenon, as it was previously described in Section 3.6.1. As a consequence of the reduction of T_{amb} under the value of $T_{amb,switch}$ = 33°C, the fourth and fifth ON periods are performed in EJ,AUX configuration.

The effects of the configuration control on the cooling effect provided by the refrigeration system can be appreciated in Figure 3.12b. For the same reasons extensively discussed in Section 3.5.2, the auxiliary evaporator contribution to the overall cooling effect is significant in the first minutes of the first ON period but, as T_i approaches its setpoint its contribution becomes null and then slightly negative. The recovery of the internal temperature setpoint is preferred for the correct preservation of the transported goods

rather than pursuing the cooling unit best performance during the entire mission. In the following ON periods, instead, the configuration leading to the best COP is selected as a function of the ambient temperature and, in fact, it is possible to observe that in the last ON periods performed in EJ,AUX configuration, the contribution of the auxiliary evaporator to the total cooling effect is always positive.

The total cooling energy and the overall quantities provided in each configuration and by the main and auxiliary evaporators are summarized in Table 3.18.

Table 3.18 – Cooling energy provided in each configuration and by the main and auxiliary evaporators during the delivery mission.

Total cooling energy [MJ]	27.0
Cooling energy in EJ config from main evaporator [MJ]	0.9
Cooling energy in EJ,AUX config [MJ]	26.1
Cooling energy in EJ,AUX config from main evaporator [MJ]	21.1
Cooling energy in EJ,AUX config from auxiliary evaporator [MJ]	5.0

Overall, 96.7% of the cooling energy provided during the mission is produced operating in EJ,AUX configuration, with a significant increase compared with the cooling energy production in the same month in the short-range mission, in which only 66% of the total cooling energy was produced in EJ,AUX configuration, as calculated from the data reported in Table 3.12. The increase in the EJ,AUX configuration operation is linked to the removal of the temperature correction due to the Urban Heat Island phenomenon, since in this case most of the mission is performed outside of metropolitan areas.

During EJ,AUX configuration operation, in which both the main and the auxiliary evaporator are involved in the cooling effect production, 19.2% of the cooling effect is provided by the auxiliary evaporator, while the remaining 80.8% is provided by the main evaporator. The cooling energy production of the main evaporator is approximately four times the one of the auxiliary evaporator, in accordance with the ratio between the external exchange area of the two heat exchangers which is close to 4:1, as reported in Table 3.1.

3.6.3 Ejector performance

The key component enabling both the EJ configuration and the EJ,AUX configuration is the two-phase ejector, inserted in the system schematic to provide a pressure lift from the main evaporator pressure to the separator pressure, thus reducing the pressure ratio of the cooling unit compressor and, consequently, its electrical power draw.

The capability of the ejector to recover energy from the motive flow is significantly dependent on the motive mass flow rate pressure and temperature properties, which are enforced by the system PI

controllers as a function of the external ambient temperature. Therefore, two ON periods of the cooling unit in different moments of the mission, corresponding to an average ambient temperature of approximately 32°C and 36°C during the ON period, are considered to investigate the variation of the performance of the ejector under different environmental temperature conditions.

Figure 3.13 and Figure 3.14 report, respectively for $T_{amb} \cong 32°C$ and for $T_{amb} \cong 36°C$, the motive nozzle mass flow rate $\dot{m}_{motive}$, the suction nozzle mass flow rate $\dot{m}_{suction}$, the ejector entrainment ratio, defined as the ratio between suction and motive mass flow rates as described in Eq. (3.5), as well as the pressure lift, defined as the difference between the pressure at the liquid separator and the pressure at the main evaporator in Eq. (3.14), and the ejector efficiency, following the definition given in Eq. (3.15) by Elbel and Hrnjak [110].

$$\Delta p_{lift} = p_{separator} - p_{evap} \tag{3.14}$$

$$\eta_{ej} = \phi \frac{h_{is}(p_{separator}, s_{evap,OUT}) - h_{evap,OUT}}{h_{gc,OUT} - h_{is}(p_{separator}, s_{gc,OUT})} \tag{3.15}$$

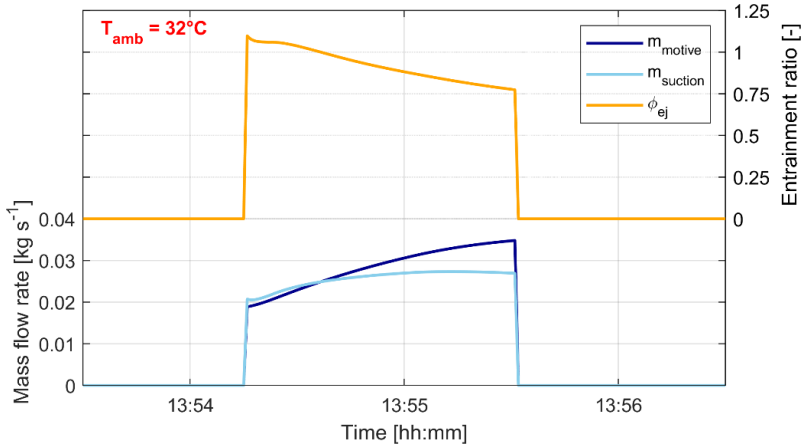

(a)

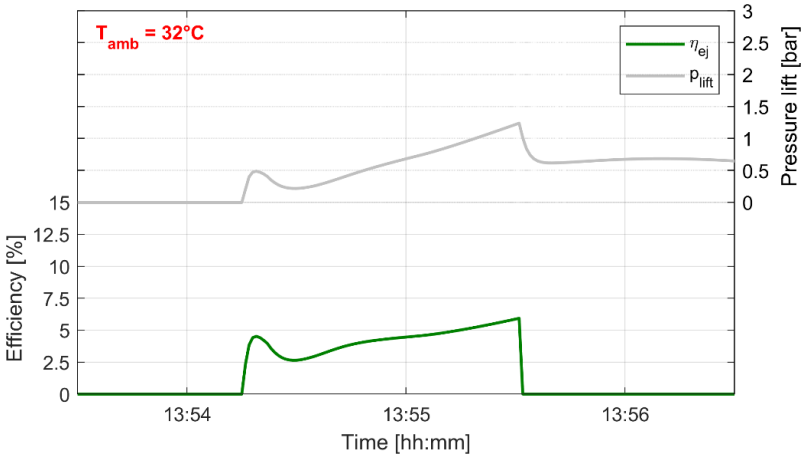

(b)

Figure 3.13 – Operating parameters of the two-phase ejector for $T_{amb} \cong 32°C$: (a) mass flow rates and entrainment ratio; (b) ejector efficiency and pressure lift.

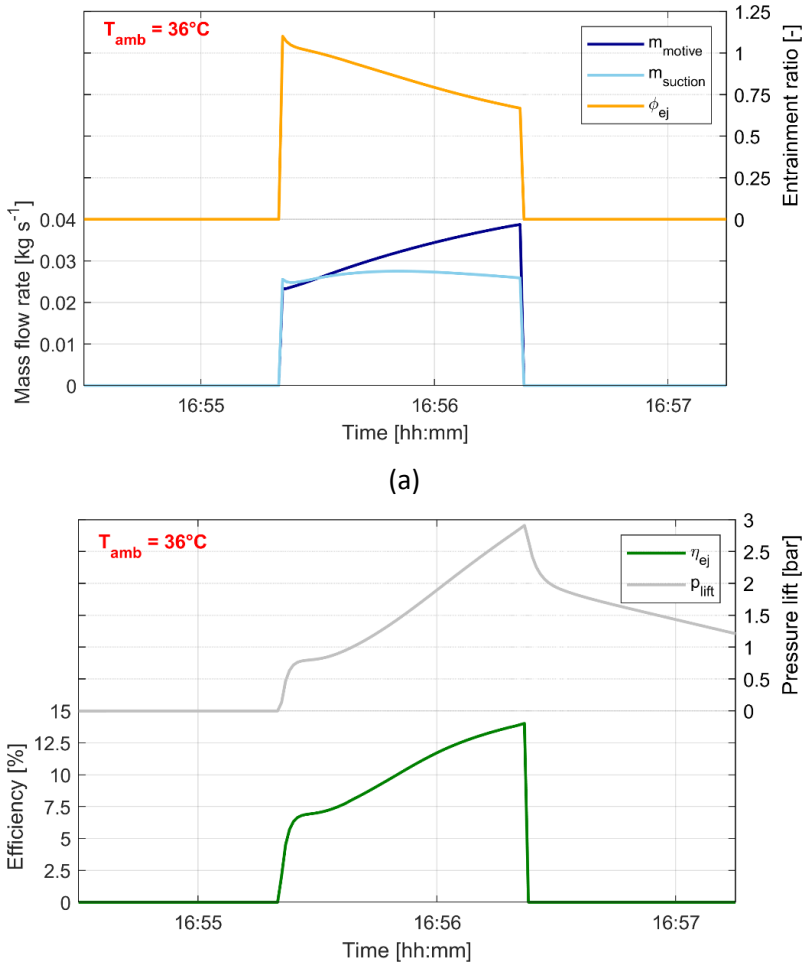

Figure 3.14 – Operating parameters of the two-phase ejector for $T_{amb} \cong$ 36°C: (a) mass flow rates and entrainment ratio; (b) ejector efficiency and pressure lift.

The ON periods highlighted in Figure 3.13 and in Figure 3.14 are determined by the system thermostat controlling the temperature of the air inside the insulated box T_i. At the beginning of the highlighted periods the unit is switched off until T_i = 3°C. At this point, the difference between the pressure at the liquid separator and the pressure at the main evaporator is null and, when the cooling unit is switched on, the ejector starts providing a pressure lift, allowing the main evaporator pressure to decrease to the value enforced by the throttling valve MTV placed between the separator and the main evaporator inlet. The cooling unit is then switched on by the thermostat when the internal air temperature reaches the value of T_i = -1°C.

The cooling unit and the ejector operation in the highlighted periods is strongly variable: the evaporating conditions, both in the main and in the auxiliary evaporator, change continuously during an ON period, as well as the separator and main evaporator pressure levels, and for this reason the ejector operating parameters present significant variations during the ON period.

The comparison between the data presented in Figure 3.13, referred to an ON occurred with $T_{amb} \cong$ 32°C, and the data presented in Figure 3.14, referred to an ON occurred with $T_{amb} \cong$ 36°C, shows that both the ejector efficiency and the average pressure lift increase significantly for higher values of the ambient temperature, consistently with the increased energy of the motive refrigerant stream.

The average entrainment ratio, ejector efficiency and pressure lift registered during the cooling unit operations highlighted in Figure 3.13 and Figure 3.14 are reported in Table 3.19. It can be observed that the maximum values of the average ejector efficiency (10.1%) and of the average pressure lift (1.59 bar) are reached during the ON period occurred at higher ambient temperature (36°C), thus underlining the better performance of the two-phase ejector under harsh environmental conditions.

Table 3.19 – Operating parameters of the ejector, averaged over a ON period, at different ambient temperatures.

$T_{amb,avg}$ [°C]	ϕ_{avg} [-]	$\eta_{ej,avg}$ [%]	$\Delta p_{lift,avg}$ [bar]
31.9 (EJ,AUX config.)	0.92	4.2	0.63
36.0 (EJ config.)	0.86	10.1	1.59

However, the absolute values of the average ejector efficiency and pressure lift evaluated during the ON periods of the mission are significantly lower than the corresponding values evaluated in steady-state operation with the same ambient temperature and internal air temperature T_i = 0°C, which are reported in Table 3.20.

Table 3.20 – Operating parameters of the ejector in steady-state operation, for T_{amb} = 36°C and T_i = 0°C.

T_{amb} [°C]	ϕ [-]	η_{ej} [%]	Δp_{lift} [bar]
31.9 (EJ,AUX config.)	0.61	17.0	3.32
36.0 (EJ config.)	0.58	15.8	3.75

The difference in the ejector performance between the steady-state operation and the ON periods registered during the delivery mission is related to the transient nature of the operation following the switch on of the cooling unit in the delivery mission. After the switch on, in fact, the cooling unit needs some time to recover its operating conditions, to bring down the separator pressure and, consequently, also the evaporation pressure from the value at which the system has established during the previous OFF period. From both Figure 3.13 and Figure 3.14 it can be observed that both the pressure lift and the ejector efficiency are still increasing at the moment of the switch off imposed by the thermostat: the short time (approximately one minute) of the ON periods leads to an ejector operation characterized by lower pressure lifts compared to the ones that would be reached in steady-state operation, thus explaining the

degradation of the ejector performance compared to the steady-state conditions, since the considered ejector efficiency increases for high pressure lifts.

It must be pointed out that, both during the highlighted ON periods and in steady-state operation, the efficiency of the ejector is quite low, always under 20%. The considered ejector, a high-pressure lift vapor cartridge (see Section 3.2.5), was chosen as it represents the solution among the ejectors currently available in the market which fits best this specific application (smallest available throat diameter), as R744 ejectors are designed and developed mostly for larger commercial refrigeration applications. The above-discussed analysis of the ejector efficiency highlights that an ejector design based on the needs of this specific application (low pressure lift, high entrainment ratio) could lead to significant performance improvements.

3.6.4 Liquid separator pressure control during long inactivity

One of the main issues to be faced when considering a R744 refrigeration system is represented by the temperature and pressure drift inside the unit pipes and components when the low-pressure side approaches the ambient temperature during long periods of inactivity.

Due to the heat exchange with the external environment, the vapor quality inside the liquid separator continuously increases and, consequently, the pressure level inside the separator and inside the pipes in the low-pressure side of the unit increases as well.

When this pressure drift effect is not contrasted, the low-pressure side has to be designed to resist to pressure levels similar to the high-pressure side of the unit, leading to an expensive and bulky system. On the other side, if the pressure drift inside the liquid separator can be somehow contrasted, the design maximum pressure of the components and pipelines in the low-pressure side of the system can be lowered to a more acceptable value.

The numerical model of the system is therefore used to test a novel safety control system integrated in the system control strategy with the objective of monitoring the pressure inside the liquid separator during long inactivity. When the maximum allowed pressure value in the separator ($p_{threshold}$) is reached, the safety control turns on the cooling unit compressor and acts on the solenoid valves S-1, S-2, S-3 and S-4 reported in Figure 3.1 to modify the circuit and realize the schematic presented in Figure 3.15.

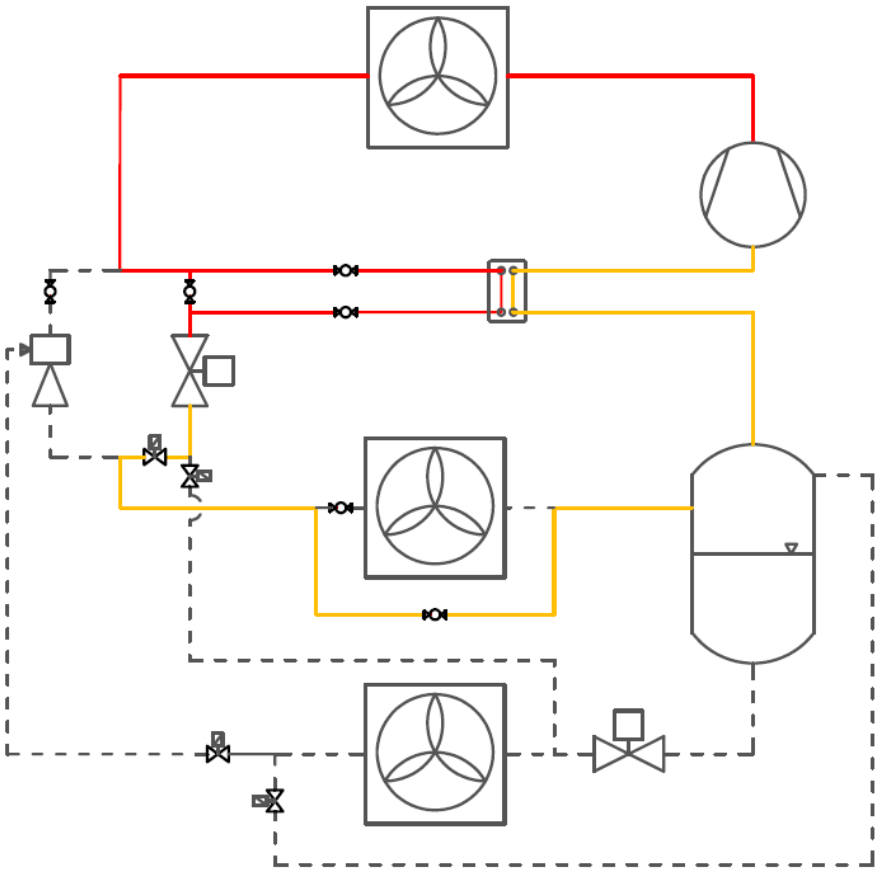

Figure 3.15 – Operational schematic of the refrigerating system to lower the liquid separator pressure from $p_{threshold}$ = 60 bar to p_{reset} = 30 bar (safety cycle).

In this phase, the objective of the safety control system is just to lower the separator pressure down to a safer reset pressure value p_{reset} and not to provide any refrigerating effect, since this phenomenon is supposed to happen during long inactivity of the cooling unit, in which the insulated box is not charged with temperature-controlled goods. For this reason, both the main and the auxiliary evaporators are bypassed, and the compressor has only the function to extract the refrigerant in vapor state from the separator and to return a low vapor quality flow to it.

Once the reset pressure value p_{reset} is reached, the control system turns off the compressor and keeps it off until the convective heat coming from the external ambient air increases the separator pressure to the $p_{threshold}$ value again.

For structural and thermodynamic safety reasons, the threshold and reset pressure values are set to $p_{threshold}$ = 60 bar and p_{reset} = 30 bar, respectively, in order to maintain the low-pressure side of the cooling unit always at safety distance from the R744 critical pressure (p_{crit} = 73.8 bar).

To evaluate the energy consumed by the system to perform a safety cycle during long periods of inactivity, the pressure increase in the liquid separator was calculated two different setups and two different ambient conditions. In one of the setups, the presence of an external insulation layer made of expanded

polystyrene, characterized by a thickness of l_{ins} = 0.05 m and a thermal conductivity of λ_{ins} = 0.04 W m^{-1} K^{-1}, is included in the model. In the other setup, no insulation is assumed to be placed around the liquid receiver. For each of these setups, the behavior of the system was evaluated under an ambient temperature which is assumed to be the average night temperature of the mean August day ($T_{avg,night}$ = 24.7 °C, averaged from 18:00 in the evening to 06:00 in the morning) and under an ambient temperature which is assumed to be the average entire mean August day temperature ($T_{avg,day}$ = 31.3 °C, averaged on the whole day from 00:00 to 24:00). The evaluation of the system behavior under $T_{avg,night}$ can be useful to estimate the system evolution between two consequent working days, while the evaluation under $T_{avg,day}$ is useful to estimate the system evolution on a daily base, for example during non-working days such as during the weekends.

The time required to the system, with the given refrigerant charge of 25 kg of R744, to reach the pressure threshold value in the above-mentioned four different scenarios is reported in Table 3.21, together with the number of expected safety cycles to be performed in the correspondent reference time to maintain the system below the threshold pressure.

Table 3.21 – Time needed to reach the maximum allowed pressure inside the separator, starting from the conditions obtained at the end of the delivery mission, with and without insulation and with different T_{amb}.

	Environmental temperature	**Reference time**	**Time to reach $p_{threshold}$**	**Expected safety cycles**
With insulation (l_{ins} = 0.05 m; λ_{ins} = 0.04 W m^{-1} K^{-1})	$T_{avg,night}$ = 24.7°C	18:00 – 06:00 [12 h]	65 h 58 min	None
	$T_{avg,day}$ = 31.3°C	00:00 – 24:00 [24 h]	33 h 00 min	None
Without insulation	$T_{avg,night}$ = 24.7°C	18:00 – 06:00 [12 h]	15 h 31 min	None
	$T_{avg,day}$ = 31.3°C	18:00 – 06:00 [24 h]	6 h 19 min	4

With the presence of the additional expanded polystyrene insulating layer, the liquid separator can be exposed for more than one entire summer day to the environmental convective heat infiltration before the maximum allowed pressure is reached. Moreover, with no insulation around the separator, an entire night (from the end of a daily mission at 18:00 to the beginning of the next one on the following day at 06:00) can be handled without the need of a safety cycle. However, if the cooling unit is kept off during an entire summer day without insulation around the liquid separator, a safety cycle will be necessary approximately every six hours.

Focusing on the worst-case scenario of ambient air temperature equal to the average day temperature ($T_{avg,day}$ = 31.3 °C) and absence of insulation around the separator, the separator pressure and the internal vapor quality variations in time are reported in Figure 3.16a, starting from the initial conditions registered at the end of the delivery mission, after the unloading of the transported goods, until a safety

cycle to lower the separator pressure is performed. Figure 3.16b highlights the pressure and vapor quality variations due to the safety cycle focusing only on the safety cycle operation, when the separator pressure is brought from $p_{threshold}$ down to p_{reset}.

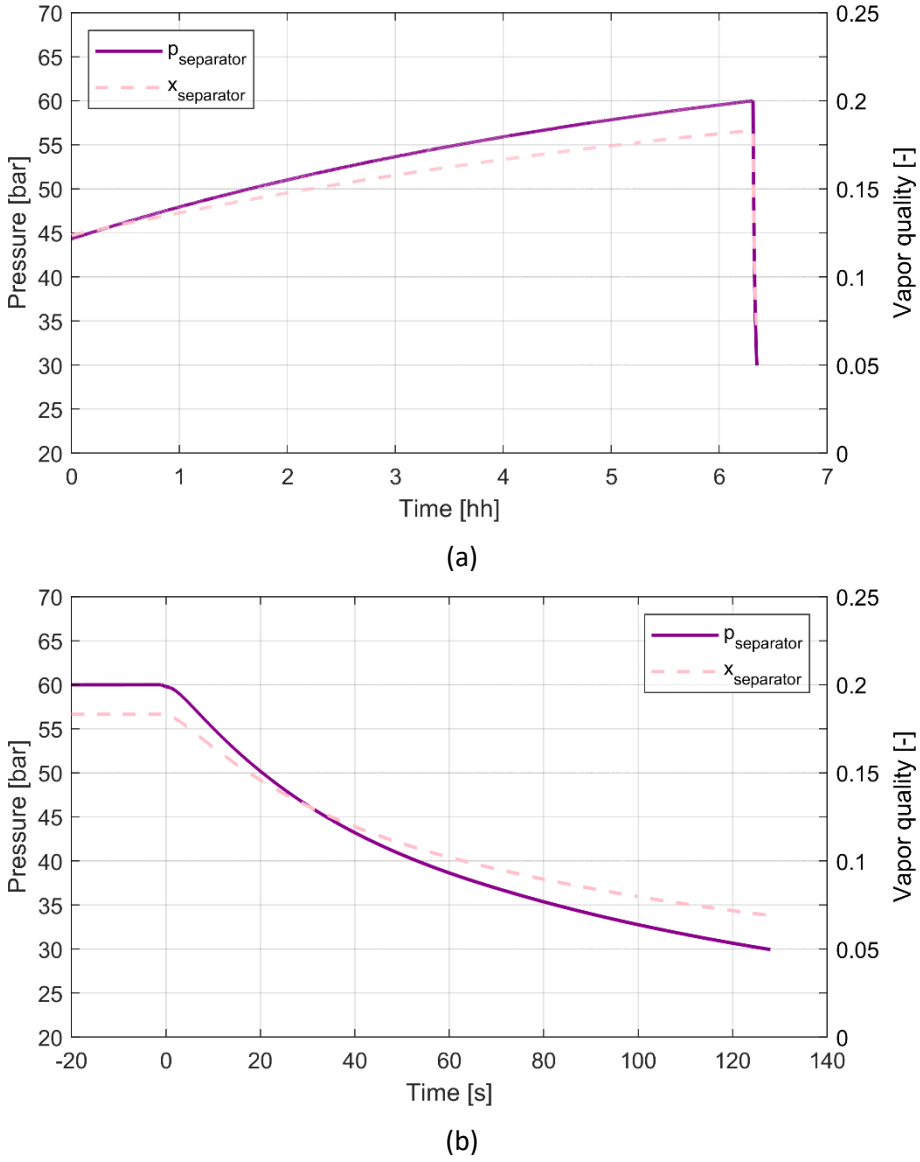

Figure 3.16 – Safety cycle with no insulation and with $T_{amb} = T_{avg,day}$: (a) Liquid separator pressure and vapor quality during an OFF period followed by a safety cycle; (b) pressure and vapor quality during the safety cycle operation.

The safety cycle requires approximately two minutes (129 s) and a total electrical energy supply of $E_{safety\ ON}$ = 0.77 MJ to run the compressor and the gas cooler fans.

While the results summarized in Table 3.21 suggest that, even in the worst-case scenario with no insulation layer, a whole night stop between consecutive working days in not long enough to require the execution of a safety cycle, it is interesting to evaluate how much the daily performance of the system could be deteriorated by the operation of one safety cycle.

The daily COP of the cooling unit also considering the addition of a safety cycle, as defined in Eq. (3.16), is therefore used to evaluate the daily COP variation due to the safety control system of the separator pressure, as described in Eq. (3.17).

$$COP_{safety\ ON} = \frac{E_{evap} + E_{evap,AUX}}{E_{comp} + E_{fans} + E_{safety\ ON}} \tag{3.16}$$

$$\Delta COP_{safety\ ON} = \frac{COP_{safety\ ON} - COP}{COP} \tag{3.17}$$

The execution of a single safety cycle during the long OFF period following the delivery mission causes a limited variation of the cooling unit daily COP ($\Delta COP_{safety\ ON}$ = -4.4%). However, with the addition of the insulating layer of expanded polystyrene around the liquid receiver, even this limited deterioration in the system daily COP can be avoided.

3.7 Comparison between R134a and R744 cooling units

As one of the main topics of this research work is to evaluate and compare transport refrigeration units employing natural refrigerants to the baseline HFC units, representative of the current market, the performance of the R744 unit described in Section 3.1 and of the R134a unit described in Section 2.1 have been compared over a short-range multi-drop delivery mission in urban environment.

The same delivery mission structure (described in Table 2.6 and Table 3.11) and the same climatic conditions (a mean day for every month in the year in the city of Athens, representative of hot European climate, whose average climatic conditions are obtained following the procedure described in Section 3.5.1) have been considered for the numerical simulations, to compare the performance of the two different cooling units working in the same operating conditions on a yearly basis.

The average mission COP of the R744 unit and of the R134a unit for every month of the year have been reported in Table 3.22, while the relationship between the average mission COP of the two units and the average ambient temperature of the mission day has been highlighted in Figure 3.17.

Table 3.22 – Comparison between the average mission COP [-] of the R744 and R134a cooling units, for every month of the year.

Month	$T_{amb,avg}$ [°C]	$COP_{R744,mission}$ [-]	$COP_{R134a,mission}$ [-]
January	14.6	1.74	2.09
February	13.4	1.77	2.21
March	15.3	1.67	1.98
April	19.7	1.96	1.73
May	24.0	2.02	1.52
June	31.8	1.61	1.24
July	34.1	1.43	1.18
August	34.8	1.40	1.16
September	28.4	1.76	1.34
October	23.6	2.01	1.54
November	18.6	1.88	1.80
December	14.5	1.72	2.09

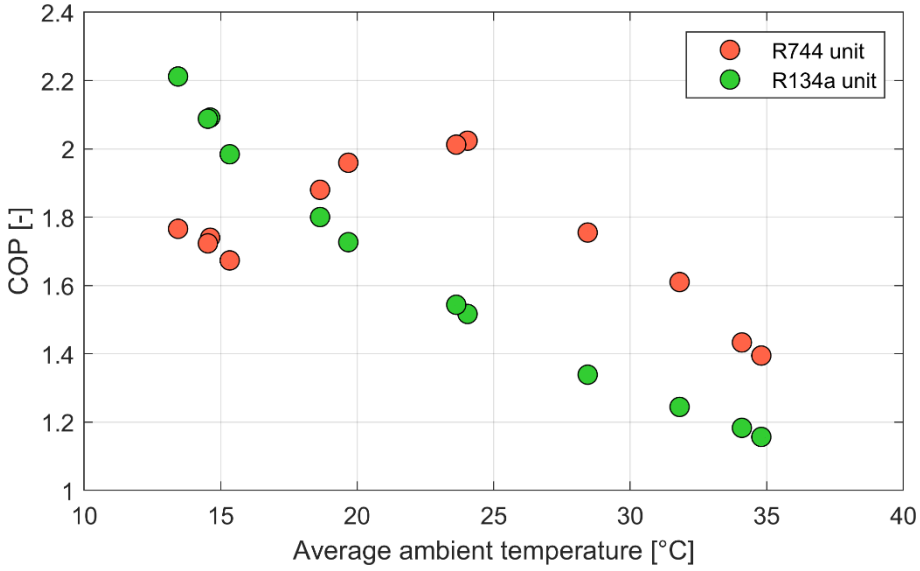

Figure 3.17 – Average delivery mission COP for the R744 and the R134a cooling units as a function of the ambient temperature.

The R744 unit presents a significantly higher average mission COP during the hottest months of the year (higher external ambient temperature conditions), while during the coldest months the baseline R134a unit presents a better COP. This is due to the performance degradation of the R744 unit during the delivery missions with low ambient temperature (and consequent low cooling demand) already discussed in Section 3.5.3: the very low Duty Cycle which characterizes the system operation along the delivery mission has a higher impact on the overall performance of the R744 unit, as the difference between cooling capacity and cooling demand is lower in the R134a unit, thus allowing operation closer to rated conditions to the R134a unit.

However, most of the yearly cooling energy production by the unit corresponds to the months characterized by the hottest ambient temperature conditions, thus reducing the impact of the coldest

months on a yearly basis. To provide the overall yearly performance of the R744 and R134a system, the overall mission COP of the two units has been evaluated considering the total cooling energy, the total energy fed to the compressor to the heat exchangers fans in all the considered months, as described in Eq. (3.18). The yearly mission COP of the considered cooling units is reported in Table 3.23.

$$COP_{year} = \frac{\sum_{i=1}^{12}(E_{evap,TOT})_i}{\sum_{i=1}^{12}(E_{comp} + E_{fans})_i} \tag{3.18}$$

Table 3.23 – Comparison between the annual average mission COP [-] of the R744 and R134a cooling units.

Period	$COP_{R744,year}$ [-]	$COP_{R134a,year}$ [-]
Year	1.69	1.46

In conclusion, the employment of the proposed R744 unit in the considered urban delivery mission, instead of the baseline R134a unit, leads to an increase of the average mission COP equal to +15.8% on a yearly basis.

3.8 Conclusions

This chapter presented the design of a R744 cooling unit designed to provide Medium-Temperature (MT) refrigeration in road temperature-controlled transport applications. Depending on the external environmental conditions, the system can operate in both subcritical and transcritical mode. The cooling unit schematic can be modified though opening and closing of four solenoid valves to realize three different operating cycles.

The reference cycle is given by a classical low-pressure receiver cycle employing a simple high-pressure valve (HPV) for the refrigerant expansion. In warm and hot environmental temperature conditions, the refrigerating system can also operate following an ejector transcritical cycle, exploiting the parallel between the HPV and a fixed-geometry two-phase ejector. Further modification of the system schematic is given by the introduction of an auxiliary evaporator in the line between the ejector outlet nozzle and the liquid separator, to extend the ejector operation towards lower ambient temperature operating conditions.

The software Simcenter Amesim v.17 was then used for the development of the numerical model of the cooling unit, including the thermal energy balance of the insulated box, the optimization of the gas cooler outlet conditions of the refrigerant and the ejector characteristic, defined through correlations obtained from experimental data. The numerical model of the heat exchangers was validated against data of commercially available heat exchangers, provided by the manufacturers.

The steady state performance of the cooling unit in the three possible configurations was numerically evaluated in different operating conditions. Moreover, also the unsteady performance of the system performing ON/OFF cycles to maintain a desired temperature range inside the insulated box was also numerically evaluated. According to the steady-state and ON/OFF cycle performance results, a configuration control strategy of the cooling unit was defined in order to maximize the cooling effect or the system COP as a function of the operating conditions.

The numerical simulation of a short-range multi-drop delivery mission (for every month of the year) and the numerical simulation of a long-range single-drop delivery mission (for the hottest month of the year) were carried out to evaluate the operation of the cooling unit when employed during delivery missions of temperature-controlled goods, both in urban and extra-urban environment.

The main results obtained in this chapter can be summarized as follows:

- In steady-state operation, the EJ configuration leads to a higher COP under higher external air temperatures, while operation in EJ,AUX configuration leads to the best performance under lower external air temperatures, thus extending the possibility to operate according to an ejector-supported cycle even with low environmental air temperature conditions. Moreover, the BP configuration is outperformed by the ejector-supported configurations in each of the considered combinations of internal and external air temperature conditions.
- In unsteady operation, when the internal air temperature is within the temperature set-point range ($T_i < 3°C$), the best performing configuration in terms of the ON/OFF cycle COP (defined differently from the steady-state COP) is preferred. In this scenario, for $T_{amb} <$ 33°C, the EJ,AUX configuration is selected, while for $T_{amb} \geq$ 33°C, the EJ configuration leads to a better performance. However, when the internal air conditions are outside of the desired temperature range ($T_i \geq 3°C$), the fast recovery of the desired temperature set-point is prioritized and the EJ;AUX configuration is selected regardless of the ambient temperature, to provide a higher overall cooling effect due to the simultaneous use of both the evaporators.
- The operation in EJ,AUX configuration for the internal air temperature pulldown after a door opening allows a fast recovery of the temperature range in which the transported products have to be maintained during transport, but it causes a counterproductive contribution of the auxiliary evaporator in the overall cooling effect in the last seconds of the ON period. However, the correct preservation of the temperature conditions for the transported products is more important in terms of cold chain safety than operation at the highest performance possible, especially since the negative contribution of the auxiliary evaporator leads to a limited impact on the overall mission performance, but it provides a crucial contribution to the safety of the cold chain of the transported products.

- The EJ configuration is used during the delivery missions in only three months in the year (June, July and August). However, these months are the hottest in the year and are characterized by the highest cooling demand to maintain the internal air temperature setpoint, representing the 37.4% of the total cooling energy provided in the entirety of the year. Therefore, the optimization given by the of the configuration control during these high cooling demand months leads to a significant improvement in the yearly performance of the system, providing an optimization for 10.5% of the yearly total cooling energy which, if operating in EJ,AUX configuration, would be provided not optimizing the system COP. Since the system configuration optimization requires limited variations to the refrigeration system operational schematic, only linked a different load management between main and auxiliary evaporator when required, switching between configurations during operation can lead to an improvement of the average performance of the system throughout the year.
- During the hottest months, the average mission COP is in good agreement with the steady-state COP of the cooling unit, decreasing as the ambient temperature increases. However, during colder months, the average mission COP presents significantly lower values compared to the steady-state ones, decreasing with decreasing temperature, while the steady-state ones increase with decreasing ambient temperature. The decrease of the needed cooling demand in the coldest months, compared to the cooling capacity in steady-state operation, leads to a lower Duty Cycle and to an increased difference between steady-state and mission performance. For the same reason, also the performance in the long-distance single-drop mission is lower than the steady-state one, even under hot environmental air temperature.
- Both the ejector efficiency and the average pressure lift, evaluated in unsteady operating conditions during the delivery mission, increase significantly for higher values of the ambient temperature, consistently with the increased energy of the motive refrigerant stream. The maximum values of the average ejector efficiency (10.1%) and of the average pressure lift (1.59 bar) are reached during the ON period occurred at higher ambient temperature (36°C). However, the absolute values of the average ejector efficiency and pressure lift evaluated during the ON periods of the mission are significantly lower than the corresponding values evaluated in steady-state operation. The short time (approximately one minute) of the ON periods leads to an ejector operation which is always in transient conditions, never reaching its steady operating conditions.
- To avoid pressure drifts inside the low-pressure side of the refrigerating system during a long time of inactivity, due to the convective heat infiltration from the external environment entering the liquid separator, a safety control system based on the definition of a maximum allowed pressure level inside the separator was proposed, turning on the compressor of the refrigerating system and bypassing the evaporators until a safe reset pressure level is reached. With the presence of

an expanded polystyrene insulating layer around the liquid separator, one entire summer day without any safety cycles can be performed and, even with no insulation around the separator, an entire night can be performed without the need of a safety cycle. However, if the cooling unit is kept off under daily environmental air temperature conditions without insulation around the separator, the operation of a safety cycle is necessary approximately every 6 h. Nevertheless, the presence of a single safety cycle during the OFF period following a delivery mission causes a limited variation of the cooling unit's daily COP (−4.4%).

- The performance of the R744 unit proposed in this chapter has been compared to the performance of the baseline R134a unit described in the previous chapter, on the same urban delivery mission and for each month of the year, in hot European climatic conditions. The R744 unit presents a significantly higher average mission COP during the hottest months of the year, characterized by higher external ambient temperature conditions, while during the coldest months the baseline R134a unit presents a better COP. However, on a yearly basis the employment of the proposed R744 unit in the considered urban delivery mission, instead of the baseline R134a unit, leads to an increase of the average mission COP equal to +15.8%.

4 Installation and preliminary setup of a R744 cooling unit experimental facility

In this chapter, the installation of the actual prototype of the R744 cooling unit described and numerically modelled in Chapter 3 is described, together with the presentation of the insulated chambers which will be used to recreate the desired heat source and heat sink temperatures under which the cooling unit has to be experimentally tested. The implementation of data monitoring equipment is carried out and the first preliminary experimental tests will be performed. Results are useful to highlight anomalous behavior of system components during the first startup phase of the system and to provide a preliminary assessment of the system performance, which can be then compared to the results provided by the numerical model. Finally, the preliminary design of the external auxiliary system to guarantee steady-state operation of the cooling unit is discussed.

4.1 Refrigerating system description

The R744 cooling unit extensively described and numerically modelled in Chapter 3 was commissioned to a major refrigeration systems manufacturer and it was delivered and installed at the ITC-CNR laboratories, located in Area della Ricerca di Padova, Italy, at the end of the second year of Ph.D. research activity.

The schematic of the cooling unit has been already outlined in Section 3.1, but it will be reported also here in Figure 4.1 for the sake of convenience and understanding.

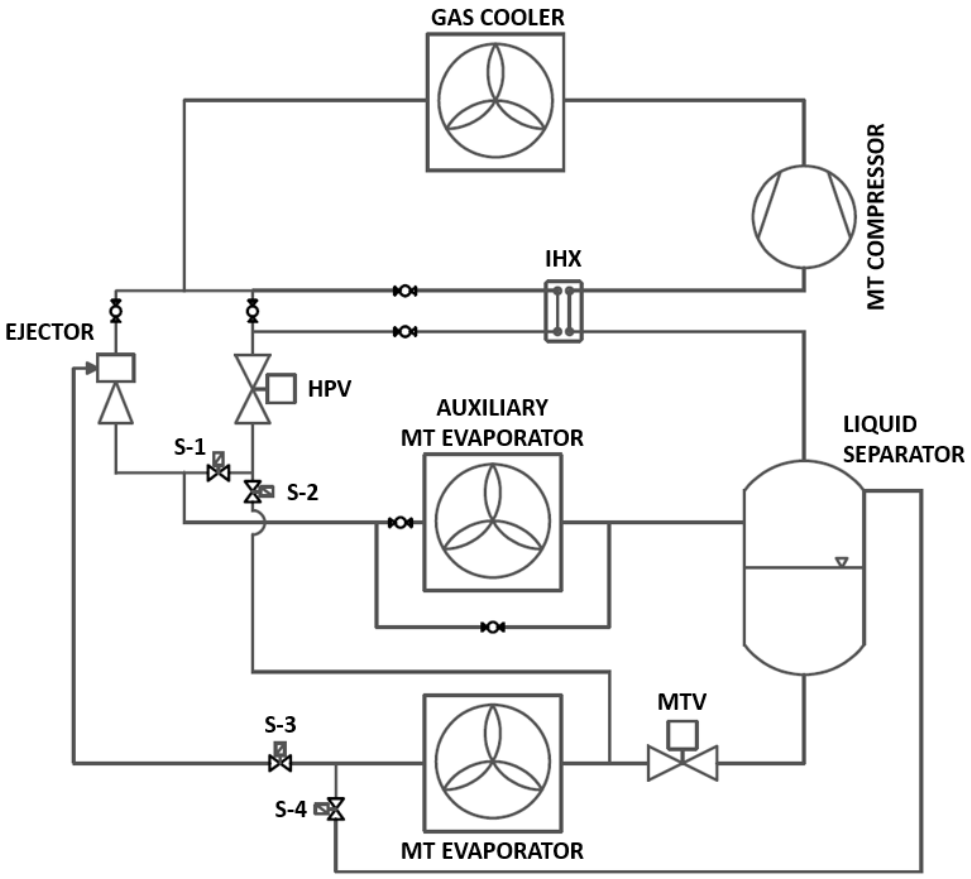

Figure 4.1 – Simplified schematic of the R744 cooling unit installed at ITC-CNR laboratories.

As previously discussed, the R744 cooling unit experimental test rig was designed and installed with the objective of allowing preliminary experimental tests to assess the best-performing configurations to provide a desired Medium-Temperature (MT) cooling effect in road temperature-controlled transport applications, evaluating the system real-life performance in steady-state conditions and validating the numerical model presented in Section 3.2 against experimental data.

Considering the schematic presented in Figure 4.1, the presence of four solenoid valves (S-1, S-2, S-3 and S-4) and of the bypass of the auxiliary evaporator allows running the refrigerating unit according to the three different configurations already described in Section 3.1, which are reported in Figure 4.2 and which will be briefly retraced here below.

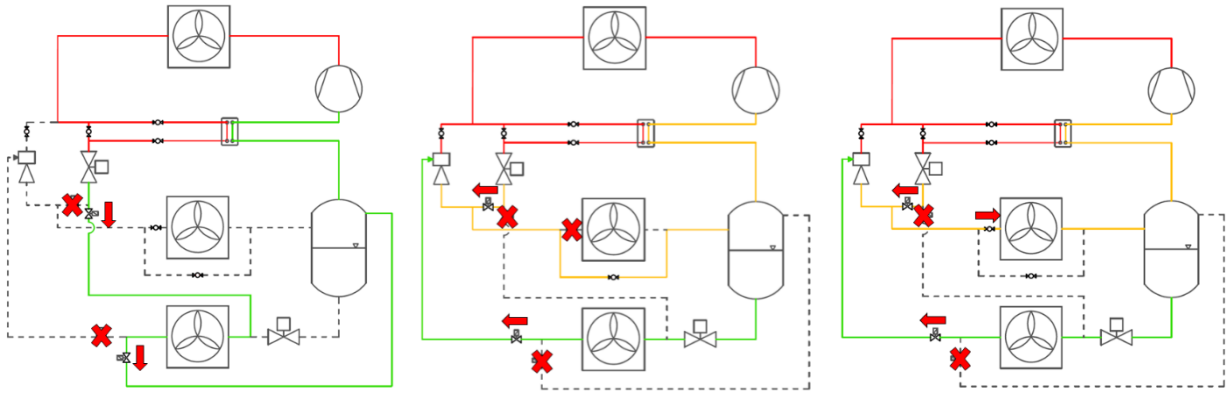

(a) (b) (c)

Figure 4.2 – Valve status (open/closed) to set the cooling unit configurations: (a) BP configuration; (b) EJ configuration; (c) EJ,AUX configuration.

The baseline back-pressure (BP) configuration is obtained closing the S-1 and S-3 solenoid valves and opening the S-2 and S-4 valves. In this configuration, the refrigerant mass flow rate coming from the gas cooler expands in a high-pressure valve (HPV) and is then sent to the main MT evaporator to provide the desired cooling effect. From the evaporator outlet, the refrigerant flows to the liquid separator, from which the vapor phase is sent to the compressor suction, flowing through an internal heat exchanger (IHX) to provide the necessary superheat to ensure absence of liquid phase at the compressor suction.

The ejector (EJ) configuration is obtained opening the S-1 and S-3 solenoid valves, closing the S-2 and S-4 valves and bypassing the MT auxiliary evaporator. In this configuration, the ejector exploits the energy of refrigerant mass flow rate at the outlet of the gas cooler to entrain the refrigerant flow at the outlet of the main MT evaporator, providing a pressure lift from the evaporation pressure to the liquid receiver intermediate pressure and thus reducing the compressor pressure ratio, and consequently its power draw, for a specific cooling effect production.

The ejector + auxiliary evaporator (EJ,AUX) configuration is obtained from the EJ configuration closing the bypass of the MT auxiliary evaporator, thus involving an additional evaporation process at the intermediate pressure level, between the ejector-HPV parallel and the liquid separator. As extensively described and proven numerically in Chapter 3, the presence of the additional MT evaporator can improve the ejector system performance at low ambient temperatures, allowing the introduction of an additional degree of freedom for the fulfillment of the liquid separator continuity equation thanks to the vapor quality increase provided by the auxiliary evaporator.

The actual experimental setup installed in the ITC-CNR laboratories in Padova, Italy, is presented in Figure 4.3, while the list of the components installed in the experimental refrigeration unit facility is reported in Table 4.1 together with the respective main geometric dimensions.

Figure 4.3 – R744 cooling unit experimental setup, installed at ITC-CNR laboratories.

Table 4.1 – List of the components of the cooling unit and corresponding main geometric dimensions.

Component	Manufacturer and model	Geometric dimensions
Compressor	Dorin CD360H	Displacement: $\dot{V}_d$ = 2.39 m^3 h^{-1} (@ 50 Hz)
Gas cooler	MODINE KCE52N3	External convective surface: $A_{e,gc}$ = 78.0 m^2
Main evaporator	LU-VE F35HC 215	External convective surface: $A_{e,evap}$ = 39.4 m^2
Auxiliary evaporator	LU-VE F35HC 106	External convective surface: $A_{e,evap\ AUX}$ = 19.7 m^2
Internal Heat Exchanger	SWEP B18	Maximum volumetric flow: $\dot{V}_{IHX}$ = 9.0 m^3 h^{-1}
Ejector	Danfoss cartridge 1 for HP Multi Ejector	Motive nozzle throat diameter: d_{EJ} = 1.0 mm
Liquid receiver	KLIMAL RCO 273.91.40.90	Volume: V = 40.0 L
Oil separator	KLIMAL TTE 09 (ODS 6)	Volume: V = 2.5 L

The oil management of the refrigeration system is reported in Figure 4.4. The oil separator reported in Table 4.1 is placed downstream the compressor discharge and upstream the gas cooler inlet and has the function of removing oil from the refrigerant mass flow. While oil is fundamental for the correct compressor lubrication, it is necessary to make it always flow back to the compressor. On the other hand, it is also advisable to reduce as much as possible the amount of circulating oil, to avoid oil accumulation in the cooling unit pipelines and components and to prevent a reduction of the system cooling effect linked to the presence of oil in the refrigerant mass flow rate in the heat exchangers. In this system it is of course possible to recover oil from the bottom of the liquid separator and to make it flow back to the compressor suction line through the opening of a manual valve. The design allows to run the system with and without the oil separator and to evaluate the need for it in this kind of applications.

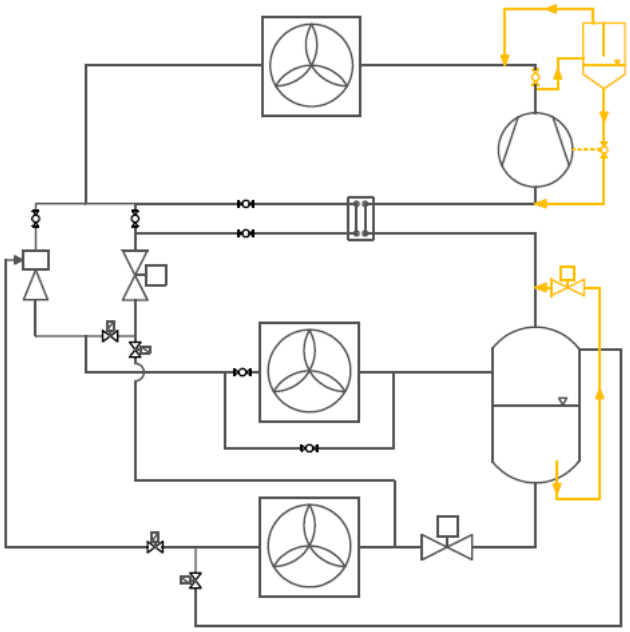

Figure 4.4 – Oil management in the refrigeration system.

Since the objective of the experimental campaign to be conducted on the R744 cooling unit prototype is to assess the best performing configuration among the above-mentioned three possible configurations under a wide range of different operating conditions, in order to define the final optimal schematic of the cooling unit to be installed and utilized on a small van for transport refrigeration applications, the prototype displayed in Figure 4.3 is not yet optimized in terms of dimensions, weight and pipelines length for an actual transport refrigeration application. Moreover, the inclusion of pressure sensors, temperature sensors, mass flow meters and the other instrumentation which allows to collect the experimental data to fully evaluate the system performance, leads to a heavier and bulkier system compared to a transport refrigeration system.

Once the optimal configurations are assessed through experimental tests on this stationary prototype, also the geometry and the structural footprint of the refrigeration system will be optimized for actual transport refrigeration purposes.

To allow experimental tests on the cooling unit under a wide range of operating conditions (i.e. different combinations of ambient temperature and air temperature inside the refrigerated box), two separate insulated chambers are installed, in which the heat exchangers of the cooling unit are placed, as presented in Figure 4.5 and Figure 4.6.

Figure 4.5 – Insulated chambers in which the heat exchangers are placed, to reproduce the desired heat sink and heat source temperatures during experimental tests.

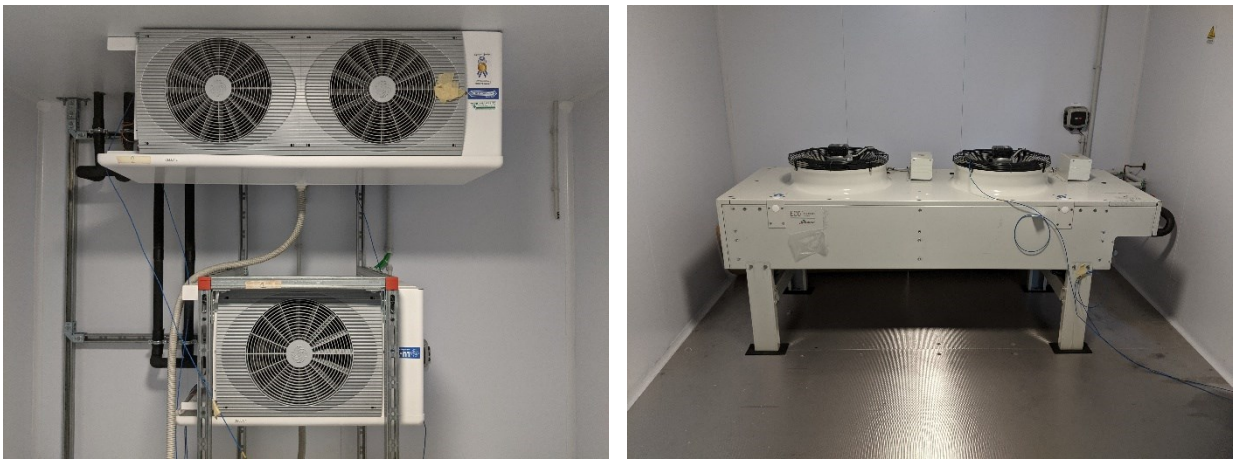

(a) (b)

Figure 4.6 – Heat exchangers inside the insulated chambers: (a) main evaporator (top) and auxiliary evaporator (bottom); (b) gas cooler.

A simplified schematic representing the thermal balance inside the insulated chambers is presented in Figure 4.7.

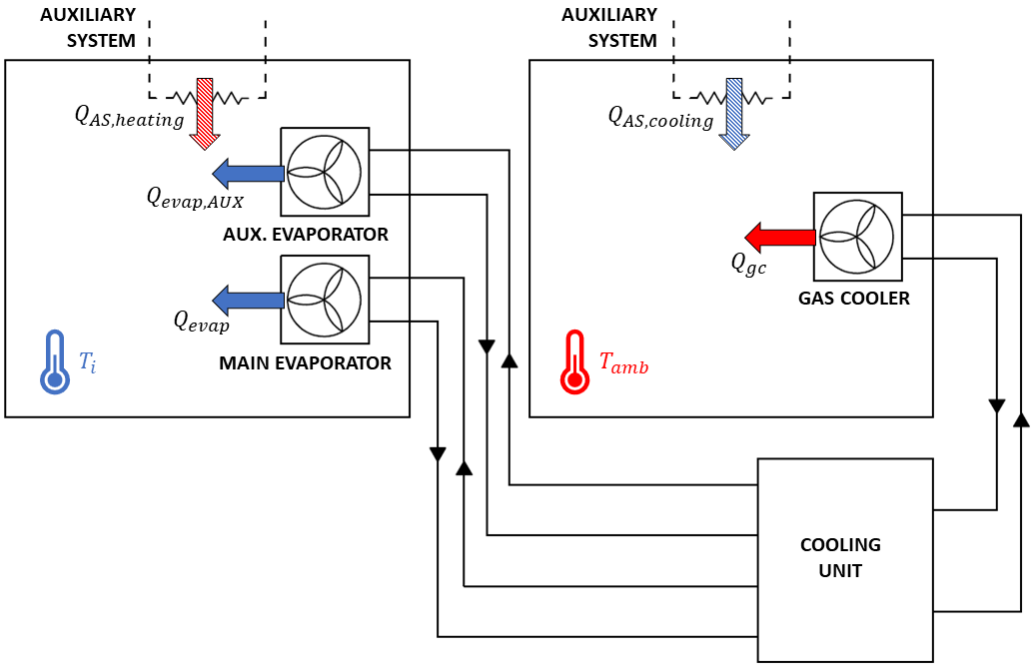

Figure 4.7 – Simplified schematic representing the thermal power balance inside the insulated chambers.

Considering the simplified schematic presented in Figure 4.7, one of the insulated chambers (hot chamber) is used to represent the heat sink of the refrigerating system, i.e. to represent the external environment temperature conditions T_{amb} corresponding to the boundary operating condition for the cooling unit gas cooler. In this insulated chamber, the gas cooler rejects heat (Q_{gc}) to the air. To allow the control of the temperature T_{amb} to the desired test conditions and to avoid a temperature drift inside the

insulated chamber, an external auxiliary system providing a cooling effect ($Q_{AS,cooling}$) counteracting the refrigeration system heat rejection needs to be included.

Conversely, the other insulated chamber (cold chamber) is used to represent the heat source of the refrigerating system, i.e. to represent the insulated box in which the perishable goods to be delivered are stored and which needs to be maintained at desired internal temperature conditions T_i corresponding to the correct preservation temperature of the products. The internal temperature T_i represents the boundary operating condition for both the main evaporator and the auxiliary evaporator. In this insulated chamber, the evaporators provide the required cooling effect ($Q_{evap} + Q_{evap,AUX}$) to the internal air. Following the same principle described for the first insulated chamber, to allow the control of the temperature T_i to the desired test conditions and to avoid temperature drifts, an external auxiliary system providing a heating effect ($Q_{AS,heating}$) counteracting the refrigeration system cooling effect is needed.

In the simplified schematic reported in Figure 4.7, the external auxiliary system contribution is presented using dashed lines and arrows, since the auxiliary system is currently not yet installed. The preliminary design of the external source to provide heating in the cold chamber and cooling in the hot chamber, to allow steady-state operation of the refrigeration system prototype at the desired temperature boundary conditions, will be later discussed in Section 4.4.

4.2 Data acquisition

The data acquisition system of the experimental facility consists of high-precision sensors which are read and logged with a sampling rate of 1 Hz through the use of National Instruments hardware (LabVIEW programming). The logged data is then used for post-processing and results analysis.

The list of the measurement equipment to be installed in the experimental facility and their respective accuracy are reported in Table 4.2. In the table, the sensors which are already installed are reported in black, while the sensors which are currently still to be installed are reported in red. As a consequence, during the preliminary startup tests of the cooling unit which will be described in the following section, no measurement was available from the equipment highlighted in red.

Table 4.2 – List of the data acquisition equipment and respective accuracy installed in the experimental facility. Instrumentation currently not yet installed is reported in red.

Type	Manufacturer and model	Accuracy
Temperature sensors	T-type thermocouples on tube	±1.1°C
Pressure transducers	WIKA P-30	±0.1% of set span
Mass flow meters (Coriolis)	Emerson MicroMotion D12 Emerson MicroMotion C25 Endress+Hauser Promass 83A	±0.4% of reading ±0.4% of reading ±0.1% of reading
Electrical power	Verivolt IsoBlock I-FG (current) Verivolt IsoBlock V (voltage)	±0.2% of reading ±(0.2% of reading + 0.005% of set span)

It has to be pointed out that the ±1.1°C accuracy for the T-type thermocouples reported in Table 4.2 corresponds to the cold-junction compensation accuracy reported in the datasheet of the National Instruments 9213 thermocouple acquisition module [111], for the temperature range -40°C < T < 70°C. Since the temperature measurements which will be described in the following section are functional only to monitor the preliminary system startup after the installation and to verify the correct operation of the cooling unit, the complete calibration of the thermocouples is still to be performed. Before carrying out any future experimental campaign on the experimental system, in which high-precision measurements are required, the calibration of the thermocouples against a reference Isotech TTI-6 Pt100 thermoresistance (characterized by an accuracy of ±0.2°C in the range -50°C < T < 150°C) will be performed, to increase the accuracy of the temperature measurements.

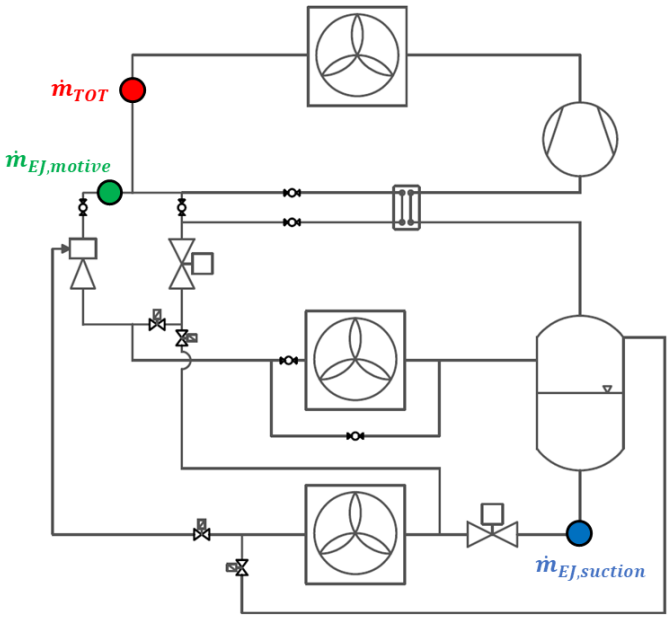

Figure 4.8 – Predisposed insertion points for the Coriolis mass flow meters.

The mass flow meters will be installed in three points of the refrigerating cycle, as reported in Figure 4.8: downstream the gas cooler, to measure the total refrigerant mass flow rate elaborated by the compressor, upstream the ejector motive nozzle, to measure the motive mass flow rate in the ejector

configurations, and downstream the liquid output of the liquid separator, to measure the suction mass flow rate in the ejector configuration, thus allowing the evaluation of the ejector entrainment ratio.

4.3 Preliminary cooling unit startup tests

After the installation of the cooling unit, preliminary experimental tests are performed to verify the correct startup of the system, the proper operation of the unit components and to perform a preliminary assessment of the cooling performance in simple back-pressure operation.

The thermodynamic points which will be presented in the remainder of this section are defined according to the nomenclature reported in Figure 4.9.

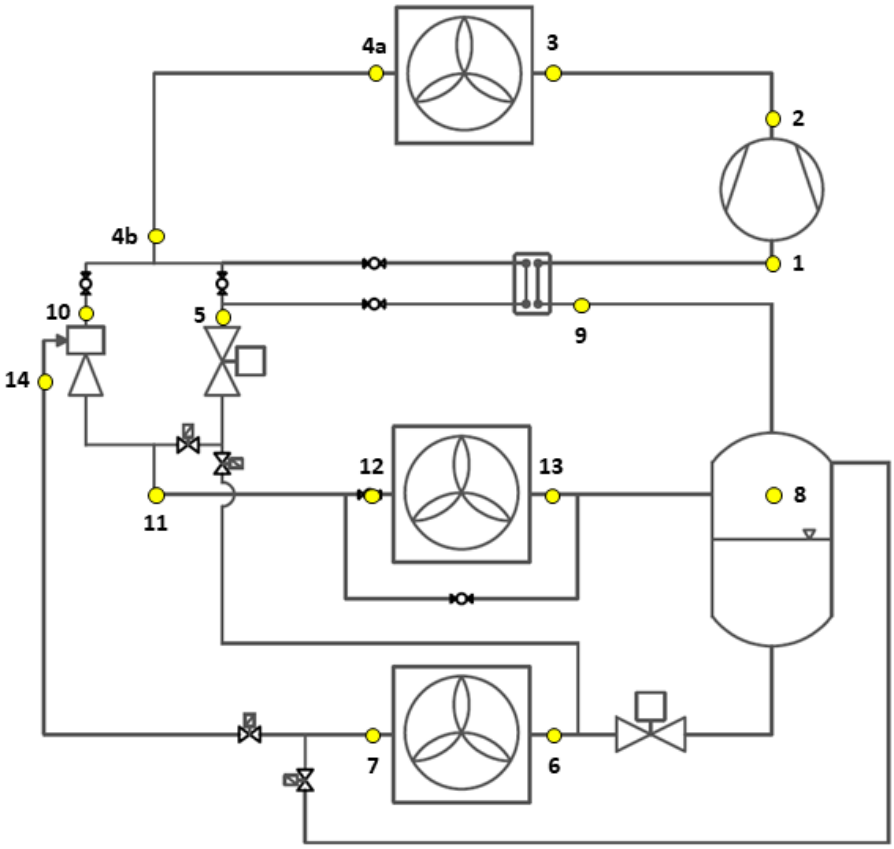

Figure 4.9 – Thermodynamic points of the cooling unit considered for the preliminary startup tests.

4.3.1 Assessment of components overall compliance with design

During the first startups of the refrigeration system, the main focus is the assessment of the correct operation of the entire unit components, with the objective of verifying the proper installation of the system.

One of the first issues that has been highlighted after the system installation, through the analysis of the experimental data logged by the measurement equipment listed in Table 4.2 (pressure transducers and

temperature sensors), is the excessive pressure loss occurring in the high-pressure side of the cooling unit during operation. In particular, a pressure loss $\Delta p_{gc} = p_2 - p_4$ of over 4 bar between the compressor discharge (p_2) and the gas cooler outlet (p_4) has been registered during the first startups of the cooling unit, as it is reported in Figure 4.10a-b. In the figure, the gray shaded area corresponds to the periods of time in which the cooling unit is switched off, according to the thermostat controlling the air temperature inside the cold insulated chamber (T_i).

A pressure loss of 4 bar in the high-pressure side of the cooling unit is not acceptable during the system operation, as it would significantly reduce the performance of the cooling unit. In fact, the discharge pressure p_2 is set as a function of the gas cooler outlet temperature, following the optimal control reported in Table 3.2. Significant pressure losses between compressor discharge and gas cooler outlet Δp_{gc} will result, for the same gas cooler outlet temperature, in a much higher gas cooler outlet enthalpy, reducing the available enthalpy difference at the evaporator side and consequently reducing the unit COP.

Following the above-mentioned results, the technicians responsible of the prototype installation performed an in-depth analysis of the pipelines and components in the high-pressure side of the unit, and found out that the pipelines of the oil separator (not displayed in the simplified schematic of Figure 4.1, but placed between the compressor discharge and the gas cooler inlet) were obstructed by unexpected welding material lodged during the installation process, causing the excessive pressure drop registered during the tests.

After the removal of the extraneous welding material from the oil separator pipelines, new tests have been performed. The pressure losses in the high-pressure side of the system have been significantly reduced and acceptable values of Δp_{gc} < 1 bar have been registered, as reported in Figure 4.10c-d.

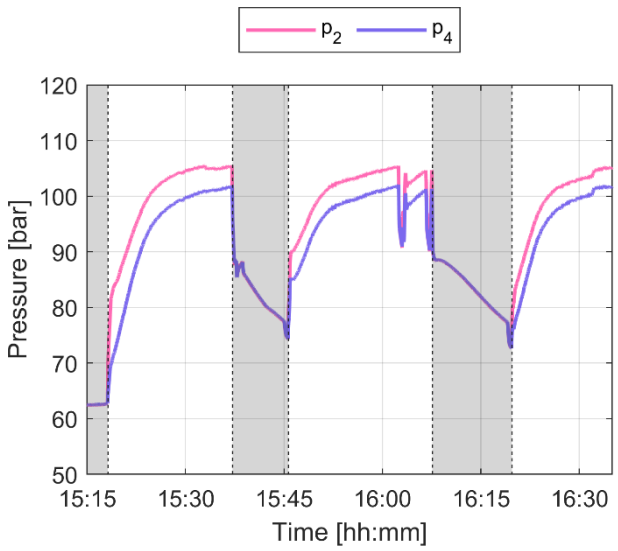

(a)

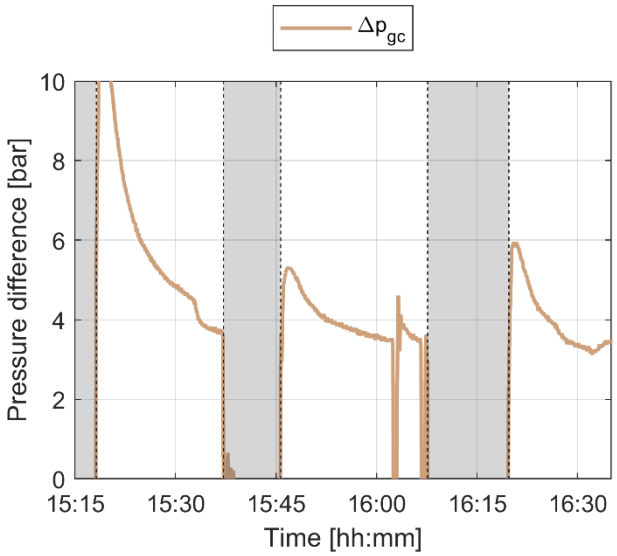

(b)

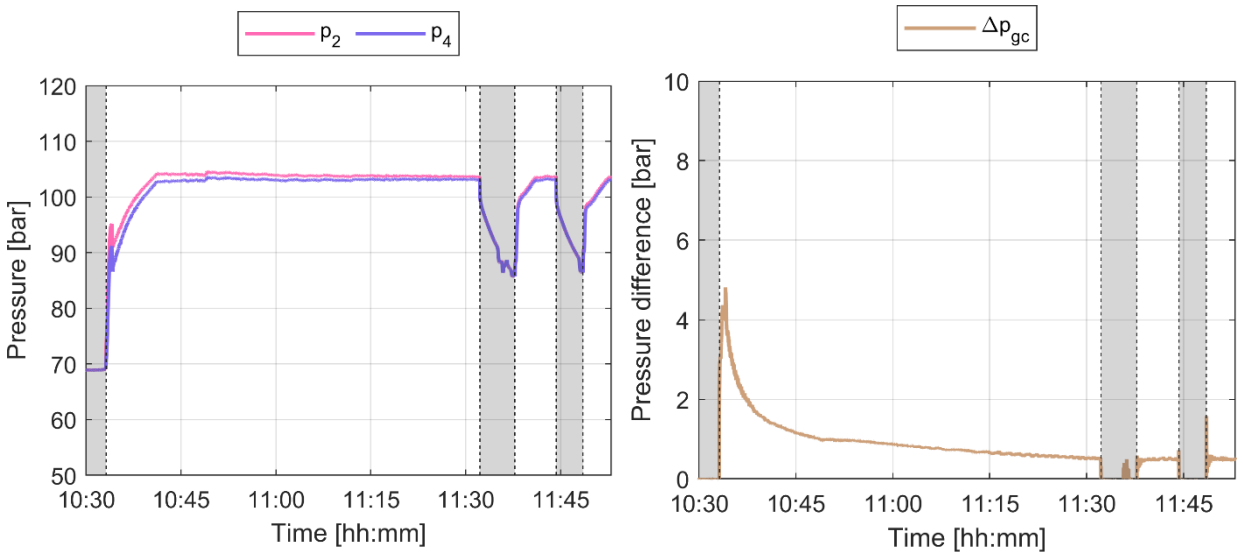

(c) (d)

Figure 4.10 – Pressure losses in the high-pressure side of the cooling unit: (a) compressor discharge pressure and gas cooler outlet pressure at first startup; (b) pressure drop at first startup; (c) compressor discharge pressure and gas cooler outlet pressure after removal of external welding material in the oil separator; (d) pressure drop after removal of external welding material in the oil separator.

Another issue that has been highlighted during the first startups of the system through the analysis of the experimental data, is that the internal heat exchanger (IHX) installed in the unit prototype has been oversized compared to the expected nominal thermal power exchange between the refrigerant mass flow rate flowing from the liquid separator to the compressor suction and the refrigerant mass flow rate flowing from the outlet of the gas cooler to the high-pressure valve HPV (as operation in BP configuration has been tested).

Considering operation in BP configuration with the bypass branch of the IHX completely closed (meaning that all the refrigerant mass flow rate in the high-pressure side flows into the IHX before flowing into the HPV), the experimental temperatures at the inlet and at the outlet of the high-pressure side of the IHX (T_4 and T_5, respectively) and at the inlet and at the outlet of the low-pressure side of the IHX (T_9 and T_1, respectively) are reported in Figure 4.11a. In addition, the temperature of the refrigerant mass flow rate at the compressor discharge (T_2) registered during the same period is reported in Figure 4.11b.

The purpose of the IHX during the correct operation of the cooling unit is to provide a desired superheat (usually in the range of 5-10 K) to the refrigerant mass flow rate in saturated vapor state flowing from the liquid separator to the compressor suction, in order to guarantee absence of liquid in the compressor, thus avoiding mechanical issues and significant compressor deterioration.

However, it can be observed from Figure 4.11a that the temperature at the compressor suction is increased to almost the same value as the temperature at the gas cooler outlet, due to the oversized convective exchange surface of the IHX, causing a superheat of more than 30 K.

An excessive temperature at the compressor suction has a significant impact on the cooling unit performance. On one hand, an increase of the temperature at the compressor suction leads to a decrease of the refrigerant density and, consequently, to a reduction of the mass flow rate elaborated by the compressor, as with decreased density the fixed volumetric capacity of the compressor corresponds to a reduced mass flow rate. As a consequence, the cooling capacity provided by the evaporator is reduced as well, while the compressor power draw remains unchanged, thus lowering the system COP. On the other hand, an increase of the compressor suction temperature causes an even greater increase of the compressor discharge temperature, due to the divergence of the isentropic lines in vapor state. In particular, it can be observed in Figure 4.11b that the excessive superheat provided by the IHX leads to temperatures at the compressor discharge over 150°C, which could potentially cause mechanical damages to the compressor itself.

Following the experimental measurements highlighted in Figure 4.11a-b, the bypass branch of the IHX has been partially opened before the cooling unit switch on in the afternoon of the same day of tests, thus allowing the bypass of the IHX to part of the refrigerant mass flow rate coming from the gas cooler outlet and the reduction of the mass flow rate flowing into the high-pressure side of the IHX.

As it can be observed in Figure 4.11c, the reduction of the high-pressure side mass flow rate leads to a lower thermal power exchanged in the IHX and to the consequent reduction of the superheat in the low-pressure side of the heat exchanger (T_1 is not increased to almost the same value of T_4 as it was before). Moreover, the reduction of the compressor suction temperature leads to a reduced temperature at the compressor discharge as well, presenting values below 140°C and granting the compressor safety, as it can be observed in Figure 4.11d.

Finally, around 17:10 the bypass branch of the IHX has been opened even more. As a result, the superheat in the low-pressure side of the IHX is lowered to the desired value (slightly less than 10 K), and the compressor discharge temperature is lowered even further as well.

Following the above-mentioned results, the installation of a modulating valve on the bypass branch of the high-pressure side of the IHX, regulating the mass flow rate bypass ratio in order to obtain a set value of the superheat at the low-pressure side of the IHX, is scheduled.

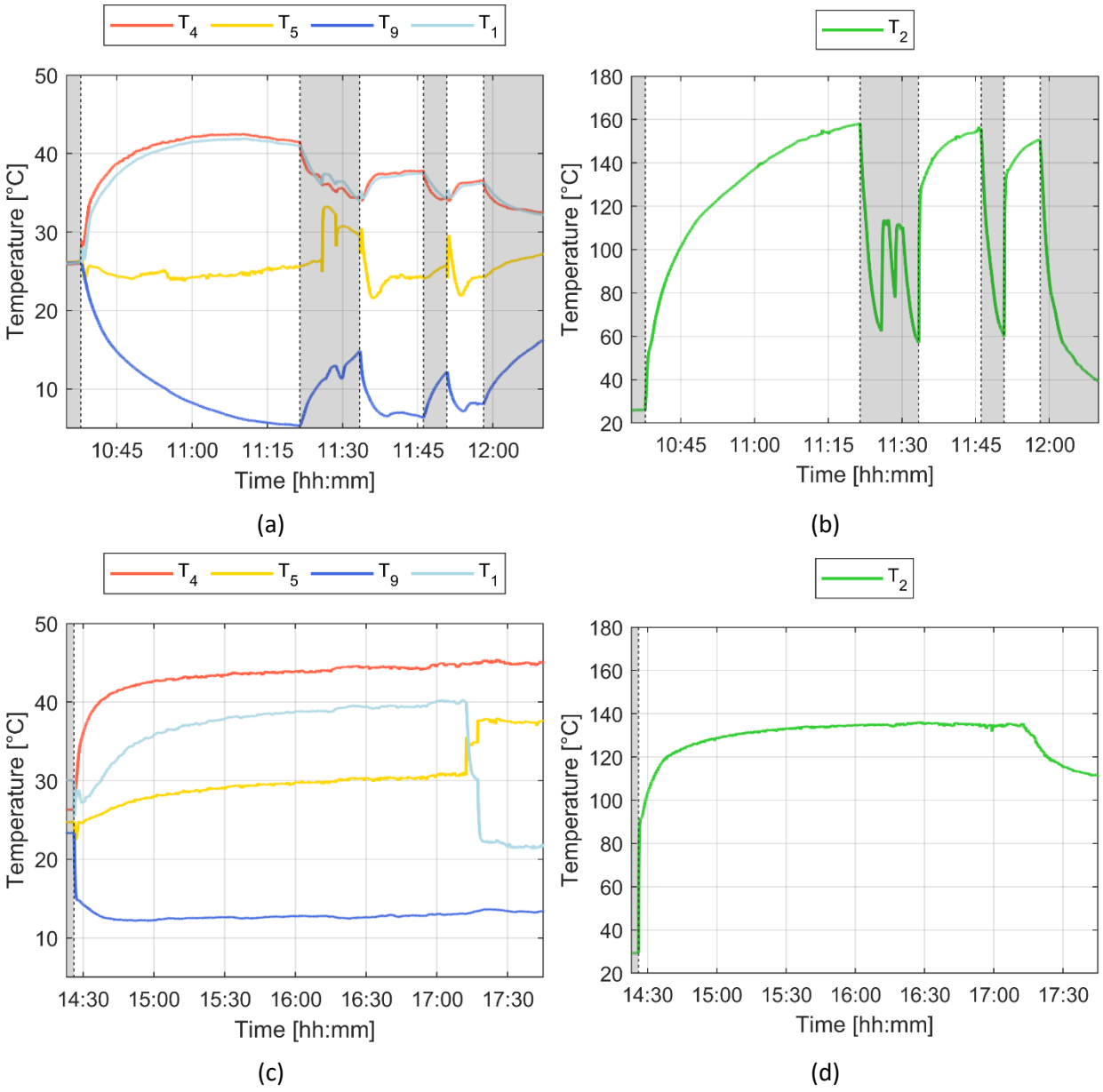

Figure 4.11 – Performance of the internal heat exchanger: (a) inlet and outlet temperatures with no IHX bypass; (b) compressor discharge temperature with no IHX bypass; (c) inlet and outlet temperatures with partial IHX bypass; (d) compressor discharge temperature with partial IHX bypass.

4.3.2 Temperature pulldown in BP configuration

In addition to the considerations regarding the compliance of components with design requirements or expected behaviors, as described in the previous sections, the experimental data logged during the initial startup of the cooling unit can be useful to perform a preliminary assessment of the refrigerating system in its entirety.

As it has been described in Table 4.2, mass flow meters and power meters are not yet installed in the prototype. However, a preliminary and indicative evaluation of the cooling unit performance can be performed through indirect calculation of the refrigerant mass flow rate and of the electrical power draw

of the compressor, considering operation in BP configuration. In particular, the on-board control panel of the refrigerating system can provide, with the frequency of 1 Hz, the values of the compressor frequency f_{comp} (analog output signal, 4-20 mA) and of the compressor power draw P_{comp} (analog output signal, 4-20 mA).

It has to be pointed out that the above-mentioned analog output signals provided by the on-board control panel of the cooling unit will not be used for future experimental campaigns, in which only high-precision sensors will be employed, as these signals have the objective of the primary on-board self-regulation of the system and not the provision of high-precision measurements. However, in the preliminary startup phase of the cooling unit, they can be useful to provide indicative values of the system performance, as it will be described hereafter.

Temperature and pressure values of the cycle operating points are directly measured through the temperature and pressure sensors reported in Table 4.2 and are then used to evaluate the specific enthalpy h of the cycle operating points through the REFPROP 9.1 database [112]. With the same method, also the density of the refrigerant at the compressor suction (ρ_1) is calculated. The refrigerant mass flow rate elaborated by the compressor can be therefore evaluated as:

$$\dot{m}_{comp} = \rho_1 \, \dot{V}_{d,comp} \left(\frac{f_{comp}}{50 \; Hz} \right) \eta_{vol} \tag{4.1}$$

in which the compressor displacement $\dot{V}_{d,comp}$ is reported in Table 4.1 and the volumetric efficiency of the compressor is interpolated as a function of the compressor pressure ratio ($r_p = {p_2}/{p_1}$) from the operating data available in the datasheet provided by the compressor manufacturer.

The thermal power exchanged by the evaporator and by the gas cooler are calculated as reported in Eq. (4.2) and Eq. (4.3), respectively.

$$Q_{evap} = \dot{m}_{comp} \, (h_7 - h_6) \tag{4.2}$$

$$\left| Q_{gc} \right| = \dot{m}_{comp} \, (h_3 - h_4) \tag{4.3}$$

As a conclusion, the system COP in BP configuration can be calculated as:

$$COP = \frac{Q_{evap}}{P_{comp}} \tag{4.4}$$

Consistently with the above-described definition of the cooling unit performance parameters, a complete pulldown performed by the cooling unit in BP configuration, in which the system (initially switched off and in thermal equilibrium with the ambient air inside the laboratory in which the system is located) is

switched on and, after reaching the desired temperature range, performs a series of ON/OFF cycles to maintain the cold chamber temperature in a specific temperature range, is presented in Figure 4.12.

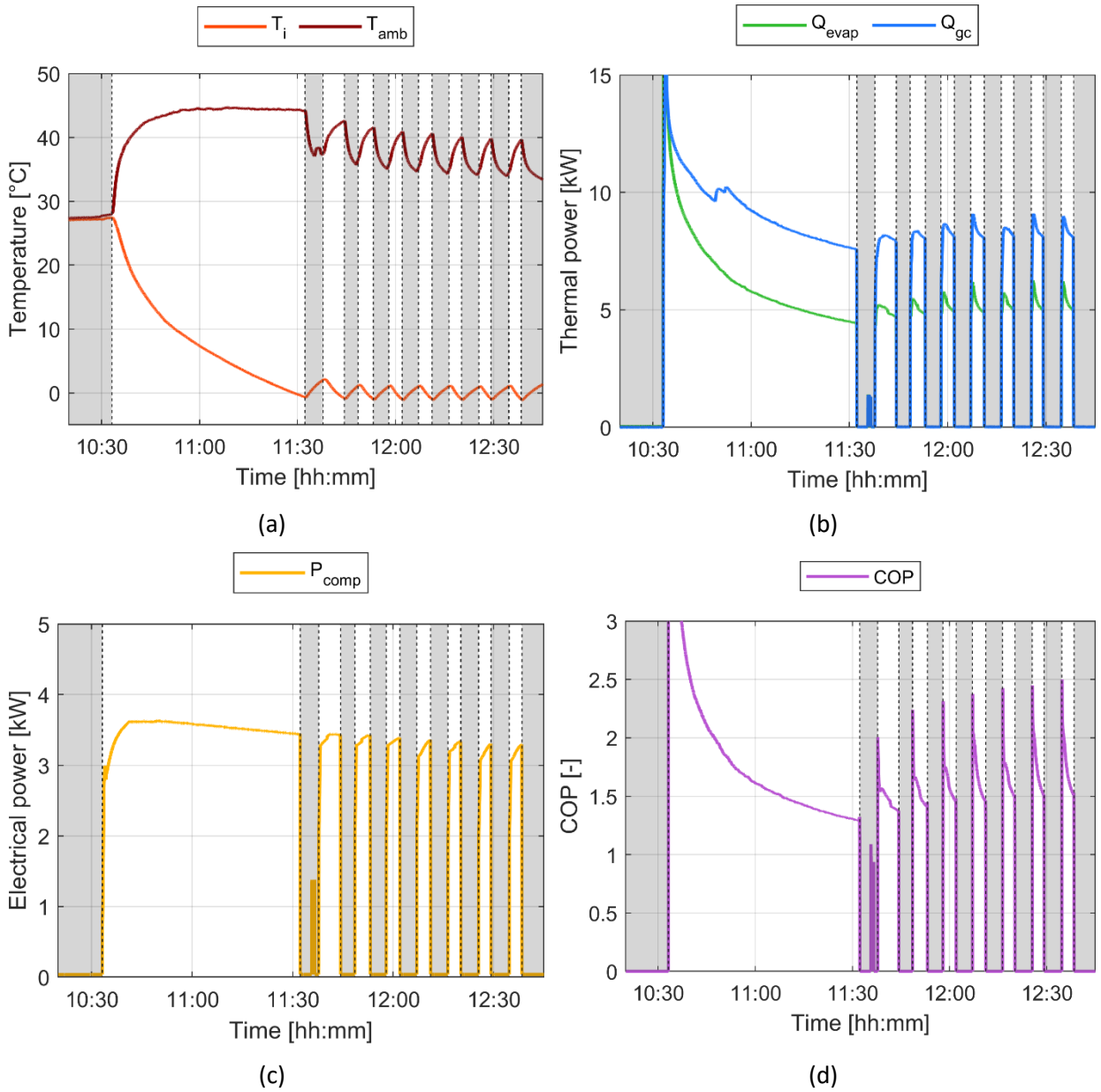

Figure 4.12 – Cooling unit performing a pulldown from thermal equilibrium with the external ambient and following ON/OFF internal temperature control in BP configuration: (a) temperatures in the cold chamber (T_i) and in the hot chamber (T_{amb}); (b) thermal power exchanged by the evaporator and by the gas cooler; (c) compressor power draw; (d) instant COP.

The evolution of the temperature of the air inside the cold insulated chamber (T_i, heat source temperature) during the pulldown process is reported in Figure 4.12a together with the temperature inside the hot insulated chamber (T_{amb}, heat sink temperature). Gray shaded areas highlight the periods in which the cooling unit is switched off, following the control of the thermostat to maintain the desired T_i range (-1°C < T_i < 2°C). According to the heat balance schematic presented in Figure 4.7, it can be observed that steady-state operation can not be reached, since the external auxiliary system is not yet

installed and, therefore, thermal equilibrium inside the insulated chambers can not be achieved. As a consequence, T_i decreases during ON periods and increases during OFF periods, as the cooling unit performs ON/OFF cycles to maintain the desired T_i range, while T_{amb} increases during ON periods and decreases during OFF periods due to the thermal power exchanged by the heat exchangers in the respective insulated chambers.

For the same period of operation, the evolution of the cooling effect provided by the evaporator in the cold chamber and of the heat rejected by the gas cooler in the hot chamber are reported in Figure 4.12b, presenting a value of approximately $Q_{evap} \cong 5$ kW and $Q_{gc} \cong 8$ kW during the highlighted period. In addition, the evolution of the compressor power draw is reported in Figure 4.12c, presenting an approximate value of $P_{comp} \cong 3.2$ kW during the considered period.

In conclusion, the evolution of the system instant COP is reported in Figure 4.12d, presenting an approximate value of $COP \cong 1.6$ in the highlighted period of operation.

4.3.3 Steady-state performance in BP configuration

Despite the absence of an external auxiliary system to provide a contrasting thermal load inside the insulated chambers during the preliminary system startup tests, necessary to guarantee the achievement of controlled steady state condition operation at a specific combination of T_i and T_{amb}, the assessment of the system performance in steady-state conditions has been possible thanks to the heat exchange between the air inside the insulated chambers and the air inside the laboratory where the chambers are located, through the control of the chamber doors opening.

In particular, the door of the hot chamber in which the gas cooler is placed has been kept completely open, to maximize the heat rejection from the air inside the chamber to the external air of the laboratory, which is significantly colder (around 25°C). Thanks to this heat exchange towards the outside of the hot chamber, operation with an almost constant temperature of around $T_{amb} \cong 45$°C was possible.

Following the same approach, the temperature inside of the cold chamber has been controlled with slight openings of the door of the cold chamber, to allow heat infiltration of the external air of the laboratory until the desired T_i was kept almost constant for a specific period of time (10 minutes), and then opened slightly more until the achievement of the following internal air temperature.

The following tests do not provide a complete mapping of the system performance in all the possible combinations of T_i and T_{amb}, as this will be the objective of the experimental campaign which will be performed once the external auxiliary system to balance the heat load inside the chambers and all the measurement equipment listed in Table 4.2 are installed. However, the experimental data collected in the cooling unit startup phase can be useful to provide a preliminary, indicative assessment of the

performance of the system and to compare it to the simulation results provided by the numerical model of the system extensively described in Chapter 3.

The experimental data are collected with the frequency of 1 Hz over a period of 10 minutes in which the system operates in BP configuration in steady-state conditions, and the performance results of the cooling unit are reported in Table 4.3. The cooling effect Q_{evap} and the system COP are calculated as reported in Eq. (4.2) and Eq. (4.4), respectively.

Table 4.3 – Steady-state performance of the cooling unit in BP configuration.

T_{amb} [°C]	T_i [°C]	Q_{evap} [kW]	P_{comp} [kW]	COP [-]
44.78	10.14	6.16	3.59	1.71
45.32	7.10	5.48	3.56	1.54
45.51	5.05	5.08	3.53	1.44
45.54	2.04	4.55	3.48	1.31
45.55	0.25	4.28	3.44	1.24

The experimental results can be compared to the simulation results provided by the numerical model of the cooling unit, extensively described in Section 3.2, providing as an input value for the numerical model the T_i and T_{amb} values registered during the experimental tests. The experimental COP and the numerical simulations COP are then compared in Table 4.4.

Table 4.4 – Comparison of the experimental and numerical steady-state COP in BP configuration.

T_{amb} [°C]	T_i [°C]	COP_{exp} [-]	COP_{sim} [-]
44.78	10.14	1.71	1.38 (-19.3%)
45.32	7.10	1.54	1.25 (-18.8%)
45.51	5.05	1.44	1.18 (-18.1%)
45.54	2.04	1.31	1.08 (-17.6%)
45.55	0.25	1.24	1.03 (-16.9%)

The experimental results and the simulations results show an acceptable agreement, with a relative error which is always under 20%, given the lack of complete measuring instrumentation and control systems at this preliminary installation stage of the cooling unit. It has to be pointed out that the comparison presented in Table 4.4 can not be considered as a validation of the numerical model, mainly because of

the very limited number of considered operating conditions, because of the sole consideration of the BP configuration and the absence of tests in the ejector configurations and because of the indirect evaluation of several parameters during the experimental tests, due to lack of the necessary measurement equipment at the moment of the system startup period. However, the results presented above can be useful for a first preliminary assessment of the numerical model accuracy range.

4.4 Auxiliary systems design

As it was mentioned in Section 4.1, currently only the refrigeration system heat exchangers are placed in the insulated chambers, while an external auxiliary system which can counteract the heat exchangers thermal load is still to be designed.

To this extent, the numerical model of the cooling unit extensively described in Section 3.2 is used to evaluate the thermal load given by the heat exchangers under different operating conditions, to assess the design of the external auxiliary system. The system will be designed to be capable of handling all the thermal load given by the refrigeration unit heat exchangers, thus neglecting the thermal losses of the insulated chambers.

The total cooling effect provided by the main and the auxiliary evaporator ($Q_{evap,TOT} = Q_{evap} + Q_{evap,AUX}$) during steady-state operation in EJ,AUX configuration under different operating conditions is reported in Table 4.5, while the heat rejected by the gas cooler under the same operating conditions is reported in Table 4.6.

Table 4.5 – Steady-state $Q_{evap,TOT}$ [kW] of the cooling system in EJ,AUX configuration.

T_{amb} [°C]/T_i [°C]	-20	-15	-10	-5	0	5	10
15	3.83	4.73	5.48	6.24	7.10	7.94	8.82
20	3.47	4.35	5.27	6.05	6.87	7.75	8.94
25	3.20	4.07	4.97	5.70	6.51	7.55	8.80
30	2.74	3.60	4.56	5.37	6.19	7.11	8.35
35	2.14	2.92	3.83	4.85	5.82	6.68	7.70
40	1.59	2.26	3.07	4.02	5.16	6.18	7.08
45	1.18	1.74	2.48	3.34	4.40	5.45	6.40

Table 4.6 – Steady-state Q_{gc} [kW] of the cooling system in EJ,AUX configuration.

T_{amb} [°C]/T_i [°C]	-20	-15	-10	-5	0	5	10
15	5.81	6.77	7.53	8.35	9.26	10.07	10.92
20	5.60	6.54	7.56	8.39	9.22	10.08	11.41
25	5.46	6.43	7.43	8.20	9.02	10.12	11.52
30	5.21	6.20	7.30	8.18	9.03	9.99	11.39
35	4.77	5.74	6.82	7.99	9.09	9.98	11.08
40	4.33	5.20	6.23	7.36	8.74	9.93	10.87
45	4.02	4.81	5.78	6.87	8.18	9.48	10.62

Since the cooling unit is designed to maintain the temperature inside the cold chamber at a nominal value of T_i = 0°C, the corresponding values of $Q_{evap,TOT}$ and Q_{gc} are highlighted in red in Table 4.5 and Table 4.6 and will be used as the heat loads in nominal operating conditions considered for the design of the external auxiliary system.

The values reported in Table 4.5 correspond to the heat which has to be provided inside the cold chamber in order to balance the cooling effect provided by the evaporators. Similarly, the values reported in Table 4.6 correspond to the heat which has to be removed inside the cold chamber in order to balance the heat rejection of the gas cooler. It can be observed that the excess heat that needs to be removed from the hot chamber can contribute to the heat request inside the cold chamber and, for the same reason, the cooling effect which has to be removed from the cold chamber can contribute to the cooling effect request inside the hot chamber. This approach can reduce the overall sizing and energy contribution of the auxiliary system to be installed.

According to the above-mentioned considerations, in addition to what has been previously presented in Figure 4.7, a ventilation system is considered for the control of the temperature inside the insulated chambers, as it is presented in Figure 4.13. The ventilation system can be used to send hot air mass flow rate from the hot chamber to the cold chamber, thus obtaining a net positive heat contribution of $(Q_{hot\ air} - Q_{cold\ air})$ in the cold chamber and a negative contribution of the same value in the hot chamber (neglecting the heat contribution given by the fans electric consumption).

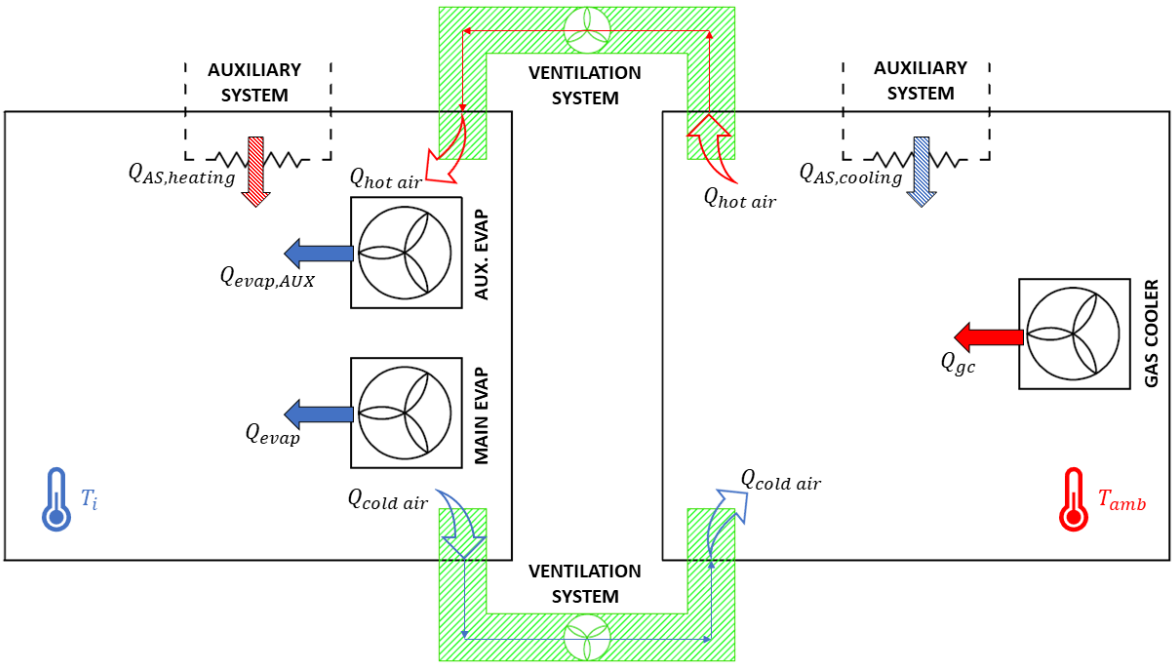

Figure 4.13 – Simplified schematic considered for the design of the auxiliary system allowing temperature control in the insulated chambers.

The cold chamber will be considered for the sizing of the ventilation system since, as it was previously mentioned, the preservation of the temperature inside the cold chamber is the main objective of the refrigeration system and its achievement needs to be granted in every possible condition. To this extent, the maximum heat request for the thermal balance inside the cold chamber is considered (7.10 kW), which can be provided by the hot air coming from the hot chamber if the ventilation system is able to guarantee a hot air volumetric flow rate equal to 1474 $m^3\ h^{-1}$ (corresponding to an air velocity of 2.1 $m\ s^{-1}$ inside a standard square air pipeline 44 cm wide). This air mass flow rate can be satisfied with an air ventilator with rated volumetric flow rate of 1500 $m^3\ h^{-1}$, commercially available in the market. This value can be used as a preliminary sizing also for the ventilator used to send cold air mass flow rate from the cold chamber to the hot chamber.

The control of the thermal load enhanced by the ventilation system can be performed through the control of the rotational speed of the ventilators, granting operational flexibility to the system. In case of a flow rate unbalance between the two chambers, the excess of the integration will be guaranteed by a small opening towards the external ambient.

However, an additional external source is still needed to guarantee operation in every condition and fine regulation of the heat balances inside the insulated chambers. Consequently, electrical heaters able to provide up to 3-4 kW of heating will be placed inside the cold chamber, while an external air conditioning system able to provide up to 6 kW of cooling effect will be placed inside the hot chamber.

The system will be regulated prioritizing the free heating/cooling provided by the air exchange. Air conditioning in the hot chamber will be used with a step regulation to reduce as much as possible the flow rate unbalance between the chambers. Electrical heater will be used as a fine-tuning system on the cold side.

4.5 Conclusions

This chapter presented the installation and the first startup of the R744 cooling unit presented and numerically modelled in Chapter 3. The unit is designed to provide Medium-Temperature (MT) refrigeration and simulate the loads and operating conditions which can characterize road temperature-controlled transport applications. As described in Chapter 3, the cooling unit can operate according to three different configurations, and the objective of the experimental analysis of the system is to define the best system configuration under a wide range of operating conditions, to allow the future development of a lighter and more compact prototype for real operation on refrigerated vehicles.

The cooling unit prototype is installed at the ITC-CNR laboratories, located in Area della Ricerca di Padova, Italy. To allow experimental tests on the cooling unit under a wide range of operating conditions, two separate insulated chambers, in which the heat exchangers of the cooling unit are placed, are installed as well, to reproduce the desired heat sink and heat source air temperatures under which the cooling unit needs to be tested.

Data measurement equipment has been installed on the experimental rig and the first startup experimental tests were performed.

The preliminary experimental tests were helpful to identify improper behaviors of non-compliance with design of some components. In particular, it was highlighted that the internal heat exchanger installed in the unit prototype has been oversized, causing a superheat at the compressor suction of over 30 K, while the desired superheat was 5-10 K. An excessive superheat at the compressor suction has a significant impact on the system performance, because of the increase of the refrigerant density at the compressor suction, causing a reduction of the elaborated refrigerant mass flow rate and consequently a reduction of the cooling effect provided by the evaporators and because of the excessive increase of the compressor discharge temperature, which presented values over 150°C, potentially causing mechanical issues to the compressor. The partial bypass of the IHX in the high-pressure side led to the recover of the desired superheat of 10 K at the compressor suction, while the compressor discharge temperature was lowered to safe values, below 120°C.

Preliminary tests were run under both transient and near-steady-state conditions, to derive the first performance evaluation of the cooling unit:

- A complete pulldown was performed by the cooling unit in BP configuration, in which the system (initially switched off and in thermal equilibrium with the ambient air inside the laboratory in which the system is located) was switched on and, after reaching the desired temperature range, performed a series of ON/OFF cycles to maintain the cold chamber temperature in a specific temperature range (-1°C < T_i < 2°C). Temperature and pressure sensors were used for the evaluation of the cycle operating points, while the refrigerant mass flow rate and the compressor power draw were indirectly calculated from available data. The evolution of the cooling effect provided by the evaporator and of the heat rejected by the gas cooler during the pulldown and consequent ON/OFF operation are assessed, presenting a value of approximately $Q_{evap} \cong$ 5 kW and $Q_{gc} \cong$ 8 kW. The compressor power draw presented an approximate value of $P_{comp} \cong$ 3.2 kW during the considered period, leading to an instant COP of around 1.6 in the considered period of operation.
- Steady-state operation was achieved through the control of the heat exchanged between the insulated chambers (which were not completely sealed through door closing) and the external air. Steady-state experimental tests with an almost constant heat sink temperature of around $T_{amb} \cong$ 45°C and various heat source temperatures ($T_i \cong$ 10°C, $T_i \cong$ 7°C, $T_i \cong$ 5°C, $T_i \cong$ 2°C, $T_i \cong$ 0°C) were performed, assessing a system COP variating from 1.71 (with $T_i \cong$ 10°C) to 1.24 ($T_i \cong$ 0°C).
- The experimental results obtained in steady-state conditions were compared to the numerical results of the cooling unit model developed in Chapter 3, providing the experimental heat source and heat sink temperatures as an input of the numerical model. The experimental results and the simulations results showed a relative error ranging from -19.3% (with $T_i \cong$ 10°C) to -16.9 % (with $T_i \cong$ 0°C).

The design of the external auxiliary system to provide the necessary thermal load inside the insulated chambers to counteract the cooling effect and the heat rejection of the cooling unit heat exchangers, thus allowing steady-state operation of the unit under several different conditions, has been discussed. An hybrid apparatus including a ventilation system able to exchange air between the insulated chambers and external thermal power sources has been proposed, and the preliminary design conditions evaluation highlighted the need of ventilators with a capacity of 1500 $m^3\ h^{-1}$ for the ventilation system, the placement of an electric heater with capacity of 3-4 kW in the cold chamber and the placement of an air conditioning system with capacity of up to 6 kW in the hot chamber.

5 Numerical evaluation of a R744 double-compression cooling unit for multi-temperature refrigerated transport applications

Traditionally, temperature-controlled logistics is organized in order to distribute goods separately for each product segment, with specific temperature requirements. However, in recent years the market is pushing more and more towards the use of trucks equipped with temperature-specific compartments, which allow the simultaneous transport of different product segments in separate chambers of the same truck, thus allowing more flexibility in the logistics and reducing the number of vehicles on the road, especially for the last-mile delivery of goods [113].

While multi-temperature transport refrigeration units employing HFC or HFO refrigerants (such as R452A and R404A) are currently available in the market [114] [115] [116], multi-temperature units employing R744 as the refrigerant are developed and available in the market only for commercial stationary applications.

According to the literature [67] [25], the commonly implemented cycle for multi-temperature R744 stationary units is given by a booster cycle with a double stage of compression. The baseline booster cycle can be further modified with the implementation of parallel compression and the use of an ejector providing the lift from the MT evaporation pressure to the liquid receiver intermediate pressure.

In this chapter, a R744 cooling unit design derived from the traditional stationary unit schematic is proposed and developed for multi-temperature refrigerated transport applications. Numerical simulations are carried out to evaluate the cooling unit performance under different operating conditions and the optimization of the operating parameters is developed through the use of a Pareto optimality criterion, to maximize the proposed system performance.

5.1 Refrigerating system description

The refrigerating system considered in this chapter is designed to remove heat from the insulated box of a multi-temperature refrigerated vehicle used for the delivery of temperature-controlled goods which need to be preserved at different temperature levels. In particular, the cooling unit is designed to provide Medium-Temperature (MT) refrigeration at an internal air temperature of $T_{i,MT}$ = 0°C in one of the two compartments in which the insulated box is divided, while Low-Temperature (LT) refrigeration at an internal air temperature of $T_{i,LT}$ = -20°C in the other compartment of the insulated box, in order to allow the simultaneous delivery of chilled and frozen goods.

The unit is charged with a total refrigerant mass equal to 25 kg of R744 and its design is based on the R744 refrigerating unit design presented and extensively described in Chapter 3 and in Chapter 4. Therefore, also for this cooling unit operation both subcritical and transcritical is allowed, depending on the external climatic conditions, and an auxiliary evaporator is placed at an intermediate pressure level, combining with the main MT evaporator to provide the MT total cooling effect.

The cooling unit design presented in Chapter 3 and in Chapter 4 is extended and adapted to multi-temperature operation through the inclusion of an additional LT evaporator, working at a lower evaporation pressure to provide refrigeration at the internal air temperature required to preserve frozen goods, and of a subcritical LT compressor to compress the refrigerant from the outlet of the LT evaporator to the intermediate pressure level of the liquid separator, corresponding to the suction conditions of the transcritical MT compressor. The refrigerating system includes the use of a parallel between a High-Pressure Valve (HPV) and a fixed geometry ejector, which provides the pressure lift from the MT evaporation pressure to the intermediate pressure level of the liquid separator.

The schematic of the refrigeration unit is presented in Figure 5.1, highlighting the different pressure levels in the system: following the same color convention used in Chapter 3, the red color is used to refer to the high pressure (HP), yellow to intermediate pressure (IP) and green to medium pressure (MP), while blue is added to refer to low pressure (LP). The unit schematic combines a standard booster cycle, representing the common practice in stationary R744 refrigerating systems such as in commercial refrigeration applications [67], with the integration of an ejector at the MT evaporation level and of the auxiliary MT evaporator to extend the operation at high efficiency of the system also at lower environmental temperatures, according to what was previously discussed in Chapter 3.

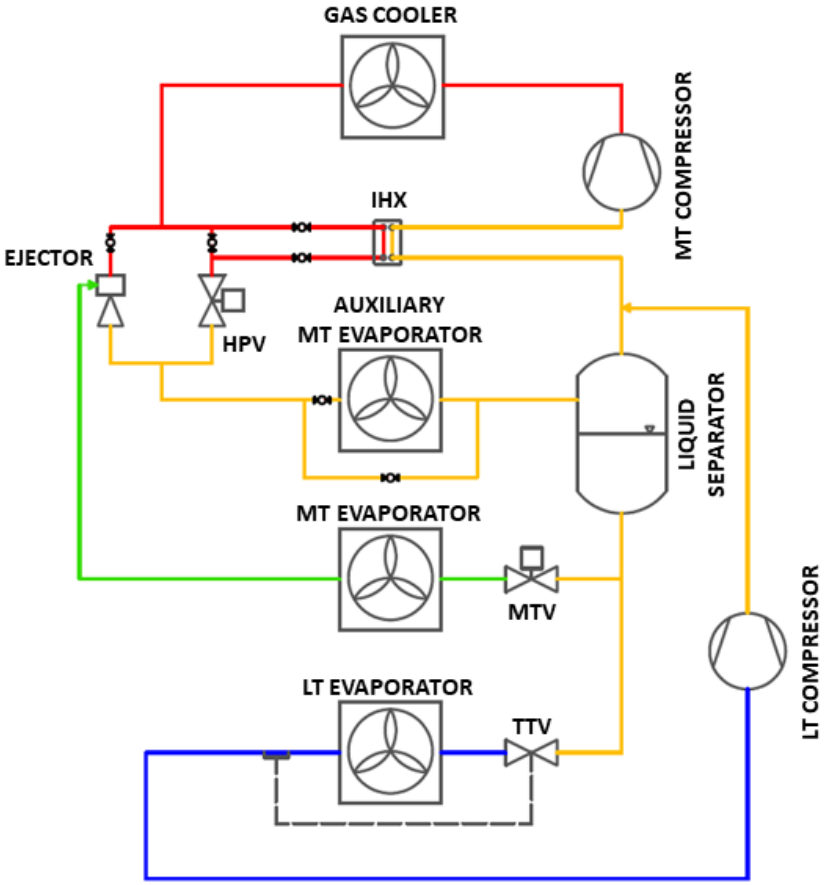

Figure 5.1 – Schematic of the refrigerating system.

Referring to the schematic presented in Figure 5.1, the refrigerant leaves the liquid separator in the state of saturated vapor and enters the MT compressor suction line. After the compression, the refrigerant flows in the gas cooler/ condenser, where it rejects heat to the external air. Since the utilization of a fixed geometry ejector was considered for the system design process, a parallel HPV is provided to control the high-pressure value working on the mass flow exceeding the mass flow rate processed by the fixed geometry ejector.

The mass flow rate at the outlet of the ejector is mixed with the one at the outlet of the HPV valve, and the two-phase mixture is returned to the liquid separator at an intermediate pressure level. In this process, the refrigerant can either flow through an auxiliary MT evaporator or bypass it. The improvements in the cycle efficiency at low external air temperature linked to the insertion of an auxiliary evaporator at this stage of the unit schematic have been extensively discussed in [78] and in Chapter 3. Moreover, comparing the schematic of the MT-LT cooling unit presented in Figure 5.1 and the schematic of the MT cooling unit presented in Figure 3.1, the auxiliary MT evaporator needs to be inserted in this MT-LT unit schematic also to guarantee MT refrigeration at very low external conditions (T_{amb} < 15°C), when the ejector does not provide any pressure lift due to the low energy conditions at the motive nozzle,

since the switching system allowing a simple back-pressure operation in the MT unit is not implemented in the MT-LT unit, to avoid excessive complexity of the system schematic.

From the liquid separator, the refrigerant in the state of saturated vapor enters the MT compressor suction line, while the refrigerant in the state of saturated liquid is partially expanded to the MT evaporation pressure (through a Mechanical Throttling Valve, MTV) and partially to the LT evaporation pressure (through a Thermostatic Throttling Valve, TTV, which controls the evaporation pressure to obtain a fixed 5 K superheating at the outlet of the LT evaporator).

The refrigerant flowing to the MT evaporator coil is evaporated and eventually superheated before entering the suction nozzle of the ejector. The refrigerant flowing to the LT evaporator is evaporated and superheated before being compressed by the LT compressor, which raises the refrigerant pressure from the LT evaporation pressure level to the MT compressor suction pressure level, as it is reported in literature that this solution represents the best practice of this kind of systems [74].

The refrigerating unit, operating with T_{amb} = 30°C, $T_{i,MT}$ = 0°C, $T_{i,LT}$ = -20°C, both compressors at the nominal rotational speed of 1450 rev min^{-1} and without any use of the auxiliary MT evaporator, provides a nominal MT cooling power of 3.6 kW and a nominal LT cooling power of 2.4 kW. The geometric dimensions of the main components of the system, which are chosen among real components available in the market, are reported in Table 5.1.

Table 5.1 – Geometric dimensions of the main components of the cooling unit.

Component	**Geometric dimensions**
MT compressor	Displacement, $V_{d,MT}$ = 27.5 cm^3
LT compressor	Displacement, $V_{d,LT}$ = 12.9 cm^3
Gas cooler/Condenser	External convective surface, $A_{e,gc}$ = 29.8 m^2
MT evaporator	External convective surface, $A_{e,evap\ MT}$ = 39.4 m^2
MT auxiliary evaporator	External convective surface, $A_{e,evap\ MT\ AUX}$ = 8.9 m^2
LT evaporator	External convective surface, $A_{e,evap\ LT}$ = 26.6 m^2
Fixed geometry ejector	Motive nozzle throat diameter d_{EJ} = 1 mm

The LT compressor is assumed to work at a fixed rotational speed, corresponding to the nominal speed of 1450 rev min^{-1}, when LT cooling effect is needed. Conversely, since the system is supposed to be capable of delivering independently MT cooling capacity, LT cooling capacity and MT+LT cooling capacities, the rotational speed of the MT compressor, which has to process a variable mass flow rate depending on the required combination of MT and LT cooling capacities, needs to be variable. Moreover, a variable speed MT compressor is needed also to allow the control the intermediate pressure value in MT+LT configuration.

The speed of the MT compressor is assumed to range from 870 rev min^{-1} (operation at the minimum frequency of 30 Hz) to 2030 rev min^{-1} (operation at the maximum frequency of 70 Hz), under control of a Proportional-Integral (PI) controller, which sets the desired value of the intermediate pressure of the liquid separator.

As regard to the control systems, in addition to the two previously mentioned (the thermostatic valve on the LT evaporator, setting the LT evaporation pressure, and the PI on the MT compressor, controlling the intermediate pressure), the unit implements two other closed-loop PI controls to control the temperature and the pressure at the gas cooler outlet thus optimizing the gas cooler operation, following the same strategy presented in Table 3.2. The temperature is controlled acting on the gas cooler fan speed, while the pressure is set by the HPV.

5.2 Numerical model description

The refrigerating system modelled in this chapter is supposed to be charged with a total refrigerant mass equal to 25 kg of R744. The numerical model of the cooling unit is developed using the commercial software Simcenter Amesim v.17.

The numerical model development is carried out following the same modelling assumptions, the same component discretization and the same equations describing the components behavior and the system energy balances as described in Section 3.2. In addition to the components whose modelling approach has already been described in Section 3.2, in this case also the additional subcritical compressor has been considered with its own displacement and efficiency maps, together with the additional evaporator, still discretized in N = 10 lumped volumes and characterized by its own external convective surface, as reported in Table 5.1. The LT thermostatic throttling valve has been modelled and controlled through a dedicated PI controller acting on the valve sectional area to realize the desired superheat at the outlet of the LT evaporator.

The high-pressure side internal flow components of the refrigerating system (gas cooler and MT evaporators lumped volumes, as well as high-pressure, intermediate-pressure and medium-pressure pipeline elements) are initialized to saturated vapor conditions at the pressure corresponding to a temperature of 30°C, while the LT side internal flow components (LT evaporator lumped volumes and low-pressure pipeline elements) are initialized to saturated vapor conditions at the pressure corresponding to a temperature of 0°C. The thermal capacity components of the refrigerating system are initialized to the mean temperature between the environment and the above-mentioned temperature of the refrigerant flow components.

However, the initialization of the state variables of the system was necessary only as an input for the first time step of the numerical solver; a total simulation time of 7200 s was proved to be enough for the

system to achieve steady state conditions and the complete independence of the solution from the initial conditions.

5.3 Numerical test conditions

The multi-temperature refrigerating system presented in this chapter was characterized considering steady-state operation with a fixed internal MT air temperature of $T_{i,MT}$ = 0°C, a fixed internal LT air temperature of $T_{i,LT}$ = -20°C and different ambient temperature conditions (T_{amb} is considered to vary between 15°C and 40°C in the numerical simulations).

The performance of the considered refrigerating system is influenced by three main parameters, besides the environmental air temperature:

- The eventual use of the MT auxiliary evaporator, which can be included in the line connecting the HPV-ejector parallel and the liquid separator or bypassed, as an input of the model;
- The liquid separator pressure level ($p_{receiver}$), which is enforced by a PI controller acting on the MT compressor rotational speed;
- The evaporation pressure level at the MT evaporator ($p_{MT\ evap}$), which depends on both the intermediate pressure level of the separator, the Δp_{lift}- ϕ characteristic of the ejector (describing the relationship between entrainment ratio and available pressure lift) and the opening ratio of the MTV throttling valve. Since $p_{MT\ evap}$ is directly derived from the above-mentioned parameters, the design of experiments will be defined through the throttling valve opening ratio ($r_{MTV} = A_{op}/A_{op,max}$).

The three described parameters, together with the external air temperature T_{amb}, were controlled to evaluate the steady-state performance of the system in specific operating conditions obtained as the combination of the parameters input values, within the variation ranges presented in Table 5.2.

Regarding the liquid separator pressure variation range, the minimum receiver pressure is assumed to be the minimum obtainable integer pressure value (which is reached with a rotational speed of the MT compressor close to its maximum value of 2030 rev min^{-1}) and the maximum receiver pressure is assumed to be the maximum obtainable integer pressure value (reached with a rotational speed of the MT compressor close to its minimum value of 870 rev min^{-1}). Since the gas cooler outlet pressure, enforced by a PI controller, depends on the external air temperature conditions (as described in Table 3.2), the liquid receiver minimum and maximum pressures depend on T_{amb} as well. The in-between receiver pressures were evaluated considering a pressure step of 1 bar.

Regarding the MT evaporation pressure, a small MTV opening ratio implies a significant throttling process occurring in the valve (leading to a lower $p_{MT\ evap}$), while a high opening ratio corresponds to an almost

null throttling process in the MTV (leading to an almost unchanged $p_{MT\ evap}$ compared to $p_{receiver}$). The final MT evaporation pressure therefore depends on the MTV opening ratio and on the intermediate pressure of the liquid receiver, which represents the pressure level from which the throttling process occurs.

Table 5.2 – Variation ranges for the input parameters of the numerical model.

External air temperature	Auxiliary MT evaporator	Liquid separator pressure	MTV opening ratio
• T_{amb} = 15°C • T_{amb} = 20°C • T_{amb} = 25°C • T_{amb} = 30°C • T_{amb} = 35°C • T_{amb} = 40°C	• Included (ON) • Excluded (OFF)	• $p_{receiver,min}$ = minimum available integer value • $p_{receiver,max}$ = maximum available integer value • $\Delta p_{receiver}$ = 1 bar	• $r_{MTV,min}$ = 0.05 (valve almost closed) • $r_{MTV,max}$ = 1 (valve fully open) • Δr_{MTV} = 0.005

5.4 Optimization of the cooling unit steady-state performance

Each of the parameters described in Section 5.3 directly affects the performance of the refrigerating system, which is evaluated through the definition of the overall MT cooling capacity (Eq. (5.1)) and of the system COP (Eq. (5.2)):

$$Q_{MT,TOT} = Q_{MT\ evap} + Q_{MT\ evap,aux} \tag{5.1}$$

$$COP = \frac{Q_{MT,TOT} + Q_{LT\ evap}}{P_{MT\ comp} + P_{LT\ comp}} \tag{5.2}$$

To assess the best combinations of parameters in terms of the objective functions COP and MT cooling effect, a Pareto optimality criterion was used, highlighting the non-dominated operating points for both the configurations including or excluding the auxiliary MT evaporator.

Pareto optimality is a criterion used to account the efficiency in multi-objective context, where different conflicting objectives must be optimized at the same time [117]. In general, a combination of parameters is considered Pareto optimal if there is no other parameter combination which improves the value of any of its objective functions without deteriorating at least one other objective function. In general, the dominance between two solutions (evaluated over m objective functions) can be defined as x_1 dominating x_2 if:

$$f_i(x_1) \leq f_i(x_2)\ \forall i \in \{1, \dots, m\} \text{ and } \exists j \in \{1, \dots, m\}\ |\ f_j(x_1) < f_j(x_2) \tag{5.3}$$

A specific combination of parameters x^* is therefore considered non-dominated or Pareto optimal if no other feasible parameters combination dominates it. The set of all non-dominated parameter

combinations constitutes the Pareto front, representing the optimal trade-off between all the objective functions of the system [118].

To highlight the influence of the variating parameters on the system operation, the cooling unit's operating points obtained through the numerical simulation of the system steady-state performance with ambient temperature of T_{amb} = 30°C are reported in Figure 5.2.

Each point reported in the figure corresponds to a specific combination of $p_{receiver}$, which was varied with a pressure step of 1 bar between the minimum achievable integer value of 30 bar and the maximum achievable integer value of 39 bar (for T_{amb} = 30°C), and r_{MTV}, which was varied with an opening ratio step of 0.005 between the values of 0.05 (almost closed valve) to 1.00 (fully open valve). Numerical simulations were performed both bypassing the auxiliary MT evaporator (Figure 5.2a) and including the auxiliary MT evaporator (Figure 5.2b). The Pareto optimality criterion was then used to highlight the optimal combination of parameters in terms of the objective functions $Q_{MT,TOT}$ and COP, for both cases.

The entire amount of operating points for T_{amb} = 30°C are then reported in Figure 5.2c, in which the Pareto optimality was evaluated considering both configurations (with and without the use of the auxiliary MT evaporator). The dashed red line represents a guess of the Pareto front interpolated using the available optimal points.

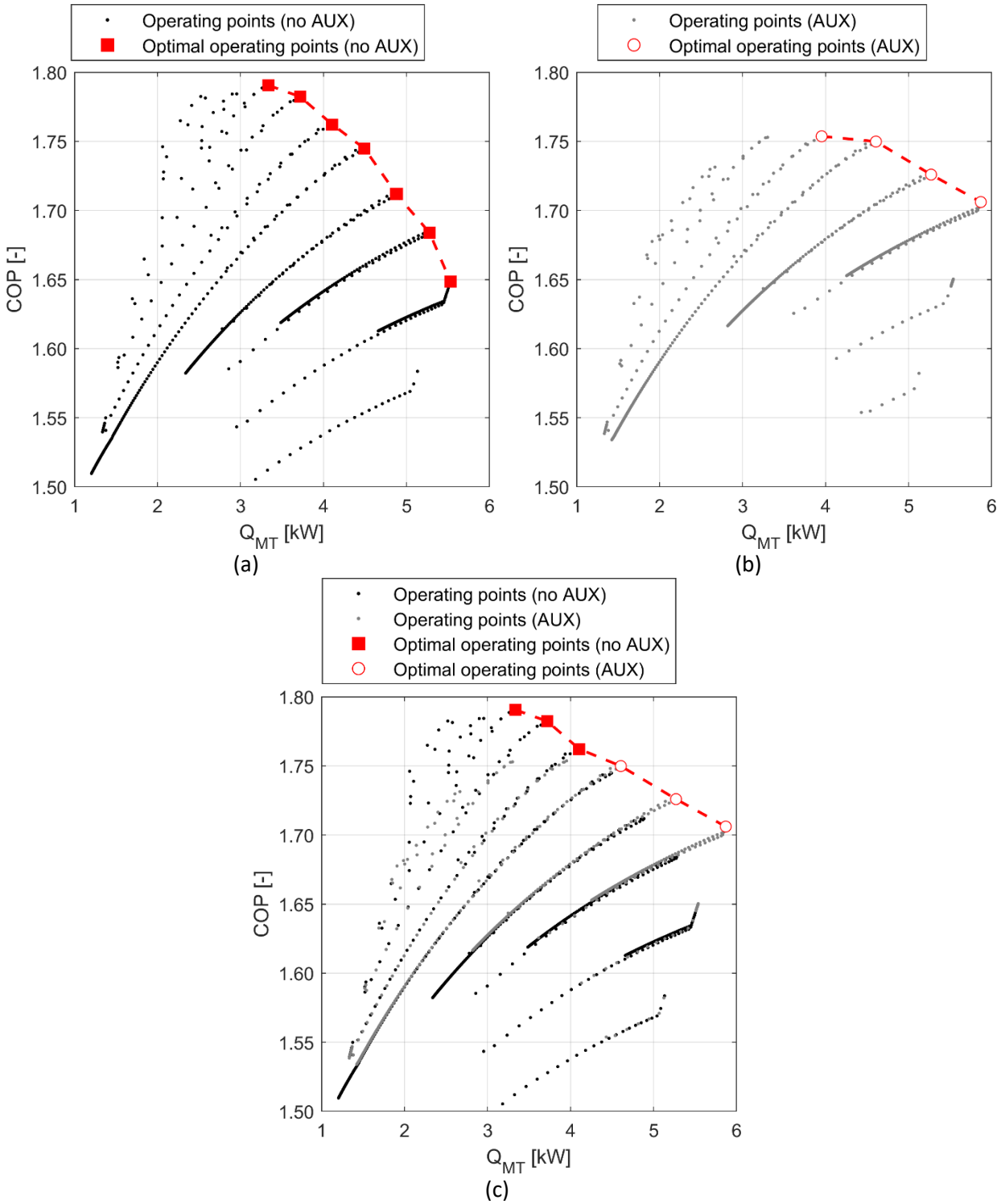

Figure 5.2 – Cooling unit operating points for different values of $p_{receiver}$ and $p_{MT\ evap}$ and Pareto optimal points for T_{amb}=30°C: (a) without auxiliary MT evaporator; (b) with auxiliary MT evaporator; (c) combined evaluation of the two configurations.

Referring to the total amount of parameters combinations presented in Figure 5.2c, the configuration and the value of $p_{receiver}$, $p_{MT\ evap}$, COP and $Q_{MT,TOT}$ for the optimal operating points at T_{amb} = 30°C are reported in Table 5.3.

Table 5.3 – Cooling unit's configuration, $p_{receiver}$, $p_{MT\ evap}$, COP and $Q_{MT,TOT}$ of the optimal operating points at T_{amb} = 30°C.

Auxiliary MT evaporator	$\boldsymbol{p_{receiver}}$ **[bar]**	$\boldsymbol{p_{MT\ evap}}$ **[bar]**	$\boldsymbol{COP}$ **[-]**	$\boldsymbol{Q_{MT,TOT}}$ **[kW]**	$\boldsymbol{Q_{LT}}$ **[kW]**	**Notes**
Off	37.0	31.3	1.79	3.33	2.26	Max COP
Off	36.0	31.0	1.78	3.72	2.30	
Off	35.0	30.7	1.76	4.11	2.33	
On	34.0	30.3	1.75	4.61	2.37	
On	33.0	29.9	1.73	5.27	2.40	
On	32.0	29.6	1.71	5.87	2.44	Max $Q_{MT,TOT}$

From the evaluation of the system performance for the total amount of possible combinations of parameters (Figure 5.2) and for the Pareto optimal solutions (Table 5.3) at ambient temperature equal to T_{amb} = 30°C, it can be observed that, for this specific environmental conditions, the highest value of the cooling unit's COP (1.79) is obtained for high values of $p_{receiver}$ (37 bar), high values of the pressure lift provided by the two-phase ejector (which corresponds to the difference between $p_{receiver}$ and $p_{MT\ evap}$ and in this case it's equal to 5.7 bar) and without the use of the auxiliary MT evaporator. Conversely, the highest value of the cooling unit's $Q_{MT,TOT}$ (5.87 kW) is obtained for low values of $p_{receiver}$ (32 bar), low values of the pressure lift of the ejector (2.4 bar) and with the use of the auxiliary MT evaporator.

From the data reported in Figure 5.2, it can be observed that, considering all the possible operating points evaluated through numerical simulations, the choice of the optimal combination of parameters leads to significant improvements in both the objective functions of the system (COP and $Q_{MT,TOT}$). In fact, operation with a non-optimized combination of parameters can lead to a reduction in the COP of up to -15.6% and to a reduction in the $Q_{MT,TOT}$ of up to -79.6% compared with the maximum achievable values.

However, considering only the Pareto optimal operating points reported in Table 5.3, even among optimal solutions the range of possible MT cooling effects is wide (from 5.87 kW to 3.33 kW, corresponding to a reduction of -43.4%). The Pareto front is in fact quite extended on the $Q_{MT,TOT}$ objective, thus the optimal control can significantly impact the system behavior depending on the refrigerating effect demanded to the cooling unit. For example, when a high cooling effect is needed (i.e. during pulldown and after a door opening of the refrigerated truck cargo space), a high $Q_{MT,TOT}$ can be provided without a significant reduction of the system COP (the COP reduction is only -4.7% along the Pareto front).

Additionally, it can be pointed out that the use of the auxiliary MT evaporator has a positive effect on both COP and $Q_{MT,TOT}$ in the high cooling power optimal solutions. This contribution will be more evident for lower ambient temperatures, consistently with the performance improvements due to the presence of the auxiliary MT evaporator in low temperature environmental conditions highlighted in Section 3.3 and Section 3.4.

The LT cooling effect is also reported in Table 5.3, and it can be observed that it follows the same trend of the total MT cooling effect, but with a very limited variation range (from 2.44 kW to 2.26 kW, corresponding to a 7.4% reduction over the Pareto front). The LT cooling effect is therefore almost uninfluenced by the operating conditions of the MT side of the system, since the LT evaporation pressure is adjusted only to maintain a 5 K superheat at the LT evaporator outlet and the LT compressor works at fixed rotational speed, as described in Section 5.1. The low dependency of Q_{LT} on the system parameters variations is the main reason why the LT cooling effect is not considered as one of the objective functions for the Pareto optimization of the refrigerating system.

The system performance analysis reported in Figure 5.2c can be extended to the whole range of external air temperature conditions considered for the system characterization (T_{amb} varying between 15°C and 40°C), and the numerical results, including the identification of the Pareto optimal solutions, are presented in Figure 5.3. Figure 5.3a highlights the system COP and the MT total refrigerating effect, while Figure 5.3b reports the same operational points in terms of system COP and LT refrigerating effect.

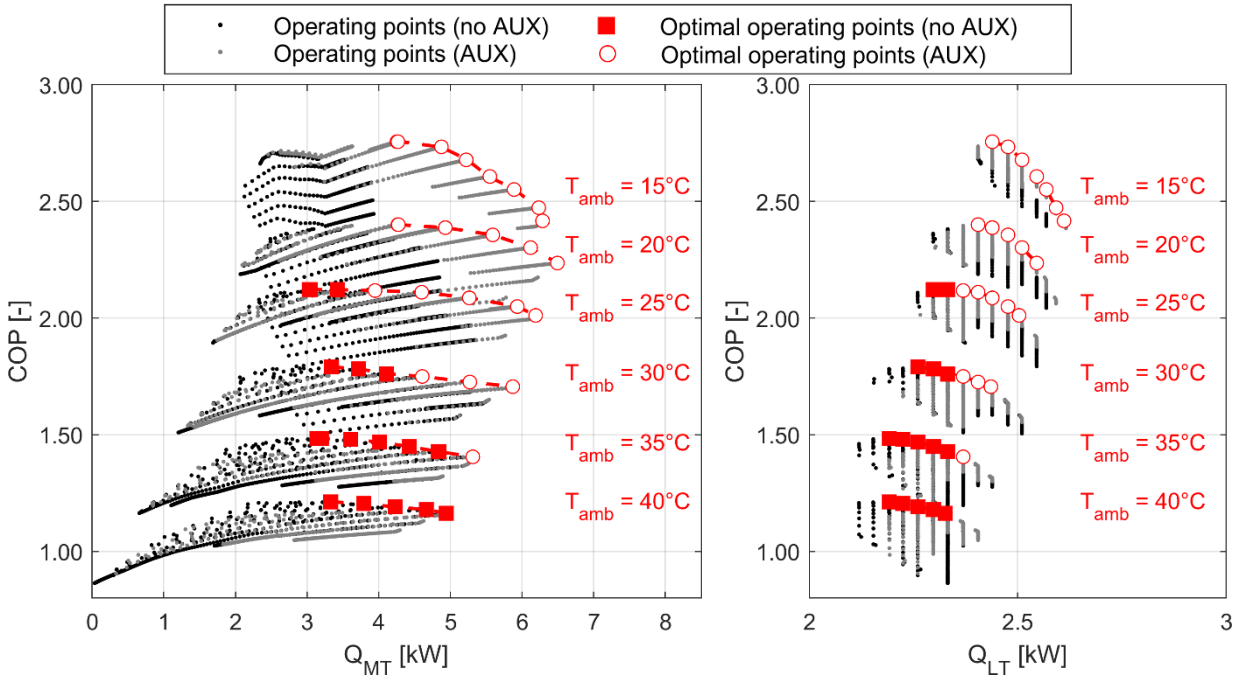

Figure 5.3 – Cooling unit operating points and Pareto optimal points for T_{amb} varying from 15°C to 40°C: (a) COP and MT cooling effect; (b) COP and LT cooling effect.

It can be observed that, for T_{amb} from 15°C to 20°C, the configuration using the auxiliary MT evaporator outperforms the configuration not using it in terms of both COP and MT cooling effect. Such a behavior is consistent with the cycle improvements at low ambient temperature linked to the presence of an auxiliary MT evaporator described in Section 3.3: the COP of the refrigerating unit is always higher with the inclusion of the additional MT evaporation at the intermediate pressure level.

For T_{amb} between 25°C and 35°C, the highest system COP is obtained without the use of the auxiliary MT evaporator, while the highest MT cooling effect is reached exploiting it. With external ambient temperature growing towards higher values, the benefits of the MT auxiliary evaporator inclusion are less significant. Still, the additional MT evaporation can be useful in case of high cooling demand of the insulated box of the truck.

Finally, for T_{amb} = 40°C the configuration without auxiliary MT evaporator presents a better performance both in terms of COP and MT cooling effect. For high environmental air temperature, the additional MT evaporation never brings to a performance improvement, and therefore the MT auxiliary evaporator can be bypassed.

As it was highlighted from the numerical results reported in Table 5.3, the LT side of the unit presents an only marginal modification as results of the different external and operating conditions along the Pareto front: the cooling power average variation from the condition of maximal COP to the condition maximizing the MT cooling power is always less than 10%. The required LT refrigerating effect can be therefore provided without being directly influenced by the variation of the operational parameters of the system, whose optimization leads mainly to the improvement of the two-phase ejector expansion work recovery and MT compressor power (and, consequently, to the improvement of the overall system COP) and to the optimal correspondence between the actual MT cooling demand and the MT cooling effect provided by the unit, resulting in the optimization of the whole system performance.

To evaluate more in detail the optimal operating points of the cooling unit in terms of $p_{receiver}$ and $p_{MT\ evap}$, which are the system parameters directly connected to the optimization of the MT compression process and of the ejector operation, Figure 5.4 reports the Pareto front optimal points highlighted in Figure 5.3 in terms of the corresponding pressure level at the liquid separator (intermediate pressure), pressure level at the MT evaporator (medium pressure) and pressure level at the LT evaporator (low pressure). The difference between $p_{receiver}$ and $p_{MT\ evap}$ for each of the Pareto front operating points represents the pressure lift which is provided by the two-phase ejector.

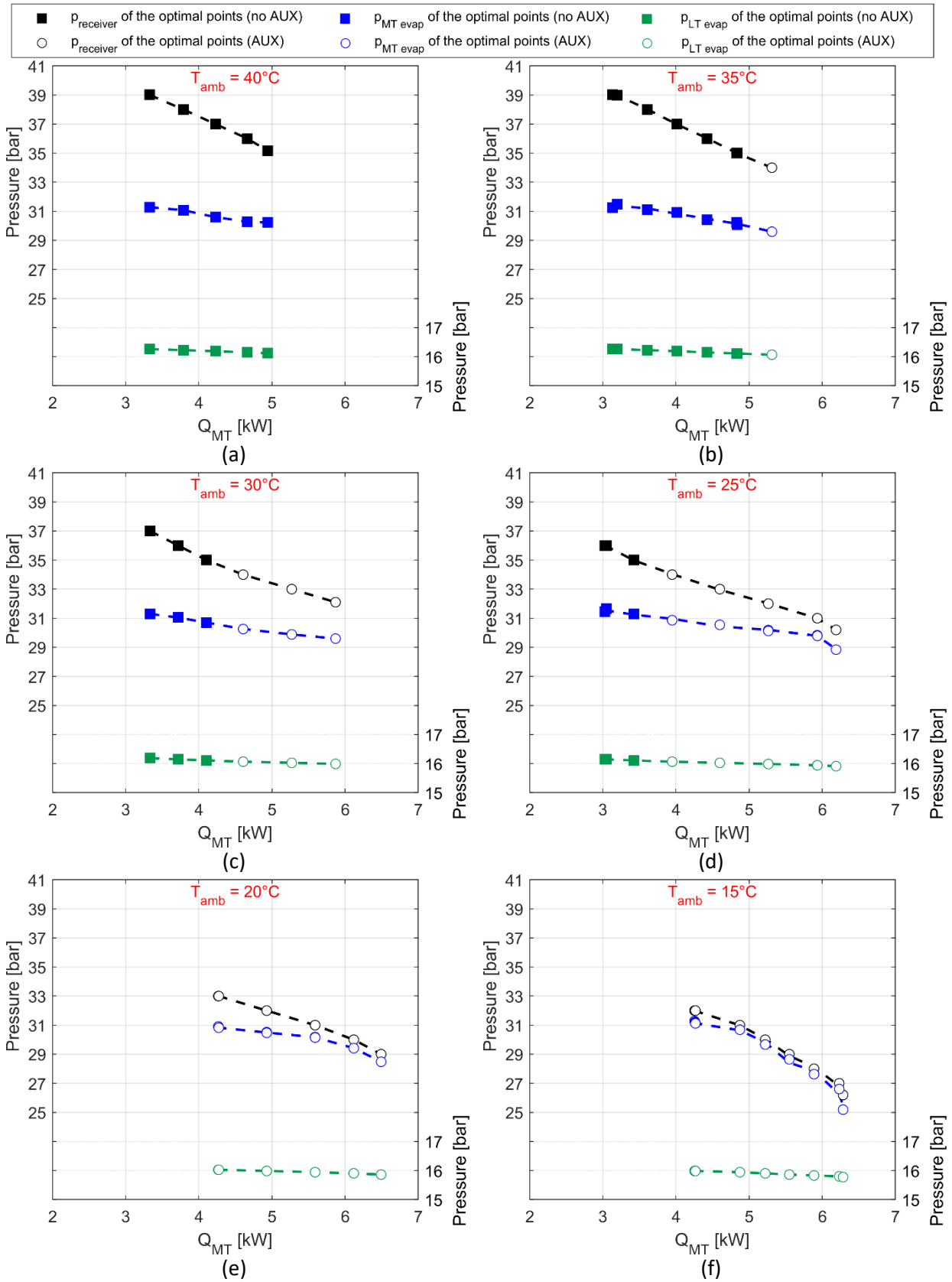

Figure 5.4 – $p_{receiver}$, $p_{MT\ evap}$ and $p_{LT\ evap}$ of the cooling unit optimal operating points: (a) for T_{amb}=40°C; (b) for T_{amb}=35°C; (c) for T_{amb}=30°C; (d) for T_{amb}=25°C; (e) for T_{amb}=20°C; (f) for T_{amb}=15°C.

First of all, it should be pointed out that, for all the Pareto optimal points reported in Figure 5.4, for $p_{receiver}$ ≥ 35 bar the configuration using only the main MT evaporator presents a better performance,

while for $p_{receiver}$ < 35 bar the configuration including the auxiliary MT evaporator is preferable, regardless of the external air temperature. The reason for such a behavior is to be found in the saturation temperature of R744, which at 35 bar is equal to 0.16°C. Since the MT internal air is assumed to be fixed at 0°C as an input parameter of the system, the auxiliary evaporator can provide a positive contribution to the overall MT cooling power $Q_{MT,TOT}$ only if the refrigerant temperature flowing inside its heat exchanger coils is at a lower temperature than the outside air of the insulated box. Therefore, for $p_{receiver}$ ≥ 35 bar the auxiliary MT evaporator is not able to exchange cooling power and, instead, has a negative contribution to the overall MT cooling effect.

In general, regardless of the ambient air temperature, higher $Q_{MT,TOT}$ operating points correspond to lower values of $p_{receiver}$, $p_{MT\ evap}$ and $\Delta p_{lift} = p_{receiver} - p_{MT\ evap}$. On the contrary, lower $Q_{MT,TOT}$ points of the Pareto fronts (which correspond to higher COP values operating points) present higher values of $p_{receiver}$, $p_{MT\ evap}$ and Δp_{lift}: an increase in the system COP is dependent on the fact that higher values of receiver pressure and pressure lift lead to a reduction in MT compression power, and a greater exploitation of the ejector energy recovery capability, respectively.

Furthermore, it can be observed that, for decreasing external air temperatures, the optimal intermediate pressure level range shifts towards lower values: at T_{amb} = 40°C, the optimal $p_{receiver}$ ranges between 35 bar and 39 bar, while at T_{amb} = 15°C the optimal $p_{receiver}$ range is 26 bar – 32 bar. This depends on the optimal high pressure level at the gas cooler, which is lower for lower values of the external air temperature, thus leading to the possibility of lowering also the intermediate and medium pressure levels of the system without increasing the MT compression work.

On the other hand, the optimal MT evaporation level is not subject to change depending on the external air conditions as much as the intermediate pressure. In fact, at T_{amb} = 40°C, the optimal $p_{MT\ evap}$ ranges between 30 bar and 31.5 bar, and this range is almost unchanged until T_{amb} = 20°C, at which the $p_{MT\ evap}$ range is 28.5 bar – 31 bar. In general, for T_{amb} > 20°C the optimal $p_{MT\ evap}$ presents an almost constant variation between approximately 31 bar (for the operating point maximizing the COP) and 29 bar (for the operating point maximizing the $Q_{MT,TOT}$), regardless of the external temperature condition.

On the contrary, for T_{amb} = 15°C the low optimal $p_{receiver}$, which becomes equal to 26 bar for the highest MT cooling effect operating point, forces the MT evaporation pressure level to be lowered as well by the MTV. It can be observed that, in this case, the $p_{MT\ evap}$ presents the maximum feasible value which can still provide a non-null pressure lift by the two-phase ejector, as the MTV optimal opening ratio is close to 1 (fully open valve) for these specific operating conditions.

Finally, consistently with what was previously highlighted from Figure 5.3, it can be observed that the LT evaporation side of the system is almost unaffected by the variation of the operating parameters: in fact,

the LT pressure of the optimal operating points presents an almost constant value of 16 bar, regardless of the external air conditions.

5.5 Conclusions

This chapter presented the numerical simulation of a R744 cooling unit developed for multi-temperature (0°C and -20°C) refrigerated transport applications. The layout integrates a traditional booster system with a two-phase ejector and auxiliary evaporator layout and relies on a double stage of compression to provide MT and LT refrigerating effect. The software Simcenter Amesim v.17 was used for the development of the numerical model of the entire system.

The system presents three parameters to be optimized, depending on the specific external air temperature conditions: the intermediate pressure level at the liquid separator, the evaporation pressure level at the MT evaporator and the eventual use of an auxiliary MT evaporator.

The theoretical performance of the unit was evaluated through steady-state simulations under different environmental temperature conditions (with ambient temperature varying between 15°C and 40°C) and different combinations of input parameters, and the system optimal operating points, in terms of system COP and total MT cooling effect, were highlighted through the implementation of a Pareto optimality criterion.

The main results obtained in this chapter can be summarized as follows:

- For low external temperatures (15°C and 20°C) the configuration using the auxiliary MT evaporator outperforms the configuration not using it in terms of both COP and MT cooling effect, while for high temperatures (40°C) the auxiliary MT evaporator has to be bypassed to obtain the system optimization. Instead, for mild outdoor temperatures (25°C, 30°C and 35°C), the use of the sole main MT evaporator leads to the optimization of the system COP, while the use of the auxiliary MT evaporator allows obtaining the highest MT cooling power.
- Considering all the possible operating points evaluated through numerical simulations, the choice of the optimal combination of parameters leads to significant improvements in both the objective functions of the system (COP and $Q_{MT,TOT}$). In particular, for external air conditions equal to T_{amb} = 30°C, operation with a non-optimized combination of parameters can lead to a reduction in the COP of up to -15.6% and to a reduction in the $Q_{MT,TOT}$ of up to -79.6% compared with the maximum achievable values.
- The Pareto front of the system operating points presents a high extension on the $Q_{MT,TOT}$ objective, thus the optimal control can significantly impact the system behavior depending on the actual system cooling demand. For external air conditions equal to T_{amb} = 30°C, a variation of up

to -43.4% of the MT cooling effect can be achieved. At the same time, moving along the Pareto front, the COP reduction never exceeds -4.7%. This flexibility in the MT cooling effect objective, while still keeping high COP values, can be useful to exploit a high cooling effect production when needed (i.e. during pulldown and after a door opening of the refrigerated truck cargo space).

- Higher MT cooling effect operating points correspond to lower values of intermediate pressure and ejector lift, while on the contrary higher COP operating points present higher values of intermediate pressure and ejector lift, due to the reduction in MT compression power, and a greater exploitation of the ejector energy recovery capability.
- The optimal value of the intermediate pressure presents a higher dependency on the external air temperature conditions than the optimal value of the MT evaporation, which for T_{amb} > 20°C is always approximately in the 29 bar – 31 bar range. An exception to this behavior is highlighted in low external temperature operation (T_{amb} = 15°C), in which the optimal MT evaporation pressure corresponds to the maximum feasible value which can still provide a non-null pressure lift by the ejector.
- The LT side of the cooling unit presents an only marginal modification as results of the different external conditions and of the different parameters combination along the Pareto front: the cooling power average variation from the condition of maximal COP to the condition maximizing the MT cooling power is always less than 10%, and the LT evaporation pressure is always approximately equal to 16 bar. The required LT refrigerating effect can be therefore provided without being directly influenced by the variation of the operational parameters of the system.

6 Experimental characterization of a R744 ejector at low-temperature suction conditions

The refrigeration system described and analyzed in Chapter 5 presented the application to the road transport refrigeration sector of the commonly implemented cycle schematic utilized for multi-temperature R744 stationary cooling units. In the described system, two stages of compression are needed to provide a cooling effect at two different temperature levels, namely a subcritical compressor to increase the refrigerant pressure from the LT evaporation pressure to the intermediate pressure of the liquid separator and a transcritical compressor to provide the necessary pressure increase from the separator level and the optimal gas cooler pressure, as a function of the ambient temperature.

In this chapter, a novel R744 cooling unit concept for multi-temperature refrigerated transport applications is proposed, based on the implementation of an ejector as the only component dedicated to the increase of the refrigerant pressure from the LT to the MT evaporating pressure, thus allowing the removal of the LT subcritical compressor from the system schematic and the operation of the multi-temperature unit with only one stage of compression. The removal of the LT subcritical compressor would reduce the overall electrical power draw of the refrigeration system, leading to an improvement of the system COP.

To verify the actual feasibility of such a unit arrangement, experimental tests were performed on a commercially available ejector to assess its performance in the desired low-temperature range (down to -25°C LT saturation temperature), far from the operational field in which R744 ejectors are traditionally employed in the current market.

A numerical evaluation of two R744 refrigeration unit concepts employing an ejector to provide pressure lift after the LT evaporation has been carried out by Banasiak et al. [119], but an experimental study on ejectors operating in such applications was still to be performed.

This chapter firstly illustrates the novel refrigerating unit concept, then it describes the experimental setup and the operating conditions used for the assessment of the ejector performance under LT suction conditions. Finally, the ejector performance results are provided and discussed.

6.1 Refrigerating system description

Similarly to the cooling unit presented in Chapter 5, the refrigerating system considered in this chapter is designed to remove heat from the insulated box of a multi-temperature refrigerated vehicle used for the delivery of temperature-controlled goods at different temperature levels. In particular, the cooling unit is designed to simultaneously provide Medium-Temperature (MT) refrigeration at an internal air

temperature of $T_{i,MT}$ = 0°C and Low-Temperature (LT) refrigeration at an internal air temperature of $T_{i,LT}$ = -20°C, for the simultaneous delivery of chilled and frozen goods with a single vehicle.

However, differently from the system schematic presented in Figure 5.1, the cooling unit design illustrated in this chapter is intended to propose a novel and simplified unit arrangement for the fulfillment of the above-mentioned refrigerating effect needs by taking advantage of the pressure lift provided by an ejector, whose placement and implementation inside the unit represents the different aspect with regards to the cooling unit presented in Chapter 5.

The simplified schematics of the refrigeration unit concept is presented in Figure 6.1.

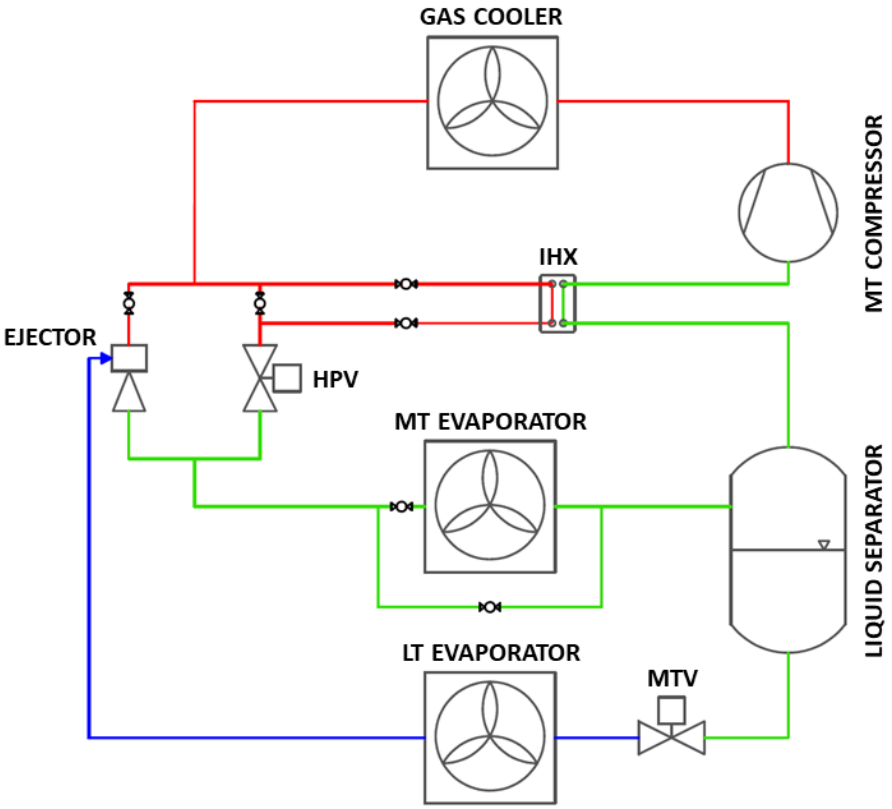

Figure 6.1 – Schematic of the refrigerating system.

In the cooling unit schematic presented in Figure 6.1, the ejector has not the function of providing a pressure lift from the MT evaporation pressure to an intermediate pressure level in which the liquid receiver is placed, as it was done in the schematic reported in Figure 5.1, with a consequent reduction of the MT compression work. Instead, in the proposed unit concept the ejector is employed to provide the pressure lift from the LT evaporation pressure to the MT evaporation pressure, thus allowing the complete removal of the additional subcritical compressor and enabling the realization of a multi-temperature cycle with only one compression stage, as the LT to MT pressure increase is provided by the ejector without external work requirement.

After the compression, the refrigerant flows in the gas cooler coils to reject the heat to the external ambient and then it is sent to the ejector motive nozzle to provide the energy required to entrain mass flow rate from the suction nozzle. Since a fixed-geometry ejector is suggested for this application, due to the expected cooling effect needs inside the insulated box mounted on the vehicle used for transport refrigeration (preliminarily evaluated from the results presented in Chapter 5), a high-pressure valve (HPV) is implemented in parallel to adjust the high-pressure according to environmental conditions and cooling load.

The mixture at the outlet of the HPV-ejector stage is sent to the MT evaporator, where it provides the required chilled-storage cooling effect, and then to a liquid separator. The liquid separator works as a suction accumulator before the MT compressor, to deliver the refrigerant vapor phase (eventually superheated in an internal heat exchanger) to the compressor suction, while the liquid phase is expanded to the LT evaporator inlet, providing the required frozen-storage cooling effect, and then entrained by the ejector.

Notably, the proposed schematic allows the system operation not only in the design case of simultaneous production of MT and LT cooling effect, but also in case only one of the two refrigerating effects is needed. In fact, in case of LT-only load requirement, the MT evaporator can be bypassed, while in case of MT-only load requirement, the refrigerant flow coming from the outlet of the gas cooler can be expanded in the HPV exclusively, thus realizing a classic backpressure cycle with MT cooling effect production and not employing the ejector.

While the refrigerating unit concept presented in Figure 6.1 could potentially work, depending on the ejector performance assessment which represents the main focus of this chapter, for different ranges of MT and LT cooling load requirements, the evaluations which will be carried out onwards are referred to the usual needs of a medium-size refrigerated van employed for short-range delivery of goods, consisting of a MT load in the range of 4-5 kW and a LT load in the range of 1-2 kW. Therefore, the choice of the ejector size to be experimentally tested are consistent with the expected refrigerating effects that the system is required to provide.

6.2 Experimental setup

As mentioned at the beginning of the chapter, ejectors are traditionally employed in R744 cooling units to increase the pressure level from the MT evaporator pressure level (corresponding to a saturation temperature of approximately -8°C to -12 °C, depending on the application) to an intermediate pressure level in which the liquid separator is placed.

However, the ejector included in the schematic presented in Figure 6.1 is intended to operate with suction nozzle corresponding to the outlet of the LT evaporation, occurring at a pressure level corresponding to a saturation temperature of down to -25°C.

To assess the capability of a commercially available ejector to entrain mass flow rate from LT suction nozzle conditions, an experimental campaign has been carried out.

The experimental tests on the ejector under LT operating conditions have been performed in the SuperSmart-Rack test facility located in NTNU/SINTEF laboratories in Trondheim (Norway). The SuperSmart-Rack test facility is a flexible and versatile experimental setup offering the implementation of various solutions and configurations to recreate completely the refrigerating needs of a supermarket for both chilled and frozen storage over a wide range of operating conditions. The refrigeration system is in fact designed to provide a cooling effect at two different temperature levels in multiple evaporators, to reproduce the supermarket operating conditions, in which several cabinets with separate evaporators are present, and at the same time to satisfy eventual additional needs such as heating, ventilation and air conditioning (HVAC) and hot water demands.

A detailed description of the system and its possible configurations is provided in [69], while a simplified schematics of the complete SuperSmart-Rack unit is provided in Figure 6.2. Since, as mentioned above, the system can be used to reproduce a vast quantity of operating conditions through the inclusion or the exclusion of components and through the modification of the refrigerant path through opening and closing of valves, part of the system was not necessary for the experimental camapign aimed at the characterization of the ejector in LT suction conditions. For this reason, in the schematic presented in Figure 6.2 the dashed lines and components highlight the portions of the system which were not used during the experimental campaign.

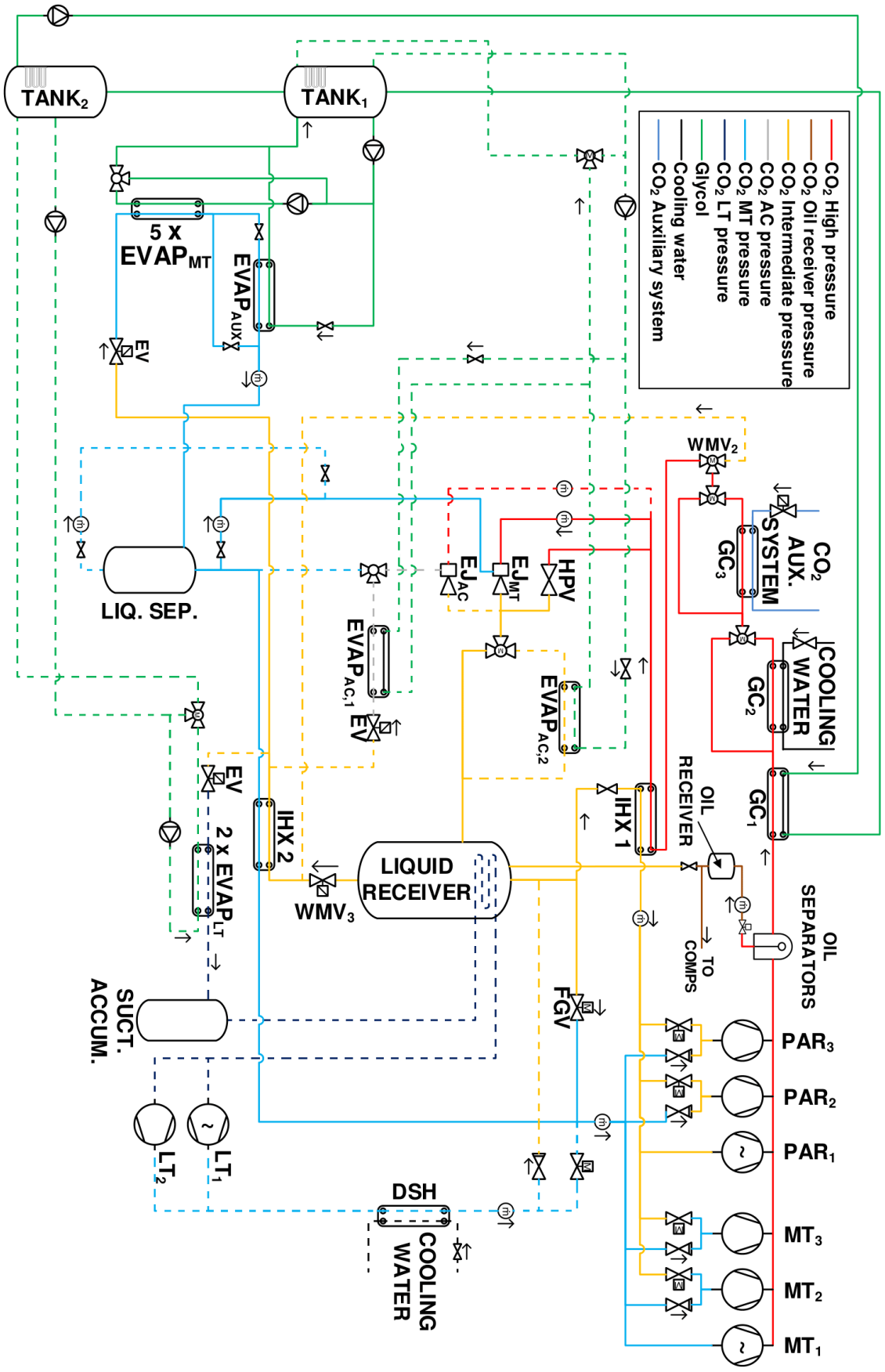

Figure 6.2 – Simplified schematic of the experimental setup used for the ejector performance tests. Dashed lines and components were not in use during the experiment.

Two different racks of ejector are installed in the experimental test facility, one designed to provide a higher pressure lift and a lower entrainment ratio to the refrigerant mass flow rate at the outlet of the MT evaporators (EJ_{MT} in the figure) and one designed to provide, on the contrary, a lower pressure lift and a higher entrainment ratio to the refrigerant mass flow rate used to provide air conditioning cooling, when required (EJ_{AC} in the figure). Only the first of the two ejector racks (EJ_{MT}) has been considered for the experimental tests, while the EJ_{AC} ejector rack has been excluded from the tested unit schematic.

The EJ_{MT} rack is a Multi Ejector CTM Combi HP 1875 LE 600 from Danfoss and it is composed by four vapor ejector cartridges (with increasing capacity) and two liquid ejector cartridges (with increasing capacity) in parallel. Through the combined use of the different cartridges, the ejector rack is capable to provide the required pressure lift to a refrigerant mass flow rate corresponding to the cooling needs of a supermarket (up to 70 kW of MT refrigeration and up to 20 kW of LT refrigeration, approximately).

However, the cooling unit concept presented in Figure 6.1 is intended to be used for limited load requirements (4-5 kW of MT load and 1-2 kW of LT load) compared with the total Multi Ejector capacity. For this reason, the experimental campaign was conducted engaging only the smallest cartridge of the Multi Ejector pack (VEJ1), whose geometrical characteristics are reported in Table 6.1. Further information about the Multi Ejector can be found in [102], while the complete description of the VEJ1 ejector and the empirical correlations describing its characteristics when employed in standard MT suction operation are reported in [108].

Table 6.1 – Main geometrical parameters of the VEJ1 ejector cartridge considered for the experimental tests.

Parameter	Geometry
Motive nozzle inlet diameter	$3.80 \cdot 10^{-3}$ m
Motive nozzle throat diameter	$1.00 \cdot 10^{-3}$ m
Motive nozzle outlet diameter	$1.12 \cdot 10^{-3}$ m
Motive nozzle converging angle	30°
Motive nozzle diverging angle	2°
Diffuser outlet diameter	$7.30 \cdot 10^{-3}$ m
Diffuser angle	5°

Referring to the system schematic reported in Figure 6.2, after the compression, the refrigerant rejects heat to three gas coolers (plate heat exchangers), working in series at different temperature levels against glycol, cooling water and CO_2 coming from an auxiliary system, respectively. The individual gas coolers can be partially or completely bypassed depending on the desired temperature at the outlet of the gas cooler section. The pressure and temperature conditions at the outlet of the gas cooler correspond to the refrigerant conditions at the motive nozzle of the ejector.

The fluid at the desired gas cooler outlet conditions is sent to the parallel between the ejector and the High-Pressure Valve (HPV). The amount of refrigerant mass flow rate which can be processed by the VEJ1

ejector cartridge is limited by the cartridge specific geometry. As mentioned above, the choice of the single VEJ1 cartridge to be experimentally tested is consistent with the resolution of designing a transport refrigeration unit with rated capacity based on the needs of a small refrigerated van (4-5 kW of MT load and 1-2 kW of LT load), which is significantly lower than the full load capacity for which the SuperSmart-Rack experimental unit was originally designed (up to 70 kW of MT load and 20 kW of LT load). The refrigerant mass flow rate which can be elaborated by the VEJ1 is therefore sent to the ejector motive nozzle, while the exceeding mass flow rate is expanded in the HPV, granting at the same time the needed high-pressure control.

The R744 mix at the outlet of the HPV and at the ejector discharge nozzle is sent to the liquid receiver, whose pressure represents the ejector discharge nozzle pressure and it is controlled through the parallel compressors capacity (or through the Flash Gas Valve FGV) and from which the liquid refrigerant is expanded and sent to the evaporators (helical coaxial tube-in-tube heat exchangers).

The control of the MT evaporation pressure is achieved adjusting the MT compressor capacity, while the evaporators feeding valves operate to guarantee a desired superheat (in the range of 8 – 10 K) at the evaporators outlet. The pressure and temperature conditions at the outlet of the MT evaporators correspond to the refrigerant conditions at the suction nozzle of the ejector. The difference between MT evaporation pressure and liquid receiver pressure levels represents the pressure lift provided by the ejector. As described above, due to the large rated capacity of the SuperSmart-Rack unit, only part of the mass flow rate at the evaporators outlet will be entrained by the VEJ1 ejector cartridge, while the exceeding mass flow rate will be elaborated by the MT compressors.

It can be observed that the refrigeration system schematic employed for the experimental campaign (Figure 6.2) is completely different from the concept schematic of the multi-temperature unit presented Figure 6.1. This is due to the completely different design purpose of the SuperSmart-Rack system (intended to simulate the needs of a complete stationary commercial refrigeration application) compared with the design purpose of the cooling unit concept presented in this chapter (to be employed in small refrigerated vehicles). Therefore, the direct implementation of the schematic reported in Figure 6.1 was not feasible in the SuperSmart-Rack test facility. However, the only objective of the experimental campaign was the evaluation of the performance of the VEJ1 ejector cartridge under specific operating conditions. The SuperSmart-Rack operational schematic used for the experimental campaign was therefore only functional with the achievement of the desired conditions at the ejector cartridge motive, suction and discharge nozzles and not to reproduce the entire refrigeration system schematic illustrated in Figure 6.1.

6.3 Data acquisition

The data acquisition system of the SuperSmart-Rack experimental setup consists of a hybrid combination of Danfoss controllers with industrial quality sensors (characterized by a sampling rate of 5 s) and of National Instruments hardware (LabVIEW programming) with high-precision sensors (characterized by a sampling rate of 1 s), whose recorded data are then synchronized for data post-processing.

The data acquired by the Danfoss industrial sensors are necessary for the complete monitoring of the whole refrigerating system and for the control of the operating conditions, in order to reach and maintain steady-state operation. However, the data analysis related to the evaluation of the ejector performance during the experimental campaign was based only on the high-quality data acquired by the LabVIEW sensors.

The whole refrigerating system is entirely equipped with sensors of various nature: temperature sensors, pressure transducers, differential pressure transducers, mass flow meters, volumetric flow meters, active power meters. However, since the experimental campaign was focused exclusively on the evaluation of the ejector performance, only the sensors monitoring the ejector motive nozzle conditions (pressure, temperature, mass flow rate), the suction nozzle conditions (pressure, temperature, mass flow rate), the pressure lift (differential pressure) and the discharge nozzle conditions (pressure) are considered for data analysis. The list of the considered sensors and their accuracy are reported in Table 6.2.

Table 6.2 – List of the data acquisition equipment and respective accuracy, used for the experimental campaign.

Type	Manufacturer and model	Placement	Accuracy
Mass flow meters	Rheonik RHM	motive nozzle, suction nozzle	±0.2 % of reading
Pressure transducers	Endress+Hauser PMP21	motive nozzle, suction nozzle, discharge nozzle	±0.3 % of set span
Differential pressure transducers	Endress+Hauser PMD75	discharge nozzle – suction nozzle	±0.035 % of set span
Temperature sensors	Pt 100 Class B DIN 1/3 on tube	motive nozzle, suction nozzle	±1/3(0.3 K + 0.005*temp(°C))

6.4 Test conditions

The objective of the experimental campaign was to verify the feasibility of operating the ejector at relatively low suction nozzle pressures and the consequent operating constraints and limiting parameters.

To this extent, several different combinations of motive nozzle conditions, suction nozzle conditions and pressure lift requirements were tested, to provide a complete performance mapping of the ejector under

different operating conditions. The test conditions selected for the experimental campaign are listed in Table 6.3.

Table 6.3 – List of the ejector test conditions of the experimental campaign.

Parameter	Test conditions
Motive nozzle conditions	• T_{motive} = 35°C, p_{motive} = 90 bar; • T_{motive} = 25°C, p_{motive} = 66 bar; • T_{motive} = 15°C, p_{motive} = 54 bar.
Suction nozzle conditions	• $p_{suction}$ = 16.8 bar (T_{sat} = -25°C); • $p_{suction}$ = 19.7 bar (T_{sat} = -20°C); • $p_{suction}$ = 22.9 bar (T_{sat} = -15°C); • $p_{suction}$ = 26.5 bar (T_{sat} = -10°C); • $p_{suction}$ = 30.5 bar (T_{sat} = -5°C); • SH = 8 – 10 K.
Pressure lift	• Minimum: $\Delta p_{lift,min}$ = 2 bar (for T_{motive} = 15°C-25°C) $\Delta p_{lift,min}$ = 3 bar (for T_{motive} = 35°C) • Maximum: $\Delta p_{lift,max}$ = maximum achievable lift; • Step: $\Delta p_{lift,step}$ = 1 bar.

Three different motive nozzle conditions were considered, to evaluate the performance of the ejector when operating under both hot environmental conditions and mild environmental conditions, therefore assessing the effects of the reduction of the motive nozzle energy on the ejector operation.

For each of the described motive nozzle conditions, five different suction nozzle conditions were tested, ranging from usual LT suction conditions (corresponding to a saturation temperature of T_{sat} = -25°C, thus ensuring the supply of the necessary cooling effect to maintain the internal air conditions at -20°C) to usual MT suction conditions (corresponding to a saturation temperature of T_{sat} = -5°C). This choice was made in order to assess the ejector performance in the desired low temperature suction conditions described in Section 6.1 (therefore determining the feasibility of the refrigeration system concept presented in Figure 6.1) but also in operating points which could be experienced during dynamic transitions from higher suction pressures to the nominal LT suction conditions (i.e. during the pulldown at the refrigeration system start or during ON/OFF operation of the unit).

Finally, for each of the combinations of motive and suction nozzle conditions, different pressure lift requirements (enforced through the control of the discharge nozzle pressure) were tested, with a pressure step of 1 bar, starting from the minimum achievable pressure lift up to the maximum achievable pressure lift, where the ejector is not able to entrain any mass flow rate at the suction nozzle due to an excessive pressure lift requirement.

6.5 Experimental results

The performance of an ejector is determined by the primary stream mass flow rate at the motive nozzle ($\dot{m}_{motive}$) and by the secondary stream mass flow rate at the suction nozzle ($\dot{m}_{suction}$) or, alternatively, by the ejector mass entrainment ratio, as previously defined in Eq. (3.5) and here reported in Eq. (6.1).

Moreover, the ejector efficiency represents its ability to recover expansion work with respect to the maximum possible expansion work rate recovery potential, following the definition given by Elbel and Hrnjak [110] previously described in Eq. (3.15) and here reported in Eq. (6.2).

$$\phi = \frac{\dot{m}_{suction}}{\dot{m}_{motive}} \tag{6.1}$$

$$\eta_{ej} = \phi \frac{h_{is}(p_{discharge}, s_{suction}) - h_{suction}}{h_{motivge} - h_{is}(p_{discharge}, s_{motive})} \tag{6.2}$$

As reported by [108], the motive nozzle mass flow rate is independent from both the suction pressure and the pressure lift, due to the supersonic flow conditions which characterize the motive nozzle outlet. For this reason, the motive nozzle experimental points, achieved according to the test matrix described in Table 6.3, are presented only as a function of the motive inlet conditions (pressure and temperature) in Figure 6.3, which also reports the mass flow rate at the ejector motive nozzle.

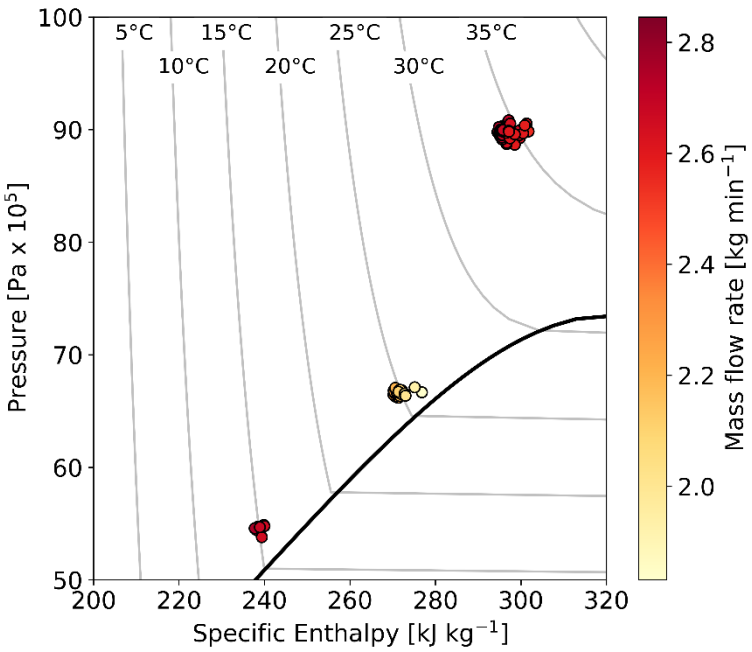

Figure 6.3 – Motive nozzle inlet conditions and mass flow rate.

The average motive nozzle conditions (temperature and pressure) achieved during the experimental tests are reported in Table 6.4 with the respective standard deviations. It can be observed that the three desired motive nozzle conditions are accurately achieved during the experimental campaign.

Table 6.4 – Average experimental motive nozzle temperature and pressure.

Desired conditions	Average experimental data	Standard deviation
T_{motive} = 35°C p_{motive} = 90 bar	$\bar{T}_{motive}$ = 34.53°C $\bar{p}_{motive}$ = 89.70 bar	σ_T = 0.35°C σ_p = 0.46 bar
T_{motive} = 25°C p_{motive} = 66 bar	$\bar{T}_{motive}$ = 24.92°C $\bar{p}_{motive}$ = 66.66 bar	σ_T = 0.26°C σ_p = 0.24 bar
T_{motive} = 15°C p_{motive} = 54 bar	$\bar{T}_{motive}$ = 15.05°C $\bar{p}_{motive}$ = 54.52 bar	σ_T = 0.22°C σ_p = 0.30 bar

The average motive mass flow rates are reported in Table 6.5 with the respective standard deviation. It can be observed that, for a specific gas cooler outlet condition, the experimental points present very limited variations of the mass flow rate, confirming that neither suction pressure nor pressure lift can influence the motive nozzle mass flow rate, as mentioned above.

Table 6.5 – Average experimental motive nozzle mass flow rate.

Motive nozzle conditions	Average experimental motive mass flow rate	Standard deviation
T_{motive} = 35°C p_{motive} = 90 bar	$\bar{\dot{m}}_{motive}$ = 2.688 kg min^{-1}	σ_m = 0.063 kg min^{-1}
T_{motive} = 25°C p_{motive} = 66 bar	$\bar{\dot{m}}_{motive}$ = 2.173 kg min^{-1}	σ_m = 0.111 kg min^{-1}
T_{motive} = 15°C p_{motive} = 54 bar	$\bar{\dot{m}}_{motive}$ = 2.736 kg min^{-1}	σ_m = 0.056 kg min^{-1}

Differently from the ejector motive mass flow rate, the suction nozzle mass flow rate is a function of more than two independent parameters, since it is strongly dependent on the expansion energy provided by the motive mass flow rate, on the suction nozzle inlet conditions and on the discharge pressure level (directly linked to the pressure lift requirement to be provided by the ejector).

However, as it was reported in Table 6.3, the superheat at the ejector suction nozzle was always maintained by the evaporators feeding valves in the range of 8 - 10 K. According to Banasiak et al. [108], within a limited range (from 0 K to 10 K) the influence of superheating at the suction nozzle on the ejector performance is barely measurable and, since all of the experimental points fall under these conditions, the effect of superheating at the suction nozzle on the ejector performance will not be considered in the analysis of the experimental results. The only suction nozzle parameter which will be considered as a significant influence on the ejector operation is therefore the suction nozzle pressure.

Following these considerations, the ejector mass entrainment ratio and the ejector efficiency are therefore presented in Figure 6.4, Figure 6.5 and Figure 6.6 as a function of the motive nozzle conditions (pressure and temperature, grouped within the three desired motive conditions), of the suction pressure and of the required pressure lift.

As it can be observed from Figure 6.4, for T_{motive} = 35°C and p_{motive} = 90 bar, the experimental results show a wide range of possible operating points for the ejector. Firstly, it can be observed that the ejector is able to entrain mass flow rate even from the lowest suction pressure condition, corresponding to a saturation temperature of T_{sat} = -25°C. This means that, in case of operation following the schematic of the unit concept presented in Figure 6.1, the ejector can allow maintaining an LT evaporation at a pressure level low enough to grant the preservation of the desired temperature of the air inside the LT truck compartment ($T_{i,LT}$ = -20°C). Operation in transient conditions, i.e. at the system start or during a pulldown, is ensured as well by the results at other suction pressure conditions.

The ejector mass entrainment ratio decreases as the pressure lift requirement increases, with the exception of the experimental points at $p_{suction}$ = 16.8 bar and $p_{suction}$ = 19.7 bar, which present a slight increase for low pressure lifts and, after reaching a maximum, start decreasing for high pressure lift requirements. On the contrary, the ejector efficiency shows a clear parabolic trend for each of the suction pressure conditions.

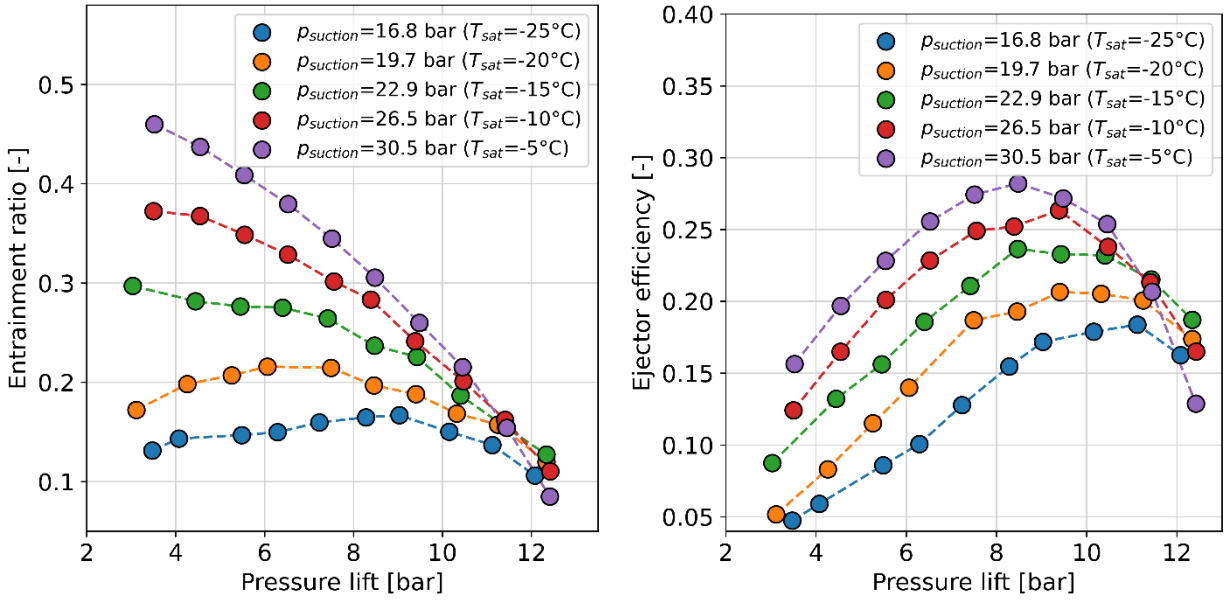

Figure 6.4 – Performance of the ejector with motive nozzle conditions equal to T_{motive} = 35°C and p_{motive} = 90 bar: (a) ejector entrainment ratio; (b) ejector efficiency.

Figure 6.5 presents the entrainment ratio and the ejector efficiency for T_{motive} = 25°C and p_{motive} = 66 bar. It can be observed that the reduced expansion energy available at the ejector motive nozzle, due to the lower values of both temperature and pressure of the motive refrigerant flow, is reflected in a reduction of the maximum achievable pressure lift. However, the trend for both the entrainment ratio and the efficiency are the same compared with the trend obtained for T_{motive} = 35°C and p_{motive} = 90 bar, where in this case also the points at $p_{suction}$ = 16.8 bar and $p_{suction}$ = 19.7 bar present an almost monotonic decrease in the entrainment ratio with increasing lift requirements.

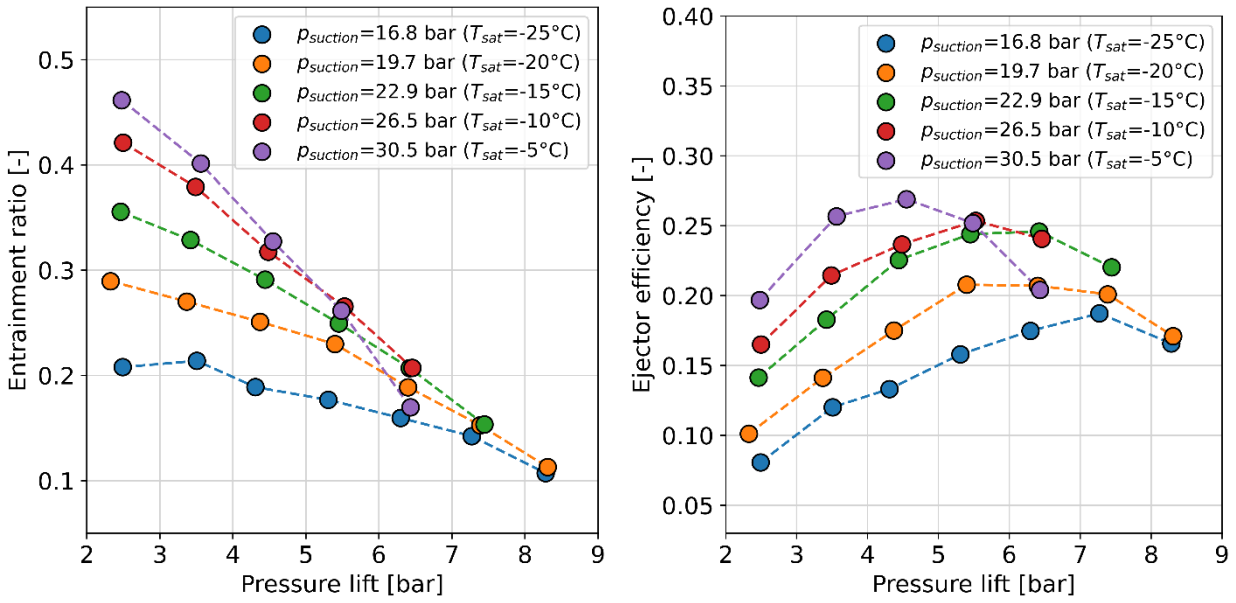

Figure 6.5 – Performance of the ejector with motive nozzle conditions equal to T_{motive} = 25°C and p_{motive} = 66 bar: (a) ejector entrainment ratio; (b) ejector efficiency.

Figure 6.6 reports the ejector performance for T_{motive} = 15°C and p_{motive} = 54 bar. In such conditions, the available expansion energy at the motive nozzle is so low that the ejector is not able to entrain mass flow rate from a suction pressure of $p_{suction}$ = 16.8 bar. In case of low ambient temperature conditions, therefore, the desired temperature of the air inside the LT truck compartment ($T_{i,LT}$ = -20°C) can not be achieved employing the ejector cartridge considered in this experimental campaign. Moreover, even for higher suction pressure conditions, the maximum pressure lift that can be provided by the ejector is very limited and never exceeds a value of approximately 4.5 bar.

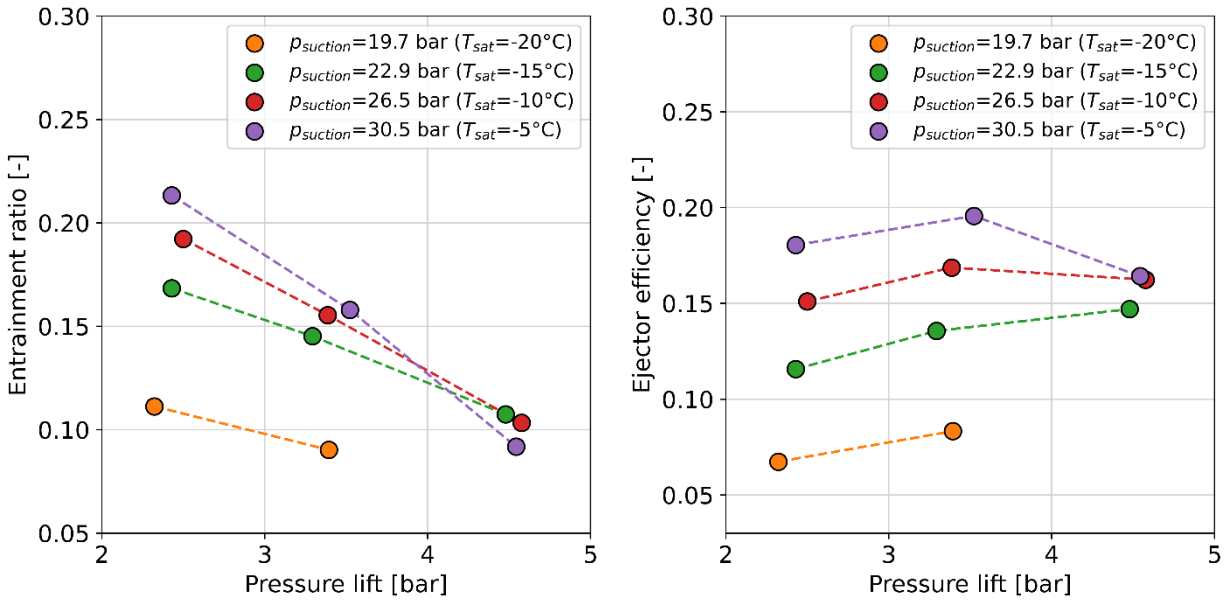

Figure 6.6 – Performance of the ejector with motive nozzle conditions equal to T_{motive} = 15°C and p_{motive} = 54 bar: (a) ejector entrainment ratio; (b) ejector efficiency.

A few interesting considerations on the ejector performance can be made from the observation of the experimental results in their entirety.

Firstly, as it can be expected in normal operating conditions of the ejector, the general behavior is that the performance is higher, both in terms of entrainment ratio and efficiency, for higher suction pressure conditions. However, it can be observed consistently between each of the three motive conditions experimentally tested that, for high values of pressure lift requirement, close to the maximum achievable lift, the general trend can be not respected, and the higher suction pressure experimental points can present performance parameters which are comparable and, in some cases, worse than lower suction pressure points. The experimental results highlight, in fact, a significant degradation of the ejector performance of higher suction pressure points towards the maximum achievable pressure lifts.

In addition, even the maximum achievable lift value that can be handled by the ejector is influenced by the suction pressure. As it can be clearly observed in Figure 6.5, the maximum lift of the experimental points at $p_{suction}$ = 16.8 bar and $p_{suction}$ = 19.7 bar presents a value of Δp_{lift} ≈ 8.5 bar, for the points at $p_{suction}$ = 22.9 bar the maximum lift is equal to Δp_{lift} ≈ 7.5 bar and for the points at $p_{suction}$ = 26.5 bar and $p_{suction}$ = 30.5 bar the maximum achievable lift is reduced to Δp_{lift} ≈ 6.5 bar. The physical properties of the R744 refrigerant at the suction nozzle (i.e. the refrigerant density, linked to the suction pressure value) show therefore a significant effect on the fluid mechanics inside the ejector, thus influencing its performance, even with fixed motive nozzle energy.

In conclusion, the results of the experimental campaign clearly show the importance of a careful choice of the design ejector operating point, since its performance is significantly dependent on the pressure lift

requirement, given fixed motive nozzle and suction nozzle conditions (which will be indirectly determined according to the temperature values of the environment and of the air inside the refrigerated box, respectively).

However, it must be pointed out that the specific ejector considered in this experimental campaign (the VEJ1 cartridge of the Multi Ejector CTM Combi HP 1875 LE 600 from Danfoss) was originally designed and optimized for very different operating conditions than the ones considered in the application described in this chapter. In fact, the Multi Ejector was originally designed to operate with suction pressure corresponding to a saturation temperature not lower than T_{sat} = -12°C, as it can be observed from Figure 6.2 that the EJ_{MT} suction nozzle corresponds to the outlet of the MT evaporators, which are intended to never operate at saturation temperatures lower than the above-mentioned one.

Therefore, the results of the experimental campaign presented in this chapter, which was conducted on a non-optimized ejector at suction pressures corresponding to LT saturation temperatures, highlight that an even better performance could be reached with a specific ejector design matching the needs of the proposed application.

6.6 Conclusions

This chapter presented the preliminary design of a novel R744 cooling unit to be employed for multi-temperature (0°C and -20°C) refrigerated transport applications. The novelty of the presented schematic concept lies in the use of an ejector as the only component to increase the refrigerant pressure from the LT evaporation pressure to the MT evaporation pressure, thus allowing the removal of a dedicated subcritical compressor, usually necessary in traditional R744 multi-temperature unit configurations, and enabling operation with the use of only one compressor.

To verify the feasibility of this cooling unit concept, the ability of a commercially available R744 ejector to entrain mass flow rate from LT suction conditions (with a suction pressure corresponding to a saturation temperature down to -25°C) was experimentally evaluated, since R744 ejectors are currently designed, optimized and available in the market for the operation at MT suction conditions (with a suction pressure corresponding to a saturation temperature down to -12°C)

The main results obtained in this chapter can be summarized as follows:

- An experimental campaign on the performance of the VEJ1 cartridge of the Multi Ejector CTM Combi HP 1875 LE 600, manufactured by Danfoss, has been carried out at the SuperSmart-Rack experimental facility, located in the NTNU/SINTEF laboratories at NTNU, Trondheim.
- The ejector performance has been experimentally testes under several different operating conditions, ranging from the design LT suction conditions (with a suction pressure corresponding

to a saturation temperature of -25°C) to MT suction conditions (with a suction pressure corresponding to a saturation temperature of -5°C), to assess the performance also in conditions which could occur during pulldown or transitory operation. Three motive nozzle conditions (35°C, 25°C and 15°C) have been considered, to represent operation under different climatic conditions. Several different pressure lift requirements have been tested, to determine the optimal ejector operating conditions, given fixed ambient and internal temperatures.

- The experimental results highlight that for a specific gas cooler outlet condition, the motive nozzle mass flow rate presents very limited variations, as neither the suction pressure condition nor the pressure lift requirement can influence the motive nozzle mass flow rate;
- The results show that, globally, the ejector mass entrainment ratio decreases as the pressure lift requirement increases. On the contrary, the ejector efficiency shows a clear parabolic trend as a function of the pressure lift.
- A reduced expansion energy available at the ejector motive nozzle, due to the lower values of both temperature and pressure of the motive refrigerant flow, is reflected in a reduction of the maximum achievable pressure lift.
- The general ejector behavior is that the performance is higher, both in terms of entrainment ratio and efficiency, for higher suction pressure conditions. However, the experimental results highlight that, for high values of pressure lift requirement, close to the maximum achievable lift, the general trend can be not respected, and the higher suction pressure experimental points can present performance parameters which are comparable and, in some cases, worse than lower suction pressure points. A significant degradation of the ejector performance of higher suction pressure points towards the maximum achievable pressure lifts is experienced.
- The maximum achievable lift value that can be handled by the ejector is influenced by the suction pressure, as for higher suction pressures the maximum achievable lift can be lower than for lower suction pressures. The physical properties of the R744 refrigerant at the suction nozzle show therefore a significant effect on the fluid mechanics inside the ejector, thus influencing its performance, even with fixed motive nozzle energy.
- In conclusion, the experimental results demonstrate the ability of the tested ejector to entrain mass flow rate in a wide range of operating points, including LT suction nozzle conditions, under different climatic conditions. However, the results highlight the crucial importance of the choice of the ejector operating point, as the pressure lift requirement has a significant influence on both the ejector entrainment ratio and efficiency.

The application of the experimental results of the ejector performance will be used in the following chapter for a preliminary numerical evaluation of the performance of the multi-temperature refrigeration unit concept presented in Figure 6.1.

7 Design of a R744 single-compression cooling unit for multi-temperature refrigerated transport applications

The experimental campaign described in Chapter 6 and carried out to evaluate the performance of a commercially available ejector in low-temperature suction conditions highlighted the feasibility of a single-compression multi-temperature cooling unit employing the ejector as the only component dedicated to the pressure increase from the LT evaporation pressure to the MT evaporation pressure, thus allowing the removal of the traditionally employed additional subcritical compressor.

In this chapter, the experimental results presented in Chapter 6 will be used to size and evaluate the performance of the cooling unit operating according to the preliminary concept schematic presented in Chapter 6.

Following this preliminary performance evaluation, the operational issues linked to the presented layout will be highlighted, and an improved schematic based on the presence of two separate ejectors (a MT ejector and a LT ejector) will be discussed.

Finally, the design operating conditions and the desired performance of the MT ejector and of the LT ejector will be numerically evaluated, to assess the nominal performance for which the ejectors geometry will be designed and optimized, with the objective of manufacturing the MT ejector and LT ejector prototypes to be experimentally tested in the future.

7.1 Preliminary performance evaluation of the R744 multi-temperature unit concept

Following the experimental evaluation of the performance of a commercially available ejector (VEJ1 of the Multi Ejector CTM Combi HP 1875 LE 600 from Danfoss) during operation in low-pressure suction conditions described in Chapter 6, a preliminary thermodynamical evaluation of the performance of the cooling unit concept presented in Section 6.1 is carried out, to assess the system COP and the cooling effect production in specific operating conditions. For the sake of convenience, the schematic of the refrigeration system concept is reported here in Figure 7.1.

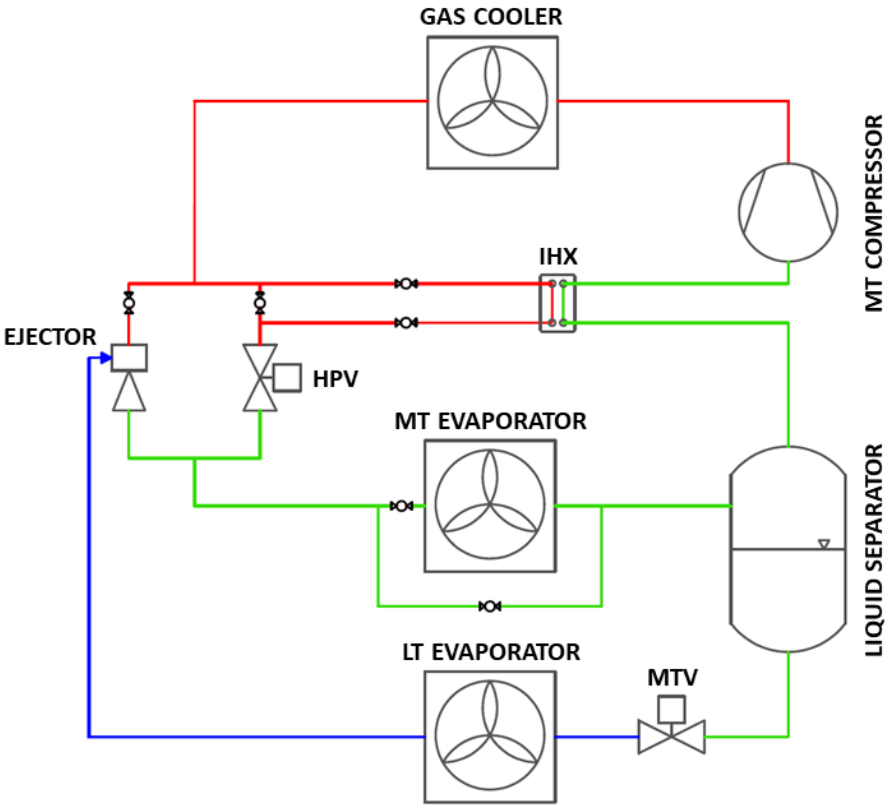

Figure 7.1 – Schematic of the refrigeration unit concept.

The ejector experimental data measured in the experimental campaign with motive nozzle conditions equal to T_{motive} = 35°C and p_{motive} = 90 bar are used for the assessment of the refrigeration system cooling effect production and for the evaluation of the system energy consumption under warm ambient conditions. The numerical evaluation of the cooling unit performance is carried out considering the design suction nozzle conditions in which the system is assumed to operate, i.e. with suction pressure equal to $p_{suction}$ = 16.8 bar, corresponding to a saturation temperature at the suction nozzle equal to T_{sat} = -25°C. All the possible pressure lifts obtained during the experimental tests with the above-mentioned motive nozzle and suction nozzle conditions are considered, to assess the influence of the operating point of the ejector on the overall performance of the complete cooling unit.

The experimental data considered for the numerical preliminary evaluation are reported in Table 7.1.

Table 7.1 – Ejector experimental data used for the numerical preliminary evaluation of the cooling unit performance.

T_{motive} [°C]	p_{motive} [bar]	$p_{suction}$ [bar]	$SH_{suction}$ [K]	Δp_{lift} [bar]	$\dot{m}_{motive}$ [kg min^{-1}]	$\dot{m}_{suction}$ [kg min^{-1}]	ϕ [-]	η_{ej} [-]
34.29	89.91	17.01	4.04	3.48	2.818	0.370	0.131	0.047
34.63	88.87	17.23	2.71	4.08	2.713	0.389	0.143	0.059
34.63	89.96	17.08	4.46	5.49	2.770	0.407	0.147	0.086
34.68	89.28	17.04	3.57	6.29	2.703	0.405	0.150	0.101
34.73	89.29	17.07	5.76	7.23	2.673	0.427	0.160	0.128
34.84	89.29	17.04	6.82	8.28	2.646	0.436	0.165	0.155
34.94	89.25	17.22	6.58	9.03	2.625	0.438	0.167	0.172
35.08	89.91	17.18	7.77	10.15	2.669	0.401	0.150	0.179
34.97	89.49	17.22	8.53	11.12	2.631	0.360	0.137	0.184
34.59	88.65	17.15	10.05	12.08	2.591	0.275	0.106	0.163

Considering the experimental values of pressure, temperature and mass flow rate reported in Table 7.1, the other points of the thermodynamic cycle of the unit presented in Figure 7.1 are defined according to the following assumptions:

- the cooling unit compressor is equipped with an inverter which can adjust the compressor speed in order to deliver to the high-pressure side of the system exactly the refrigerant mass flow rate measured at the ejector motive nozzle during the experimental tests ($\dot{m}_{comp} = \dot{m}_{motive}$). As a consequence, no excess mass flow rate is expanded in the HPV ($\dot{m}_{HPV}$ = 0);
- the conditions at the outlet of the liquid separator are assumed to be saturated vapor (sent to the compressor) and saturated liquid (sent to the expansion valve, which performs an isenthalpic expansion to the LT evaporation pressure);
- the compressor isentropic efficiency, required to evaluate the thermodynamic point after the compression and, consequently, the power draw of the compressor, is evaluated as a function of the compressor pressure ratio from the database of the manufacturer catalogue [104].

The MT cooling effect and the LT cooling effect obtained from the thermodynamic solution of the system operation with motive nozzle conditions equal to T_{motive} = 35°C and p_{motive} = 90 bar and suction nozzle conditions equal to $p_{suction}$ = 16.8 bar are reported in Figure 7.2 and in Table 7.2 as a function of the experimental pressure lift, as well as the system COP, defined as:

$$COP = \frac{Q_{MT\ evap} + Q_{LT\ evap}}{P_{comp}} \tag{7.1}$$

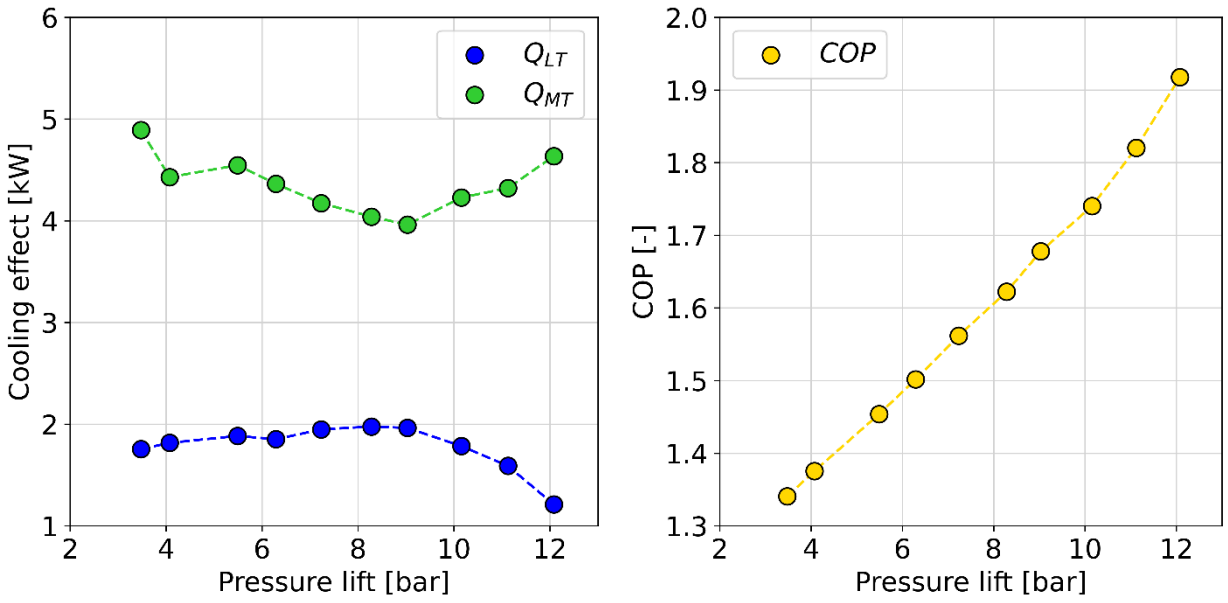

Figure 7.2 – Performance of the refrigeration unit concept with motive conditions equal to T_{motive} = 35°C and p_{motive} = 90 bar and suction conditions equal to $p_{suction}$ = 16.8 bar: (a) MT cooling effect and LT cooling effect; (b) unit COP.

Table 7.2 – Cooling effect production and COP of the cooling unit with motive conditions equal to T_{motive} = 35°C and p_{motive} = 90 bar and suction conditions equal to $p_{suction}$ = 16.8 bar.

Δp_{lift} [bar]	$Q_{MT\ evap}$ [kW]	$Q_{LT\ evap}$ [kW]	P_{comp} [kW]	COP [-]	Notes
3.48	4.89	1.76	4.96	1.34	Max $Q_{MT\ evap}$
4.08	4.43	1.82	4.54	1.38	
5.49	4.55	1.88	4.42	1.45	
6.29	4.36	1.85	4.14	1.50	
7.23	4.17	1.95	3.92	1.56	
8.28	4.04	1.98	3.71	1.62	Max $Q_{LT\ evap}$
9.03	3.96	1.96	3.53	1.68	
10.15	4.23	1.78	3.46	1.74	
11.12	4.32	1.59	3.25	1.82	
12.08	4.64	1.21	3.05	1.92	Max COP

Based on the ejector experimental data, during operation with motive nozzle conditions equal to T_{motive} = 35°C and p_{motive} = 90 bar and suction nozzle conditions equal to $p_{suction}$ = 16.8 bar the system is able to provide up to 4.89 kW of MT cooling and up to 1.98 kW of LT cooling, depending on the ejector lift requirement. The MT and LT cooling effect production matches with the usual cooling effect requirement expected for medium-size refrigerated vans (4-5 kW of MT cooling effect and 1-2 kW of LT cooling effect).

From the numerical results of the preliminary cooling unit evaluation, it can be observed that the overall system COP is maximized (reaching a value of 1.92) at the maximum available lift provided by the ejector, as higher pressure lifts lead to an increased pressure of the liquid receiver (since the LT evaporation

pressure is fixed for these calculations) and, consequently, to a reduced power draw in the compression section to bring the refrigerant from the receiver pressure level to the gas cooler high-pressure value.

However, as emerged from the experimental data of the ejector, the maximum pressure lift achievable by the ejector does not correspond to the best ejector performance, in terms of entrainment ratio and ejector efficiency, as these performance parameters are significantly degraded at the maximum lift operating point. As a consequence, the LT cooling effect production is significantly reduced from the maximum $Q_{LT\ evap}$ operating point to the maximum system COP operating point.

The reduction between the maximum and the minimum $Q_{LT\ evap}$ production is significant (-38.9%) over the range of the ejector operating points, while the variation between maximum and minimum $Q_{MT\ evap}$ production is lower (-19.0%). It has also to be noticed that the MT cooling effect could be increased without affecting the LT cooling effect production with the selection of an adequate compressor, able to deliver to the high-pressure side (and therefore, through the HPV, to the MT evaporator) more mass flow rate than the one elaborated by the ejector motive nozzle, giving to the refrigeration system more flexibility in the MT cooling effect production.

In conclusion, the system design point (i.e. the pressure lift requirement to be provided by the ejector and the compressor size and rotational speed) has to be carefully chosen according to the ejector performance, to the system thermodynamic COP and to the expected MT and LT refrigeration needs for the specific application, in order to obtain the best trade-off between cooling effect production and overall system performance.

7.2 Design of a single compression R744 multi-temperature unit with MT and LT ejectors

While the simple cooling unit schematic presented in Figure 7.1 is useful for a preliminary evaluation of the performance and of the cooling effect ranges of a R744 multi-temperature refrigeration system with only one stage of compression, as presented in Section 7.1, such a schematic leads to some operational issues which have to be faced in the design phase of an actual refrigeration system which could still exploit the presence of an ejector to remove the subcritical compressor in a multi-temperature system, but at the same time guarantee operation in a wide range of conditions in road transport refrigeration applications.

In current transport refrigeration sector, for small and medium size refrigerated vehicles used for multi-temperature deliveries, it is common practice to exploit compact cooling units with traditional HFC refrigerants and a single stage of compression, with the simplified schematic presented in Figure 7.3. These cooling units operate with a single evaporation pressure and two evaporators in parallel (one placed in the MT compartment and the other placed in the LT compartment of the insulated box).

The common practice consists in operating the cooling unit setting an MT evaporation pressure (corresponding to a saturation temperature ranging from -5°C to -10°C, depending on the specific application) for most of the time, bypassing the evaporator placed in the LT compartment (Figure 7.3a). This is done since the LT compartment presents a higher degree of insulation (as it is built with specific materials which lead to a lower global heat transfer coefficient) and it is usually subject to less openings during a delivery mission compared to the MT compartment, due to the specific type of products which have be stored and transported in frozen conditions. Consequently, less infiltrations of external air are present in the LT compartment, and the desired temperature range can be maintained for a longer time without providing a cooling effect.

Once the maximum allowed temperature in the LT compartment is reached, the single evaporation pressure of the cooling unit is lowered to LT evaporation pressure conditions (corresponding to a saturation temperature of around -25°C), and both the evaporator placed in the MT compartment and the evaporator placed in the LT compartment operate simultaneously at the same evaporation pressure (Figure 7.3b) until the minimum allowed temperature in the LT compartment is reached, the evaporator in the LT compartment is bypassed again and the evaporation pressure is increased to MT conditions. In case the MT compartment temperature reaches its minimum allowed value during MT+LT operation, or I case of LT-only cooling effect requirement, the MT evaporator can be bypassed.

The above-mentioned control of multi-temperature units for transport refrigeration follows the test procedure defined in Annex 1 of the ATP agreement [82], which requires the determination of the nominal refrigerating capacity of the cooling unit with both evaporators operating simultaneously at the same temperature (-20°C and 0°C, in two separate mono-temperature tests), and the determination of the capacity in multi-temperature operation with the LT evaporator tested at -20°C and the MT evaporator operating under control of a thermostat set at 0°C with a determined heat load. The datasheets of transport refrigeration units available in the market [115] [116] provide in fact the capacity of the unit working at 0°C and -20°C, following the procedure prescribed by the ATP agreement.

Therefore, the cooling unit must be designed to allow operation with a single evaporation temperature, which is set according to the requirement of MT cooling effect or LT cooling effect.

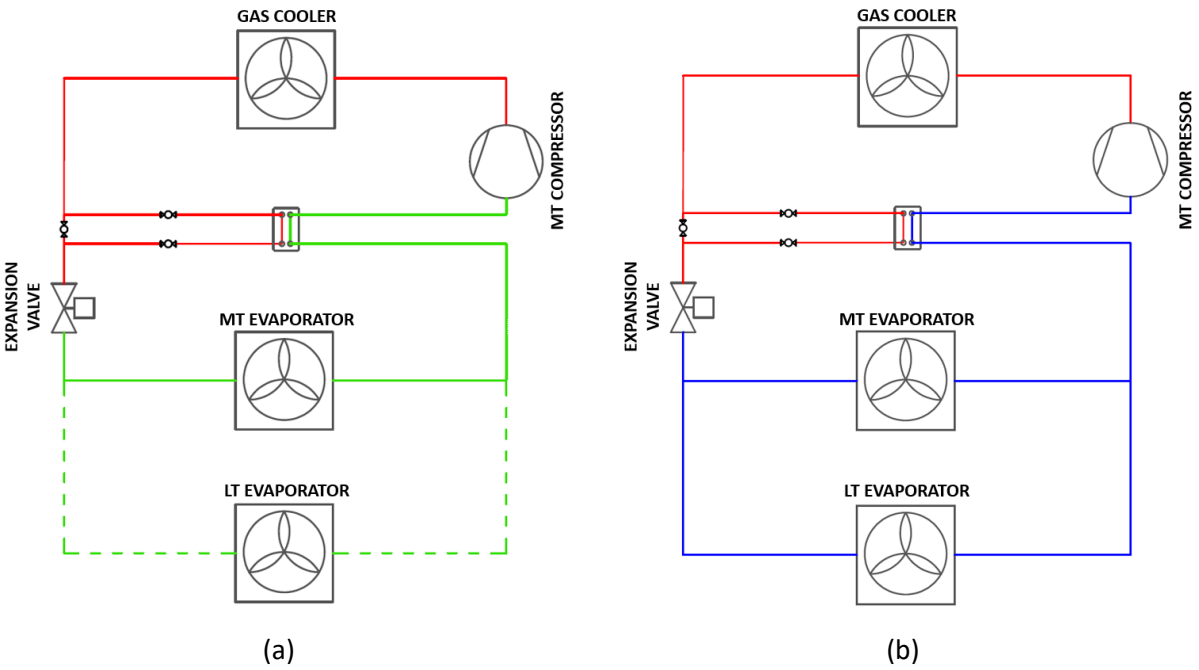

Figure 7.3 – Simplified schematic of HFC cooling units with single compression currently used in multi-temperature transport in small and medium vehicles: (a) MT operation; (b) MT+LT operation. Dashed lines and components are not in use.

The simplified schematic of the HFC multi-temperature units currently used in the market presented in Figure 7.3 helps highlighting some operational limits which characterize the R744 multi-temperature unit concept schematic presented in Figure 7.1. In particular:

- Considering the above-described common practice to operate the cooling unit to provide only MT refrigeration for most of the delivery mission time, due to the better insulation and to the lower heat infiltration inside the LT compartment, the concept schematic presented in Figure 7.1, if operating in MT-only cooling production, is reduced to a simple back-pressure cycle. As extensively described in Chapter 3, the simple back-pressure cycle COP can be significantly improved with the insertion of a MT ejector, and it does not represent the optimized system schematic to operate for a vast amount of delivery mission time in MT-only cooling production.
- On the other side, the ability of the ejector included in the schematic presented in Figure 7.1 to provide an entrainment of mass flow rate from the outlet of the LT evaporator to the MT evaporation pressure is strictly dependent on the motive mass flow rate and on the motive pressure and temperature conditions, as pointed out by the experimental results presented in section 6.5. As a consequence, to guarantee the supply of the desired LT cooling effect, the compressor needs to elaborate the required motive mass flow rate whether the MT cooling effect is required or not. In case the MT cooling effect is not required, the COP of the system is strongly degraded, since the total cooling effect is reduced to the LT cooling effect only, while the compressor power draw remains unchanged, to allow the operation of the ejector. The presented

schematic therefore does not represent the optimized system schematic to operate in LT-only cooling production.

- The system performance is optimized only in case of simultaneous production of MT and LT cooling effect. However, as above mentioned, the LT cooling effect is usually not required for the same amount of time compared to the MT cooling effect during transport refrigeration applications. Moreover, the ON/OFF control strategy of the single compressor might present some challenges, due to the different desired temperature ranges and heat infiltration of the MT and the LT compartments.
- In addition, the schematic is not compliant with the Annex 1 of the ATP agreement [82] which prescribe the characterization of multi-temperature systems with both evaporators at the same evaporation pressure: this operational mode is in fact not possible, for the intrinsic principle of operation of the ejector.

As a conclusion, the concept schematic presented in Figure 7.1 presents some limits in operational flexibility. Therefore, an improved cooling unit schematic has been developed, which is presented in Figure 7.4.

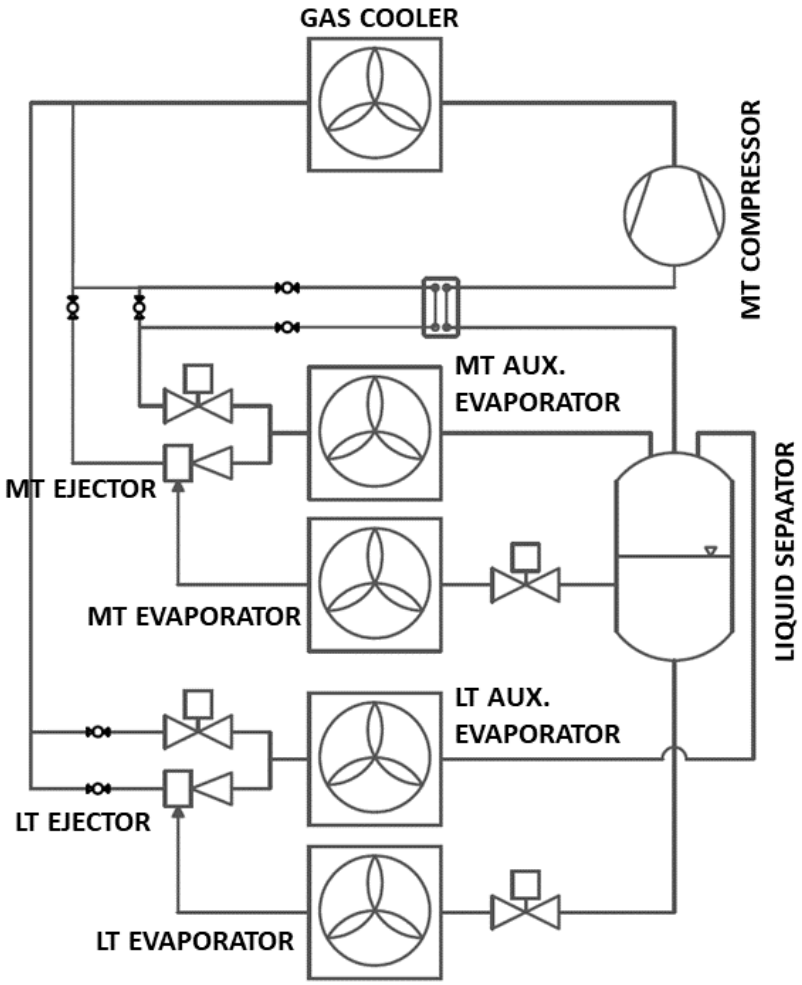

Figure 7.4 – Schematic of the improved refrigeration unit concept.

The general idea behind the development of the improved schematic of the R744 single-compression multi-temperature unit presented in Figure 7.4 is to combine the optimization of the MT system performance carried out in Chapter 3 with the optimization of the LT system performance through the insertion of a dedicated LT ejector, following the results of the experimental campaign described in Chapter 6.

Consistently with the common practice described for HFC multi-temperature units to adjust the evaporation pressure in order to operate in MT-only or in MT+LT or LT-only configuration, the improved system schematic allows operation in each of the above-mentioned configurations.

The schematic of the cooling unit operating in MT-only cooling effect production is presented in Figure 7.5, in which the red color is used to refer to the high pressure level, while the green color refers to medium pressure level, for MT refrigeration production. The dashed lines represent the portion of the cooling unit which is bypassed during operation in this configuration, since no LT cooling effect is required.

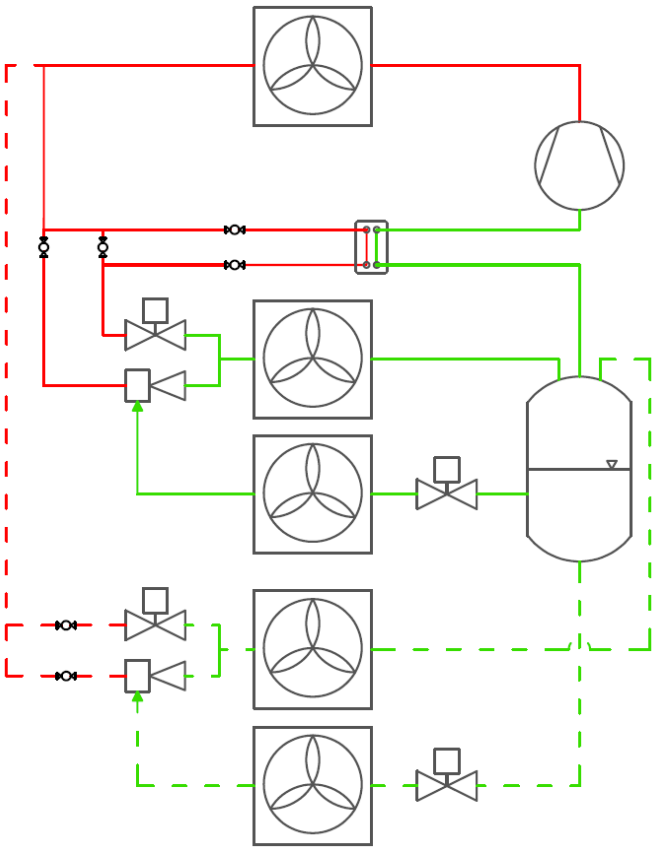

Figure 7.5 – Schematic of the refrigeration unit providing MT cooling effect. Dashed lines and components are not in use in this configuration.

This configuration, providing MT cooling effect only, operates following the same ejector cycle presented and discussed in Section 3.1 (EJ configuration and EJ,AUX configuration).

In this configuration, the refrigerant leaves the liquid separator in the state of saturated vapor, it is superheated in the internal heat exchanger (IHX) and then it enters the compressor suction line. After compression to the high pressure level, the refrigerant flows in the gas cooler coils and rejects heat to the external environment.

A parallel between the MT ejector and the High Pressure Valve (HPV) is enforced: the ejector operates with a fixed geometry, so the HPV is kept in parallel to the ejector, to handle the mass flow rate exceeding the one processed by the ejector motive muzzle. The IHX is placed in the bypass branch connected only to the HPV valve, in order to provide the refrigerant superheat required to guarantee absence of liquid at the compressor suction without affecting the mass flow at the MT ejector motive nozzle. The contemporary presence of an inverter driven compressor and the HPV allows also to increase the MT cooling power by increasing the compressor speed and consequently the mass flow rate on the HPV line if required.

The mass flow rate at the outlet of the MT ejector-HPV parallel is sent to the liquid separator flowing through the auxiliary MT evaporator or bypassing it, according to the external ambient temperature, as

extensively discussed in Section 3.1 and Section 3.3. Since in this operating mode the system is required to provide MT cooling effect only, the separator pressure level is set to allow providing MT cooling effect in both the main MT evaporator and in the auxiliary MT evaporator (with the pressure difference between these evaporators being provided by the MT ejector).

From the separator, the vapor phase is sent to the IHX and then to the compressor, while the liquid phase is expanded in a mechanical throttling valve (MTV) to the MT evaporation pressure and then evaporated in the heat exchanger coils. The refrigerant at the outlet of the evaporator is then entrained by the MT ejector providing the lift from the main MT evaporator pressure level to the separator pressure level.

The MT ejector insertion in the cooling unit schematic has the objective of increasing the efficiency of the system in MT-only cooling effect production, thanks to the reduction of the compressor pressure ratio allowed by the pressure lift provided by the MT ejector.

In this configuration, no refrigerant mass flow rate is sent to the portion of the cooling unit placed in the LT compartment of the insulated box.

On the other hand, the schematic of the cooling unit operating in LT-only cooling effect production is presented in Figure 7.6, in which the red color is used to refer to the high pressure level, while the blue color refers to low pressure level, for LT refrigeration production. The dashed lines represent the portion of the cooling unit which is bypassed during operation in this configuration.

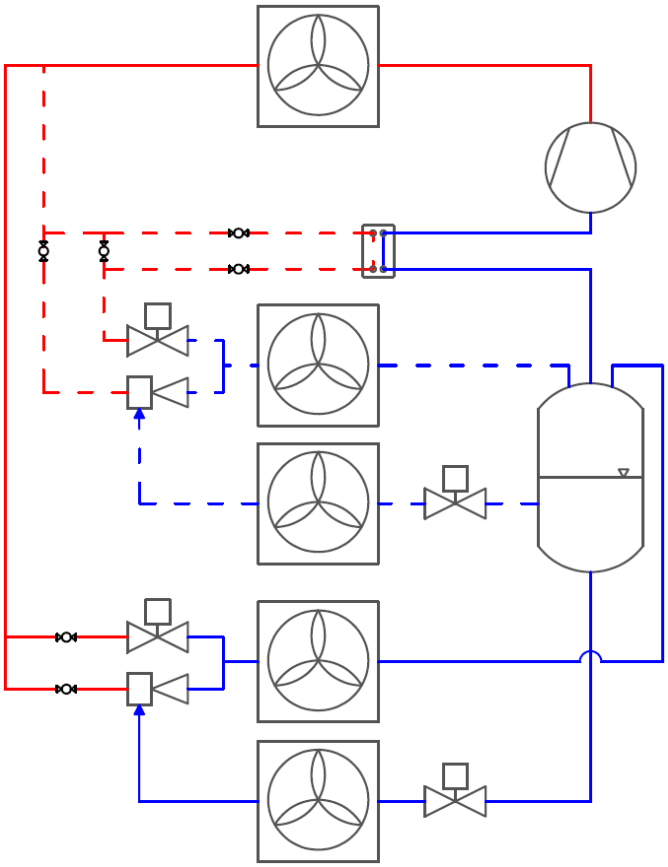

Figure 7.6 – Schematic of the refrigeration unit providing LT cooling effect. Dashed lines and components are not in use in this configuration.

In this configuration, the high pressure side of the cycle is unchanged, with the refrigerant leaving the liquid separator in the state of saturated vapor, entering the compressor suction line and, after the compression to the high pressure level, the rejecting heat to the external environment in the gas cooler coils.

Differently from the previous operating mode, in this operating mode the system is required to provide LT refrigeration only, and consequently the separator pressure level is lowered to allow providing LT cooling effect in both the main LT evaporator and in the auxiliary LT evaporator (with the pressure difference between these evaporators being provided by the LT ejector).

Following the same structure of the MT side of the cooling unit, also in the LT side of the unit a parallel between the LT ejector and the HPV is enforced. The mass flow rate at the outlet of the LT ejector-HPV parallel is sent to the liquid separator flowing through the auxiliary LT evaporator or bypassing it. The eventual use of the auxiliary LT evaporator is linked to the fulfillment of the continuity equation of each phase in the liquid separator, as the presence of the auxiliary LT evaporator allows operation even when the vapor quality of the two-phase mixture obtained at the mixing point between the LT ejector and the HPV does not necessarily coincide with the vapor quality at the inlet of the separator, as discussed in Section 3.1.

From the separator, the vapor phase is sent to the to the compressor, while the liquid phase is expanded in the MTV to the LT evaporation pressure and then evaporated in the heat exchanger coils. The refrigerant at the outlet of the evaporator is then entrained by the LT ejector providing the lift from the main LT evaporator pressure level to the separator pressure level.

Although the insertion of the LT ejector in the cooling unit schematic can provide an increase of the efficiency of the system in LT-only cooling effect production compared to a simple back-pressure cycle, for the same reasons discussed for the MT-only configuration, the main objective of the insertion of the LT ejector in the unit schematic is to guarantee the system operation even in very hot external ambient temperature conditions.

In fact, in case of LT operation under high external temperature conditions, the compressor pressure ratio required for the system operation increases and it has to be maintained within the compressor application limits. The application field of a compressor suitable for the application is reported in Figure 7.7 [104]. In the figure, the compressor is assumed to operate in a simple back-pressure cycle (with compressor, condenser, expansion valve and evaporator), in which the outlet of the evaporator coincides with the compressor suction. Therefore, the x-axis indicates the saturation temperature at the evaporator (and, consequently, determines the compressor suction pressure), while the y-axis indicates the minimum and the maximum allowed values of the pressure at the condenser (i.e. the discharge pressure) supported by the compressor. The application limits presented in the figure are valid for superheating values at the compressor suction lower than 10 K.

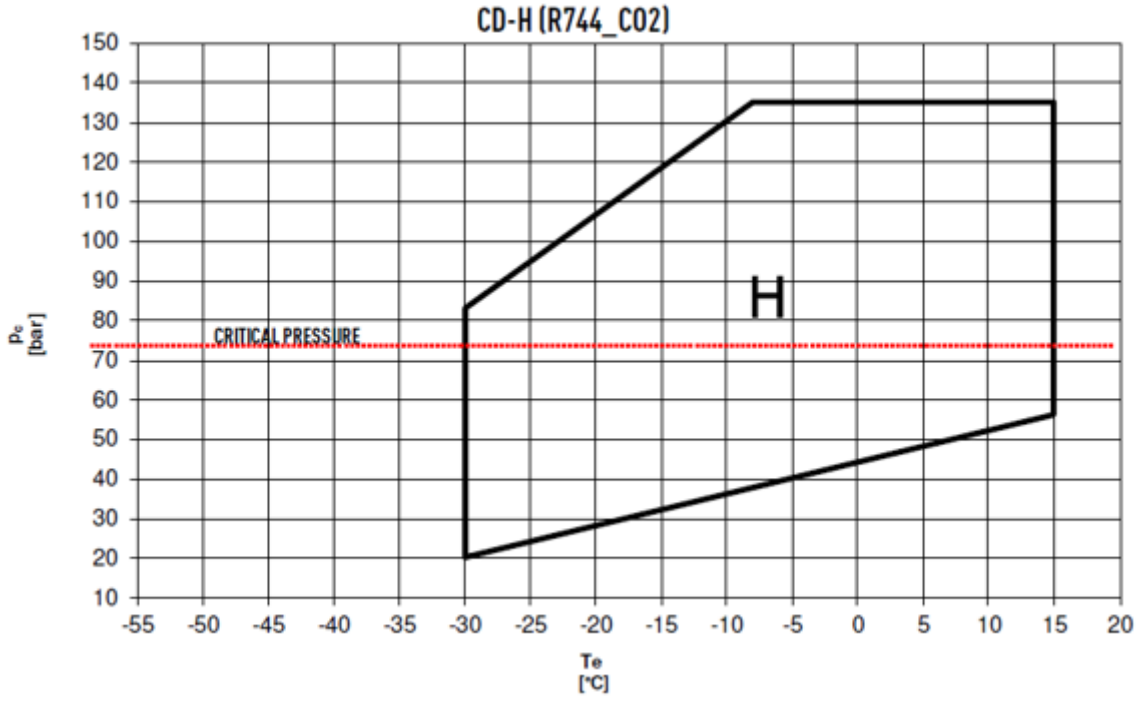

Figure 7.7 – Maximum discharge pressure range of a compressor suitable for the application [104], as a function of the evaporation saturation temperature of a simple back-pressure cycle.

In case of LT cooling effect requirement to guarantee a LT compartment temperature of -20°C, a simple back-pressure schematic of the LT side of the cooling unit would require evaporation (and, consequently, compressor suction) at a pressure level corresponding to a saturation temperature of -25°C. From the compressor application limits presented in Figure 7.7, for such compressor suction conditions, the maximum discharge pressure allowed by the compressor is around 95 bar which, according to the gas cooler pressure control presented in Table 3.2, would not allow the compressor operation in case the external temperature is greater than 35°C.

Instead, with the insertion of the LT ejector and the schematic presented in Figure 7.6, the compressor suction pressure and the LT main evaporator pressure are different, thanks to the pressure lift provided by the ejector. Therefore, the LT main evaporator pressure can be set at a pressure level corresponding to a saturation temperature of -25°C, while the separator pressure level (and the compressor suction pressure) can be increased according to the ejector performance.

Assuming a pressure lift provided by the LT ejector of Δp_{lift} = 6 bar, the compressor suction pressure is increased from 16.8 bar to 22.8 bar, corresponding to a saturation temperature of around -15°C. From the compressor application limits presented in Figure 7.7, for such compressor suction conditions, the maximum discharge pressure allowed by the compressor is around 120 bar which, according to the gas cooler pressure control presented in Table 3.2, would guarantee the compressor operation up to an external temperature of 44°C, thus significantly extending the external temperature range in which the refrigeration system can operate.

It has to be noticed that, in case of simultaneous requirement of MT cooling effect and LT cooling effect, the MT side of the system can be engaged, operating at the same pressure level of the LT side of the system, until the LT cooling effect requirement ceases, and the liquid separator pressure is increased to the MT evaporation level again.

As a conclusion, the schematic presented in Figure 7.4 leads to an increased operational flexibility compared to the concept schematic presented in Figure 7.1, employing an MT ejector for the optimization of the system operation in case of MT-only cooling effect production (corresponding to the majority of the delivery mission time, as previously described) and an LT ejector for the optimization of the LT cooling effect production and to allow operation of the system also in harsh external temperature conditions.

7.3 MT ejector and LT ejector design operating points

After the definition of the final schematic of the R744 multi-temperature unit with a single compression stage, the design operating points of both the MT ejector and the LT ejector have to be evaluated, in order to assess their desired performance.

Once the desired operating point are defined, through the evaluation of the expected motive nozzle conditions and mass flow rate, suction nozzle conditions and mass flow rate and pressure lift requirement, the mechanical and geometrical design of the MT ejector and of the LT ejector can be carried out, since both the ejectors are supposed to be designed with a fixed geometry, which has to fit the desired ejector performance.

The definition of the design point of the MT ejector has been carried out considering the schematic and the refrigeration cycle points presented in Figure 7.8.

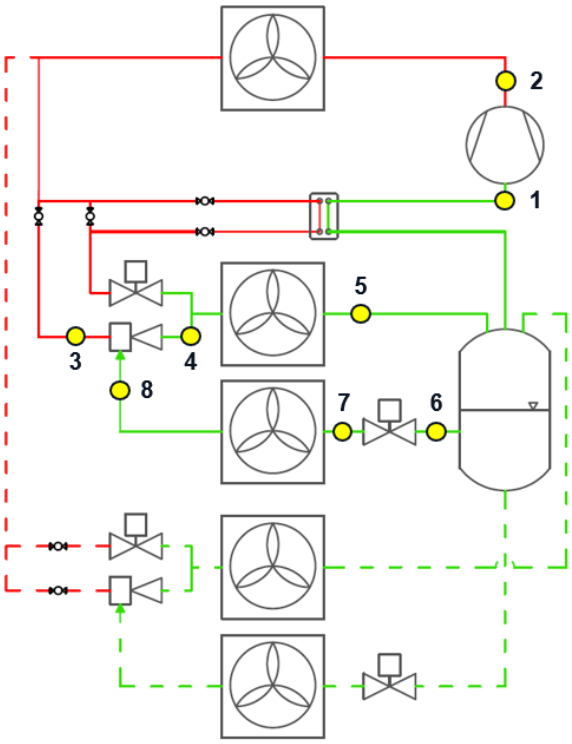

Figure 7.8 – Cooling unit cycle considered for the evaluation of the MT ejector design operating point.

The MT ejector dimensioning has been performed under the design operating conditions of ambient temperature equal to T_{amb} = 30°C and temperature of the air inside the MT compartment of the refrigerated vehicle equal to $T_{i,MT}$ = 0°C and considering the following assumptions:

- The refrigerant at the outlet of the liquid separator is assumed to be saturated vapor flowing to the compressor suction (x_1 = 1) and saturated liquid flowing to the mechanical throttling valve (x_6 = 0).
- The compressor considered for the following numerical evaluation is suitable for a MT cooling effect production of around 4-5 kW [104]. The compressor is characterized by a displacement of $\dot{V}_d$ = 1.46 m^3/h at the nominal rotational speed of ω_{comp} = 1450 rev min^{-1} (at a frequency of 50 Hz). To assess the maximum MT cooling effect that the system is able to provide, during the following numerical evaluation the compressor is assumed to operate at a frequency of 60 Hz.

The volumetric efficiency η_{vol} and the overall compression efficiency η_{comp} are interpolated as a function of the pressure ratio r_p and the rotational speed ω_{comp} from the compressor operating data provided by the manufacturer.

- No excess mass flow rate is expanded in the HPV, as all the refrigerant mass flow rate elaborated by the compressor is sent to the MT ejector motive nozzle ($\dot{m}_3 = \dot{m}_{comp}$). This assumption allows the definition of the minimum acceptable entrainment ratio of the MT ejector ($\phi_{MT} = \phi_{min,MT}$). In fact, if the MT ejector is able to provide a higher entrainment ratio compared to the one calculated under these assumptions, it means that the ejector is able to entrain the desired mass flow rate from the suction nozzle (and, consequently, the system is able to provide the desired MT cooling effect in the MT main evaporator) with a lower mass flow rate at the motive nozzle, thus reducing the mass flow rate that the compressor has to elaborate.
- The motive nozzle pressure and temperature are defined as a function of the ambient temperature, following the control strategy for the optimal conditions at the gas cooler outlet presented in Table 3.2 (p_3 = 83 bar, T_3 = 33°C).
- The suction nozzle pressure and temperature are defined by assuming a fixed evaporation pressure in the MT main evaporator (p_8 = 26.49 bar), according to a desired saturation temperature equal to $T_{sat,MT\ evap}$ = -10 °C. The superheat at the suction nozzle is assumed to be equal to SH_8 = 5 K.
- Different possible pressure lift requirements, from a minimum of $\Delta p_{lift,min}$ = 2 bar to a maximum of $\Delta p_{lift,max}$ = 8 bar, with a step of 1 bar, are considered for the definition of the possible MT ejector operating point. Since the suction pressure is fixed as mentioned above, different pressure lift requirements will result in different receiver pressures and, consequently, to different mass flow rates flowing to the compressor and to the MT main evaporator, since the continuity equation of each phase in the liquid separator has to be fulfilled at different pressure levels.
- The use of the MT auxiliary evaporator is not considered in the operating point design phase, since the system must be able to operate with good efficiency even without the flexibility given by the insertion of the MT auxiliary evaporator. Therefore, the possible operating points are selected in order to realize the condition $Q_{MT\ evap,AUX} \approx 0$ W ($h_5 \approx h_4$).

Under the above-mentioned assumptions, the numerical evaluation determined the possible design operating points for the MT ejector reported in Table 7.3.

Table 7.3 – MT ejector possible design operating points.

T_{motive} [°C]	p_{motive} [bar]	$p_{suction}$ [bar]	$SH_{suction}$ [K]	Δp_{lift} [bar]	$\dot{m}_{motive}$ [kg min^{-1}]	$\dot{m}_{suction}$ [kg min^{-1}]	ϕ [-]	η_{ej} [-]	Q_{MT} [kW]
33.00	83.00	26.49	5.00	2	1.71	0.90	0.525	0.101	3.9
33.00	83.00	26.49	5.00	3	1.80	0.96	0.530	0.157	4.1
33.00	83.00	26.49	5.00	4	1.90	1.01	0.535	0.217	4.3
33.00	83.00	26.49	5.00	5	1.99	1.07	0.539	0.281	4.5
33.00	83.00	26.49	5.00	6	2.09	1.13	0.544	0.349	4.7
33.00	83.00	26.49	5.00	7	2.18	1.20	0.548	0.421	4.9
33.00	83.00	26.49	5.00	8	2.28	1.26	0.552	0.450	5.1

Since the MT ejector will be developed and designed in order to guarantee specific operating conditions, in Table 7.3 the chosen operating conditions for which the MT ejector will be designed are reported highlighted in red, since in practical applications the ejector efficiency usually does not exceed the value of 0.3. The MT ejector final geometry will be commissioned for development with the objective of being able to provide an entrainment ratio and an efficiency in the range of the ones determined numerically under those specific operating conditions.

After the definition of the design point of the MT ejector, the design operating conditions for the LT ejector have been evaluated considering the schematic and the refrigeration cycle points presented in Figure 7.9.

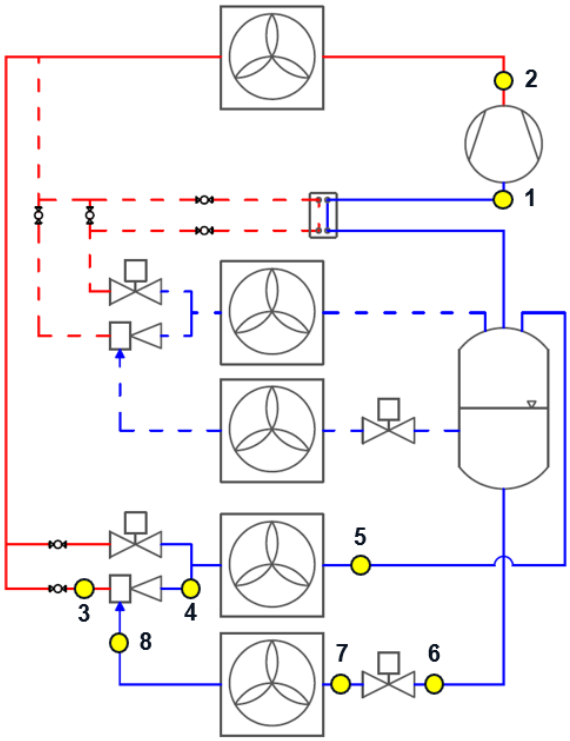

Figure 7.9 – Cooling unit cycle considered for the evaluation of the LT ejector design operating point.

The LT ejector dimensioning has been performed under design operating conditions with the same ambient temperature as for the MT ejector, equal to T_{amb} = 30°C, but with temperature of the air inside

the LT compartment of the refrigerated vehicle equal to $T_{i,LT}$ = -20°C. For the numerical evaluation, the following assumptions were considered:

- As done for the MT ejector evaluation, the refrigerant at the outlet of the liquid separator is assumed to be saturated vapor flowing to the compressor suction (x_1 = 1) and saturated liquid flowing to the mechanical throttling valve (x_6 = 0).
- The same compressor was considered in the numerical evaluation, since a single compressor will be installed in the cooling unit. In this case, to assess the minimum LT cooling effect that the system is able to provide, during the following numerical evaluation the compressor is assumed to operate at a frequency of 30 Hz.
- As described for the MT ejector evaluation, no excess mass flow rate is expanded in the HPV, as all the refrigerant mass flow rate elaborated by the compressor is sent to the LT ejector motive nozzle ($\dot{m}_3 = \dot{m}_{comp}$). Consequently, also in this case this assumption allows the definition of the minimum acceptable entrainment ratio of the LT ejector ($\phi_{LT} = \phi_{min,LT}$).
- The motive nozzle pressure and temperature are defined as a function of the ambient temperature, following the control strategy for the optimal conditions at the gas cooler outlet presented in Table 3.2 (p_3 = 83 bar, T_3 = 33°C).
- Differently from the MT ejector evaluation, in this case the liquid separator pressure is fixed at a value of p_5 = 19.10 bar), corresponding to a saturation temperature equal to $T_{sat,separator}$ = -21°C. With this assumption, the LT ejector is defined according to operating conditions in which the LT auxiliary evaporator can always provide a positive cooling effect if needed, as the refrigerant flowing in the LT auxiliary evaporator will be always colder than the air inside the LT compartment of the insulated box.
- Different possible pressure lift requirements, from a minimum of $\Delta p_{lift,min}$ = 2 bar to a maximum of $\Delta p_{lift,max}$ = 6 bar, with a step of 1 bar, are considered for the definition of the possible LT ejector operating point. Since the separator pressure is fixed as mentioned above, an increase of the pressure lift requirement will result in a decrease of the LT evaporator pressure and in the consequent change of the suction nozzle pressure. However, the superheat at the suction nozzle is still assumed to be equal to SH_8 = 5 K. According to the LT ejector evaluation assumptions, since the separator is always at the same pressure level, the same mass flow rates flow to the compressor and to the LT main evaporator for all the considered pressure lift requirements.
- As done for the MT ejector evaluation, the use of the LT auxiliary evaporator is not considered in the operating point design phase, since the system must be able to operate with good efficiency even without the flexibility given by the insertion of the LT auxiliary evaporator. Therefore, the possible operating points are selected in order to realize the condition $Q_{LT\ evap,AUX}$ ≈ 0 W ($h_5 \approx h_4$).

Under the above-mentioned assumptions, the numerical evaluation determined the possible design operating points for the LT ejector reported in Table 7.4.

Table 7.4 – LT ejector possible design operating points.

T_{motive} [°C]	p_{motive} [bar]	$p_{suction}$ [bar]	$SH_{suction}$ [K]	Δp_{lift} [bar]	$\dot{m}_{motive}$ [kg min^{-1}]	$\dot{m}_{suction}$ [kg min^{-1}]	ϕ [-]	η_{ej} [-]	Q_{LT} [kW]
33.00	83.00	17.10	5.00	2	0.46	0.21	0.449	0.092	1.0
33.00	83.00	16.10	5.00	3	0.46	0.21	0.449	0.144	1.0
33.00	83.00	15.10	5.00	4	0.46	0.21	0.449	0.199	1.0
33.00	83.00	14.10	5.00	5	0.46	0.21	0.450	0.260	1.0
33.00	83.00	13.10	5.00	6	0.46	0.21	0.450	0.326	1.0

Also in this case, the chosen operating conditions for which the LT ejector will be commissioned and designed are reported highlighted in red in Table 7.4, following the same choice criteria described for the MT ejector.

As a conclusion, the desired performance of both the MT ejector and the LT ejector has been numerically evaluated under nominal operating conditions. The desired performance data will be provided to the ejectors manufacturers with the objective of their geometrical design and optimization, which will result in the manufacturing of ejectors prototypes to be experimentally tested in the future.

7.4 Conclusions

This chapter presented the preliminary evaluation of the performance of a R744 single-compression multi-temperature unit, based on the ejector performance results in low-temperature suction conditions obtained from the experimental campaign presented in Chapter 6. The concept schematic is based on the use of an ejector as the only component to increase the refrigerant pressure from the LT evaporation pressure to the MT evaporation pressure, thus allowing the simultaneous production of MT and LT cooling effects.

After the preliminary evaluation of the concept cooling unit performance, the operational limits of the first concept schematic were highlighted, and the development of an improved and more flexible schematic, based on the insertion of separate MT ejector and LT ejector, was carried out to improve the operational issues connected to the first concept schematic.

Finally, the design operating points of the MT ejector and of the LT ejector have been used to assess the desired operational points for which the ejectors geometry will be designed and optimized.

The main results obtained in this chapter can be summarized as follows:

- The performance of the multi-temperature cooling unit based on the first concept schematic (with the presence of a single LT ejector) was numerically evaluated in nominal operating conditions, based on the ejector performance experimental results measured with motive nozzle conditions equal to T_{motive} = 35°C and p_{motive} = 90 bar and suction pressure equal to $p_{suction}$ = 16.8 bar (corresponding to a saturation temperature at the suction nozzle equal to T_{sat} = -25°C). In such operating conditions, the system is able to provide up to 4.89 kW of MT cooling and up to 1.98 kW of LT cooling, depending on the ejector lift requirement. The maximum overall system COP is equal to 1.92 and it is obtained when the ejector provides the maximum available pressure lift. However, at maximum pressure lift the LT cooling effect production is significantly reduced (-38.9% compared to the operating conditions with maximum LT cooling effect production). As a consequence, the system design point has to be carefully chosen according to the ejector performance, to the system thermodynamic COP and to the expected MT and LT refrigeration needs for the specific application, in order to obtain the best trade-off between cooling effect production and overall system performance.
- The first cooling unit concept schematic leads to some operational issues which have to be faced in transport refrigeration applications: in case of MT-only operation (which is the operating mode realized for the majority of a delivery mission period) the refrigeration cycle is reduced to a non-optimized, baseline back-pressure cycle with low COP; operation in LT-only cooling effect production would require the operation of the compressor at full capacity, to guarantee the necessary mass flow rate at the ejector motive nozzle, even if the MT cooling effect is not required, lowering the overall system COP; even in simultaneous MT+LT cooling effect production, the ON/OFF control strategy of the single compressor might present some challenges, due to the different desired temperature ranges and heat infiltration of the MT and the LT compartments.
- An improved, more flexible cooling unit schematic has been developed to address the above-mentioned operational issues linked to the first concept schematic. The improved schematic includes the use of a MT ejector, to optimize the system performance during operation in MT-only cooling effect production, thanks to the pressure lift provided by the ejector and the consequent reduction of the compressor pressure ratio, and the use of a separate LT ejector, to optimize the system performance during operation in LT-only cooling effect production. Moreover, the insertion of the LT ejector allows the cooling unit operation even under harsh environmental conditions, due to the reduction of the compressor pressure ratio under the maximum pressure ratio achievable by the compressor. In particular, with a LT evaporation pressure corresponding to a saturation temperature of -25°C, a pressure lift provided by the LT

ejector of Δp_{lift} = 6 bar would extend the environmental conditions in which the operation of the cooling unit is guaranteed from T_{amb} = 35°C to T_{amb} = 44°C.

- The MT ejector and LT ejector design operating points have been defined through a numerical evaluation of the cooling unit refrigeration cycle in MT-only and LT-only cooling effect production, respectively. The possible design performance of the MT ejector has been defined as a design motive mass flow rate of $\dot{m}_{motive\ MT}$ = 1.01-1.07 kg min^{-1}, entrainment ratio of ϕ_{MT} = 0.535-0.539, efficiency of η_{MT} = 0.217-0.281 and pressure lift of $\Delta p_{lift\ MT}$ = 4-5 bar, under the nominal operating conditions of T_{amb} = 30°C and $T_{i,MT}$ = 0°C. On the other hand, the possible design performance of the LT ejector has been defined as a design motive mass flow rate of $\dot{m}_{motive\ LT}$ = 0.46 kg min^{-1}, entrainment ratio of ϕ_{LT} = 0.449-0.450, efficiency of η_{LT} = 0.199-0.260 and pressure lift of $\Delta p_{lift\ LT}$ = 4-5 bar, under the nominal operating conditions of T_{amb} = 30°C and $T_{i,LT}$ = -20°C.

8 Conclusions

The main objective of this thesis was to propose and analyze solutions to improve the environmental sustainability of road transport refrigeration systems through the reduction of both indirect and direct emissions of transport cooling units.

As a first step, reduction of indirect GHG emissions through the overall improvement of the efficiency of transport refrigeration systems has been addressed.

The numerical model of a R134a cooling unit serving the needs of a small refrigerated van in an urban delivery mission of perishable goods was developed using the software Simcenter Amesim v.17, to represent the baseline technology in current refrigerated transport sector. A comprehensive modelling approach simultaneously accounting for the dynamic behavior of the cooling unit, of the insulated box in which the products are stored and of the vehicle engine during a typical daily multi-drop delivery mission in urban environment was used. The fuel consumption and the pollutant emissions of the engine were evaluated throughout the delivery mission and operation under different climatic conditions (Athens, representative of hot European climate, and Strasbourg, representative of mild European climate) was considered.

Three different system layouts, which differ for the type of connection between the cooling unit compressor and the vehicle prime engine, were considered: a direct-drive connection between the vehicle main shaft and the refrigerating system compressor, an alternator to disconnect the compressor rotational speed from the engine rotational speed, enabling the optimization of the compressor efficiency and of the refrigerating system cooling effect, and finally a battery pack to store and provide the required energy to the refrigerating system, thus leading to the possibility to switch off the vehicle engine during some sections of the delivery mission.

Considering operation in hot European climatic conditions (Athens), the average mission COP of the refrigerating system is equal to 1.31 with a direct connection between cooling unit and vehicle engine (BELT-CONF) and to 1.65 when an alternator is used to decouple the rotational speed of the engine and of the compressor, providing an optimization of the latter (ALT-CONF and BAT-CONF). In addition, an overall Duty Cycle equal to 0.28 for the belt-driven configuration and to 0.39 for the electrically driven configurations was calculated. The introduction of the alternator to disconnect the cooling unit from the engine led to a 26% increase of the mission COP and a 39.3% increase of the Duty Cycle of the refrigerating system.

The compressor connection to the vehicle engine has a significant effect on the temperature of the air inside the insulated box, as in the BELT-CONF the heavily varying compressor speed causes irregular ON/OFF cycles of the refrigerating unit and a not constant cooling capacity profile, while in the electrically-

driven configurations the compressor speed control leads to a better management of the internal air conditions and to a lower internal air temperature on the average, thus improving the preservation of the transported cargo during the delivery mission.

The introduction of a battery as an electrical energy storage dedicated to the cooling unit operation (BAT-CONF) leads to the disconnection between the power demand of the refrigerating system and the power production to be performed by the engine. Thanks to the energy storage device, the engine can be switched off when the vehicle is still, as the power required by the cooling unit is withdrawn from the battery, which will be then recharged when the engine is already switched on to perform the mission driving cycles.

The presence and the operation of the cooling unit during the daily delivery mission lead to a 19.0% increase of the fuel consumption, a 33.2% increase of the CO emissions, a 9.5% increase of the NOx emissions, a 32.2% increase of the THC emissions and a 23.5% increase of the PM emissions, on the average, compared to the same vehicle performing the same delivery mission without powering a cooling unit. However, when the use of a cooling unit is mandatory to preserve the cold chain, the use of a battery can significantly mitigate the impact of the presence of the cooling unit on the engine operation, giving the possibility to switch off the engine when the vehicle is still. The implementation of the battery leads to a 11.1% reduction of the fuel consumption, a 24.0% reduction of the CO emissions, a 1.1% reduction of the NOx emissions, a 25.0% reduction of the THC emissions and a 16.6% reduction of the PM emissions compared with the use of a direct belt connection between the engine shaft and the cooling unit.

Considering operation in BELT-CONF in mild European climatic conditions (Strasbourg), the average mission COP of the refrigerating system becomes equal to 1.59 thanks to the less severe external temperature level. Overall, the variation of the fuel consumption and of the pollutant emissions due to the cooling unit presence with climatic conditions is always comprised in the ±1% range, approximately.

Following the above-mentioned assessment of the thermal and environmental improvement of the transport refrigeration unit performance linked to the insertion of a battery pack, the introduction in the refrigeration system schematic of photovoltaic panels for energy production from the renewable solar source, which can be stored in the batteries and then used by the cooling unit, was evaluated. Stationary experimental tests were conducted, demonstrating the ability of the solar system to significantly contribute to the overall energy balance under early summer conditions, providing 65.5% of the energy required to run the cooling unit on the first full day of activity and 56.0% of the energy on the last full day after five consecutive days of activity.

The photovoltaic panels were then added to the previously developed numerical model of the system, and numerical simulations of the solar-aided refrigeration system employed in a typical daily delivery mission in an urban environment highlight that the presence of the PV panels can reduce by 95% the

power drawn from the vehicle engine, in case of small battery pack capacity (2.16 MJ). With the use of a larger battery pack (8.64 MJ), the performance of the system can be improved up to 17%, leading to a net +12% energy excess on a yearly basis. The effects of shading were also considered, leading to a 68% reduction of the power drawn from the vehicle engine, in case of small battery pack capacity (2.16 MJ). Full shading conditions, however, limit the ability to exploit a larger battery pack capacity, as the switch to a 8.64 MJ battery pack leads to a 3% improvement of the net energy balance on a yearly basis.

After focusing on the development of solutions which can improve the performance and the efficiency of current transport refrigeration systems, thus reducing the indirect emissions of road transport cooling units, the development of novel units employing natural refrigerants, which are characterized by a low GWP and which can therefore nullify the direct emissions linked to refrigerant leakage in the atmosphere, was carried out. A simple preliminary evaluation highlighted that the use of a low-GWP refrigerant, such as R744, leads to a reduction of around -23.5% of the total direct + indirect emissions compared to a standard R404A HFC refrigerant unit, over a 10-year service lifetime.

Therefore, the design of a R744 cooling unit designed to provide MT refrigeration in road temperature-controlled transport applications was presented. Depending on the external environmental conditions, the system can operate in both subcritical and transcritical mode and three different operating cycles were evaluated. The reference cycle is given by a classical low-pressure receiver cycle (BP configuration) employing a simple high-pressure valve (HPV) for the refrigerant expansion. In warm and hot environmental temperature conditions, the refrigerating system can also operate following an ejector transcritical cycle (EJ configuration), exploiting the parallel between the HPV and a fixed-geometry two-phase ejector. Further modification of the system schematic is given by the introduction of an auxiliary evaporator in the line between the ejector outlet nozzle and the liquid separator (EJ,AUX configuration), to extend the ejector operation towards lower ambient temperature operating conditions. The software Simcenter Amesim v.17 was then used for the development of the numerical model of the cooling unit.

The steady state performance of the cooling unit and the unsteady performance of the system performing ON/OFF cycles to maintain a desired temperature range inside the insulated box were evaluated in each of the three possible configurations. Results allowed the development of a configuration control strategy of the cooling unit, to maximize the cooling effect or the system COP as a function of the operating conditions. When the internal air temperature is within the temperature set-point range ($T_i < 3°C$), the best performing configuration in terms of the ON/OFF cycle COP is preferred. In this scenario, for $T_{amb} <$ 33°C, the EJ,AUX configuration is selected, while for $T_{amb} \geq$ 33°C, the EJ configuration leads to a better performance. However, when the internal air conditions are outside of the desired temperature range ($T_i \geq 3°C$), the fast recovery of the desired temperature set-point is prioritized and the EJ;AUX

configuration is selected regardless of the ambient temperature, to provide a higher overall cooling effect due to the simultaneous use of both the evaporators.

The numerical simulation of a short-range multi-drop delivery mission (for every month of the year) and the numerical simulation of a long-range single-drop delivery mission (for the hottest month of the year) were carried out to evaluate the operation of the cooling unit when employed during delivery missions of temperature-controlled goods, both in urban and extra-urban environment.

The EJ configuration is used during the delivery missions in the hottest months in the year (June, July and August), resulting in 10.5% of the yearly total cooling energy provided using this configuration. The ejector performance was evaluated in unsteady operating conditions during the delivery mission, and the maximum values of the average ejector efficiency (10.1%) and of the average pressure lift (1.59 bar) are reached during an ON period occurred at higher ambient temperature (36°C). However, the absolute values of the average ejector efficiency and pressure lift evaluated during the ON periods of the mission are significantly lower than the corresponding values evaluated in steady-state operation. The short time (approximately one minute) of the ON periods leads to an ejector operation which is always in transient conditions, never reaching its steady operating conditions.

To avoid pressure drifts inside the low-pressure side of the refrigerating system during a long time of inactivity, due to heat infiltration from the external environment, a safety control system based on the definition of a maximum allowed pressure level inside the separator was proposed. With the presence of an expanded polystyrene insulating layer around the liquid separator, one entire summer day without any safety cycle can be performed and, even with no insulation around the separator, an entire night can be performed without the need of a safety cycle. However, if the cooling unit is kept off under daily environmental air temperature conditions without insulation around the separator, the operation of a safety cycle is necessary approximately every 6 h. Nevertheless, the presence of a single safety cycle during the OFF period following a delivery mission causes a limited variation of the cooling unit's daily COP (−4.4%).

The performance of the proposed R744 unit has been compared to the performance of the baseline R134a unit previously considered as representative of the current market, on the same urban delivery mission and for each month of the year, in hot European climatic conditions. The R744 unit presents a significantly higher average mission COP during the hottest months of the year, characterized by higher external ambient temperature conditions, while during the coldest months the baseline R134a unit presents a better COP. However, on a yearly basis the employment of the proposed R744 unit in the considered urban delivery mission, instead of the baseline R134a unit, leads to an increase of the average mission COP equal to +15.8%.

After the numerical analysis of the above-described R744 cooling unit, an actual prototype of the unit was commissioned and installed at the ITC-CNR laboratories in Padova, Italy. Data measurement equipment has been installed on the experimental rig and the first startup experimental tests were performed.

Experimental startup tests were useful to identify unexpected behavior of some components and to define proper solutions.

A complete pulldown and subsequent ON/OFF operation was performed by the cooling unit in BP configuration, with no control of the heat sink temperature. An average cooling effect provided by the evaporator of around 5 kW and an average heat rejected by the gas cooler of around 8 kW were registered during the pulldown and consequent ON/OFF operation. The compressor power draw presented an approximate value of 3.2 kW during the considered period, leading to an instant COP of around 1.6 in the considered period of operation.

Steady-state experimental tests with an almost constant heat sink temperature of around $T_{amb} \cong 45$°C and various heat source temperatures ($T_i \cong 10$°C, $T_i \cong 7$°C, $T_i \cong 5$°C, $T_i \cong 2$°C, $T_i \cong 0$°C) were performed, assessing a system COP variating from 1.71 (with $T_i \cong 10$°C) to 1.24 ($T_i \cong 0$°C). The experimental results obtained in steady-state conditions were compared to the numerical results of the previously developed cooling unit model. The experimental results and the simulations results showed a relative error ranging from -19.3% (with $T_i \cong 10$°C) to -16.9 % (with $T_i \cong 0$°C).

After focusing on single-temperature R744 cooling units for transport refrigeration applications, R744 multi-temperature solutions were considered, in line with the market requirements, and the numerical model of a R744 cooling unit for multi-temperature (0°C and -20°C) refrigerated transport applications was developed in the software Simcenter Amesim v. 17.

A first layout integrating a traditional booster system with a two-phase ejector and auxiliary evaporator layout and relying on a double stage of compression was initially considered. The theoretical performance of the unit was evaluated through steady-state simulations under different environmental temperature conditions and different combinations of input parameters, and the system optimal operating points, in terms of system COP and total MT cooling effect, were highlighted through the implementation of a Pareto optimality criterion.

Considering all the possible operating points evaluated through numerical simulations, the choice of the optimal combination of parameters leads to significant improvements in both the COP and MT cooling effect objective functions. In particular, for external air conditions equal to T_{amb} = 30°C, operation with a non-optimized combination of parameters can lead to a reduction in the COP of up to -15.6% and to a reduction in the MT cooling effect of up to -79.6% compared with the maximum achievable values. The Pareto front of the system operating points presents a high extension on the MT cooling effect, as for

external air conditions equal to T_{amb} = 30°C, a variation of up to -43.4% of the MT cooling effect can be achieved. At the same time, moving along the Pareto front, the COP reduction never exceeds -4.7%. This flexibility in the MT cooling effect objective, while still keeping high COP values, can be useful to exploit a high cooling effect production when needed (i.e. during pulldown and after a door opening of the refrigerated truck cargo space).

The LT side of the cooling unit presents an only marginal modification as results of the different external conditions and of the different parameters combination along the Pareto front: the cooling power average variation from the condition of maximal COP to the condition maximizing the MT cooling power is always less than 10%, and the LT evaporation pressure is always approximately equal to 16 bar. The required LT refrigerating effect can be therefore provided without being directly influenced by the variation of the operational parameters of the system.

Finally, a novel R744 cooling unit concept for multi-temperature refrigerated transport applications was proposed, based on the implementation of an ejector as the only component dedicated to the increase of the refrigerant pressure from the LT to the MT evaporating pressure, thus allowing the removal of the LT compressor, with both performance and cost benefits.

To verify the actual feasibility of such a unit arrangement, dedicated experimental tests were performed on a commercially available ejector to assess its performance in the desired low-temperature range (down to -25°C LT saturation temperature. Tests were carried out at the NTNU/SINTEF laboratories in Trondheim, Norway.

The results show that, globally, the ejector mass entrainment ratio decreases as the pressure lift requirement increases. On the contrary, the ejector efficiency shows a clear parabolic trend as a function of the pressure lift. Typically, the performance is higher, both in terms of entrainment ratio and efficiency, for higher suction pressure conditions. A significant degradation of the ejector performance of higher suction pressure points towards the maximum achievable pressure lifts wa experienced. Moreover, the maximum achievable lift value that can be handled by the ejector is influenced by the suction pressure, as for higher suction pressures the maximum achievable lift can be lower than for lower suction pressures.

In conclusion, the experimental results demonstrate the ability of the tested ejector to entrain mass flow rate in a wide range of operating points, including LT suction nozzle conditions, under different climatic conditions. However, the results highlight the crucial importance of the choice of the ejector operating point, as the pressure lift requirement has a significant influence on both the ejector entrainment ratio and efficiency.

The experimental results of the ejector operating in LT suction conditions were used to perform a numerical evaluation of the performance of the novel multi-temperature R744 cooling unit concept with

only one stage of compression. The analysis shows that the system design point has to be carefully chosen according to the ejector performance, to the system thermodynamic COP and to the expected MT and LT refrigeration needs for the specific application, in order to obtain the best trade-off between cooling effect production and overall system performance.

After highlighting some operational issues linked to the above-considered cooling unit concept schematic, an improved schematic based on the presence of two separate ejectors (a MT ejector and a LT ejector) was developed. In particular, the insertion of the LT ejector allows the cooling unit operation even under harsh environmental conditions, due to the reduction of the compressor pressure ratio under the maximum pressure ratio achievable by the compressor. With a LT evaporation pressure corresponding to a saturation temperature of -25°C, a pressure lift provided by the LT ejector of 6 bar would extend the environmental conditions in which the operation of the cooling unit is guaranteed from T_{amb} = 35°C to T_{amb} = 44°C. The MT ejector and LT ejector design operating points have been defined through a numerical evaluation of the cooling unit refrigeration cycle in MT-only and LT-only cooling effect production, respectively.

In conclusion, the research work carried out during the three years of Ph.D. has highlighted that sustainable alternatives to replace the traditionally used HFC/HFO transport refrigeration systems are possible and under practical development, both in terms of improvement of the refrigerating system performance and efficiency, through innovative solutions and electrification, and in terms of development of highly efficient units employing natural refrigerants such as R744.

The achievements described in this thesis introduce to future research activities. The first step will be the full experimental assessment of the performances of the R744 single-temperature unit installed at ITC-CNR and the validation of the numerical model developed in the Ph.D. period. Moreover, the experimental test rig will be helpful to define the final, simplified refrigeration system schematic to be developed for real road transport refrigeration applications, including only the configurations optimizing the system performance. The final foreseen goal built on the achievements of this work is a prototype of the complete system, composed by the vehicle and the R744 refrigeration unit, including the specifically designed MT ejector and LT ejector and the presence of photovoltaic solar panels, to fully instrument it and to test it experimentally during typical temperature-controlled delivery missions in the field. The design developed for the refrigeration unit multi-temperature application has already been positively evaluated and its development and implementation will continue under the EU H2020 Project ENOUGH.

References

[1] A. Meneghetti, G. Da Rold and G. Cortella, "Sustainable refrigerated food transport: searching energy efficient routes," *IFAC-PapersOnLine 51(11),* pp. 618-623, 2018.

[2] Z. Yang, J. E. Tate, E. Morganti and S. P. Shepherd, "Real-world CO2 and NOx emissions from refrigerated vans," *Science of Total Environment 763(X),* no. 142974, 2021.

[3] S. Mercier, S. Villeneuve, M. Mondor and I. Uysal, "Time-temperature management along the food cold chain: a review of recente developments," *Comprehensive Reviews in Food Science and Food Safety, 16 (4),* pp. 647-667, 2017.

[4] Food and Agriculture Organization of the United Nations, "The future of food and agriculture: trend and challenges," Rome, 2017.

[5] F. Bagheri, M. A. Fayazbakhsh and M. Bahrami, "Real-time performance evaluation and potential GHG reduction in refrigerated trailers," *International Journal of Refrigeration 73,* pp. 24-38, 2017.

[6] H. M. Stellingwerf, A. Kanellopoulos, J. G. A. J. Van Der Vorst and J. M. Bloemhof, "Reducing Co2 emissions in temperature-controlled road transportation using the LDVRP model," *Transportation Research Part D: Transport and Environment 58,* pp. 80-93, 2018.

[7] M. Ahmed, O. Meade and M. A. Medina, "Reducing heat transfer across the insulated walls of refrigerated truck trailers by the application of phase change materials," *Energy Conversion and Management 51,* pp. 383-392, 2010.

[8] A. Rai and S. A. Tassou, "Environmental impact of vapour compression and cryogenic transport refrigeration technologies for temperature-controlled food distribution," *Energy Conversion and Management 150,* pp. 914-923, 2017.

[9] S. James, C. James and J. Evans, "Modelling of food transportation systems - A review," *International Journal of Refrigeration 29 (6),* pp. 947-957, 2006.

[10] S. Estrada-Flores and A. Eddy, "Thermal performance indicators for refrigerated road vehicles," *International Journal of Refrigeration 29,* pp. 889-898, 2006.

[11] P. Jara, J. Rivera, C. Merino, E. Silva and G. Farfan, "Thermal behavior of a refrigerated vehicle: process simulation," *International Journal of Refrigeration 100,* pp. 124-130, 2019.

[12] P. Artuso, A. Rossetti, S. Minetto, S. Marinetti, L. Moro and D. Del Col, "Dynamic modeling and thermal performance analysis of a refrigerated truck body during operation," *International Journal of Refrigeration 99,* pp. 288-299, 2019.

[13] G. Li, "Comprehensive investigation of transport refrigeration life cycle climate performance," *Sustainable Energy Technologies and Assessments 21,* pp. 33-49, 2017.

[14] X. Wu, S. Hu and S. Mo, "Carbon footprint model for evaluating the global warming impact of food transport refrigeration systems," *Journal of Cleaner Production 54,* pp. 115-124, 2013.

[15] R. Haass, P. Dittmer, M. Veigt and M. Lutien, "Reducing food losses and carbon emission by using autonomous control - A simulation study of the intelligent container," *International Journal of Production Economics 164,* pp. 400-408, 2015.

[16] O. Adekomaya, T. Jamiru, R. Sadiku and Z. Huan, "Sustaining the shelf life of fresh food in cold chain - A burden on the environment," *Alexandria Engineering Journal 55,* pp. 1359-1365, 2016.

[17] S. A. Tassou, G. De-Lille and Y. T. Ge, "Food transport refrigeration - Approaches to reduce energy consumption and environmental impacts of road transport," *Applied Thermal Engineering 29 (8-9),* pp. 1467-1477, 2009.

[18] G. Cavalier and S. A. Tassou, "Sustainable refrigerated road transport. 21st Informatory Note on refrigerating technologies," International Institute for Refrigeration, 2011.

[19] T. Michineau, G. Cavalier and E. Devin, "F-gases in refrigerated transport," in *Proceedings of the 3rd IIR International Conference on Sustainability and the Cold Chain*, London, England, 2014.

[20] R. A. Barnitt, D. Chernich, M. Burnitzki, A. Oshinuga, M. Miyasato, E. Lucht, D. Van Der Merwe and P. Schaberg, "Emissions of transport refrigeration units with CARB diesel, gas-to-liquid diesel and emission control devices," *SAE Technical Papers,* 2009.

[21] R. Lawton, T. Mynott, N. Marshall and F. Wagner, "Emission testing of a transport refrigeration unit," in *Proceedings of the 25th IIR International Congress of Refrigeration*, Montreal, Canada, 2019.

[22] J. Houghton, L. Meira Filho, B. Lim, K. Treanton, I. Mamaty, Y. Bonduki, D. Griggs and B. (. Callender, "Revised 1996 IPCC Guidelines for National Greenhouse Gas Inventories," IPCC/OECD/IEA, UK Meteorological Office, Bracknell, UK, 1996.

[23] European Commettee for Standardization (CEN) Technical Committee (TC), "CEN/TC 182 - Refrigerating systems, safety and environmental requirements".

[24] European Commission, "Regulation (EU) No 517/2014 of the European Parliament and of the Council of 16th April 2014 on fluorinated greenhouse gases and repealing Regulation (EC) No 842/2006," 2014.

[25] M. Karampour and S. Sawalha, "State-of-the-art integrated CO2 refrigeration systems for supermarket: a comparative analysis," *International Journal of Refrigeration 86,* pp. 239-257, 2018.

[26] C. Aprea, A. Greco and A. Maiorino, "An experimental evaluation of the greenhouse effect in the substitution of R134a with CO2," *Energy, 45 (1),* pp. 753-761, 2012.

[27] M. Rossi, C. Favi, M. Germani and M. Omicioli, "Comparative life cycle assessment of refrigeration systems for food cooling: eco-design actions towards machines with natural refrigerants," *International Journal of Sustainable Engineering, 14 (6),* pp. 1623-1646, 2021.

[28] European Union, "Transport and the Green Deal," [Online]. Available: https://ec.europa.eu/info/strategy/priorities-2019-2024/european-green-deal/transport-and-green-deal_en. [Accessed November 2022].

[29] European Commission, "Sustainable & Smart Mobility Strategy," 2020. [Online]. Available: https://ec.europa.eu/info/strategy/priorities-2019-2024/european-green-deal/transport-and-green-deal_en. [Accessed November 2022].

[30] V. Nair, "HFO refrigerants: a review of present status and future prospects," *International Journal of Refrigeration 122,* pp. 156-170, 2021.

[31] A. K. S. Al-Sayyab, J. Navarro-Esbrì, A. Barragan-Cervera, S. Kim and A. Mota-Babiloni, "Comprehensive experimental evaluation of R1234yf-based low GWP working fluids for refrigeration and heat pumps," *Energy Conversion and Management 258,* 2022.

[32] S. Daviran, A. Kasaeian, S. Golzari, O. Mahian, S. Nasirivatan and S. Wongwises, "A comparative study on the performance of HFO-1234yf and HFC-134a as an alternative in automotive air conditioning systems," *Applied Thermal Engineering 110,* pp. 1091-1100, 2017.

[33] S. Vashisht and D. Rakshit, "Recent advances and sustainable solutions in automobile air conditioning systems," *Journal of Cleaner Production 329,* 2021.

[34] M. Z. Sharif, W. H. Azmi, N. N. M. Zawawi, R. Mamat and A. H. Hamisa, "R1234yf vs R134a in automotive air conditioning system: a comparison of the performance," *IOP Conference Series: Materials Science and Engineering 863,* 2020.

[35] Z. Wang, Y. Wang, J. Li, S. Henne, B. Zhang, J. Hu and J. Zhang, "Impacts of the degradation of 2,3,3,3-Tetrafluoropropene into Trifluoroacetic from its application in automobile air conditioners in China, the United States and Europe," *Environmental Science and Technology 52,* pp. 2819-2826, 2018.

[36] Y. Wang, Z. Wang, M. Sun, J. Guo and J. Zhang, "Emissions, degradation and impact of HFO-1234ze from China PU foam industry," *Science of the Total Environment 780,* 2021.

[37] European Chemicals Agency (ECHA), "Five European state calls for evidence on broad PFAS restriction," ECHA/NR/20/13, 2020. [Online]. Available: https://echa.europa.eu/-/five-european-states-call-for-evidence-on-broad-pfas-restriction.

[38] X. Chen, Q. Yang, W. Chi, Y. Zhao, G. Liu and L. Li, "Energy and exergy analysis of NH3/CO2 cascade refrigeration system with subcooling in the low-temperature cycle based on an auxiliary loop of NH3 refrigerants," *Energy Reports 8,* pp. 1757-1767, 2022.

[39] W. Chi, Q. Yang, X. Chen, G. Liu, Y. Zhao and L. Li, "Performance evaluation of NH3/CO2 cascade refrigeration system with ejector subcooling for low-temperature cycle," *International Journal of Refrigeration 136,* pp. 162-171, 2022.

[40] S. Zhou, G. He, X. Liang, Y. Li, Q. Pang and D. Cai, "Comparison of experimental performance of absorption refrigeration cycle using NH3/LiNO3+H20 working fluids with different water component proportions," *International Journal of Refrigeration 139,* pp. 25-40, 2022.

[41] M. Wirtz, B. Stutz, H. T. Phan and F. Boudehenn, "Performance improvement of NH3/H20 absorption chiller with a combined generator," *International Journal of Refrigeration,* 2022.

[42] P. H. Jorgensen, T. Ommen and B. Elmegaard, "Quantification and comparison of COP improvement approaches for large-scale ammonia heat pump systems," *International Journal of Refrigeration 129,* pp. 301-316, 2021.

[43] D. S. Ayou, R. Hargiyanto and A. Coronas, "Ammonia-based compression heat pumps for simultaneous heating and cooling applications in milk pasteurization processes: performance evaluation," *Applied Thermal ENgineering 217,* 2022.

[44] W. Meesenburg, W. B. Markussen, T. Ommen and B. Elmegaard, "Optimizing control of two-stage ammonia heat pump for fast regulation of power uptake," *Applied Energy 271,* 2020.

[45] K. Harby, "Hydrocarbons and their mixtures as alternatives to environmental unfriendly halogenated refrigerants: an updated overview," *Renewable and Sustainable Energy Reviews 73,* pp. 1247-1264, 2017.

[46] Q. Tian, D. Cai, L. Ren, W. Tang, Y. Xie, G. He and F. Liu, "An experimental investigation of refrigerant mixture R32/R290 as drop-in replacement for HFC410A in household air conditioners," *International Journal of Refrigeration 57,* pp. 216-228, 2015.

[47] Y. Jeon, S. Kim, S. H. Lee, H. J. Chung and Y. Kim, "Seasonal energy performance characteristics of novel ejector-expansion air conditioners with low-GWP refrigerants," *Applied Energy 278,* 2020.

[48] H. Zheng, G. Tian, Y. Zhao, C. Jin, F. Ju and C. Wang, "Experimental study of R290 replacement R134a in cold storage air conditioning system," *Case Studies in Thermal Engineering 36,* 2022.

[49] H. K. Hsieh and T. P. Teng, "Retrofit assessment of automobile air conditioners using hydrocarbon refrigerants," *Applied Thermal Engineering 214,* 2022.

[50] M. Ozsipahi, H. A. Kose, H. Kerpicci and H. Gunes, "Experimental study of R290/R600a mixtures in vapor compression refrigeration system," *International Journal of Refrigeration 133,* pp. 247-258, 2022.

[51] Q. Chen, Y. Hwang, G. Yan and J. Yu, "Theoretical investigation on the performance of an ejector enhanced refrigeration cycle using hydrocarbon mixture R290/R600a," *Applied Thermal Engineering 164,* 2020.

[52] J. V. H. D'Angelo, V. Aute and R. Radermacher, "Performance evaluation of vapor injection refrigeration system using mixture refrigerant R290/R600a," *International Journal of Refrigeration 65,* pp. 194-208, 2016.

[53] K. Nawaz, B. Shen, A. Elatar, V. Baxter and O. Abdelaziz, "R290 (propane) and R600a (isobutane) as natural refrigerants for residential heat pump water heaters," *Applied Thermal Engineering 127,* pp. 870-883, 2017.

[54] D. Colbourne, P. Solomon, R. Wilson, L. De Swardt, R. Nosbers and M. Schuster, "Development of R290 transport refrigeration system," Institute of Refrigeration, Carshalton, UK, 2017.

[55] M. Ramaube and Z. Huan, "Testing and performance evaluation of a R404A transport refrigeration system retrofitted with R290," in *Proceedings of the AIUE 17th Industrial and Commercial Use of Energy (ICUE) Conference*, Cape Town, South Africa, 2019.

[56] J. M. Corberan, J. Segurado, D. Colbourne and J. Gonzalvez, "Review of standards for the use of hydrocarbon refrigerants in A7C, heat pump and refrigeration equipment," *International Journal of Refrigeration 31,* pp. 748-756, 2008.

[57] A. Jones, A. Wolf and S. M. Kwark, "Refrigeration system development with limited charge of flammable refrigerant, R290," *Thermal Science and Engineering Progress 34,* 2022.

[58] M. O. McLinden, A. F. Kazakov, S. J. Brown and P. A. Domanski, "A thermodynamic analysis of refrigerants: possibilities and tradeoffs for low-GWP refrigerants," *International Journal of Refrigeration 38,* pp. 80-92, 2014.

[59] M. H. Kim, J. Pettersen and C. W. Bullard, "Fundamental process and system design issues in CO2 vapor compression systems," *Progress in Energy and Combustion Science 30 (2),* pp. 119-174, 2004.

[60] H. Inokuty, "Approximated graphical method of finding compression pressure of CO2 refrigeration machine for max coefficient of performance," Read before the 92nd meeting of the Japan Society of Mechanical Engineers, 8 March 1923, 1923.

[61] G. Lorentzen, "Revival of carbon dioxide as a refrigerant," *International Journal of Refrigeration 17 (5),* 1994.

[62] H. Inokuty, "Theory and experiments on vapour compression refrigeration machine with some modified cycles," Read before the 101st meeting of the Japan Society of Mechanical Engineers, 17 July 1924, 1924.

[63] G. Lorentzen, "Throttling: the internal haemorrhage of the refrigeration process," Institute of Refrigeration, London, UK, 1983.

[64] S. Elbel, "Historical and present developments of ejector refrigeration systems with emphasis on transcritical carbon dioxide air-conditioning," *International Journal of Refrigeration 34 (7),* pp. 1545-1561, 2011.

[65] P. Gullo, A. Hafner, K. Banasiak, S. Minetto and E. Kriezi, "Multi-Ejector concept: a comprehensive review on its latest technological developments," *Energies 12 (3),* 2019.

[66] M. Karampour and S. Sawalha, "Energy efficiency evaluation of integrated CO2 trans-critical system in supermarkets: a field measurements and modelling analysis," *International Journal of Refrigeration 82,* pp. 470-486, 2017.

[67] P. Gullo, A. Hafner and K. Banasiak, "Transcritical R744 refrigeration systems for supermarket applications: current status and future perspectives," *International Journal of Refrigeration 93,* pp. 269-310, 2018.

[68] D. Tsimpoukis, E. Syngounas, D. Petsanas, G. Mitsopoulos, S. Anagnostatos, E. Bellos, C. Tzivanidis and M. G. Vrachopoulos, "Energy and environmental investigation of R744 all-in-one configurations for refrigeration and heating/air conditioning needs of a supermarket," *Journal of Cleaner Production 279,* 2021.

[69] Á. Á. Pardiñas, A. Hafner and K. Banasiak, "Novel integrated CO2 vapour compression racks for supermarkets. Thermodynamic analysis of possible system configurations and influence of operational conditions," *Applied Thermal Engineering 131,* pp. 1008-1025, 2018.

[70] B. Yu, J. Yang, D. Wang, J. Shi and J. Chen, "An updated review of recent advances on modified technologies in transcritical CO2 refrigeration cycle," *Energy 189,* pp. 116-147, 2019.

[71] Y. Song, C. Cui, X. Yin and F. Cao, "Advanced development and application of transcritical CO2 refrigeration and heat pump technology - A review," *Energy Reports 8,* pp. 7840-7869, 2022.

[72] R. B. Barta, E. A. Groll and D. Ziviani, "Review of stationary and transport CO2 refrigeration and air conditioning technologies," *Applied Thermal Engineering 185,* 2021.

[73] N. Lawrence, S. Elbel and P. Hrnjak, "Design and validation of a transcritical CO2 mobile refrigerated container system for military applications," in *Proceedings of the 13th IIR Gustav Lorentzen Conference on Natural Refrigerants*, Valencia, Spain, 2018.

[74] N. Lawrence, S. Elbel and P. Hrnjak, "Advanced R744 technology applied to a multi-temperature refrigerated container," in *Proceedings of the 14th IIR Gustav Lorentzen Conference on Natural Refrigerants*, Kyoto, Japan, 2020.

[75] R. B. Barta, J. J. Hugenroth and E. A. Groll, "Modeling and control strategy of a transcritical carbon dioxide cycle for application in multi-temperature refrigerated container systems," in *Proceedings of the 13th IIR Gustav Lorentzen Conference on Natural Refrigerants*, Valencia, Spain, 2018.

[76] J. Bodys, A. Hafner, K. Banasiak, J. Smolka and Y. Ladam, "Design and simulations of refrigerated sea water chillers with CO2 ejector pumps for marine applications in hot climates," *Energy 161,* pp. 90-103, 2018.

[77] E. Söylemez, K. N. Widell, C. H. Gabrielii, Y. Ladam, T. Lund and A. Hafner, "Overview of the development and status of carbon dioxide (R-744) refrigeration systems onboard fishing vessels," *International Journal of Refrigeration 140,* pp. 198-212, 2022.

[78] P. Artuso, S. Marinetti, S. Minetto, D. Del Col and A. Rossetti, "Modelling the performance of a new cooling unit for refrigerated transport using carbon dioxide as the refrigerant," *International Journal of Refrigeration 115,* pp. 158-171, 2020.

[79] Fiat Professional, "Ducato - Technical specifications," 2021. [Online]. Available: https://www.fiatprofessional.com/brochure.

[80] Siemens PLM Software, "Simcenter Amesim 17 - Mechanical Library. User's guide," 2018.

[81] L. De Simio, M. Gambino and S. Iannaccone, "Dual fuel engines for utilization of waste vegetable oil and municipal organic fraction as energy source in urban areas," in *Proceedings of the 4th International Conference on Sustainable Energy & Environmental Protection*, Bari, Italy, 2010.

[82] United Nations, "Agreement on the International Carriage of Perishable Food-stuffs and on the Special Equipment to be Used for Such Carriage (ATP)," UNECE Transport Division, Geneva, Switzerland, 2020.

[83] T. Lafaye De Micheaux, M. Ducoulombier, J. Moureh, V. Sartre and J. Bonjour, "Experimental and numerical investigation of the infiltration heat load during the opening of a refrigerated truck body," *International Journal of Refrigeration 54,* pp. 170-189, 2015.

[84] M. Benedict, G. Webb and L. Rubin, "An empirical equation for thermodynamic properties of light hydrocarbons and their mixtures I. Methane, Ethane, Propane and n-Butane," *The Journal of Chemical Physics 8 (4),* pp. 334-345, 1940.

[85] Bitzer, "Transport applications // Open drive reciprocating compressors. Technical brochure," 2013. [Online]. Available: https://www.bitzer.de/us/us/reciprocating-compressors/roadstar/.

[86] V. Gnielinski, "New equations for heat and mass transfer in turbulent pipe and channel flow," *International Chemical Engineering 16,* pp. 359-368, 1976.

[87] D. Steiner and J. Taborek, "Flow boiling heat transfer in vertical tubes correlated by an asymptotic model," *Heat Transfer Engineering 13,* pp. 322-329, 1992.

[88] M. Shah, "A general correlation for heat transfer during film condensation inside pipes," *International Journal of Heat and Mass Transfer 22,* pp. 547-556, 1979.

[89] L. Friedel, "Improved friction pressure drop correlation for horizontal and vertical two-phase pipe flow," in *Proceedings of the European Two-Phase Flow Group Meeting*, Ispra, Italy, 1979.

[90] F. McQuiston, "Correlation of heat, mass and momentum transport coefficients for plate-fin-tube heat transfer surfaces with staggered tubes," *ASHRAE Transaction 84 (1),* pp. 294-309, 1978.

[91] Siemens PLM Software, "Simcenter Amesim 17 - Integration algorithms used in Simcenter Amesim. Technical bulletin n.102," 2018.

[92] ASHRAE, Refrigeration Handbook, Chapter R09, Thermal properties of foods, Atlanta, GA, USA: American Society of Heating, Refrigerating and Air-Conditioning Engineers, 2006.

[93] M. Harris, J. Carson, J. Willix and S. Lovatt, "Local surface heat transfer coefficients on a model lamb carcass," *Journal of Food Engineering 61,* pp. 421-429, 2004.

[94] European Commission, "Commission Regulation (EU) 2017/1151," 2017.

[95] Energy Plus, "Energy Plus Weather Data," [Online]. Available: https://energyplus.net/.

[96] A. Bahaj, "World's first solar powered transport refrigeration system," *Renewable energy 15 (1-4),* pp. 572-576, 1998.

[97] A. Bahaj, "Photovoltaic power for refrigeration of transported perishable goods," in *28th IEEE Photovoltaic Specialists Conference*, Anchorage, AK, USA, 2000.

[98] B. Elliston and M. Dennis, "Feasibility of solar-assisted refrigerated transport in Australia," in *47th ANZSES Annual Conference*, Townsville, Queensland, Australia, 2009.

[99] A. Meneghetti, F. Dal Magro and A. Romagnoli, "Renewable energy penetration in food delivery: coupling photovoltaics with transport refrigerated units," *Energy 232, 120994,* 2021.

[100] A. Rossetti, S. Marinetti, P. Artuso, F. Fabris and S. Minetto, "Implementation of a solar aided refrigeration unit for refrigerated trucks employing photovoltaic generators," *Energy Reports 8,* pp. 7789-7799, 2022.

[101] A. Vartholomaios, "Classification of the influence of urban canyon geometry and reflectance on seasonal solar irradiation in three European cities," *Sustainable Cities and Society 75, 103379,* 2021.

[102] P. Kalinski, "The Danfoss Multi-Ejector range for CO2 refrigeration: design, applications and benefits," Danfoss, 2019. [Online]. Available: https://www.multiejectorsolution.danfoss.com.

[103] S. Elbel and P. Hrnjak, "Effect of internal heat exchanger on performance of transcritical CO2 systems witg ejector," in *Proceedings of the International Refrigeration and Air Conditioning Conference*, Purdue, USA, 2004.

[104] Dorin, "CD Series. Semi-hermetic motor compressors. Transcritical CO2 application - 50/60 Hz," 2022. [Online]. Available: https://www.dorin.com/documents/Download/18/1LTZ016_CD_02.22.pdf.

[105] S. Dugaria, L. Calabrese, M. Azzolin, S. Minetto and D. Del Col, "Energy analysis of CO2 refrigeration systems using measured values of compressor efficiency," in *Proceedings of the 13th IIR Gustav Lorentzen Conference on Natural Refrigerants*, Valencia, Spain, 2018.

[106] S. Churchill and H. Chu, "Correlating equations for laminar and turbulent free convection from a vertical plate," *International Journal of Heat and Mass Transfer 18 (11),* pp. 1323-1329, 1975.

[107] R. Hilpert, "Heat transfer from cylinders," *Forsch. Geb. Ingenieurwes, 4,* p. 215, 1933.

[108] K. Banasiak, A. Hafner, E. Kriezi, K. Madsen, M. Birkelund, K. Fredslund and R. Olsson, "Development and performance mapping of a multi-ejector expansion work recovery pack for R744 vapour compression units," *International Journal of Refrigeration 57,* pp. 265-276, 2015.

[109] G. Mihalakakou, M. Santamouris, N. Papanikolaou, C. Cartalis and A. Tsangrassoulis, "Simulation of the urban heat island phenomenon in Mediterranean climates," *Journal of Pure and Applied Geophysics 161,* pp. 429-451, 2004.

[110] S. Elbel and P. Hrnjak, "Experimental validation of a prototype ejector designed to reduce throttling losses encountered in transcritical R744 system operation," *International Journal of Refrigeration 34 (7),* pp. 411-422, 2008.

[111] National Instruments, "NI 9213 Datasheet," 2017. [Online]. Available: https://www.ni.com/it-it/support/model.ni-9213.html.

[112] E. Lemmon, M. Huber and M. McLinden, "NIST Standard Reference Database 23: Reference Fluid Thermodynamic and Transport Properties-REFPROP, Version 9.1, Natl Std. Ref. Data Series (NIST NSRDS)," National Institute of Standards and Technology, Gaithersburg, Maryland, U.S.A., 2013.

[113] M. Frank, M. Ostermeier, A. Holzapfel, A. Hübner and H. Kuhn, "Optimizing routing and delivery patterns with multi-compartment vehicles," *European Journal of Operational Research 293 (2),* pp. 495-510, 2021.

[114] Thermo King, "Multi-Temperature Trailer Units," 2022. [Online]. Available: https://www.thermoking.com/na/en/road/trailers/multi-temperature-controlled-units.html#s-610m.

[115] Daikin, "Transport Refrigeration," 2022. [Online]. Available: https://www.daikin.eu/en_us/product-group/transport-refrigeration.html.

[116] Carrier Transicold, "Trailer Refrigeration Units," 2022. [Online]. Available: https://www.carrier.com/truck-trailer/en/eu/products/eu-truck-trailer/trailer/.

[117] A. Chinchuluun and P. Pardalos, "A survey of recent developments in multiobjective optimization," *Annals of Operations Research, 154(1),* pp. 29-50, 2007.

[118] S. Brisset and F. Gillon, "Approaches for multi-objective optimization in the ecodesign of electric systems," in *Eco-friendly innovation in electricity transmission and distribution networks*, 2015, pp. 83-97.

[119] K. Banasiak, Á. Á. Pardiñas and E. Kriezi, "Modelling and development of high-pressure lift ejector for low temperature evaporators in R744 refrigeration systems for supermarkets," in *Proceedings of the 25th IIR International Congress of Refrigeration*, Montreal, Canada, 2019.

List of publications

Peer-reviewed journals:

- Fabris, F., Artuso, P., Marinetti, S., Minetto, S., Rossetti, A. (2021). Dynamic modelling of a CO2 transport refrigeration unit with multiple configurations. Applied Thermal Engineering 189 (2021), 116749.
- Fabris, F., Artuso, P., Marinetti, S., Minetto, S., Rossetti, A. (2022). Cooling unit impact on energy and emissions of a refrigerated light truck. Applied Thermal Engineering 216 (2022), 119132.
- Rossetti, A., Marinetti, S., Artuso, P., Fabris, F., Minetto, S. (2022). Implementation of a solar aided refrigeration unit for refrigerated trucks employing photovoltaic generators. Energy Reports 8, 7789-7799.

Conference proceedings:

- Fabris, F., Artuso, P., Rossetti, A., Minetto, S., Marinetti, S. (2020). Impact of the refrigeration system on the fuel consumption and on the emissions of a small refrigerated truck. 6th IIR International Conference on Sustainability and the Cold Chain, 26-28 August 2020, Nantes, France.
- Fabris, F., Artuso, P., Minetto, S., Marinetti, S., Rossetti, A. (2020). Numerical investigation of a CO2 cooling unit for refrigerating transport operating switching between different configurations. 14th IIR Gustav Lorentzen Conference on Natural Refrigerants, 7-9 December 2020, Kyoto, Japan.
- Fabris, F., Artuso, P., Minetto, S., Marinetti, S., Rossetti, A. (2021). Numerical analysis of the thermal performance of a CO2 refrigerating unit for multi-temperature transport applications. 6th IIR Conference on Thermophysical Properties and Transfer Processes of Refrigerants, 1-3 September 2021, Vicenza, Italy.
- Fabris, F., Pardiñas, Á. Á., Marinetti, S., Rossetti, A., Hafner, A., Minetto, S. (2022). Experimental evaluation of the performance of an ejector for a single compression multi-temperature CO2 refrigeration unit. 15th IIR Gustav Lorentzen Conference on Natural Refrigerants, 13-15 June 2022, Trondheim, Norway.
- Rossetti, A., Fabris, F., Marinetti, S., Minetto, S. (2022). Field-data based model for integrated supermarkets system seasonal performance evaluation. 7th IIR International Conference on Sustainability and the Cold Chain, 11-13 April 2022, Newcastle, United Kingdom.
- Pardiñas, Á. Á., Fabris, F., Contiero, L., Selvnes, H., Banasiak, K., Hafner, A. (2022). Ejector for the World: simplified ejector-supported CO2 refrigeration systems for all climates. 15th IIR Gustav Lorentzen Conference on Natural Refrigerants, 13-15 June 2022, Trondheim, Norway.

- Contiero, L., Fabris, F., Pardiñas, Á. Á., Hafner, A. (2022). Performance improvements of supermarket R744 systems by pivoting compressor arrangements. 15th IIR Gustav Lorentzen Conference on Natural Refrigerants, 13-15 June 2022, Trondheim, Norway.